



The
University
Of
Sheffield.

Characterisation Of Parkinson's Disease Risk Gene, GTP Cyclohydrolase I, In Zebrafish

Hannah Larbalestier

June 2020

Thesis Submitted for The Degree of Doctor of Philosophy
University of Sheffield, Department of Neuroscience

Acknowledgements

Firstly, thank you to my supervisor, Oliver Bandmann, for guiding me throughout my PhD, and providing me with such an exciting project. Thank you also to my secondary supervisor, Ryan MacDonald, for imparting your IHC expertise and for always being on hand for feedback and advice.

Thank you to Lisa and Marcus, who have supported me throughout the entirety of my PhD, despite not being in the lab with me for most of it. Thank you to all the other past and present members of the Bandmann group with whom I've greatly enjoyed working alongside: Emily, Emma, Deepak, Seyi, Beckah, Sarah and Siri. Thanks also to everyone in C06/C10 space: Karishma, Eli, Karen, Aaron, Ryan, Yan, Jane, Julia, Mat, Rings, Rosemary, Eleanor, Stone, and Freek.

Thank you to other members of Bateson and Sitran, Adrian Higginbottom, Alex McGown, Noemie Hamilton, Mike Thomas, Vickie Thomas-McArthur, and JP Ashton, for your help and expertise. Thank you also to Dirk Sieger and Julie Mazzolini, for giving up your valuable time to share your methods with me.

Finally, thank you to my family, and to Liam, for all your support.

Abstract

GTP Cyclohydrolase I (*GCH1*) is a known Parkinson's Disease (PD) risk gene, identified in sporadic and familial PD cases. Additionally, mutations in *GCH1* are a causative factor for the childhood-onset disorder dopa-responsive dystonia (DRD). *GCH1* catalyses the rate-limiting step in the synthesis of tetrahydrobiopterin (BH4), which is an essential cofactor for the synthesis of dopamine and other catecholaminergic neurotransmitters. We hypothesised that *GCH1* deficiency may lead to dopaminergic cell degeneration, and thus development of PD, as a direct result of metabolic dopamine deficiency. We generated a *gch1* mutant zebrafish line (*gch1*^{-/-}) to investigate this hypothesis, and to explore additional pathomechanisms by which *GCH1* deficiency may contribute to PD risk. *gch1*^{-/-} zebrafish develop neurotransmitter deficits by 5 dpf, a hypoactive motor phenotype by 8 dpf, and mortality by 12 dpf. Despite striking neurotransmitter deficits, dopaminergic neurons show no evidence of degeneration, however, protein levels of the dopamine-producing enzyme, tyrosine hydroxylase, are depleted. Gene expression analysis from larval brains revealed metabolic dysregulation, induction of matrix metalloproteinases, and inflammatory activation in *gch1*^{-/-}. Morphological analysis and functional activity assays of microglial activation identified a heightened activation state of microglia in *gch1*^{-/-}, indicative of a neuroinflammatory phenotype. We reject our hypothesis that dopamine deficiency directly predisposes to degeneration, as despite severe biochemical deficits we do not observe a reduction in the number of dopaminergic neurons in *Gch1*-deficient zebrafish; however, this project identifies 2 mechanisms – tyrosine hydroxylase (TH) depletion, and neuroinflammation - in *Gch1*-deficient larvae, which both represent potential pathological mechanisms which may lead to neurodegeneration. We propose that in cases of *GCH1*-deficiency, PD symptoms appear at an early subclinical stage of nigral degeneration as a result of dopamine deficiency, and this is exacerbated by depletion of TH protein.

Table of Contents

Characterisation Of Parkinson’s Disease Risk Gene, GTP Cyclohydrolase I, In Zebrafish	0
Acknowledgements	1
Abstract.....	2
Table of Figures	6
List of Tables.....	8
List of abbreviations.....	9
Chapter 1. Introduction.....	11
1.1. Parkinson’s Disease	12
1.1.1. Incidence	12
1.1.2. Neuropathology of PD	12
1.1.3. Symptoms and Diagnosis	13
1.1.4. Treatment.....	14
1.1.5. Mortality	15
1.2. Etiology of Parkinson’s Disease.....	16
1.2.1. Environmental risk factors.....	16
1.2.2. Identifying Genetic Causes of Familial PD	17
1.2.3. Identifying Genetic Risk Factors for Sporadic PD	18
1.3. <i>GCH1</i> as a PD risk gene	22
1.3.1. Identification of <i>GCH1</i> as a familial and sporadic PD risk factor	22
1.3.2. Physiological roles of <i>GCH1</i> and <i>BH4</i> – neurotransmitter synthesis.....	27
1.3.3. Physiological roles of <i>BH4</i> – Nitric Oxide Synthase activity.....	28
1.3.4. Factors influencing <i>GCH1</i> expression	30
1.3.5. Multiple forms of parkinsonism in <i>GCH1</i> mutation carriers.....	31
1.3.6. Proposed mechanisms contributing to dopaminergic degeneration	32
1.4. Models of <i>GCH1</i> deficiency	33
1.4.1. <i>Gch1</i> knockout mouse model is embryonic lethal	33
1.4.2. <i>hph-1</i> mouse model shows DRD-like biochemical deficits	34
1.4.3. TH depletion in dopamine-depleted PC12D cells.....	34
1.4.4. <i>Gch1</i> -deficient murine macrophages exhibit elevated superoxide production.....	35
1.4.5. Literature review summary	36
1.5. Zebrafish as a model for studying <i>GCH1</i> deficiency	36
1.5.1. The Dopaminergic system in zebrafish.....	38
1.6. Aims and Objectives	41
Chapter 2. Materials and Methods	44
2.1. Zebrafish Husbandry	45
2.1.1. Larval Husbandry.....	45
2.1.2. Imaging Larvae	46
2.1.3. Adult Husbandry	46
2.2. CRISPR/Cas9 – Generating a <i>gch1</i> Zebrafish Line	46
2.3. Nucleic Acid Extraction and Polymerase Chain Reaction (PCR).....	46
2.3.1. DNA Extraction	46
2.3.2. Polymerase Chain Reaction (PCR).....	47
2.3.3. PCR Purification.....	47
2.3.4. Gel Electrophoresis	48

2.3.5. RNA Extraction	48
2.3.6. cDNA Synthesis.....	48
2.3.7. Reverse Transcriptase PCR.....	49
2.3.8. Quantitative PCR (qPCR)	50
2.4. Survival Analysis	50
2.5. High Performance Liquid Chromatography (HPLC).....	51
2.6. Fixing Fish	51
2.7. Wholemount In Situ Hybridisation (WISH).....	51
2.7.1. WISH Probe Generation	51
2.7.2. WISH Protocol	52
2.7.3. <i>gch1</i> WISH	54
2.7.4. Neuron Counting In <i>th</i> -WISH Stained Larvae	54
2.7.5. Neuron counting in MPP+ treated larvae.....	54
2.8. Neuron Counting in <i>etVmat2-GFP</i> Larvae	55
2.9. Immunohistochemistry	55
2.9.1. Cryosectioning Larval Samples	55
2.9.2. Immunohistochemistry on Cryosections.....	56
2.9.3. Wholemount Immunohistochemistry	56
2.10. Western Blot	57
2.10.1. Protein Lysate Preparation	57
2.10.2. SDS-PAGE.....	58
2.10.3. Western Blot Transfer to Membrane	58
2.11. RNAseq	58
2.11.1. RNA Sample Preparation	58
2.11.2. Differential Gene Expression Analysis.....	59
2.11.3. Pathway Analysis	59
2.11.4. Gene Ontology Enrichment Analysis	60
2.12. Microglial Methods	60
2.12.1. High Throughput Imaging of 4c4-Immunostained Larvae.....	60
2.12.2. Counting of Microglia.....	60
2.12.3. Analysis Of The Percentage Of Microglia Showing Activated Morphology.....	61
2.12.4. Zymosan-Injection Experiment.....	61
2.12.5. Zymosan Phagocytic Activity Assay	62
2.13. Drug Treatments	63
2.13.1. Drug application	63
2.13.1. Larval Movement Analysis.....	64
Chapter 3. Results	65
3.1. Establishing a <i>gch1</i>^{-/-} Zebrafish Line	66
3.1.1. Identifying the Zebrafish Ortholog of <i>GCH1</i>	66
3.1.2. Confirming Spatiotemporal Expression of <i>gch1</i>	68
3.1.3. CRISPR/Cas9 Mediated Knockout of <i>gch1</i>	71
3.1.4. Loss of Function of <i>gch1</i> is Homozygous Lethal	74
3.2. Characterisation of the DA Neurons	76
3.2.1. HPLC Analysis of Monoaminergic Neurotransmitters and Metabolites.....	76
3.2.2. Electrophysiological Assessment of DA Neurons.....	80
3.2.3. DA Neuron Counts	81
3.2.4. Neurotoxin Exposure.....	83
3.2.5. Tyrosine Hydroxylase Depletion in <i>gch1</i> ^{-/-}	84

3.3. Gene-gene interaction study.....	87
3.3.1. <i>gch1</i> ; <i>gba</i>	88
3.4. RNAseq to Assess Transcriptional Changes in WT, <i>gch1</i> ^{+/−} and <i>gch1</i> ^{−/−} Larval Brain Samples	92
3.4.1. Principal component analysis	93
3.4.2. Differential gene expression analysis	94
3.4.3. Pathway analysis	96
3.4.4. Gene Ontology enrichment analysis.....	104
3.4.5. Validation of upregulation of <i>irg1l</i>	112
3.5. Microglial analysis	113
3.5.1. Validating microglial specific staining with α-4c4	113
3.5.2. High throughput imaging of 4c4-stained larvae for microglial analysis	114
3.5.3. Functional assessment of microglial activity by quantifying phagocytic efficiency of zymosan engulfment	117
3.6. Effect of targeted drug treatments on <i>gch1</i> ^{−/−} survival	121
3.6.1. Sepiapterin treatment fails to modify survival in <i>gch1</i> ^{−/−}	121
3.6.2. L-DOPA treatment prolongs survival but does not ameliorate hypoactive motor phenotype ..	124
3.6.4. L-N ⁶ -(1-Iminoethyl)lysine treatment has no effect on <i>gch1</i> ^{−/−} survival	130
3.6.5. Nitric oxide donor, Sodium Nitroprusside, prolongs median survival of <i>gch1</i> ^{−/−}	133
Chapter 4. Discussion	135
4.1. Key findings	136
4.2. DA Neuron Characterisation.....	136
4.2.1. HPLC analysis of neurotransmitter levels.....	136
Suitability of the <i>gch1</i> ^{−/−} zebrafish for modelling autosomal dominant GCH1 deficiency	140
4.2.2. Electrophysiology	141
4.2.3. Dopaminergic neuronal cell counts	141
4.2.4. MPP+ treatment.....	143
4.2.5. Tyrosine hydroxylase depletion.....	146
4.3. Gene-gene interactions	147
4.4. RNAseq and microglial activation	149
4.5. Microglial characterisation	153
4.6. Drug treatments.....	155
4.6.1. Sepiapterin	156
4.6.2. L-DOPA.....	156
4.6.3. Etomoxir	157
4.6.4. L-NIL.....	157
4.6.5. Sodium nitroprusside.....	158
4.7. Concluding summary.....	159
4.8. Future outlook	159
Bibliography	161
Appendix	193

Table of Figures

Figure 1: Feasibility of identifying genetic variants by risk allele frequency and strength of genetic effect. ...	20
Figure 2: Manhattan plot for significant PD GWAS variants.	21
Figure 3: Pedigrees and ¹²³ I-FP-CIT SPECT scan images of the four families with GCH1 mutations involved in the Mencacci et al. (2014) study.....	24
Figure 4: The Tetrahydrobiopterin (BH4) synthesis pathway.	28
Figure 5: Schematic illustrating production of nitric oxide under conditions of saturated BH4.....	29
Figure 6: Schematic demonstrating how subsaturated BH4 levels leads to production of peroxynitrite.....	30
Figure 7: Illustrative schematic of zymosan injection procedure.....	62
Figure 8: GCH1 protein homology	66
Figure 9: GCH1 synteny map	67
Figure 10: gch1 RT-PCR.....	68
Figure 11: Wholemount In situ hybridisation for gch1.	69
Figure 12: Gch1 and Th immunostain.	70
Figure 13: gch1 PCR. The WT band is shown at ~300bp on the DNA ladder, and mutant band at ~200bp.....	71
Figure 14: Predicted mutant protein sequence.....	72
Figure 15: qPCR of gch1 transcript levels in WT and gch1 ^{-/-}	73
Figure 16: Phenotypic images of WT and gch1 ^{-/-} larvae from 4-8 dpf.....	74
Figure 17: Survival proportions of larvae from a gch1 ^{+/-} incross.....	75
Figure 18: HPLC analysis of monoaminergic neurotransmitters and metabolites at 5 dpf.	77
Figure 19: HPLC analysis of monoaminergic neurotransmitters and metabolites at 8 dpf.	78
Figure 20: HPLC analysis of neurotransmitters and metabolites at 12 mpf.....	79
Figure 21: Electrophysiological assessment of DA neurons.....	80
Figure 22: th+ neuron counts at 5 dpf.....	81
Figure 23: Representative th WISH image.	82
Figure 24: Representative et-vmat2;GFP image of DC2-DC4/5 neurons.	82
Figure 25: Vmat2+ neuron counts at 8 dpf.....	83
Figure 26: th+ counts in MPP+ treated larvae.....	84
Figure 27: Reduced Th-immunofluorescence in gch1 ^{-/-} DA neurons.	85
Figure 28: qPCR and Western blotting reveals depletion of Th protein in gch1 ^{-/-} at 8dpf.....	86
Figure 29: gch1;gba1 th+ neuron counts, 5dpf.....	89
Figure 30: Survival curve of larvae from gch1 ^{+/-} ;gba1 ^{+/-} incross.	90
Figure 31: Survival curve of adult fish from a gch1 ^{+/-} ;gba1 ^{+/-} incross.	91
Figure 32: Principal component analysis of RNAseq data.....	93
Figure 33: Volcano plot to illustrate DE genes in gch1 ^{-/-}	95
Figure 34: GO term clusters of downregulated genes in gch1 ^{-/-}	107
Figure 35: GO term clusters of upregulated genes in gch1 ^{-/-}	111
Figure 36: qPCR to quantify irg1l expression levels at 3, 5 and 8 dpf in gch1 ^{-/-} larvae.	112
Figure 37: Comparison of microglial specificity of mpeg-mCherry and 4c4 immunostain.	114
Figure 39: Microglial counts, 8dpf.	115
Figure 40: Percentage of amoeboid microglia in the midbrain.....	116
Figure 40: Representative image of WT vs gch1 ^{-/-} microglia.....	116
Figure 44: Zymosan engulfment by microglia, representative image.	117
Figure 45: Quantification of phagocytic engulfment of zymosan.	118
Figure 46: Counting of microglia in zymosan- vs PBS-injected samples.	119
Figure 47: Microglial activation in response to zymosan injection.	120
Figure 48 Sepiapterin toxicity assessment.	122
Figure 49: Sepiapterin treatment.	123
Figure 50: L-DOPA toxicity test.....	124
Figure 51: Survival analysis of L-DOPA-treated gch1 ^{-/-}	125
Figure 52: Representative movement trace from L-DOPA treatment.....	126
Figure 53: Movement analysis of L-DOPA-treated larvae from a gch1 ^{+/-} incross at 8 dpf.....	126
Figure 54: Etomoxir toxicity assessment #1.....	127
Figure 55: Survival analysis of 1 μM etomoxir-treated gch1 ^{-/-}	128

Figure 56: Etomoxir toxicity assessment #2.	129
Figure 57: : Survival analysis of 5 μ M etomoxir-treated $gch1^{-/-}$	130
Figure 58: L-NIL toxicity assessment #1.	131
Figure 59: L-NIL toxicity assessment #2.	131
Figure 60: Survival analysis of L-NIL-treated $gch1^{-/-}$	132
Figure 61: SNP toxicity assessment.....	133
Figure 62: Survival analysis of SNP-treated $gch1^{-/-}$	134
Figure 63: MPTP neurotoxicity mechanism.	145

List of Tables

Table 1: Primer list	45
Table 2: Differentially expressed genes in the $gch1^{+/-}$ vs WT dataset.	94
Table 3: Differentially expressed pathways in $gch1^{-/-}$	97
Table 4: GO enrichment analysis of downregulated transcripts in $gch1^{-/-}$	105
Table 5: GO enrichment analysis of upregulated transcripts in $gch1^{-/-}$	109
Table 6: Reports of hyperphenylalanemia as a result of homozygous or compound-heterozygous GCH1 mutations	139
Supplementary table 1: list of PD risk loci (Nalls et al., 2019), their nearest gene in the human genome, and the zebrafish ortholog(s) of each gene.	189
Supplementary table 2: DE genes in $gch1^{-/-}$ vs WT.	193

List of abbreviations

$-/-$ - homozygous

$+/-$ - heterozygous

3-MT - 3-Methoxytyramine

5-HIAA - 5-hydroxyindoleacetic acid

ARS – aminoacyl tRNA synthetase

BH4 – tetrahydrobiopterin

Cas9 - CRISPR associated protein 9

cDNA – complementary DNA

CNS – central nervous system

CRISPR - clustered regularly interspaced short palindromic repeats

DA - dopaminergic

DOPAC - 3,4-Dihydroxyphenylacetic acid

dpf – days post fertilisation

gch1 – GTP cyclohydrolase I

GWAS – genome wide association study

HPA - hyperphenylalanemia

HPLC – high performance liquid chromatography

HVA - Homovanillic acid

iNOS – inducible nitric oxide synthase

irg1l – immunoresponsive gene 1, like

KO – knockout

L-dopa - L-3,4-Dihydroxyphenylalanine

MeOH – methanol

MIP – maximal intensity projection

mM – millimolar

MO - morpholino

mpf – months post fertilisation

mRNA – messenger RNA

mROS - mitochondrial ROS

NMS – non-motor symptoms

NO – nitric oxide
NOS – nitric oxide synthase
PBS – phosphate buffered saline
PBT – phosphate buffered saline + 0.01% Tween-20
PCR – polymerase chain reaction
PFA – paraformaldehyde
PKU - phenylketonuria
PVDF - polyvinylidene difluoride
qPCR – quantitative polymerase chain reaction
RNAseq - RNA sequencing
RNS – reactive nitrogen species
ROS – reactive oxygen species
rpm – revolutions per minute
RT - room temperature
RT-PCR – reverse transcriptase polymerase chain reaction
sgRNA – single guide RNA
SNP – single nucleotide polymorphism
TAE – Tris-acetate-EDTA
th – tyrosine hydroxylase
WISH – wholemount in situ hybridisation
WT – wild type
 μ l - microlitre
 μ M - micromolar

Chapter 1. Introduction

1.1. Parkinson's Disease

1.1.1. Incidence

Parkinson's disease (PD) is the 2nd-most common neurodegenerative disease globally, and affects 1-2 people per 1000 in the general population, or 1% of the population over 60 (Tysnes and Storstein, 2017). With global population growth and an increasing elderly population, the global burden of PD is expected to double between 2007 and 2030 (Dorsey et al., 2007). The major risk factor for PD is age; a meta-analysis of 14 epidemiological studies on PD confirmed that in males and females, incidence of PD rises steadily over time (Hirsch et al., 2016). In females, the meta-analysis revealed an incidence of 3.26 per 100,000 person-years at age 40-49, increasing to 103.48 at age 80+. In males, incidence rises from 3.57 per 100,000 person-years at age 40, to 258.47 at age 80+. Males were confirmed to have significantly higher incidence of PD than females in the age brackets 60-69 and 70-79. It has been suggested that females have delayed incidence and more benign PD, due to higher striatal dopamine levels as a result of estrogen activity (Haaxma et al., 2007).

1.1.2. Neuropathology of PD

Key neuropathological features of PD are degeneration of dopaminergic (DA) neurons in the substantia nigra pars compacta (SNpc), and the presence of alpha-synuclein-containing Lewy bodies (Braak et al., 2003a). From post-mortem analyses, it has become clear that loss of DA neurons in the SNpc is clearly linked with PD, however, it can also be observed in a wide-range of other Parkinsonian disorders which do not necessarily also show alpha-synuclein pathology (Dickson et al., 2009). Alpha-synuclein pathology, in the form of aggregated and misfolded alpha-synuclein in Lewy-Bodies (LBs) and Lewy-neurites is similarly found in the majority of PD cases, but not all. Even in some classical monogenic-mutation forms of PD, such as PD caused by LRRK2 or parkin variants, pathology may present as neuronal degeneration without evidence of alpha-synuclein inclusions (Hasegawa et al., 2009; Johansen et al., 2018).

Investigations into the diagnostic accuracy of PD estimates that only 74% of PD cases correlate with positive neuropathological criteria at autopsy (Tolosa et al., 2006). This is likely due to a combination of initial misdiagnosis of different brain diseases with similar

clinical signs to PD, in addition to the heterogeneity of pathology in PD cases. Variation in PD pathology is likely due to the heterogeneity in the molecular mechanisms underpinning the disease - developing knowledge of these mechanisms may therefore give rise to new molecular markers for neuropathological diagnosis.

1.1.3. Symptoms and Diagnosis

PD is primarily considered to be a movement disorder, and can be recognised by the cardinal signs of bradykinesia, resting tremor, rigidity and postural instability. Motor symptoms are often unilateral at disease onset, with one side of the body more affected than the other (Djaldeiti et al., 2006). The correct diagnosis of PD is important for the sake of treatment, however, as mentioned previously, PD is often misdiagnosed. Differential diagnosis of PD from other forms of Parkinsonism can be challenging, due to the similarity of signs and symptoms, particularly in the early stages of disease. The most common misdiagnoses include progressive supranuclear palsy, multisystem atrophy, or corticobasal degeneration (Hughes et al., 2002), which are all alternative forms of degenerative parkinsonism.

Clinical diagnosis of PD, following the UK Parkinson's disease brain bank criteria, requires presence of bradykinesia, in addition to one other of the cardinal signs – usually tremor or rigidity, as postural instability is a symptom which generally occurs late in the progression of the disease. In 2015, the Movement Disorder Society revised the clinical diagnostic criteria for Parkinson's (Postuma et al., 2015), retaining the typical diagnosis of motor parkinsonism as a core diagnostic feature, but including several additional criteria. Absolute exclusion criteria are required to rule out other potential sources of parkinsonism, “red flags” (indicators of alternative pathology which must be counterbalanced with inclusion criteria that supports a PD diagnosis) must be considered, and additional supportive criteria indicative of PD are considered. The revised criteria aims to standardise PD diagnosis globally, and to provide explicit instructions to clinicians defining the cardinal symptoms. Diagnosis by these criteria results in either a certain diagnosis, or a “probable” diagnosis.

Whilst PD is primarily a movement disorder, patients can also develop a number of non-motor symptoms. Non-motor symptoms (NMS) are diverse, and can be just as debilitating

as the motor symptoms of PD. While they have garnered renewed attention over recent years, they were originally noted at the time of James Parkinson's observations (reviewed by Garcia-Ruiz et al., 2014). Mood disturbances are frequent symptoms, including depression, hallucinations, cognitive dysfunction and complex behavioural disorder. Sensory dysfunction can cause anosmia (inability to smell), pain, and affect circadian rhythm. Autonomic dysfunction is also common, with a majority of patients reporting constipation and other bowel/bladder related symptoms (Poewe, 2008). Appearance of NMS may occur several years prior to appearance of motor symptoms, and as such, may provide a useful pre-clinical screening approach for PD. However, given that many of the common NMS, such as constipation, are quite ordinary complaints, they are easily overlooked. The presence of bowel-related NMS prior to the onset of motor symptoms give credence to the Braak hypothesis, which proposes that an ingested pathogen triggers Lewy-pathology, which then follows an ascending course from the digestive tract to the brain (Braak et al., 2003b, 2003a).

1.1.4. Treatment

Clinical manifestation of PD only begins to occur once pathology has already reached an advanced stage. At disease onset, around 60% of cells in the SNpc have already degenerated (Dauer and Przedborski, 2003) - reversing progression of the disease is therefore unrealistic, and there is no cure. However, symptomatic treatment of PD is very effective, and is able to improve motor features in addition to some NMS. Treatment with L-3,4-Dihydroxyphenylalanine (L-Dopa/Levodopa), a precursor to dopamine, supplements not only dopamine production, but additionally adrenaline and noradrenaline production, which require dopamine as a precursor. Treatment with L-Dopa has been in use for over 50 years (Kofman, 1971), and is still the most effective form of treatment for PD. Unfortunately, long-term treatment with L-dopa is commonly associated with levodopa-induced dyskinesias, which typically develop 3-5 years after treatment commences, and can affect roughly half of patients treated with L-dopa (Pandey and Srivanitchapoom, 2017). L-dopa is now commonly prescribed alongside other drugs to modify dopamine levels, signalling and metabolism.

Dopa-decarboxylase inhibitors (DDI), such as carbidopa, are commonly prescribed alongside L-dopa in order to inhibit the conversion of L-dopa to dopamine in systemic circulation;

Carbidopa cannot cross the blood-brain barrier, therefore conversion of L-dopa is not inhibited in the brain. As a result, lower dosages of L-dopa can be used, reducing side-effects of vomiting and nausea, and reducing risk of developing levodopa-induced dyskinesia (Kaufman and Milstein, 2013; Montioli et al., 2016). Additionally, treatment with drugs to slow the process of dopamine metabolism, such as inhibitors of catechol-O-methyl transferase and monoamine oxidase, can prolong the half-life of L-dopa, thus preventing symptoms linked to the wearing-off effect of L-dopa in between doses (Muller, 2015).

Treatment with dopamine agonists, such as ropinirole or pramipexole, can be used to directly activate dopamine receptors, independently of degenerating pre-synaptic DA neurons. As such, treatment with dopamine agonists may be increased in later stages of PD, and L-Dopa dosages may be decreased (Lindsay et al., 2010).

1.1.5. Mortality

Parkinson's disease is not considered a fatal disease, and it is commonly stated that patients die "with" rather than "of" Parkinson's. Nonetheless, the disease does reduce life expectancy. A meta-analysis of 88 studies of mortality in PD (Macleod et al., 2014) revealed that the majority of studies show increased mortality in PD cases. Heterogeneity across studies was high, ranging from 0.9 - 3.8 mortality ratio in cases vs controls, and on average, the overall mortality ratio was 1.52. Patients had an annual 5% decrease in survival, and average time from disease onset until death ranged from 6.9 to 14.3 years across post-mortem studies. Due to the effect of the disease on mobility, patients suffer increased risk of falls, which can have knock-on effects on their physical health, such as being bedridden and developing pneumonia. In a 10-year population incident cohort study, tracking PD development from diagnosis, pneumonia was identified to be the most common cause of death, accounting for 33% of mortalities. Occurrence of aspiration pneumonia is likely due to impaired ability to swallow, which increases risk of aspirating food, drink, or saliva into the lungs (Williams-Gray et al., 2013). Other causes of death in PD are primarily age-linked, with cancer being the 2nd-most common, accounting for 19% of mortalities, and cardiac cases accounting for 16% of mortalities. The data demonstrate that while PD itself is not the cause of mortality in the majority of cases, it does contribute to increased risk of death, often via repercussions of increased falls.

1.2. Etiology of Parkinson's Disease

PD is a multifactorial disease, with a large number of genetic risk factors known to contribute to sporadic disease risk, in addition to a small number of genes in which mutations can cause rare familial (i.e. highly heritable) forms of PD. Additionally, several environmental risk factors such as smoking and pesticide exposure are known to alter disease susceptibility. PD risk is considered to be caused by genetic factors, environmental factors, and gene-environment interactions.

1.2.1. Environmental risk factors

Inverse associations of PD have been established with smoking (Chen et al., 2010; Ritz et al., 2014), physical activity (Chen et al., 2005a; Xu et al., 2010), coffee consumption (Ascherio et al., 2004; Liu et al., 2012), non-steroidal anti-inflammatory use (Chen et al., 2005b; Gao et al., 2011), and blood plasma urate levels (Chen et al., 2009; Gao et al., 2016). Positive associations of PD with head injuries (Fang et al., 2012; Gao et al., 2015) and pesticide exposure (Allen and Levy, 2013; Ascherio et al., 2006; Costello et al., 2009; Liew et al., 2014; Tanner et al., 2011) are additionally well established.

For several of these factors, mechanisms have not been robustly established, and the correlation between these environmental effects or lifestyle factors does not necessarily constitute a causative link. However, the link between pesticide exposure and PD is well characterised and has led to the development of toxin-induced animal models of PD which recapitulate DA cell death as observed in PD pathology, in addition to motor deficits and Lewy-pathology. 6-hydroxydopamine (6-OHDA), 1-methyl-4-phenyl-1,2,3,6-tetrahydropyridine (MPTP), paraquat, and rotenone have all been used to produce neurotoxin-induced models of PD and have contributed to understanding of processes contributing to PD, particularly mitochondrial dysfunction (Zeng et al., 2018).

1-methyl-4-phenyl-1,2,3,6-tetrahydropyridine (MPTP)

MPTP was initially discovered as a Parkinsonism-inducing neurotoxin due to development of parkinsonian symptoms in illicit drug abusers, who intravenously injected drugs

contaminated with MPTP (Langston et al., 1983). MPTP, as a lipophilic molecule, is able to cross the blood brain barrier. Once in the brain, MPTP is taken up by astrocytes, and converted to the intermediate 1-methyl-4-phenyl-2, 3, dihydropyridinium (MPDP⁺) by monoamine oxidase-B (MAO-B), and then rapidly oxidised to the neurotoxin 1-methyl-4-phenylpyridinium (MPP⁺) (Chiba et al., 1984). As a structural analogue of dopamine, MPP⁺ is selectively taken up into DA neurons through dopamine transporters. Application of a dopamine uptake inhibitor, Mazindol, is capable of blocking uptake of MPP⁺ (Schinelli et al., 1988). Once taken up into the neuron, it accumulates in the mitochondria and inhibits complex I of the mitochondrial electron transport chain. This inhibition causes a reduction in ATP synthesis, an increase in mitochondrial ROS (mROS) production, and increased peroxynitrite production, thus contributing to damage to proteins via oxidative and nitrative mechanisms, resulting in neurotoxic effects and cell death (Przedborski et al., 2000). MPTP-induced nigrostriatal degeneration has been observed in multiple models, including mice, dogs, primates, and zebrafish (Burns et al., 1983; Johannessen et al., 1989; Lam et al., 2005; Zeng et al., 2014).

1.2.2. Identifying Genetic Causes of Familial PD

Familial, monogenic forms of PD are caused by autosomal recessive or autosomal dominant mutations in a small number of genes, which carry high risk for PD. Only 6 causative genes exist, in which SNCA and LRRK2 act in an autosomal dominant manner, and Parkin, PINK1, DJ-1 and ATP13A2 are autosomal recessive. These monogenic familial cases are rare, and account for <10% of PD cases in total (Thomas and Beal, 2007).

Genes underlying heritable PD can be determined using genetic mapping and linkage analysis, by comparing affected and unaffected family members in a pedigree. Linkage analysis is dependent on the fact that a disease-causing gene will likely be in linkage disequilibrium with closely situated “markers” on the same chromosome, and will thus be inherited together; a lod (logarithm of odds) score summarises the probability that the disease-causing gene has been inherited with the marker. Performing linkage analysis with a larger number of markers, at closer intervals therefore increases the lod score, and increases confidence of the location of the disease-causing gene. Sequencing of genes

within the region can then be performed to confirm the location of the disease-causing mutation.

In 1996, a linkage analysis study in a large pedigree showing autosomal dominant inheritance identified the first genetic locus, 4q21-q23, to be positively linked to PD (Polymeropoulos et al., 1996). This locus was subsequently identified as alpha-synuclein (Polymeropoulos et al., 1997), which harboured a G209A base pair change in the affected subjects, resulting in a Ala53Thr substitution. This mutation showed 100% penetrance in the studied pedigree, and was replicated in several kindreds, thus providing the first conclusively genetic causative factor for PD. In the years following, several studies assessed PD patients for mutation in this region, and found no evidence of mutation of SNCA, thus confirming it as a rare mutation, and demonstrating the heterogenous nature of PD etiology (Farrer et al., 1998; Munoz et al., 1997; Scott et al., 1997, 1999). A recent multi-centre study in Sweden assessed the prevalence of known pathogenic mutations in SNCA (duplications/triplications, p.Ala30Pro, and p.Ala53Thr) in 2,206 PD patients, representing approximately 10% of PD cases in Sweden. 21.6% of cases reported first or second-degree family history of PD, and SNCA mutation (a duplication) was identified in only one patient, accounting for 0.045% of cases (Puschmann et al., 2019).

Since the discovery of SNCA as a causative PD gene, linkage analysis has also been utilised to identify PINK1, Parkin/PARK2, DJ-1, LRRK2, and ATP13A2 as familial PD genes (Klein and Westenberger, 2012). The use of linkage studies in identifying these Mendelian risk factors for PD has formed an important part in our understanding of PD etiology, however, its use is limited to identifying risk factors of large effect, and is an ineffective method to identify risk factors with low to modest effect.

1.2.3. Identifying Genetic Risk Factors for Sporadic PD

Sporadic PD accounts for over 90% of cases (Thomas and Beal, 2007), hence the importance in understanding the etiology underlying these cases. Over the past decade, genome-wide association studies (GWAS) have vastly increased our comprehension of the genetics of sporadic PD. GWAS enable the identification of genotype-phenotype correlations at a population level, by testing common genetic variants across the genome in a large sample

size. GWAS can assess from several hundred thousand variants to millions of variants, throughout the genome, either by utilising genotyping arrays, or from whole genome sequencing data. Single nucleotide polymorphisms (SNPs) are common genetic variants spread across the genome, and association with a phenotype of interest is assessed. Meta-analyses of multiple GWAS can be used to produce larger datasets and increase the statistical power of genetic associations. The SNPs that reach genome-wide significance for association with a phenotype are in linkage disequilibrium with the causative gene, therefore, further investigation, such as extensive sequencing of the region to identify potentially pathogenic mutations, in addition to functional genomics studies, must be used to validate the definite causal variant.

It is assumed that the majority of heritability of a complex disease can be explained by common variants of low effect, low-frequency variants of intermediate effect, and rare variants of large effect (**Figure 1**, Manolio et al., 2009; McCarthy et al., 2008). GWAS focuses on common variants of low effect, which are present in >5% of the population. As a result of this, there is a large component of heritability that goes undetected. This missing heritability is due to the contribution of variants of minor allele frequency (present in 0.5-5% of the population) and from rare variants (<0.5% of the population) which cannot be observed by GWAS. These variants are thus missed by GWAS due to their low frequency, in addition to being missed out by genetic linkage studies due to an insufficient effect size (Manolio et al., 2009; Pritchard, 2001). As genome sequencing has become more commonplace, in addition to projects such as the 1000 Genomes Project, variants at low allele frequencies are now more extensively catalogued and are incorporated into more SNP arrays and GWAS analyses. Additionally, the boom in genome sequencing over the last decade has enabled increased sample sizes in GWAS, thus resulting in greater power of statistical associations between variants and phenotype, and narrowing the gap in missing heritability.

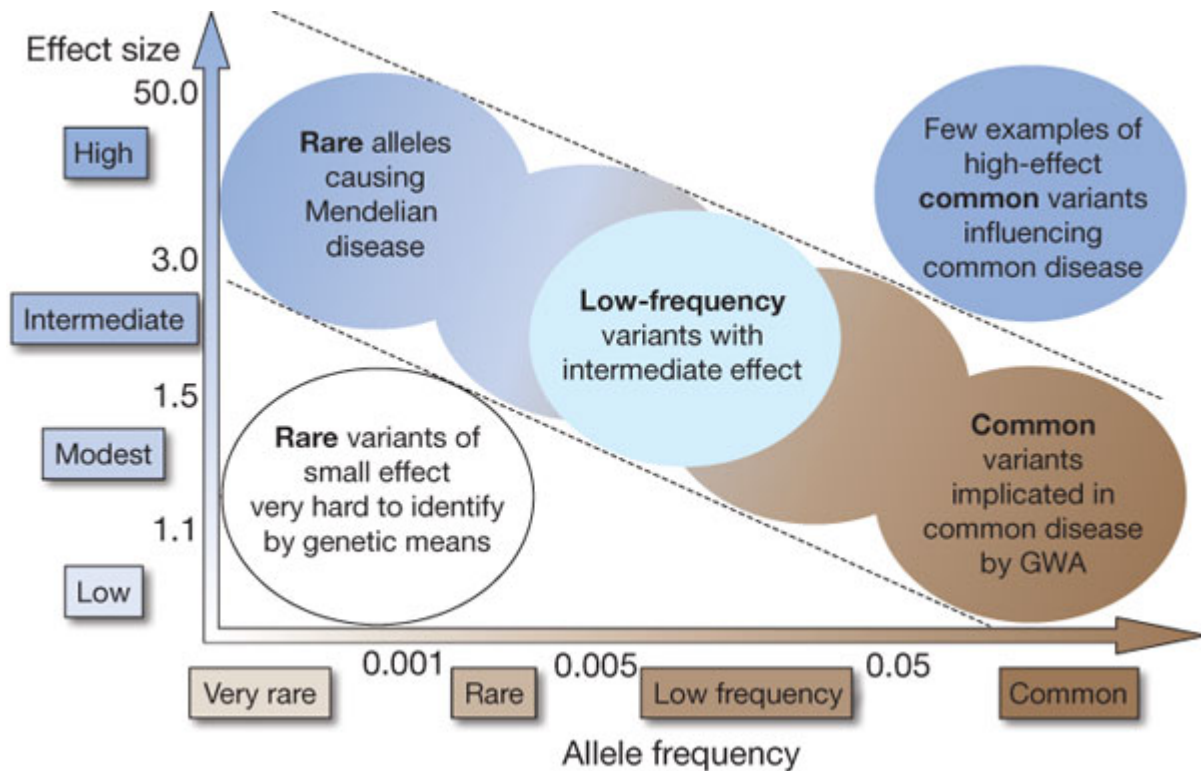


Figure 1: Feasibility of identifying genetic variants by risk allele frequency and strength of genetic effect. Reproduced with permission (Manolio et al., 2009).

GWAS has been instrumental in identifying genetic risk in sporadic PD, in which we now know there to be 90 loci of genome-wide significance (Figure 1, Nalls et al., 2019). This most recent PD GWAS meta-analysis compiled results from 17 datasets, and assessed 7.8 million SNPs across 37,688 cases, 18,618 “proxy-cases” (first degree relatives of PD cases), and 1.4 million controls. Heritability estimates from this meta-analysis propose that the variants identified at 90 loci account for somewhere between 16-36% of heritability in PD, indicating that there are a large number of risk-contributing variants still undiscovered. Genome-wide significant risk variants had a median minor-allele frequency (MAF) of 25.1% and a median effect size of 0.081; sub-significant risk variants had a median MAF of 21.3% and median effect estimate of 0.047. These sub-significant variants of lower MAF and smaller effect size are representative of potential future GWAS hits, and the authors calculated that to achieve genome wide significance at 80% power, an increase in sample size up to 99,000 cases would enable further identification of novel hits.

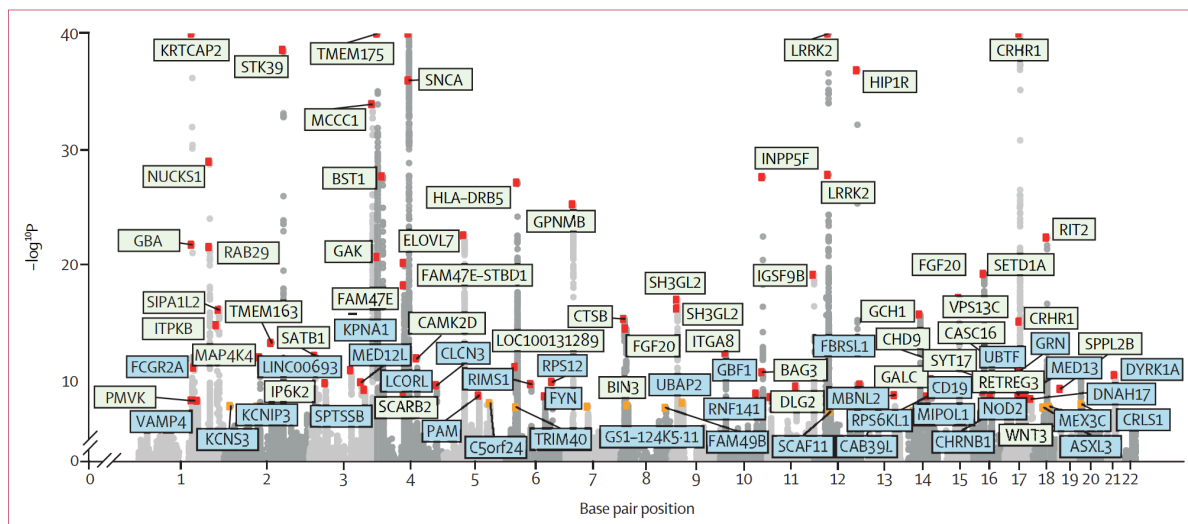


Figure 2: Manhattan plot for significant PD GWAS variants. The nearest gene to each of the 90 significant variants are labelled in green for previously identified loci and in blue for novel loci. $-\log_{10} p$ values were capped at 40. Variant points are colour-coded red and orange, with orange representing significant variants at $p=5 \times 10^{-8}$ and 5×10^{-9} and red representing significant variants at $p < 5 \times 10^{-9}$. The X axis represents the base pair position of variants from smallest to largest per chromosome (1–22), only autosomes were included in this analysis. Figure and legend reproduced with copyright permission (Nalls et al., 2019).

A commonly cited limitation of GWAS is the challenge of validating risk variants following identification of genome-wide significant loci. By utilising quantitative trait locus (QTL) mapping, the authors nominated 70 genes as the putative causal variants under the genome-wide significant loci, which are most likely contributing to PD risk.

Risk genes were assessed for enrichment in a total of 53 tissue types, and were found to be significantly enriched in 13 tissues – all of which were brain-derived. Use of single-cell RNA sequencing data from mouse brains enabled enrichment analysis within 88 different neuronal-derived cell types within the brain, which revealed significantly enriched expression in 7 cell types. The most significant of these was within the DA neurons of the substantia nigra. Additionally, enrichment was observed in the globus pallidus, thalamus, posterior cortex, frontal cortex, hippocampus, and entopeduncular nucleus. Furthermore, pathway analysis revealed enrichment of risk genes within chemical signalling pathways and pathways involving response to a stressor.

The finding of enrichment of risk genes within common tissue types has important implications for additive risk effects of multiple loci. It is commonly assumed that variants identified by GWAS, of common frequency and low effect, contribute to complex disease risk in an additive manner, and likely in combination with environmental risk factors. This is termed the “common disease, common variant” hypothesis (Hemminki et al., 2008). Expression of multiple PD risk genes within one tissue type gives credence to this hypothesis due to the higher likelihood of interacting or additive effects of these variants. Moreover, involvement of risk genes in pathways involved in response to a stressor reinforces the notion that risk genes likely interact with environmental factors to increase disease risk.

In addition to identifying risk loci, the study utilised Mendelian randomisation to assess the association of a small number of phenotypic factors with disease risk, which have the potential to be used as biomarkers for the disease. Positive correlations were observed between putamen volume and intracranial volume, and negative correlations were observed with academic qualifications and current tobacco use. When assessed for causal effect, cognitive performance and educational attainment had large positive causal effects on disease risk (cognitive performance: Mendelian randomisation effect 0.213, SE 0.041; Bonferroni-adjusted $p=8.00 \times 10^{-7}$; educational attainment: Mendelian randomisation effect 0.162, SE 0.040, Bonferroni-adjusted $p=2.06 \times 10^{-4}$), suggesting that individuals without higher education qualifications may be at lower risk of developing PD. Tobacco use was not found to have a causal effect on disease risk, however, presence of disease was found to have a small positive causal effect on smoking initiation (Mendelian randomisation effect 0.027, SE 0.006, Bonferroni-adjusted $p=1.62 \times 10^{-5}$).

1.3. *GCH1* as a PD risk gene

1.3.1. Identification of *GCH1* as a familial and sporadic PD risk factor

GCH1 was first identified as a PD risk factor in 2014, in two independent studies. The first of which was a study of 4 unrelated family pedigrees with dopa-responsive dystonia (DRD), in which rare heterozygous pathogenic variants of *GCH1* were also identified in family members with adult-onset PD (Mencacci et al., 2014).

DRD is a childhood-onset disorder presenting with generalised dystonia, in which patients show biochemical striatal dopamine depletion in the absence of nigral cell loss, and have a dramatic and long-lasting response to treatment with L-DOPA (Jeon, 1997). Pathologic findings of lack of nigral degeneration are strengthened by dopamine transporter (DAT) imaging and fluorodopa positron emission tomography (PET) analyses, which show normal uptake of dopamine in DRD cases (Jeon et al., 1998; Snow et al., 1993).

Autosomal dominant mutation of *GCH1* is the most common cause of DRD. In recombinant studies of the autosomal dominant G201E *GCH1* mutation, the mutant protein was found to have enzyme activity of just 5% compared to WT activity (Hwu et al., 2000). Mutant protein is synthesised as normal, but rapidly undergoes lysosomal degradation after synthesis. As a result of the homodecameric *GCH1* protein complex, mutant protein interacts with WT protein to exert a dominant negative effect, resulting in degradation of WT protein in addition to degradation of the mutant protein. A single copy of the mutant allele can therefore result in a reduction to less than 50% of normal *GCH1* activity. The reduction in *GCH1* activity has a direct effect on levels of pterins and catecholaminergic neurotransmitters, which are severely depleted in pathogenic mutation carriers. In the pedigrees studied by Mencacci et al. (2014), the familial pathogenic mutations which were causative for DRD in some family members also resulted in PD development in others (Figure 3).

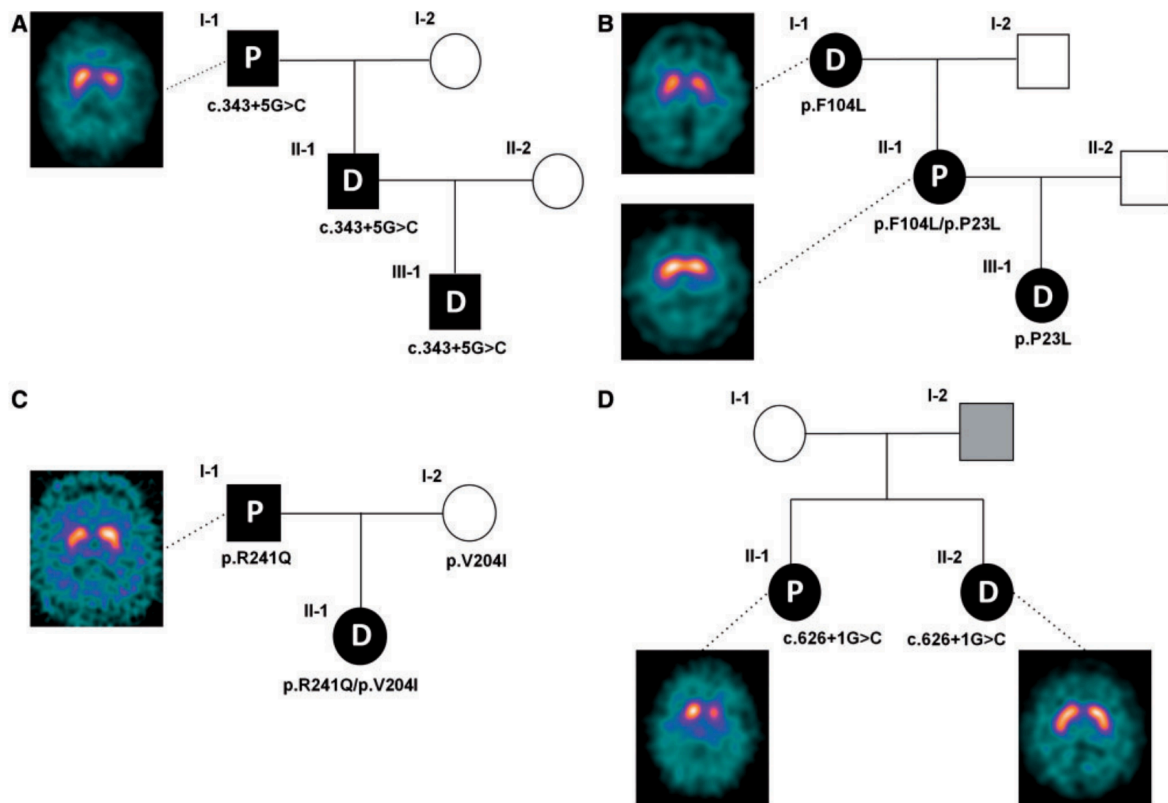


Figure 3: Pedigrees and ^{123}I -FP-CIT SPECT scan images of the four families with *GCH1* mutations

involved in the Mencacci et al. (2014) study. Subject I-2 of Family D was reported to be affected by a movement disorder (hand tremor) but was not available for clinical or genetic assessment. P = Parkinson's disease; D = DOPA-responsive dystonia. Figure and legend reproduced with permission (Mencacci et al., 2014).

PD subjects in the studied pedigrees displayed clinical features that met the criteria for PD diagnosis (as defined by the UK PD Society Brain Bank), whilst not displaying features associated with DRD. Consistent with a typical PD phenotype, family members with PD displayed abnormal dopamine transporter imaging (**Figure 3**), indicative of nigrostriatal denervation. To identify whether *GCH1* variants could contribute to PD in patients without family history of DRD, the authors examined whole-exome sequencing data from a cohort of primarily early-onset PD and familial PD patients and controls, with additional controls from the Exome Variant Server (total 1318 PD cases, 5935 controls). 11 different *GCH1* heterozygous variants were identified (Table 1), and the frequency of variants was significantly higher in cases (10/1318 = 0.75%) vs. controls (6/5935 = 0.1%, odds ratio [OR] of 7.5, Fisher's exact test P-value 0.0001).

Table 1: List of GCH1 variants identified by exome sequencing in patients with Parkinson disease and controls. Reproduced from Mencacci et al. (2014)

Mutation	Exon	dbSNP	Prediction score ^b	Previously described in DRD?	PD patients (n = 1318)	UCL-ex controls (n = 1635)	OR (95% CI)	P-value	EVS controls (n = 4300)	OR (95% CI)	P-value	Total controls (n = 5935)	OR (95% CI)	P-value
All variants					10 (0.75%)	1 (0.06%)	12.4 (1.7–541.1)	0.003	5 (0.11%)	6.5 (2.0–24.5)	0.0004	6 (0.1%)	7.5 (2.4–25.3)	0.0001
c.328C > T; p.Q110X	1		NA	Yes, in dominant and recessive pedigrees	1	0			0			0		
c.328C > G; p.Q110E	1		2	No	1	0			0			0		
c.334A > G; p.T112A	2	rs199990434	2	No	0	0			1			1		
c.358G > T; p.A120S	2		4	No	1	0			0			0		
c.401A > G; p.D134G	2		4	No	1	0			0			0		
c.460A > G; p.I154V	3		2	No	0	1			0			1		
c.593G > A; p.R198Q	5	rs201238926	0	No	0	0			1			1		
c.610G > A; p.V204I	5	rs200891969	4	Yes, in sporadic and recessive cases	3	0			1			1		
c.650G > T; p.G217V	6		4	No	1	0			0			0		
c.671A > G; p.K224R	6	rs41298442	2	Yes, in dominant and recessive pedigrees	1	0			2			2		
c.690G > A; p.M230I	6		4	Yes, in a sporadic case	1	0			0			0		

NA = not applicable; DRD = DOPA-responsive dystonia; PD = Parkinson disease; UCL-ex = University College of London exomes consortium; EVS = Exome Variant Server. P-values were calculated by means of Fisher's exact test.

^a NCBI transcript NM_000161.2. This count includes all detected coding and splice-site variants at any frequency, but the two benign variants P23L and P69L.

^b This score, ranging from 0 to 4, indicates the number of tools (Polyphen-2, SIFT, LRT and MutationTaster) predicting a pathogenic effect on the protein function.

Mencacci et al.'s finding of increased frequency of *GCH1* variants in PD cases appears to be in contradiction to other studies which have failed to identify an association. For example, Rengmark et al. performed sequencing of the *GCH1* gene in 509 PD patients and 230 controls from Norway and Sweden, and found no pathogenic *GCH1* mutations in either group (Rengmark et al., 2016). However, the PD cohort was primarily late-onset PD, in contrast to the EOPD and familial PD cohort studied in Mencacci et al. (2014), therefore the result only suggests that *GCH1* pathogenic mutations are rare in late-onset PD cases. This is consistent with a recent case-control exome-sequencing study which demonstrates that deleterious *GCH1* mutations in coding regions are associated with early onset of symptoms (Pan et al., 2020).

Mencacci and co-authors' finding of *GCH1* as a risk factor for PD was independently corroborated by a PD GWAS meta-analysis published shortly after, identifying the intronic *GCH1* rs11158026 SNP as one of 26 loci with genome-wide significant association for sporadic PD (Nalls et al. 2014). 7,893,274 variants were assessed for association with PD cases, over a number of cohorts. The effect allele (T allele, MAF=0.335) was identified as genome-wide significant at the discovery phase (13,708 cases and 95,282 controls) with an OR of 0.889 ($P = 7.13 \times 10^{-11}$). This was validated in the replication phase (5,353 cases and 5,551 controls, OR = 0.948, $p = 0.039$), and in the combined cohort (OR = 0.904, $p = 5.85 \times 10^{-11}$). The OR of <1 represents a reduced prevalence of the minor allele in PD cases vs. controls, indicating a protective effect against PD in rs11158026 SNP carriers. This finding has since been replicated in the more recent GWAS meta-analysis (Nalls et al., 2019), which analysed 37,688 cases, 18,618 proxy-cases, and 1.4 million controls. From this meta-analysis, the rs11158026 SNP was validated as genome-wide significant, with a regression coefficient (β) of -0.0842 [equivalent to an OR of 0.9138] (MAF = 0.3245, $p = 1.66 \times 10^{-16}$), indicating a protective effect of the minor allele, lowering risk of developing PD by 9.1%.

In summary, rare autosomal dominant *GCH1* pathogenic mutations have been identified to be significantly more common in EOPD and familial patients, with an odds ratio of 7.5 (indicating a 7.5-fold increase in risk of developing PD; Mencacci et al., 2014); whereas

meta-analysis of PD GWAS identifies the *GCH1* rs11158026 variant to be associated with mildly attenuated risk of PD (Nalls et al., 2019).

1.3.2. Physiological roles of *GCH1* and *BH4* – neurotransmitter synthesis

GCH1 is a homodecameric protein complex, which catalyses the rate limiting step in the *de novo* synthesis of tetrahydrobiopterin (*BH4*) from GTP (Figure 4). *BH4* is an essential cofactor for the aromatic amino acid hydroxylases (AAAHs) tyrosine hydroxylase (TH) and tryptophan hydroxylase (TPH), which synthesise L-DOPA and 5-hydroxytryptophan respectively (5-HT). L-DOPA and 5-HT undergo decarboxylation by DOPA decarboxylase (DDC) to produce the catecholaminergic neurotransmitters dopamine and serotonin, respectively. In addition to its role as a neurotransmitter, dopamine is also required for the biosynthesis of noradrenaline and adrenaline.

The AAAHs require one mole of *BH4* to support a single catalytic turnover of L-DOPA or 5-HT (Crabtree and Channon, 2011). During the catalytic process, *BH4* is oxidised, via a 2-step mechanism: first pterin-4a-carbinolamine dehydratase (PCD) catalyses the oxidation of *BH4* to the intermediate *BH4*-4a-carbinolamine (Haavik and Flatmark, 1987), which is then converted to quinonoid-*BH2* (q-*BH2*, Rebrin et al., 1995). q-*BH2* can be reduced to *BH4* by the NADPH-dependent dihydropteridine reductase (DHPR, Kaufman, 1991), otherwise it undergoes rapid rearrangement into the stable isomer 7,8-dihydrobiopterin (*BH2*). *BH2* is then reduced to *BH4* by dihydrofolate reductase (DHFR).

BH4 availability is therefore a delicate balance between *de novo* synthesis, oxidation of *BH4* to *BH2*, and the recycling of *BH2* to *BH4*. Imbalances in any of these processes can therefore lead to *BH4* deficiencies. Mutations in the DHPR and PCD genes, which catalyse the recycling of *BH4*, are associated with *BH4* deficiency and hyperphenylalaninemia (Crabtree and Channon, 2011).

DHPR is ubiquitously expressed at much higher concentrations than that of the AAAHs (Kaufman, 1991)(Crabtree and Channon, 2011); the high expression of this enzyme enables efficient *BH4* recycling, therefore, recycling of *BH4* in *GCH1*-deficient cases is not a limiting factor, but the availability of *BH4* itself is reduced. Exogenous supplementation of

sepiapterin is a commonly used pharmacological approach to supplement BH4 levels in experimental models; sepiapterin reductase reduces sepiapterin to BH2, which is reduced to BH4 by DHFR. This route is termed the “salvage pathway”.

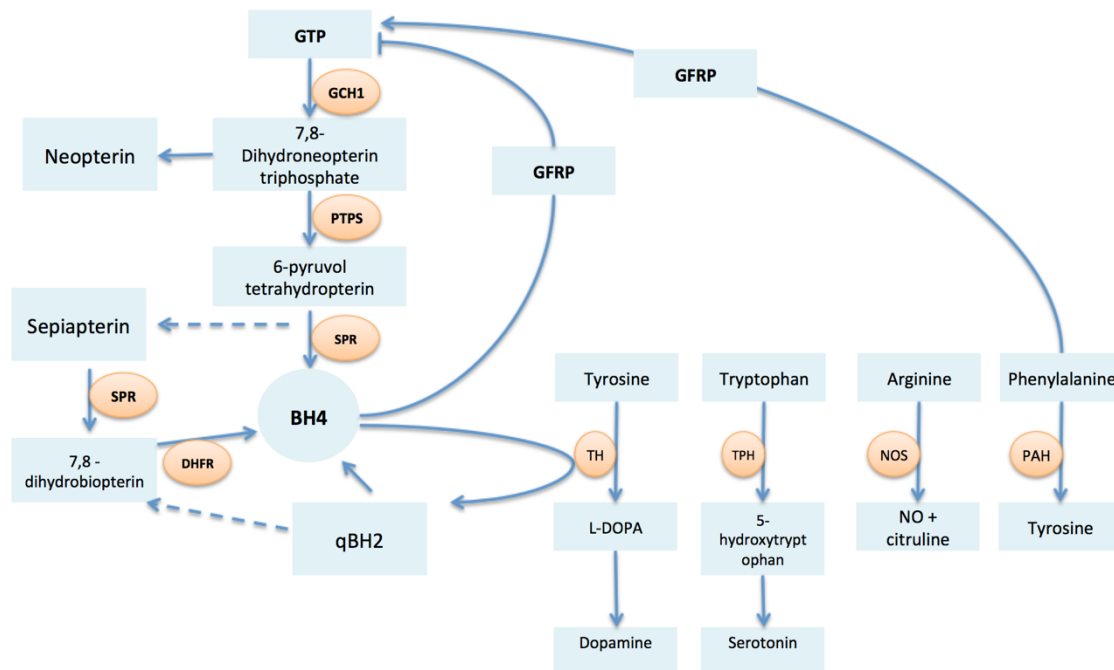


Figure 4: The Tetrahydrobiopterin (BH4) synthesis pathway. GTP-cyclohydrolase I (GCH1) catalyses the first rate-limiting step in the de novo synthesis of BH4, followed by reactions catalysed by 6-pyruvyltetrahydropterin synthase (PTPS) and sepiapterin reductase (SPR). Alternatively, the salvage pathway recycles sepiapterin - a product of the reduction of 6-pyruvyl tetrahydropterin under certain physiological conditions – into 7,8-dihydrobiopterin and BH4 in 2 reduction reactions catalysed by SPR and dihydrofolate reductase (DHFR), respectively. BH4 acts as a cofactor for tyrosine hydroxylase (TH) in L-DOPA synthesis, tryptophan hydroxylase (TPH) in 5-hydroxytryptophan synthesis, nitric oxide synthase (NOS) in the production of nitric oxide (NO), and phenylalanine hydroxylase (PAH) in tyrosine synthesis (Nagatsu and Ichinose, 1999). BH4 and phenylalanine feedback to inhibit and stimulate GCH1 activity, respectively, by associating with GCH1 feedback regulatory protein (GFRP)(Hussein et al., 2015). Figure produced by myself.

1.3.3. Physiological roles of BH4 – Nitric Oxide Synthase activity

In addition to its role in neurotransmitter synthesis, BH4 is required as a cofactor for the family of nitric oxides synthases, for the synthesis of nitric oxide (NO) from L-arginine. NO is a messenger molecule with different targets, with roles in neurotransmission (Kuriyama and Ohkuma, 1995), maintenance of vascular tone (Jin and Loscalzo, 2010), transcriptional regulation (Contestabile, 2008), regulation of mRNA processing (Wang et al., 2006), and

post-translational modifications (Brune et al., 1994). The NOS family consists of 3 isoforms: endothelial NOS (eNOS), inducible NOS (iNOS) and neuronal NOS (nNOS). eNOS is expressed constitutively in endothelial tissue, and nNOS is expressed constitutively in central and peripheral neuronal tissue. iNOS is typically expressed at low levels under normal conditions, and expression is upregulated under inflammatory conditions.

Under conditions of saturated BH4 availability (Figure 5), NOS isoforms catalyse the production of NO, utilising L-arginine, molecular oxygen (O₂) and nicotinamide-adenine-dinucleotide phosphate (NADPH) as substrates. Electron transfer occurs from NADPH via the reductase domain of NOS, to the oxygenase domain. BH4, O₂ and L-arginine are bound to the oxygenase domain, and the electrons are transferred to O₂ and L-arginine, reducing O₂ to NO, and oxidising L-arginine to L-citrulline (reviewed by Förstermann and Sessa, 2012).

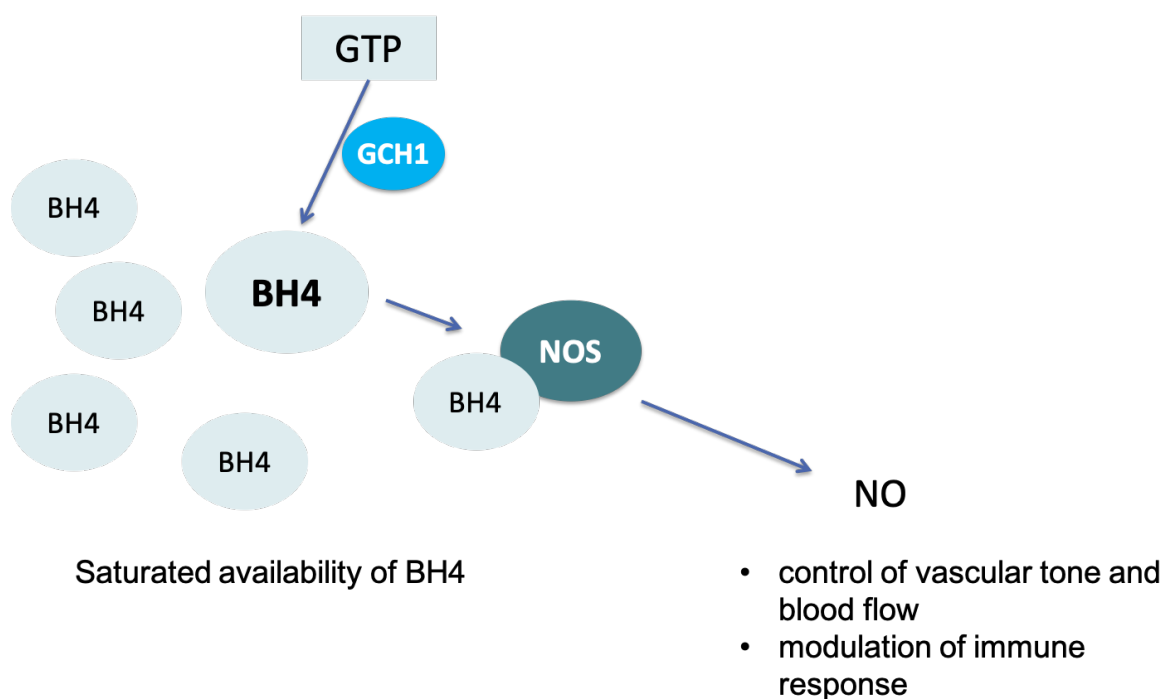


Figure 5: Schematic illustrating production of nitric oxide under conditions of saturated BH4

However, in conditions of subsaturated BH4 availability (Figure 6), NOS can become uncoupled, leading to production of superoxide (O₂⁻) instead of NO (Vásquez-Vivar et al., 1998). This can happen in cases of GCH1 deficiency, resulting in reduced production of BH4, or in highly oxidising conditions (such as in the mitochondria, or in states of oxidative

stress), which results in oxidation of BH4 to BH2. BH2 has the same affinity for NOS as BH4, however, is catalytically inactive; BH4 to BH2 ratio is thus negatively correlated to superoxide production (Crabtree et al., 2008). The reaction of superoxide with NO results in formation of peroxynitrite (ONOO⁻), which, as mentioned earlier, is a strong oxidising and nitrating agent and can cause damage to proteins, lipids and organelles, leading to neurotoxic effects (Beckman and Koppenol, 1996; Crow and Ischiropoulos, 1996; Ischiropoulos and al-Mehdi, 1995). Peroxynitrite-induced neurotoxicity provides a potential mechanism by which GCH1 deficiency may be implicated in DA neuronal degeneration.

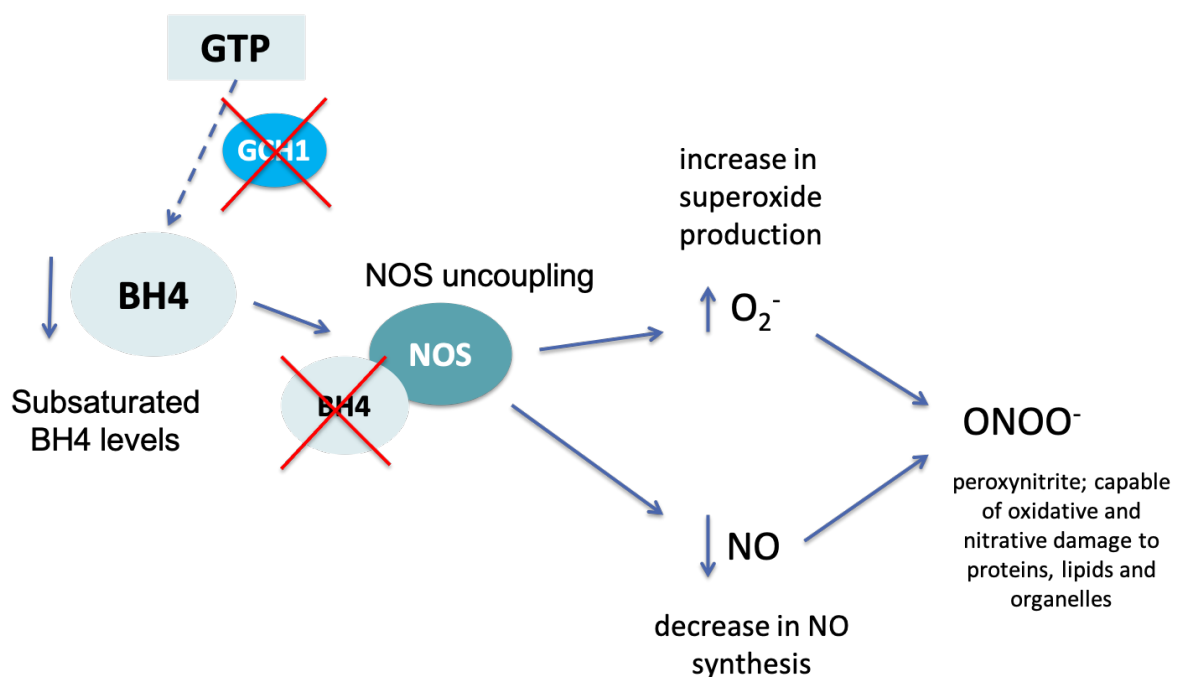


Figure 6: Schematic demonstrating how subsaturated BH4 levels leads to production of peroxynitrite.

1.3.4. Factors influencing GCH1 expression

GCH1 expression, and consequently BH4 synthesis, is increased by a wide range of factors, including arginine, insulin, estrogen, statins, cyclosporine A, hydrogen peroxide, and several proinflammatory cytokines (Interleukin-1 β , Interferon- γ , TNF- α and LPS); alternatively, GCH1 expression can be reduced in response to anti-inflammatory cytokines (Interleukin-4, Interleukin-10 and TGF- β) and glucocorticoid hormones (Shi et al., 2004).

The GCH1 feedback regulatory protein (GFRP) has historically been associated with GCH1 regulation. BH4 negatively regulates GCH1 by binding GFRP, which forms an inhibitory complex to regulate GCH1. Phenylalanine, conversely, binds GFRP to positively modulate GCH1 activity, reversing BH4-induced inhibition (Yoneyama and Hatakeyama, 1998). This mechanism has been validated in hepatocytes (Geller et al., 2000; Pastor et al., 1996), however, more recent in vivo research across multiple rat organs has demonstrated a lack of GFRP expression across brain, heart and kidney samples, with expression only detected in liver tissue (Du et al., 2012). Eukaryotic translation initiation factor 3 subunit I (EIF3I), another GCH1 protein partner, however, was detected by pull-down purification across all tissue samples, leading Du et al. to propose EIF3I as a general regulator of GCH1 activity. Alternatively, regulation of GCH1 may be tissue specific, and regulated by different mechanisms dependent on isoform or tissue-specific function of GCH1. Regulation of *GCH1* expression remains a contentious topic, and there are likely more unidentified mechanisms by which GCH1 levels are controlled.

1.3.5. Multiple forms of parkinsonism in *GCH1* mutation carriers

Furukawa and Kish, in response to the Mencacci publication, proposed there to be 2 kinds of parkinsonism in *GCH1* mutation carriers: “benign” parkinsonism, or “neurodegenerative” parkinsonism (2014). Benign parkinsonism appears to be an additional phenotype of autosomal dominant DRD, which presents as a metabolic GCH1-related dopamine deficiency during adulthood. Patients respond well to treatment with levodopa over long periods, and appear resistant to side effects of treatment such as dyskinesia and motor response fluctuations. This form is presumed to be caused by an age-related decline in tetrahydrobiopterin availability, resulting in deficiency of dopamine in the absence of DA degeneration.

On the other hand, neurodegenerative parkinsonism, such as the PD cases described by Mencacci et al. (2014), features progressive nigrostriatal degeneration. In these cases, abnormal DA transporter imaging is observed, and patients require increasing dosage of treatment with levodopa. Motor complications of treatment are common in these cases, most notably levodopa-induced dyskinesia.

The mechanism for “benign” and “neurodegenerative” parkinsonism in *GCH1* mutation carriers remains unclear. Furukawa and Kish propose that genetic and/or environmental factors act to modulate the effects of *GCH1* mutation, resulting in the heterogeneity of parkinsonism and DRD symptoms in *GCH1*-mutation carrying pedigrees.

1.3.6. Proposed mechanisms contributing to dopaminergic degeneration

Several mechanisms are proposed by Mencacci and co-authors by which loss of function variants in *GCH1* may contribute to PD and nigral degeneration. The first hypothesis is that dopamine deficiency may contribute to DA neuronal loss via a mechanism by which innervation of the dopamine D2 autoreceptor acts as an anti-apoptotic signal, and lack of signal may thus reduce the survival of neurons (Nair et al., 2003; Vaarmann et al., 2013).

Another hypothesis put forward by Mencacci et al. is that mutation carriers who do not develop childhood-onset DRD may possess other mechanisms that assist DA metabolism and/or transmission, but these mechanisms may contribute to neuronal vulnerability in combination with aging. One such mechanism which could fit with this hypothesis would be modulation of *GCH1* activity by other genetic or environmental factors.

In response to the Mencacci et al. (2014) study, Ryan et al. proposed that additional cellular roles of BH4 should also be considered to evaluate the risk mechanism. These additional roles include the requirement of BH4 for production of NO, and the role of BH4 as an antioxidant (Ryan et al., 2014a). Uncoupling of NOS in conditions of subsaturating levels of BH4 results in superoxide production instead of NO production (Crabtree et al., 2009; Vasquez-Vivar et al., 2003); furthermore, superoxide can react with nitric oxide to produce peroxynitrite, a reactive species capable of causing nitrative stress. BH4, which acts as an antioxidant, has been identified as a target for oxidation by peroxynitrite, producing 5,6-dihydrobiopterin and 7,8-dihydrobiopterin, resulting in a self-perpetuating downward spiral of BH4 availability (Milstien and Katusic, 1999). Additionally, peroxynitrite has been identified to cause damage to multiple cellular targets implicated in PD pathogenesis, including alpha-synuclein, tyrosine hydroxylase, and complexes of the mitochondrial electron transport chain. Accumulation of alpha-synuclein with nitrated tyrosine residues has been identified in Lewy-body inclusions in PD, implicating nitrative and oxidative stress

by peroxynitrite in the progression of PD pathology (Giasson et al., 2000). Tyrosine hydroxylase has also been identified as a selective target for nitration by peroxynitrite, resulting in loss of enzymatic activity, which would further exacerbate DA deficits (Ara et al., 1998). Complex I, II, and V of the mitochondrial electron transport chain have been shown to be inhibited as a result of peroxynitrite-induced nitration of tyrosine residues and oxidation of tryptophan residues (Murray et al., 2003), which would cause impaired ATP production and exacerbated free radical production.

Finally, three different SNPs at the *GCH1* locus have previously been described, which result in reduced plasma and vascular BH4 levels, reduced GCH1 mRNA expression, and increased vascular superoxide production via eNOS uncoupling (Antoniades et al., 2008). Furthermore, they have since identified increased GCH1 expression and BH4 induction as an endothelial defence mechanism against inflammation, which is impaired when GCH1 is inhibited (Antoniades et al., 2011). These findings indicate a mechanism between *GCH1* polymorphisms and oxidative stress and neuroinflammation, which could contribute to PD risk.

1.4. Models of GCH1 deficiency

1.4.1. *Gch1* knockout mouse model is embryonic lethal

A mouse *Gch1* knockout (KO) model has demonstrated that GCH1 is essential in embryonic development, with whole-body genetic ablation of *Gch1* resulting in embryonic lethality at E13.5 (Douglas et al., 2015). Heterozygotes, however, are unaffected. BH4 levels in the *Gch1* KO were observed to be normal as a result of maternal contribution until E11.5, and at this time point there was no difference in size of *Gch1*-KO and WT littermates. However, after this time point, BH4 levels were reduced, with maternal transfer of BH4 no longer sufficient to maintain normal levels. *Gch1*-KO embryos displayed no gross morphological abnormalities, but showed reduced heart rate, which was proposed to be the cause of lethality. Supplementation of BH4 (by treatment with sepiapterin) and L-DOPA via maternal feeding was able to prolong embryonic survival, but not completely rescue survival, to E15.5, indicating there are additional roles for GCH1 independent of BH4 synthesis, which are required for survival.

1.4.2. *hph-1* mouse model shows DRD-like biochemical deficits

Deficiency of GCH1 has been studied in the *hph-1* mouse, which, unlike the *Gch1* mouse described above, is not homozygous lethal. The *hph-1* mouse was generated from a *N-ethyl-N'-nitrosurea* screen for hyperphenylalaninemia, with the aim of generating a model for phenylketonuria (Bode et al., 1988). The genomic location of the mutation is predicted to be in *Gch1*, however, there are no coding sequence changes in the *Gch1* open reading frame in *hph-1* mutants (Mouse Genome Informatics: 1856903). The *hph-1* mouse shows only transient hyperphenylalaninemia after birth, but phenylalanine levels normalise as BH4 levels accumulate in the liver; however, the *hph-1* mouse does show biochemical deficits in the brain similar to those seen in patients with GCH1-deficient DRD. GCH1 activity in the mutant is approximately 20% of WT controls (Gutlich et al., 1994). Biochemical analysis by Hyland et al. (2003) reveals a 60% reduction of BH4, compared to WT controls. Dopamine shows a 14% reduction, and its metabolite HVA is reduced by 26%. Serotonin is decreased by 22%, and its metabolite 5-HIAA is decreased by 44%. Additionally, analysis of TH activity in vitro revealed a 30% reduction in activity in conditions of BH4 saturation, and further analysis revealed a reduction in total TH protein in the striatum. The finding of reductions in TH protein is consistent with data from postmortem brains in a small number of DRD cases (Furukawa et al., 1999; Rajput et al., 1994), which showed TH protein levels as low as 1.5% of controls. Despite biochemical deficits, the *hph-1* mouse shows no dystonia-like symptoms or signs of motor impairment (Nasser et al., 2013).

1.4.3. TH depletion in dopamine-depleted PC12D cells

Kawahata et al. (2015) investigated the mechanism for degradation of TH under conditions of GCH1 inhibition in PC12D cells, and identified that phosphorylation of serine-40 and subsequent ubiquitination target the protein for proteasomal degradation. This mechanism was found to be dopamine dependent, as inhibition of the dopamine-producing enzyme, aromatic l-amino acid decarboxylase (AADC), or inhibition of GCH1 both resulted in reduced dopamine content, and an increase in phosphorylated TH at serine-40. The authors identified that the dopamine deficient state is recognised by the dopamine D2-autoreceptor, which regulates cAMP-dependent protein kinase (PKA). PKA mediates the

phosphorylation of TH serine-40, which resulted in ubiquitination and proteasomal degradation. This mechanism highlights how persistent dopamine depletion in cases of DRD and PD can lead to TH depletion, further impairing dopamine production.

1.4.4. Gch1-deficient murine macrophages exhibit elevated superoxide production

McNeill et al. (2015) produced a novel mouse mutant, lacking *Gch1* expression in leukocytes. *Gch1*-KO macrophages were thus incapable of synthesising BH4, the essential cofactor for NO production from iNOS. Incubation of isolated *Gch1*-KO macrophages with the superoxide indicator dihydroethidium revealed a substantial increase in superoxide production in the presence of iNOS expression, which was induced by treatment with LPS+IFN- γ . Induction of iNOS expression was additionally found to elevate macrophage ROS production, however, even when NOS was inhibited with L-NAME, ROS production remained highly elevated in GCH1-deficient cells. The results indicate that BH4 is important in regulating superoxide production through iNOS, and additionally through (unidentified) iNOS-independent, ROS-producing mechanisms. Gene expression analysis of LPS+IFN- γ induced *Gch1*-KO macrophages revealed a decrease in NRF2 pathway activation, a known cytoprotective response pathway to oxidative stress; this implicates BH4-dependent NO production and iNOS regulation in the macrophage inflammatory response.

In succession to this article, the authors performed siRNA-mediated *Gch1*-knockdown (KD) in murine endothelial cells, to identify the major source of ROS, and to investigate the effects of BH4 depletion on mitochondrial redox (Bailey et al., 2017). *Gch1*-KD resulted in a 90% reduction in BH4 levels, and elevated ROS production, as observed previously (McNeill et al., 2015). To identify the superoxide producing-mechanisms, the authors systematically inhibited cellular contributors of superoxide generation, and identified that inhibition of mitochondrial CI completely normalised ROS to WT levels. This effect was additionally observed in NOS-devoid BH4-depleted fibroblasts, indicating that the mitochondrial ROS production was NOS-independent. Elevated ROS production was found to further oxidise mitochondrial BH4, leading to an elevated ratio of BH2:BH4, thus exacerbating the oxidising conditions within the mitochondria and diminishing BH4 further. Mitochondrial basal respiratory function was found to be mildly impaired, and cell metabolism was also affected, with accumulation of the tricarboxylic acid (TCA) cycle intermediates succinate and

fumarate observed in the *Gch1*-depleted cells. Given the well-known contribution of mitochondrial dysfunction in PD, this finding provides another potential pathomechanism by which GCH1-depletion may contribute to PD.

1.4.5. Literature review summary

From the existing data on *GCH1* models, there is no evidence to suggest if or how GCH1 deficiency may lead to nigrostriatal degeneration. It also remains unclear why some *GCH1* familial mutation carriers may develop DRD, while some develop PD. From the mouse *Gch1*-KO model, it appears there are additional essential roles of GCH1 in addition to its requirement for BH4 synthesis, which remain to be identified. There is, however, strong evidence of oxidative stress and mitochondrial dysfunction, which are already known mechanisms contributing to PD.

1.5. Zebrafish as a model for studying GCH1 deficiency

Model organisms exist on a spectrum of complexity and of similarity to humans. Typically, the model organisms which possess closest homology to humans, such as mice or primates, are also the most challenging to work with, in terms of life-span, ethics, and ease of generating mutants; the simplest organisms such as *C elegans*, or *Drosophila*, are often unable to recapitulate various aspects of human disease, have lower homology, but are easy to work with. Zebrafish occupy a useful middle ground in the spectrum of model complexity.

Importantly, as a vertebrate model, zebrafish share a high percentage of gene homology with humans, with an estimated 82% of human disease genes sharing an ortholog in zebrafish (Howe et al., 2013). In addition, the organisation of the zebrafish genome remains fairly well conserved, with large blocks of conserved synteny despite rearrangements between chromosomal regions, and a similar number of chromosomes (Ehrlich et al., 1997; Postlethwait et al., 2000). However, whole genome duplication, which occurred early in teleost radiation, poses difficulty in the study of gene function due to compensation by additional orthologs. It has been estimated that roughly 20% of zebrafish genes are still present in duplicate (Postlethwait et al., 2000); annotation of the zebrafish genome has

revealed the presence of upwards of 26,000 genes, which constitutes the biggest annotated gene set of any vertebrate (Collins et al., 2012).

As a model to characterise sporadic PD genes, high genetic homology is important, given the number of novel risk genes that require characterisation to validate their designation as a risk factor and the mechanism by which they contribute to risk. Of the 90 genes most closely situated to the novel risk loci identified by Nalls et al. (2019), 62 genes have an ortholog in zebrafish, and 20 of these genes have one or more ortholog (*Supplementary table 1*, appendix). However, *SNCA*, encoding alpha-synuclein, crucially does not have an ortholog in zebrafish, therefore modelling PD in zebrafish will not recapitulate Lewy-pathology, which is a hallmark of the disease.

The ease of generating zebrafish mutant lines, as a result of the efficiency of using CRISPR/Cas9, in addition to the short generation time (roughly 3 months) of zebrafish, means that we can produce many different zebrafish mutants for different sporadic PD risk genes. Furthermore, generating double-mutant crosses enables the investigation of gene-gene interactions, either for the identification of novel interactors or to confirm putative gene-gene interactions identified from genetic studies.

Characteristics of zebrafish that are useful across all research practices, and particularly developmental biology, are their rapid, external development and their optical transparency. Within 36 hpf the zebrafish body plan is already established and most major organs are formed, and by 72 hpf embryonic development is complete (Kimmel et al., 1995). The optical transparency of the larvae enables visualisation of development and imaging of internal structures in a non-invasive approach. Furthermore, the availability of transgenic lines, such as reporter lines tagged with fluorescent transgenes, enables visualisation of specific cell populations in the live embryo or larvae.

The high fecundity of zebrafish enables production of large numbers of embryos, which, paired with their ease of maintenance, can facilitate a fairly high-throughput approach. This is useful for practices such as drug screening, in which large numbers of drugs may be tested at once during initial phases of drug discovery, or large numbers of larvae may be treated

with a single drug to enable a large sample size. Another benefit of the zebrafish which is useful in drug screening is the ability to deliver drug by immersion in a small amount of solution. An embryo can be maintained in as little as 200 µl media, thus reducing drug costs and enabling drugging of a large sample. Furthermore, *In vivo* analysis of the effects of drugs can be also be undertaken at an early stage of drug screening processes, such as behavioural analysis or imaging of transgenic markers.

1.5.1. The Dopaminergic system in zebrafish

Imperative for the purposes of studying PD risk genes, the zebrafish DA system is well characterised. Neurons of the posterior tuberculum and the ventral diencephalon correspond to the mammalian A11 DA system, which is implicated in locomotion and sensory processes. The mammalian A11 population of DA neurons is located in the periventricular gray matter of thalamus, hypothalamus and rostral midbrain (Smeets and Gonzalez, 2000); in zebrafish, the A11 homologous population is located in the ventral diencephalon (the DA groups labelled DC2, and DC4-6), the preoptic region, the pretectum, the ventral thalamus, and the hypothalamus (Rink and Wullimann, 2001), but not in the mesencephalon. Both the mammalian A11 group, and the zebrafish homologous population (DC2, DC4-6) are specified by the transcription factor *Orthopedia* (*Otp*) (Blechman et al., 2007). Retrograde neuronal tracing experiments, in tandem with tyrosine hydroxylase immunohistochemistry, have established that 2 populations in the zebrafish posterior tuberculum ascend to the basal telencephalon, which includes the subpallium (analogous to the human striatum). These 2 populations are described as the “small round neurons in the periventricular nucleus of the posterior tuberculum and large pear-shaped cells adjacent to it”, and are understood to be the teleostean equivalent of the SNpc (Rink and Wullimann, 2001).

The DC2 and DC4/5 population are relatively easy to distinguish and count in wholemount zebrafish larvae due to their large soma – hence being labelled “large pear-shaped cells” by Rink and Wulliman. In mice and rats, the DA neurons can only be observed by performing serial sectioning and immunostaining (Blechman et al., 2007), therefore, the ability to quantify these neurons in wholemount is a considerable advantage. These cells may be labelled by immunostaining or *in situ* hybridisation for tyrosine hydroxylase, or with the

transgenic zebrafish line *ETvmat2-GFP*. Vesicular monoamine transporter 2 (*vmat2*) is a membrane-bound protein, responsible for the uptake of monoaminergic neurotransmitters from the cytosol into vesicles at the pre-synaptic terminal. *ETvmat2-GFP* labels all monoaminergic neuron populations and has been confirmed to label the DC2 and DC4/5 populations by co-immunostaining with anti-tyrosine hydroxylase (Jay et al., 2015).

In a mapping study of the zebrafish dopaminergic and noradrenergic projectome, Tay et al. (2011) used genetic mosaics with individually GFP-tagged catecholaminergic neurons to trace the projections of each neuron population in the larvae. The authors confirmed that the A11-like population are the major far-projecting dopaminergic population, with projections to the telencephalon (including the subpallium), the diencephalon, the hindbrain, and the spinal cord. The DC2 and DC4 populations, importantly, were the only ascending dopaminergic populations identified (homologous to the ascending pathway from the pars compacta to the striatum). Furthermore, individual neurons from these populations also connected with axon branches from the diencephalon, the hindbrain and the spinal cord, indicating that these neurons may integrate both ascending and descending circuits to modulate motor control.

Evidence of the A11-like population of dopaminergic neurons modulating locomotor behaviour has been observed in cases of neurotoxin-mediated loss of DA neurons, and laser and chemogenetic ablation studies of specific neuronal groups. For example, Jay et al. (2015) performed specific laser ablation of DC2 neurons at 1dpf in zebrafish, which led to selective loss of dopaminergic diencephalospinal neurons (DDNs) at all larval stages (Jay et al 2015); at 4dpf, reduced number of large-diameter DC2 cells persisted (with the surrounding cells still intact), and motor deficits were observed at this time. These motor deficits included a reduced cumulative swimming distance over a 10-minute period, and impaired beat-glide swimming behaviour as a result of decreased proportion of time actively swimming. However, duration and velocity of beat-glide episodes were unchanged, but intervals between episodes were increased. This is in contrast to findings from (Lambert et al., 2012), that chemogenetic ablation of *otp*-neurons (including DDNs) resulted in an increase in the duration of individual locomotor episodes – but overall also identified depressed locomotor activity. Discrepancies in findings may be due to a number of factors,

such as ablation of non-DDNs in the Lambert study, or methodological differences in the timing of neuron ablation, or in the recording or analysis of locomotor episodes. Jay et al (2015) also observed that widespread ablation of DC2 and DC4/5 neurons resulted in even more exacerbated reduction in beat-glide swimming behaviour and total swim distance.

Conversely, in adult fish (>4 mpf), ablation of the DDNs as a result of intraventricular 6-OHDA injection results in no observed changes in basic swimming parameters (Caldwell et al., 2019); this was assessed by an open field test to measure distance and velocity of swimming activity, in addition to a light/dark test and a novel tank test to assess anxiety-like behaviour. However, social behaviour was impaired in the 6-OHDA-injected group (versus sham-injection controls). Shoaling activity was impaired, as observed by a ~2x-fold increase in the pairwise distance that 6-OHDA-injected fish maintained between each other. Additionally, a breeding test revealed significant reductions in the mating success of the 6-OHDA-injected fish.

These findings of impaired motor behaviour in DDN-ablated fish reinforce our understanding of these neuron populations to provide a useful model for studying the mammalian midbrain dopaminergic system. Our primary research question for this project is “how does deficiency of Gch1 contribute to dopaminergic cell death and the development of Parkinson’s Disease?”; overall, we conclude that zebrafish provide a useful model to address this hypothesis by studying Gch1/BH4 depletion *in vivo*, and its effect on DA neuron development, neuronal firing activity, neuronal death, response to drugs or neurotoxins, behavioural changes due to alterations in neurotransmission, and the interface between the CNS and the different tissue types, such as the immune system.

1.6. Aims and Objectives

Aim:

The role of GCH1-deficiency in the development of PD is not established. The aim of this thesis was to gain an understanding of whether deficiency of GCH1 may contribute to dopaminergic cell degeneration, and development of PD, using a zebrafish model (*gch1*^{-/-}). In addition to the effects of loss of function of *gch1*, we also investigated the consequences of gene-gene interaction, and gene-environment interaction – mechanisms which are well established in contributing to PD risk. Additionally, we undertook transcriptional analysis of *gch1*^{-/-} and *gch1*^{+/-} brains in order to identify dysregulated pathways, which would provide insight into the biological processes which are disrupted by Gch1-deficiency.

Objectives:

- 1) Develop a zebrafish *gch1*-KO line which phenocopies the monoaminergic neurotransmitter deficiencies observed in pathogenic *GCH1* mutation cases.
- 2) Characterise the DA neuron phenotype in *gch1*^{-/-}, using in situ hybridisation, immunostaining and transgenic reporters to label the ventral diencephalic neurons. We hypothesise that deficiency of Gch1 contributes to loss of DA neurons.
- 3) Investigate whether *gch1* interacts with other *gba1* (another PD risk gene) to modify PD risk. Both *gch1* and *gba1* are associated with inflammatory phenotypes; we hypothesise that mutation of multiple PD risk genes contributes to greater risk of dopaminergic degeneration and reduced survival.
- 4) Use RNAseq to identify pathomechanisms in *gch1*^{-/-} and *gch1*^{+/-} larval brain tissue in a hypothesis-free, unbiased approach. We propose that characterisation of the transcriptional changes will provide insight into mechanisms that may contribute to PD development.
- 5) Assess microglial activation in larval zebrafish. Existing literature, and results from our transcriptional analysis, provide evidence of increased inflammatory activity in GCH1-deficient states; we hypothesise that *gch1*^{-/-} will show morphological and functional evidence of microglial activation, which will be assessed by immunostaining with the microglial-specific antibody 4C4.
- 6) Perform drug treatments on *gch1*^{-/-} to identify modulators of phenotype.

- i. We hypothesise that treatment with a selection of targeted treatments will ameliorate the *gch1*^{-/-} phenotype, which will be assessed by survival analysis and movement analysis; treatments include:
- (1) sepiapterin - to supplement BH4 synthesis
 - (2) L-DOPA - to supplement dopamine synthesis
 - (3) etomoxir - a candidate drug selected to inhibit the downstream effects of *irg1l* (a transcript which shows significant upregulation in *gch1*^{-/-})
 - (4) L-NIL - iNOS inhibition
 - (5) SNP - nitric oxide supplementation

Summary of contributors for each results section:

<p>3.1. Establishing a <i>gch1</i>^{-/-} Zebrafish Line</p>	<p>¹ Protein homology analysis, gene synteny analysis, RT-PCR, Gch1/Th immunostain, <i>gch1</i> genotyping PCR, phenotypic images – performed by myself.</p> <p>Generation of mutant line, qPCR, <i>gch1</i> WISH and survival curve performed by Marcus Keatinge; statistical analysis of these experiments was performed by myself.</p>
<p>3.2. Characterisation of the DA Neurons</p>	<p>HPLC neurotransmitter analysis performed by Svetlana Semenova. Genotyping and preparation of samples performed jointly by Marcus Keatinge and myself. Statistical analysis was performed by myself.</p> <p>Electrophysiology performed by Neal Rimmer.</p> <p>5 dpf and 8dpf neuron counts (and images) performed by myself.</p> <p>MPP+ neuron exposure performed by Siri Gowda; statistical analysis performed by myself.</p> <p>Vmat2/Gch1/Th immunostain – sectioning performed by Emma White, stain and imaging performed by myself <i>th</i> qPCR and Th Western blot performed by myself.</p>
<p>3.3. Gene-gene interaction study</p>	<p><i>gch1</i> ; <i>gba</i> interaction study jointly undertaken by myself, Marcus Keatinge and Rebeckah Grassby</p>
<p>3.4. RNAseq to Assess Transcriptional Changes in WT, <i>gch1</i>^{+/-} and <i>gch1</i>^{-/-} Larval Brain Samples</p>	<p>Sample preparation was performed by Marcus Keatinge and Lisa Watson. Alignment of reads was performed by Wenbin Wei. Differential gene expression analysis, principal component analysis, pathway analysis and GO enrichment analysis was performed by Katjusa Koler.</p> <p>Analysis of the RNAseq data was performed by myself.</p>
<p>3.5. Microglial analysis</p>	<p>All experiments were undertaken by myself</p>
<p>3.6. Effect of targeted drug treatments on <i>gch1</i>^{-/-} survival</p>	<p>All experiments were undertaken by myself</p>

Chapter 2. Materials and Methods

Table 2: Primer list

Method	Target	Oligo sequence	
CRISPR sgRNA	<i>gch1 exon1</i>	5'-AGAAGAGCGCACCCGGAGCCTGG-3' (guide #1)	
		5'-GGGAGGATCCGCAGCGCCAGGGG-3' (guide #2)	
PCR	<i>gch1</i>	F 5'- AAAGTACGAGCGATCAAC-3'	
		R 5'- TCTCCTGGTATCCCTTGGTG-3'	
	<i>gba1</i>	F 5'-AAAGCAGCACGATATGTCCA-3'	
		R 5'-ATGTCATGGGCGTAGTCCTC-3'	
qPCR	<i>gch1</i>	F 5'- CCACGATGAGATGGTGATTG -3' (exon 2)	
		R 5'- CTGTTTGGTCAGACGCTCCT -3' (exon 5)	
	<i>th</i>	F 5'- GACGGAAGATGATCGGAGACA-3'	
		R 5'- CCGCCATGTTCCGATTTCT-3'	
	<i>irg1l</i>	F 5'- ACATCTGGGAATGCACTGGA -3'	
		R 5'- TTGGAGAGTGGCACCCCTAAG -3'	
	<i>ef1a</i>	F 5'-TGGTACTTCTCAGGCTGACT-3'	
		R 5'-TGACTCCAACGATCAGCTGT-3'	
	<i>rps29</i>	F 5'-TTTGCTCAAACCGTCACGGA -3'	
		R 5'-ACTCGTTTAATCCAGCTTGACG -3'	
	WISH	<i>gch1</i>	F 5'-ATGGAGCGCTCCAAACAGAA -3'
			R 5'-TCAGCTCCGGATCAGGGTCA-3'
<i>th</i>		F 5'-AGTGCACCTGTCGGATGTTA-3'	
		R 5'- TAATACGACTCACTATAGGGG CGTCCACAAAGCTTTCTGA-3'	

2.1. Zebrafish Husbandry

All zebrafish husbandry and experimental procedures were performed in accordance with the UK Home Office Animals (Scientific Procedures) Act. Project license PPL 70/8437, held by Dr Oliver Bandmann.

2.1.1. Larval Husbandry

Embryos (0 - 72 hpf) and larvae (72 hpf – 30 dpf) were maintained at 28°C in E3 media (5 mM NaCl, 0.17 mM KCL, 0.33 mM CaCl₂, 0.33 mM MgSO₄) with methylene blue, unless otherwise stated, until 5.2 dpf. A 14:10 hour light:dark cycle was introduced after 5.2 dpf.

For experiments requiring embryos/larvae lacking pigmentation, embryos were treated with phenylthiourea (PTU) from 8 hpf. Stock solution of PTU was prepared at a concentration of 75 mg/ml in DMSO, and 12 µl of stock solution was added per plate of embryos (i.e. 12 µl PTU solution : 25 ml of E3).

2.1.2. Imaging Larvae

Phenotypic images of live larvae were obtained on the Leica M165 MC microscope with a Leica DFC310 FX camera. Larvae were maintained in E3 with 4.3% tricaine while imaged.

2.1.3. Adult Husbandry

Zebrafish were maintained at in Tecniplast tanks at 28.5°C with a 14:10 hour light:dark cycle.

2.2. CRISPR/Cas9 – Generating a *gch1* Zebrafish Line

A loss of function *gch1* zebrafish line was generated by Marcus Keatinge using the CRISPR/Cas9 method as previously described (Hruscha et al., 2013). In brief, 2 sgRNAs (5'-AGAAGAGCGCACCCGGAGCCTGG-3' and 5'-GGGAGGATCCGCAGCGCCAGGGG-3') targeting exon 1 of *gch1* were co-injected with Cas9 mRNA into zebrafish embryos at the single cell stage, to induce a large deletion. Efficacy of mutagenesis was assessed by performing a restriction digest of a unique restriction enzyme site positioned at the protospacer adjacent motif (PAM) sequence, to identify if the target site was successfully mutagenised. Injected embryos were raised to adulthood, and founders carrying large indels in germ cells were identified by outcrossing to WT and performing PCR for the *gch1* target region on offspring DNA. A successful founder carrying a large frameshift deletion was then outcrossed to WT to generate a stable heterozygous *gch1* mutant colony.

2.3. Nucleic Acid Extraction and Polymerase Chain Reaction (PCR)

2.3.1. DNA Extraction

The alkaline lysis method was used for genomic DNA extraction for genotyping. Larvae or larval tissue was isolated into individual wells of a 96-well PCR plate. For genotyping whole embryos, 100 µl of alkaline lysis buffer (50 mM NaOH) was added to each well. For

genotyping larval fin clips, 20 µl 50 mM NaOH was used. Following incubation at 95°C for 10 minutes, 1/10 volume of neutralisation buffer (i.e. 10 µl per 100 µl NaOH; 10 mM Tris-HCl pH 8.0) was added to each well and the samples were then vortexed. The DNA was subsequently used for polymerase chain reaction (PCR).

2.3.2. Polymerase Chain Reaction (PCR)

1 µl of DNA was used per reaction with 5 µl of BioMix™ Red (Bioline, Meridian Life Science), 2 µl MilliQ H₂O (Millipore) and 1 µl of each forward and reverse primer flanking the deletion site (10 mM, Integrated DNA Technologies). PCR primers are listed in **Table 2** (pg 18).

Samples were cycled in a thermocycler with the following protocol:

95°C - 3 minutes

37 cycles of:

95°C - 30s

60°C - 30s

72°C - 1 minute

72°C – 5 minutes

2.3.3. PCR Purification

PCR product purification was performed by phenol-chloroform precipitation. Equal volume of phenol:chloroform:isoamyl alcohol (25:24:1) was added to the sample and vortexed for approximately 20 seconds. The sample was then centrifuged at room temperature for 5 minutes at 16,000 × g. The upper aqueous phase was carefully removed and transferred to a fresh tube. Half the volume of the sample of 7.5 M NH₄OAc was then added, followed by 2.5x (volume of sample + NH₄OAc) of 100% ethanol. The sample was then precipitated at -20°C overnight before centrifugation at 4°C for 30 minutes at 16,000 × g to pellet the DNA. The supernatant was then discarded, and the pellet washed and centrifuged in 70% ethanol twice. The ethanol was then removed and the pellet air-dried for around 5 minutes, before the pellet was resuspended in ddH₂O.

2.3.4. Gel Electrophoresis

Gel electrophoresis was used to visualise PCR products. PCR products were run on 2% agarose gels, made up from 2% agarose in TAE buffer (40 mM Tris, 20 mM acetic acid, 1 mM EDTA) with ethidium bromide. TAE was used as a running buffer in the gel tank and gels were run at 150V. DNA products were then visualised using a UV light imaging system.

2.3.5. RNA Extraction

Trizol:chloroform was used for extraction of RNA. 10-20 larvae were used per sample, and 250 µl TRI reagent (SIGMA) added. Larvae were homogenised by repeatedly passing through a 25-gauge syringe needle. 50 µl chloroform (SIGMA) was then added, followed by inversion of the tube 10 times. Samples were then centrifuged at 13,000 rpm at 4°C for 15 minutes. Following centrifugation, the aqueous (upper) phase was selected, and combined with an equal volume of isopropanol in a new tube. Following a 10 minute incubation at room temperature, the samples were centrifuged again at 13,000 rpm for 15 minutes at 4°C to pellet the RNA. The supernatant was then discarded, followed by 2 wash steps in 70% ethanol, with brief centrifugation. The pellet was then air dried and resuspended in DEPC-treated water (Invitrogen). RNA purity and concentration was quantified using the Nanodrop 2000 spectrophotometer.

2.3.6. cDNA Synthesis

Complementary DNA (cDNA) was generated using the Verso cDNA synthesis kit (Thermo Fisher). 1 µg of RNA was used as a template for each reaction. The reaction was assembled at room temperature as follows:

- 4 µl 5x Verso cDNA synthesis buffer
- 2 µl dNTP mix
- 1 µl oligo-dT primer
- 1 µl RT enhancer
- 1 µl Verso enzyme
- 1 µg RNA
- DEPC-treated water up to 20 µl

Samples were incubated at 42°C for 30 minutes, prior to inactivation of the enzyme at 95°C for 2 minutes. Samples were then stored at -20°C prior to use for reverse-transcriptase PCR or qPCR.

2.3.7. Reverse Transcriptase PCR

To assess *gch1* mRNA expression levels throughout development and in adult brain, reverse transcriptase-PCR (RT-PCR) was performed. RNA was collected as described above from WT larvae at 1, 2, 3, 4 and 5 dpf, and from WT adult brain, extracted at 3 mpf. cDNA was transcribed as described above. PCR was then performed as described above using 1 µl of the cDNA template, and the *gch1* qPCR primer pair listed in

Table 2.

2.3.8. Quantitative PCR (qPCR)

qPCR was used to quantify relative mRNA transcript levels, either to assess stability of mRNA to confirm loss of function in the case of mutant genes, or to validate transcript levels from RNAseq data. qPCR was performed on 5 dpf samples, unless otherwise stated. Each biological replicate (n) for qPCR was obtained from ~20 larvae (from one set of parents), pooled into one sample. RNA and cDNA extraction was performed as described above. In the case of *irg1l* and *th* qPCR, RNA extraction was performed on larval heads. Transcript levels were quantified by qPCR using Brilliant iii SYBR-green on the Stratagene MxPro 3000P (Stratagene) qPCR machine or the BioRad CFX96. Each set of qPCR primers were optimised for primer concentration and DNA concentration, and the conditions selected were at which efficiency of DNA amplification was closest to 100%. Target gene expression was normalised using *ef1a* as a housekeeping gene (however, *rps29* was used as a housekeeping gene for quantifying *th* transcript levels), and the delta delta-Ct method was used for analysis (Livak and Schmittgen, 2001). 3 technical repeats were performed for each biological replicate.

2.4. Survival Analysis

For survival analysis of double mutants, and for the *gch1*^{-/-} survival curve, larvae were genotyped at 3 dpf, and subsequently divided into groups based on genotype. For survival analysis of drug treatment experiments on *gch1*^{-/-}, survival analysis was performed blinded to genotype, on plates of larvae from a *gch1*^{+/-} incross, and larvae were genotyped following culling.

Larvae were culled when showing signs of infirmity, primarily judged by their swimming behaviour. If larvae failed to show a robust escape response following a touch to the tail, larvae were culled. Survival curves were analysed by log-rank test.

Each survival experiment was performed on at least 3 independent clutches of larvae obtained from separate mating pairs. *n* refers to one individual larva.

2.5. High Performance Liquid Chromatography (HPLC)

For HPLC, samples of whole larvae, pooled into biological repeats (n) of 20 per genotype (each obtained from independent mating pairs), were flash frozen prior to shipment. For the adults, five individual brains (1 brain = n) were analyzed for each genotype. Upon arrival, samples were sonicated in 150 μ l 2% HClO₄, centrifuged, and 25 or 30 μ l supernatant (for 12 mpf adult brains, and 5- and 8 dpf larvae, respectively) were injected into the column for HPLC. HPLC was performed by Svetlana Semenova. Data was analysed by 2-way ANOVA by myself.

2.6. Fixing Fish

Larvae were culled in tricaine, prior to fixation in 4% paraformaldehyde (PFA; SIGMA) in PBS (Thermo Fisher™ Oxoid™ Phosphate Buffered Saline tablets) with gentle rocking, for 2h at room temperature, or overnight at 4°C.

2.7. Wholemount In Situ Hybridisation (WISH)

2.7.1. WISH Probe Generation

WISH requires digoxigenin-labelled RNA probes complementary to the mRNA transcript of interest, in order to produce specific staining to demonstrate localisation of expression. To generate the probes, we started with a cDNA transcript from WT RNA (as described above), and amplified a large amplicon (normally ~1000 bp) from the cDNA by PCR. Primers for each transcript are listed in Table 1. Primers for this reaction were tagged with a T7 promoter on the forward or reverse primer for transcribing a sense or antisense probe, respectively.

Following purification of the PCR product, and validating the product size by gel electrophoresis, the DNA was used as a template for RNA transcription with a T7 polymerase, using the following reaction:

200-400 ng PCR product – made up to 13 μ l with DEPC H₂O

2 μ l 10x T7 polymerase buffer

2 μ l DIG RNA labelling mix (SIGMA)

1 μ l RNase inhibitor (RNasin, Promega)

2 μ l T7 RNA polymerase (Promega)

The reaction was incubated at 37°C for >2h, then treated with DNase and incubated at 37°C for an additional 20 minutes.

RNA was purified by first making the RNA product up to 100 µl with DEPC-treated/RNase-free water, then mixing with ice-cold solutions of 33 µl 10 M NH₄Ac and 350 µl 100% ethanol. Samples were kept at -80°C for ~2h, and then pelleted by centrifugation at 4°C for 30 minutes (13,000 rpm). Pellets were washed in 70% ethanol, air-dried, and resuspended in DEPC-treated water. RNA concentration was assessed by Nanodrop 2000 spectrophotometer, and quality was assessed by agarose gel (1%) electrophoresis, prior to diluting the product to 1 ng/µl in pre-hybridisation buffer (50% deionised formamide [Invitrogen, Fisher Scientific UK Ltd], 50 µg/ml heparin [Sigma], 5x saline sodium citrate [SSC, Sigma], 0.1% Tween-20, 500 µg/ml yeast tRNA [Sigma], 6 mM citric acid).

2.7.2. WISH Protocol

WISH was performed using a protocol adapted from a previously published method (Thisse and Thisse, 2008). The protocol was carried out on a BioLane HTI 16Vx (Intavis), which automates the WISH process, thus reducing inter-sample variability, and allowing a high-throughput approach to the staining process. Fixed larvae were transferred to mesh-bottomed 96-well filter plates (Merck Millipore, UK), at a density of ~5 per well, thus allowing parallel processing of up to 480 embryos per plate.

All washes were at RT unless stated. All steps were carried out on the BioLane In Situ robot unless stated.

WISH Day 1

Fixed larvae were sequentially rehydrated from methanol (MeOH) into PBT (PBS, 0.1% Tween-20), over a series of 5 minute washes of:

75% MeOH : 25% PBT

50% MeOH : 50% PBT

25% MeOH : 75% PBT

4 washes in PBT

5 dpf larvae were permeabilised with Proteinase K in PBT (10g/ml, Sigma) for 45 minutes, then washed twice with PBT for 5 minutes. Samples were re-fixed in their permeabilised state with a 20 minute incubation with 4% PFA in PBT, followed by 5 x 5 minute PBT washes. Larvae were incubated in pre-hybridisation buffer (50% deionised formamide [Invitrogen, Fisher Scientific UK Ltd], 50µg/ml heparin [Sigma], 5x saline sodium citrate [SSC, Sigma], 0.1% Tween-20, 500µg/ml yeast tRNA [Sigma], 6 mM citric acid) at 68°C for 3h. Following pre-hybridisation, larvae were incubated in the WISH probe at 68°C overnight in an oven or heat block.

WISH Day 2

Larvae were briefly washed in HybB (50% deionised formamide [Invitrogen, Fisher Scientific UK Ltd], 5x saline sodium citrate [SSC, Sigma], 0.1% Tween-20, 6 mM citric acid) at 68°C, before successive 15 minute washes of 75% HybB-2x SSC, 50% HybB-2x SSC, 25% HybB-2x SSC, and 100% 2x SSC at 68°C. Larvae were then washed twice in 0.2x SSC for 30 minutes at 68°C. Samples were bridged to PBT with 10 minute successive washes of 75% 0.2x SSC : 25% PBT, 50% 0.2x SSC : 50% PBT, 25% 0.2x SSC : 75% PBT, and 100% PBT, all at RT. Samples were then incubated in blocking buffer (2 mg/ml bovine albumin serum, 2% sheep serum in PBT) for 3h, prior to overnight incubation in blocking buffer with 1:5000 Anti-Digoxigenin-AP, Fab fragments (Roche).

WISH Day 3

Samples were washed 6 x 15 minutes in PBT, before removing the plate from the BioLane In Situ Robot. Samples were then twice washed for 5 minutes in NTMT (0.1 M Tris-HCL pH9.5, 50 mM MgCl₂, 0.1 M NaCl, 0.1% Tween-20), and then transferred to NTMT staining solution (3.5 µl/ml BCIP [Roche], 4.5 µl/ml NBT [Roche], in NTMT), and left to stain while protected from light. From this step onwards, embryos were kept protected from light to prevent background staining. When larvae showed satisfactory colour development, samples were washed 3x with PBT for 5 minutes to prevent further staining, then underwent a clearing

step in 100% MeOH to reduce background stain. Larvae were re-fixed in 4% PFA in PBS for 20 minutes at RT, then thrice washed in PBT. Samples were finally transferred to 100% glycerol, and stored at 4°C, prior to mounting.

2.7.3. *gch1* WISH

WISH for *gch1* was performed on WT larval samples as described above. To generate the *gch1* antisense and sense probes, RNA was synthesised from a pGEM-T easy plasmid (Promega) containing a complete *gch1* zebrafish cDNA insert; the plasmid was linearised using *SbfI* and *NcoI* restriction enzymes (New England Biolabs), prior to RNA transcription using T7 and SP6 polymerase to generate DIG-labelled antisense and sense probes, respectively.

2.7.4. Neuron Counting In *th*-WISH Stained Larvae

Following WISH as described above, the body was dissected from the larvae for genotyping by PCR, and the head of the larvae was mounted in glycerol on a glass slide for counting of the DA neurons. Slides were coded to enable blinding of the experiment.

Counting of the DA neurons was performed on Zeiss Axioplan microscope using a Plan-Neo FLUAR 20x/0.5 objective (Carl Zeiss Ltd, Jena, Germany).

Populations DC2, DC4 and DC5, as described by (Rink and Wulliman, 2002), were counted. Counting was performed on samples from at least 3 independent clutches of larvae. *n* refers to an individual larva. Samples were un-blinded after all samples were counted, to allow for analysis of neuron count by genotype. A normality test was performed on the data in Prism to check for normality, and standard deviation was calculated to provide a measure of homoscedasticity. A two-tailed unpaired *t*-test was then used to compare means of groups.

2.7.5. Neuron counting in MPP+ treated larvae

Embryos from a *gch1*^{+/-} incross were maintained in PTU from 8 hpf until 48 hpf. At 48 hpf, embryos were exposed to 3mM MPP+ in E3 with PTU for 24h. At 72 hpf, larvae were washed with E3, prior to fixation in 4% PFA in PBT. Fixed embryos underwent WISH for *th*, prior to performing neuron counts as described above. Neuron counts were tested for

normality in Prism, and standard deviation was calculated to provide a measure of homoscedasticity, prior to performing a 2-way ANOVA.

A 2-way ANOVA was used to assess how the number of neurons (the quantitative dependent variable) differs by genotype, by treatment with MPP⁺, and by both variables in combination. The 2-way ANOVA can test 3 null hypotheses concurrently:

1. There is no difference in neuron count as a result of genotype
2. There is no difference in neuron count as a result of MPP⁺ treatment
3. The effect of MPP⁺ treatment does not depend on genotype

The 2-way ANOVA assumes that: data are homoscedastic (i.e. variation from the mean is similar across groups; the categorical variables (i.e. genotype and MPP⁺ treatment) are independent variables; finally, the dependent variables should be normally distributed.

2.8. Neuron Counting in *etVmat2-GFP* Larvae

Embryos from a *gch1^{+/-};etVmat2-GFP* incross were treated with E3 + PTU from 8hpf to prevent development of skin pigmentation. At 8 dpf, GFP-positive larvae were anaesthetised with E3 + 4.2% tricaine, and mounted dorsal-side down in low melting point agarose on a 35 mm imaging dish with a coverslip bottom. The DC2-DC4/5 region of the ventral diencephalon was imaged on the Zeiss Airyscan microscope with a 10X objective. Larvae were genotyped following the experiment, and images were subsequently blinded for analysis. The DC2 and DC4-5 neurons were counted from image z-stacks, prior to unblinding of the neuron counts for analysis. Counts were normalised to WT, and were tested for normality and standard deviation in Prism. Following confirmation that the data were normally distributed and homoscedastic, the neuron counts were statistically analysed by a two-tailed unpaired *t*-test in Prism 8.

2.9. Immunohistochemistry

2.9.1. Cryosectioning Larval Samples

Larvae were prepared for cryosectioning by initially culling and fixing in 4% PFA in PBS overnight at 4°C. After washing 3x 15 minutes in PBT, larvae were then cryoprotected in a 30% sucrose solution in PBT at 4°C until samples sunk to the bottom of the vessel (at least

overnight), indicating sufficient equilibration in sucrose. Samples were subsequently mounted in OCT and flash frozen on dry ice, before cryosectioning into 15 μm slices onto Superfrost Plus slides (Thermo Scientific). Slides were dried in a fume hood for 30 minutes, or at room temperature for $\sim 2\text{h}$, prior to freezing at -20°C for short-term storage prior to immunostaining.

2.9.2. Immunohistochemistry on Cryosections

For immunostaining on cryosections, slides were rehydrated in PBT for 3x 5 minutes, then blocked at RT for 1h in 150 μl block (1% sheep serum, 5% BSA, 0.3% Triton-X, 0.1% Tween-20 in PBS) and covered with a parafilm coverslip. After blocking, slides were incubated with 100 μl primary antibody diluted in block, covered with a parafilm coverslip, and maintained at 4°C overnight. Primary antibodies were used at the following concentrations: Gch1 1:100, Th 1:1000, Anti-GFP 1:200. After overnight incubation with primaries, slides were washed in PBT 3x 5 minutes, before adding 100 μl secondary antibody (1:200) in block, then covered with parafilm, and incubated at 37°C for 1.5h. Slides were subsequently washed in PBT 3x 20 minutes, before partially drying, adding fluoroshield with DAPI, and applying a glass coverslip.

2.9.3. Wholmount Immunohistochemistry

Wholmount immunostaining with anti-4c4 was performed as previously described (Inoue and Wittbrodt, 2011). Samples were raised in PTU-treated media to prevent development of pigment, and were fixed in 4% PFA overnight at 4°C , before undergoing dehydration in 100% MeOH at -20°C .

Fixed larvae were rehydrated through a series of MeOH-PBT washes, of 5 minutes each:

75% MeOH : 25% PBT

50% MeOH : 50% PBT

25% MeOH : 75% PBT

Larvae were then washed in PBT 3 x 5 minutes. Samples were equilibrated in 150mM Tris-HCl pH 9.0 for 5 minutes at room temperature, then incubated in fresh 150mM Tris-HCl pH9.0 at 70°C for 15 minutes. Samples were washed twice with PBT, and rinsed with MilliQ

water prior to penetration with ice-cold acetone for 20 minutes at -20°C. Samples were rinsed twice with MilliQ water, then washed 3 x 5 minutes in PBT. Samples were subsequently incubated in blocking solution (10% sheep serum, 1% BSA, PBS-triton 0.8%) overnight at 4°C with gentle agitation on a rocker.

After blocking, samples were incubated with primary antibody in incubation buffer (1% sheep serum, 1% BSA, PBS-Triton 1.0%) for 2 nights at 4°C with gentle agitation on a rocker. anti-4c4 (mouse) antibody (produced and donated by Alex McGown of Tenmore Ramesh's lab, University of Sheffield) was used at a concentration of 1:50, anti-dsRed (rabbit) (ClonTech Living Colours[®] DsRed polyclonal Antibody #632496) was used at a concentration of 1:500.

Following 2 nights incubation in primary antibody, samples were washed 3 x 1 hour in PBS-TS (10% sheep serum, PBS-Triton 0.1%). Subsequently, samples were washed in PBS-Triton 0.1% for 2 x 10 minutes. Samples were then incubated in Alexa 647 anti-mouse secondary antibody (Molecular Probes by Life Technologies) at a concentration of 1:200, at 4°C for 3 nights with agitation on a rocker.

Following staining, samples were washed 3 x 1h in PBT, prior to mounting in 1% low-melting point agarose for imaging.

2.10. Western Blot

2.10.1. Protein Lysate Preparation

Protein samples for Western blotting were isolated from larval zebrafish heads, using approximately 15 per sample. Tissue was homogenised in 25 µl RIPA buffer (Thermo Fisher Scientific) using a glass pestle and mortar-style tissue grinder. Samples were left on ice for between 10-30 minutes, then centrifuged at 13,000 rpm for 15 minutes at 4°C. Supernatant was collected and moved to a new microcentrifuge tube. 5 µl of sample was retained for a BCA assay, then an equal volume of laemmli buffer was added to the larger aliquot of protein. BCA assay (bicinchoninic acid assay; Pierce™ BCA Protein Assay Kit, Thermo Fisher Scientific) was used to quantify protein concentration as per the manufacturer's protocol.

2.10.2. SDS-PAGE

Samples (prepared as described above) were boiled for 3-5 minutes at 95°C in a heat block, before centrifugation at 5000 rpm for 1 minute. BioRad Mini-PROTEAN TGX Precast acrylamide gels were inserted into the blotting tank, and the tank then filled with a buffer solution of 25 mM Tris, 190 mM glycine, 0.1% SDS. Samples were loaded to equate to equal concentrations of total protein per well. 5 µl of BioRad Precision Plus Protein Dual Color Standards was used as a ladder. Samples were run at 120V until the 10 kDa standard reached the bottom of the gel.

2.10.3. Western Blot Transfer to Membrane

A polyvinylidene difluoride (PVDF) membrane was per-soaked in 100% MeOH prior to blotting. Gels were transferred to a PVDF membrane at 250mA for one hour, in a buffer of:

100 ml 10x transfer buffer (250 mM Tris, 1.9 M glycine)

100 ml 100% Methanol

800 ml dH₂O

Following transfer, samples were blocked in 5% skimmed-milk powder in TBST for one hour, prior to overnight incubation with primary Th antibody (Immunostar mouse Tyrosine Hydroxylase antibody [product ID 22941], 1:1000 dilution in milk-blocking solution). The membrane was then washed 3 x 5 minutes in TBST, incubated for 1h with HRP-tagged secondary antibody (Mouse, 1:10000), then washed 3x 5 minutes in TBST prior to imaging using the BioRad ChemiDoc XRS+. The membrane underwent blocking and subsequent steps with a beta-actin antibody (Abcam Anti-actin AC40), in order to normalise Th protein levels to beta-actin.

2.11. RNAseq

2.11.1. RNA Sample Preparation

RNA samples were obtained from larval brains at 8 dpf from WT, *gch1^{+/-}* and *gch1^{-/-}*. Genotypes were determined from a 3 dpf tail-fin biopsy and PCR. 20 brains were collected and pooled into each sample. In total, 4 samples were obtained per genotype, each from a

different pair of biological parents. RNA was then extracted, purified and quantified as described above.

2.11.2. Differential Gene Expression Analysis

Differential gene expression analysis was performed by Wenbin Wei and Katjusa Koler. RNA-Seq samples were pre-processed with RNA-seq pipeline bcbio (<https://github.com/bcbio/bcbio-nextgen>) using Salmon quantification (Patro et al., 2017). Salmon counts were rounded to the nearest integer, and analysed with the R package DESeq2 (Love et al., 2014) to perform differential gene expression analysis. *gch1*^{-/-} samples were compared against WT controls. Transcripts were mapped to Entrez IDs using the R package biomaRt (Durinck et al., 2009).

2.11.3. Pathway Analysis

biomaRt (Durinck et al., 2009) was used to map transcripts to human homologs. Transcripts with low reads (< 10 counts per sample in at least 3 samples) were excluded from further analysis. Homologs were annotated with Entrez IDs and normalised with trimmed mean of M values (TMM) implemented in edgeR (Robinson et al., 2010). Normalised counts were log-transformed with limma-voom (Ritchie et al., 2015). Gene-level counts were summarised into pathway-level expression scores: Genes were assigned to pathways catalogued in Molecular Signature Database (MSigDB) v6.2 C2 Canonical Pathways (Subramanian et al., 2005) and static modules (data driven pathway sets) as used in pathprint (Altschuler et al., 2013). Adapting the top 50% mean method (Hwang, 2012), we summarised z-scaled gene expression for each pathway by calculating the mean expression of the top 50% of genes within the pathway with highest |t| score, giving a pathway-level summary expression score. The pathway-level summary expression scores are analysed with limma (Ritchie et al., 2015), yielding differentially expressed pathways. We define differentially expressed pathways as all pathways meeting the adjusted p-value < 0.05 threshold and $|\log_2FC| > 1$.

2.11.4. Gene Ontology Enrichment Analysis

Differentially expressed genes from *gch1*^{-/-} vs WT analysis were tested for GO biological process enrichment. hyper (Federico and Monti, 2020) and enrichplot (<https://github.com/YuLab-SMU/enrichplot>) were used to generate enrichment and figures, respectively. Up-regulated genes were defined as all genes with adjusted p-value threshold < 0.05 and log fold change > 1. Down-regulated genes were defined as all genes with adjusted p-value threshold < 0.05 and log fold change < -1.

2.12. Microglial Methods

For microglial analysis, larvae from a *gch1*^{+/-} incross were raised in E3 + PTU to 8 dpf following standard zebrafish husbandry. At 8 dpf, larvae were fixed with 4% PFA in PBS overnight at 4°C, then dehydrated in methanol at -20°C. Larvae then underwent wholemount immunostaining with a-4c4 as described above.

2.12.1. High Throughput Imaging of 4c4-Immunostained Larvae

4c4-immunostained larvae were imaged on the Perkin Elmer Opera Phenix, using the 20X objective lens. A Z-stack image was taken of the entire brain – this may have been composed of multiple image tiles if necessary. Prior to imaging, tails were transected from the larvae for genotyping by PCR, and larvae were mounted dorsal-side down in 1-2% low-melting point agarose gel in Greiner 96-well clear-bottomed plates.

2.12.2. Counting of Microglia

Images taken by the Opera Phenix were opened as a stack in Fiji, and microglia were counted by scrolling through the stack and using the point tool to mark counted cells. Cells were counted in the telencephalon and the midbrain, prior to unblinding of genotype. Data were assessed for normality, then analysed by one-way ANOVA following confirmation of a normal distribution.

2.12.3. Analysis Of The Percentage Of Microglia Showing Activated Morphology

Following microglial counting, as described above, the number of amoeboid cells in the telencephalon and midbrain were counted. A percentage of amoeboid cells was calculated by the following formula:

$$\frac{\text{number amoeboid microglia}}{\text{total number of microglia}} \times 100$$

Results were assessed for normality, which revealed that the data were not normally distributed. As a result, data were analysed by a Kruskal-Wallis test in Graphpad Prism. The Kruskal-Wallis test makes no assumptions about the distribution of the data, and enables comparisons of the means of more than 2 groups.

2.12.4. Zymosan-Injection Experiment

In order to quantify phagocytic efficiency of microglia, pacific blue fluorescently-tagged zymosan was injected into the tectum of the brain, and the efficiency of engulfment by microglia was calculated. Additionally, activation of microglia was quantified by counting the percentage of microglia showing completely amoeboid morphology.

Larvae were maintained in E3 with PTU until 5 dpf, then anaesthetised with tricaine prior to mounting in 2% low-melting point agarose in a petri dish, dorsal-side up (Figure 7A). Once set, the petri dish was filled with E3 + 4.2% tricaine until the larvae and agarose were completely submerged. then the agarose was removed surrounding the head area, to allow a clear trajectory for injection (Figure 7B).

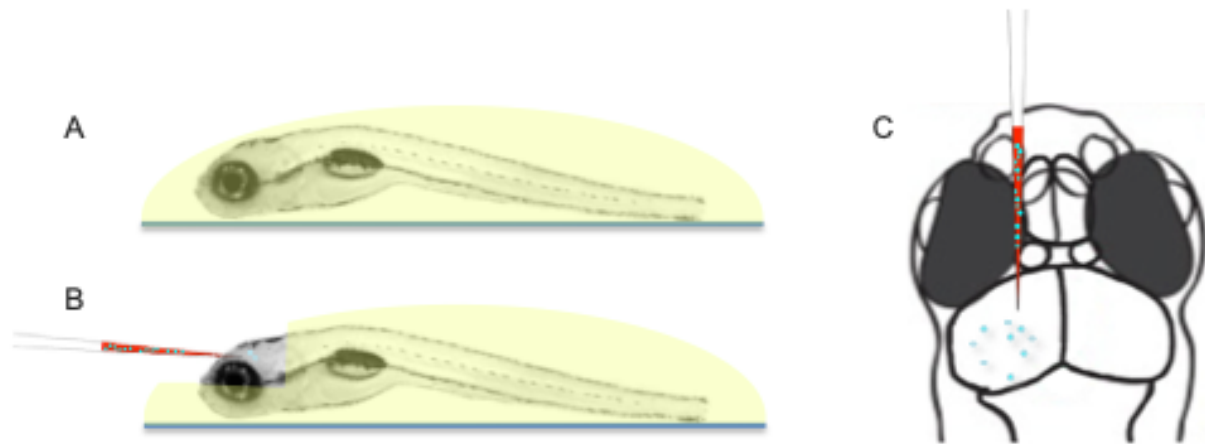


Figure 7: Illustrative schematic of zymosan injection procedure. A) larvae mounted in 2% low-melting point agarose. B) agarose is selectively removed from the head region to allow access by a microinjection needle. C) Dorsal view of injection trajectory.

Injection mixture was injected into the tectum as pictured (Figure 7B,C) using a gated (i.e. untimed) setting at a low pressure, until the tectum filled with the injection mix, but prior to the mix filling the midbrain ventricle. This was roughly 2 nL. The injection mix was composed of 1.66 μl zymosan (at a concentration of 10^3 particles/ μl), 2 μl phenol red dye, and 6.33 μl of PBS. A PBS control injection group was also included for the microglia activation assay.

Following injection, larvae were carefully removed from the agarose and transferred to fresh E3 + PTU media, and maintained at 28°C for a further 6 hours, prior to perfusion fixation in 4% PFA at 4°C overnight.

Larvae were dehydrated in methanol at -20°C, prior to immunostaining with the 4C4 antibody (as described above). Following immunostaining, tails were transected from the samples for genotyping, and the heads were imaged on the Perkin Elmer Opera Phenix, using the 20x objective.

2.12.5. Zymosan Phagocytic Activity Assay

To quantify phagocytic activity, the proportion of zymosan that had been engulfed by microglia was calculated. To achieve this, Z-stacks of immunostained, zymosan-injected larvae were imported into IMARIS as 2 separate channels (Channel 1 = zymosan, Channel 2

= microglia), and a “surface” was created to summarise the properties of the zymosan in the image.

On the Surpass Scene viewer in IMARIS, a surface was rendered manually, specific to Channel 1 using the Marching Cubes tool. Only zymosan within the tectum was selected. Specific values for the intensity sum of Channel 1 were exported and saved; these values correspond to the total fluorescent intensity of the selected zymosan within the tectum. Returning to the surface rendering function, any zymosan that had not been engulfed was deleted from the surface rendering, leaving only the engulfed particles selected. Intensity sum of these remaining zymosan particles was then exported, providing us with 2 datasets: *total zymosan fluorescent intensity*, and *engulfed zymosan fluorescent intensity*. To calculate phagocytic efficiency, the following equation was used:

$$\frac{\text{engulfed zymosan fluorescent intensity}}{\text{total zymosan fluorescent intensity}} \times 100 = \text{phagocytic efficiency}$$

Following calculation of phagocytic efficiency for each sample, data were analysed for normality in Prism. The data were not normally-distributed, therefore a Kruskal-Wallis test was used, as it allows comparison of the means of more than 2 groups with non-normally distributed values.

2.13. Drug Treatments

2.13.1. Drug application

For all drug treatments commencing at 1 dpf, larvae were maintained in E3 with methylene blue until 1 dpf, at which point they were dechorionated and transferred to fresh media with the drug solution. For treatments commencing at 5 dpf, larvae were maintained in E3 with methylene blue for the first 24h, and subsequently transferred to fresh E3 without methylene blue. For all drug treatments, larvae were transferred to fresh media daily, and survival was monitored daily.

All drugs were obtained from SIGMA Aldrich/Merck. The product details are as follows:

Etomoxir	(+)-Etomoxir sodium salt hydrate (E1905)
L-DOPA	3,4-Dihydroxy-L-phenylalanine (D9628)
L-NIL	L-N6-(1-Iminoethyl)lysine dihydrochloride (I8021)
SNP	Sodium nitroprusside (PHR1423)
Sepiapterin	(S154)

Due to the light-sensitivity of L-DOPA, SNP and sepiapterin, larvae were maintained in light-protected conditions during treatment. Preparation of L-DOPA required pH correction with 0.5 M HCl to achieve media at pH7.

2.13.1. Larval Movement Analysis

For larval movement analysis, fish were transferred to a 48-well tissue culture plate, in fresh E3 (or drug dissolved in E3 media), and then underwent behavioural analysis using the Viewpoint zebrabox system. Behaviour was analysed as previously described (Cario et al., 2011). In brief, larvae were habituated for 30mins, at 10% light intensity; larvae were then tracked for a 40min period of alternating 5min dark and light cycles (of 0% and 10% light intensity). Larvae were culled and genotyped following movement tracking.

2-way ANOVA with repeated measures was performed to assess changes in distance travelled per group. This statistical test was used to assess how the mean distance travelled (the quantitative dependent variable) differs by genotype, and by drug treatment – individually and in combination. The 2-way ANOVA can test 3 null hypotheses concurrently:

4. There is no difference in mean distance travelled as a result of genotype
5. There is no difference in mean distance travelled as a result of drug treatment
6. The effect of drug treatment does not depend on genotype

The 2-way ANOVA assumes that: data are homoscedastic (i.e. variation from the mean is similar across groups; the categorical variables (i.e. genotype and drug treatment) are independent variables; finally, the dependent variables should be normally distributed.

Chapter 3. Results

3.1. Establishing a *gch1*^{-/-} Zebrafish Line

3.1.1. Identifying the Zebrafish Ortholog of *GCH1*

GTP Cyclohydrolase I (*GCH1*) has 2 orthologs in zebrafish, GTP cyclohydrolase 1 (*gch1*) and GTP cyclohydrolase 2 (*gch2*), both of which share close homology with human *GCH1*. *gch1* shares 71% DNA sequence identity and 75% protein identity with *GCH1*, while *gch2* shares 67% identity at the DNA level and 69% protein identity. Both zebrafish orthologs have a highly conserved GTP cyclohydrolase functional domain (Figure 8). However, only *gch1* shares conserved synteny with *GCH1* (Figure 9), with *GCH1*'s surrounding genes *SAMD4A*, *WDHD1* and *SOCS4* on chromosome 14 maintaining homologs surrounding *gch1* on chromosome 17 of the zebrafish genome. *gch2* shares no synteny with *GCH1*.

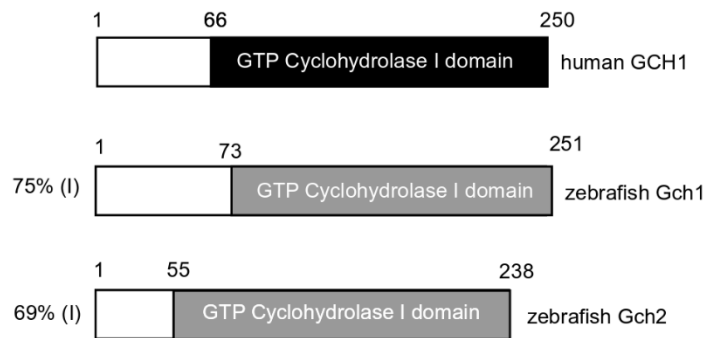


Figure 8: *GCH1* protein homology. Zebrafish *Gch1* and *Gch2* share high protein homology with human *GCH1*. All share a conserved GTP cyclohydrolase domain, spanning from residue 66-250 in *GCH1*, residue 73-251 in *Gch1*, and from residue 55-238 in *Gch2*.

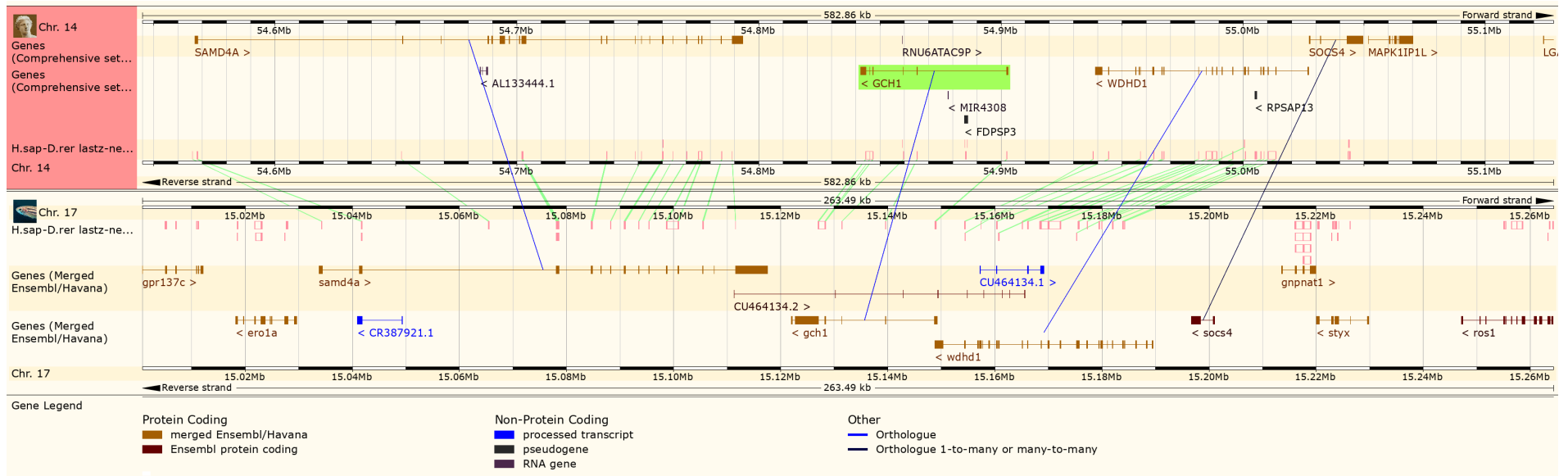


Figure 9: *GCH1* synteny map. Human *GCH1* and zebrafish *gch1* share conserved synteny, with several surrounding genes of *GCH1* maintaining orthologs surrounding *gch1* in the zebrafish genome. Orthologs with synteny are indicated with a blue line. Synteny map generated by Ensembl.

gch1 expression in zebrafish has recently been described, and shown to localise to the dopamine-producing neurons (Breuer et al., 2019); *gch2*¹ expression has been described in the migrating neural crest cells (melanophore and xanthophore progenitors) during early development, with expression becoming undetectable after 3 dpf (Pelletier et al., 2001).

3.1.2. Confirming Spatiotemporal Expression of *gch1*

We performed wholemount *in situ* hybridisation (WISH) and reverse-transcriptase PCR (RT-PCR) to confirm spatial and temporal expression patterns of *gch1*. RT-PCR revealed gradually increasing expression throughout development from 1-5 dpf, in addition to strong expression in adult brain tissue (Figure 10).

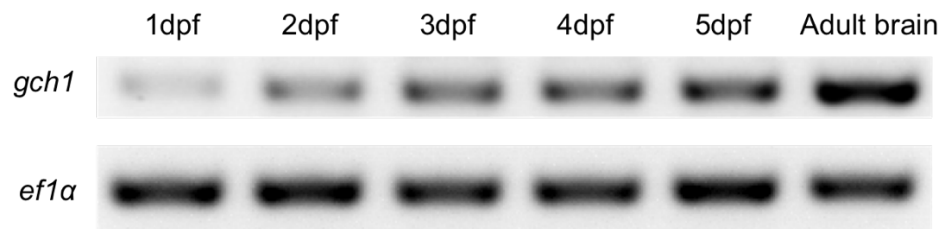


Figure 10: *gch1* RT-PCR. RT-PCR for *gch1* demonstrates increasing expression throughout development, and strong expression in adult brain. *ef1α* was used as a loading control. Each sample from 1-5 dpf was generated from ~20 embryos/larvae.

¹ Incorrectly referred to as *gch1* in the manuscript. BLAST for the in-situ probe demonstrates that the probe used is specific to *gch2*.

Using a riboprobe complementary to *gch1*, WISH demonstrated specific expression of *gch1* in neuronal populations of the ventral diencephalon and the raphe nuclei (Figure 11)², consistent with previously described expression (Breuer et al., 2019).

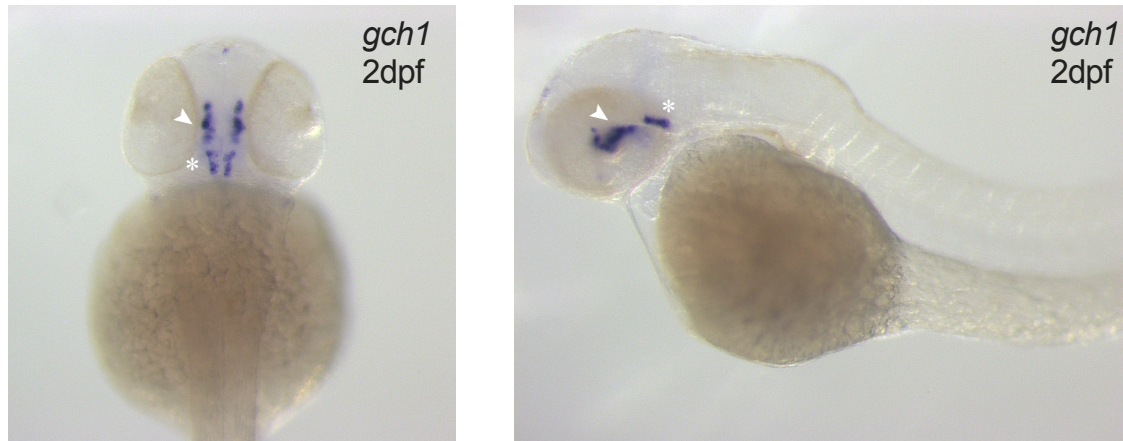


Figure 11: Wholemount In situ hybridisation for *gch1*. At 2 dpf WT larvae show *gch1* expression localised to the ventral diencephalic DA neurons (arrow) and the serotonergic neurons of the raphe nuclei (asterisk).

² WISH performed by Marcus Keatinge

We confirmed localisation of *gch1* in the diencephalic DA neurons by immunostaining with a custom Gch1 antibody in combination with anti-Th (Figure 12). Gch1 shows strong cytoplasmic expression in the cell bodies of the neurons, colocalising with Th, however, unlike Th, Gch1 does not show strong staining in the axonal projections, consistent with observations in rats of expression limited to the perikarya (Hirayama et al., 1993).

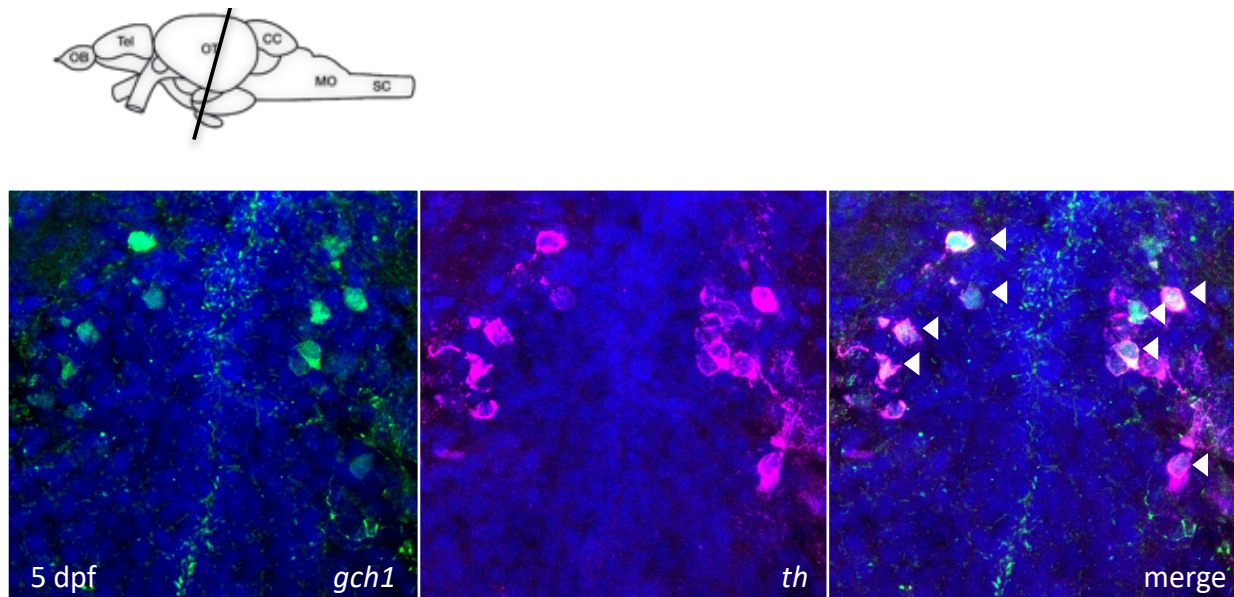


Figure 12: Gch1 and Th immunostain. Immunostaining for Gch1 in transverse plane sections of 5 dpf WT larvae confirms co-localisation with Th in the ventral diencephalic DA neurons (white arrows). Brain region from which section is derived is depicted above.

3.1.3. CRISPR/Cas9 Mediated Knockout of *gch1*

Due to the close homology, conserved synteny and expression of *gch1* within the diencephalic DA neurons, we opted to generate a zebrafish *gch1* mutant line to investigate the effects of *gch1* deficiency on pathomechanisms linked to PD. The line was generated by Marcus Keatinge using the CRISPR/Cas9 method. 2 sgRNAs targeting exon 1 of *gch1* were co-injected, producing a 94bp deletion which could be detected by standard PCR (Figure 13).

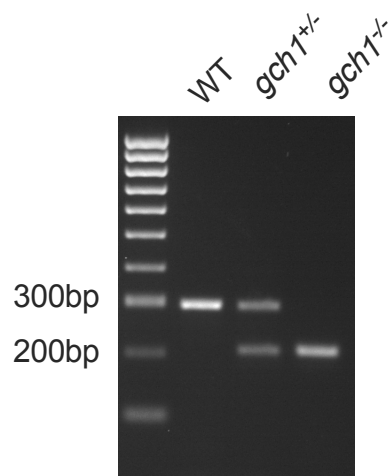


Figure 13: *gch1* PCR. The WT band is shown at ~300bp on the DNA ladder, and mutant band at ~200bp.

The mutation results in a frameshift, with a predicted nonsense protein product from residue 59 and a truncation at residue 87, deleting the entire GTP cyclohydrolase domain (Figure 14). The mutation was identified and sequenced from an outcross of a CRISPR-injected founder fish. A clutch from the outcrossed fish was raised to generate stable heterozygous mutants.

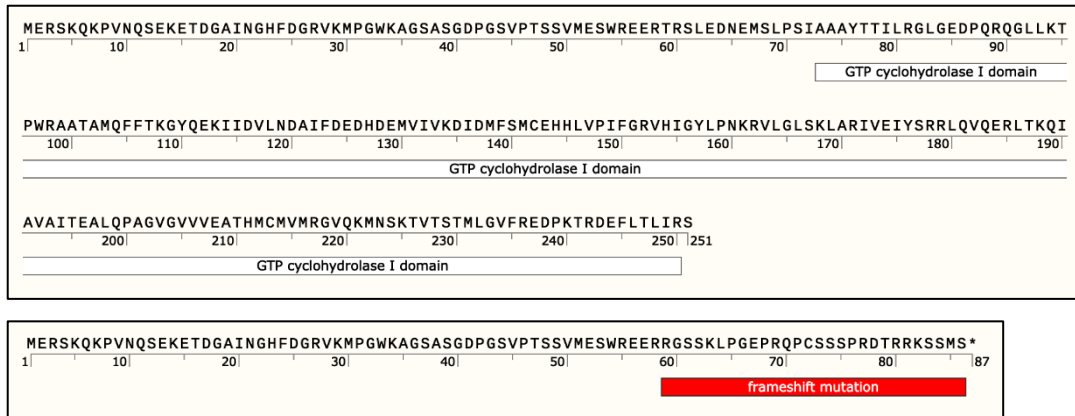


Figure 14: Predicted mutant protein sequence. Top panel: graphic of the protein sequence of WT Gch1, with the conserved region marked from residue 73-251. Lower panel: graphic of the predicted Gch1 mutant protein sequence; the red box marks the region with a predicted frameshift mutation, and the asterisk indicates the location of a premature stop codon.

To assess mRNA stability of the mutant *gch1* transcript, qPCR was performed on homozygous larval samples. mRNA levels of *gch1* were reduced to 21.3% of WT expression levels ($p = 0.0130$, Figure 15)³, indicating that the mutant *gch1* transcript undergoes nonsense mediated decay.

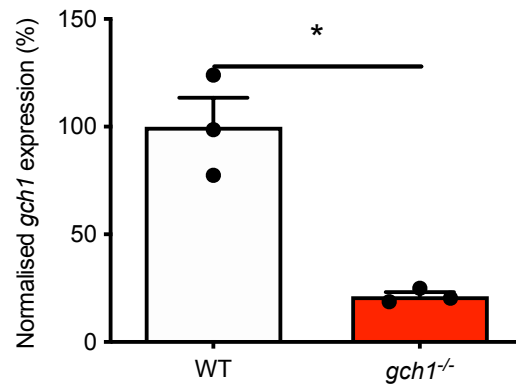


Figure 15: qPCR of *gch1* transcript levels in WT and *gch1*^{-/-}. *gch1*^{-/-} expression is expressed as a percentage of WT expression and is reduced by 78.7%. (one-tailed Welch's t-test, $n = 3$, $p = 0.0130$). "n" refers to a pooled sample of ~20 larvae, each from an independent mating pair. Error bars represent SEM.

³ qPCR performed by Marcus Keatinge

3.1.4. Loss of Function of *gch1* is Homozygous Lethal

Phenotypically, *gch1*^{-/-} larvae appear to develop normally until 5 dpf, at which point they fail to inflate their swim bladder (Figure 16).

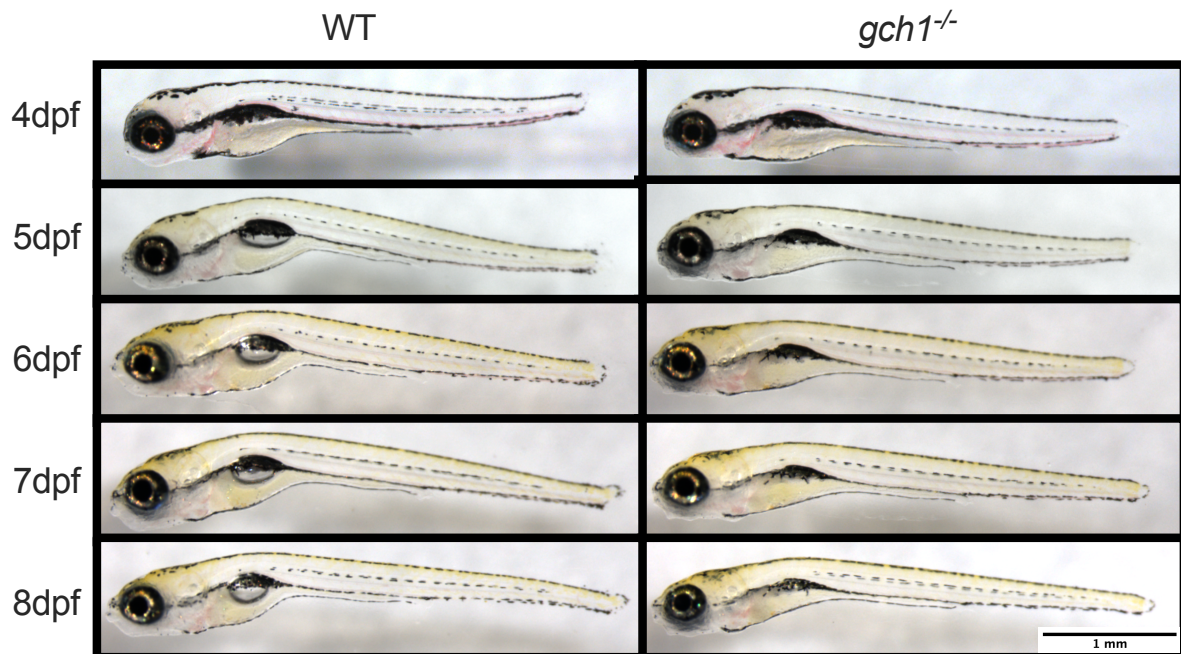


Figure 16: Phenotypic images of WT and *gch1*^{-/-} larvae from 4-8 dpf. At 4 dpf, *gch1*^{-/-} larvae are indistinguishable from WT. At 5 dpf, *gch1*^{-/-} fail to inflate their swim bladder. By 8 dpf, *gch1*^{-/-} larvae are visibly emaciated.

By 8 dpf, most *gch1*^{-/-} larvae become emaciated, with some larvae showing a curved spine. From 8 dpf onwards, larvae show a gradual decrease in survival, with no fish surviving beyond 12 dpf (Figure 17)⁴, phenocopying the lethality at E13.5 in the *Gch1*-KO mouse model (Douglas et al., 2015).

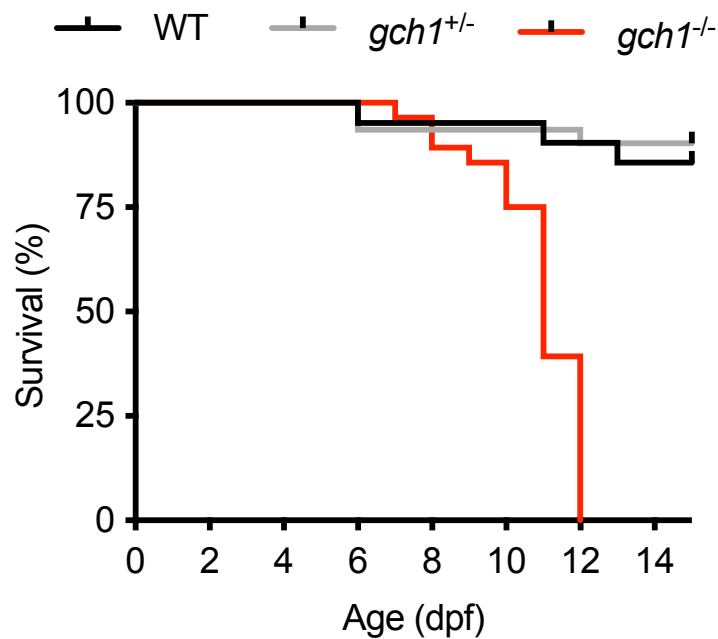


Figure 17: Survival proportions of larvae from a *gch1*^{+/-} incross. *gch1*^{-/-} larvae showed declining survival from 7 dpf, and complete mortality by 12 dpf. (log rank test, WT n = 21, *gch1*^{+/-} n = 31, *gch1*^{-/-} n = 28, p < 0.0001).

⁴ Survival curve performed by Marcus Keatinge

3.2. Characterisation of the DA Neurons

3.2.1. HPLC Analysis of Monoaminergic Neurotransmitters and Metabolites

GCH1 is an essential component of the monoaminergic neurotransmitter pathway, catalysing the first and rate-limiting step of tetrahydrobiopterin (BH4) synthesis, which, in turn, is an essential cofactor for synthesis of monoaminergic neurotransmitters. We proposed that a loss of function of this enzyme should result in reductions in the levels of dopamine, serotonin, adrenaline and noradrenaline. We extracted protein from WT, *gch1*^{+/-} and *gch1*^{-/-} larvae at 5 dpf, 8 dpf and adult brain tissue, and performed high performance liquid chromatography (HPLC) to quantify neurotransmitter levels. We assessed levels of the monoaminergic neurotransmitters: dopamine, serotonin, noradrenaline and adrenaline. Additionally, we assessed levels of the dopamine metabolites dioxyphenylacetic acid (DOPAC), 3-methoxytyramine (3-MT) and homovanillic acid (HVA), and the serotonin metabolite, 5-hydroxyindoleacetic acid (5-HIAA). Dopamine is initially broken down into either DOPAC or 3-MT, both of which are subsequently metabolised into HVA.⁵

At 5 dpf serotonin and noradrenaline were both severely depleted in *gch1*^{-/-}, and were reduced to 30% ($p = 0.0047$) and 21.9% ($p < 0.0001$) of WT levels, respectively. Adrenaline was maintained at 96% of WT levels. Dopamine appears to show a non-significant reduction ($p = 0.0708$), at 15% of WT levels. DA metabolites DOPAC, HVA and 3-MT were unchanged at 5 dpf, however, 5-HIAA was reduced to 57.3% of WT levels ($p = 0.0006$, Figure 18).

⁵ HPLC performed by Svetlana Semenova. Genotyping performed jointly by the author and Marcus Keatinge. Data analysis performed by the author.

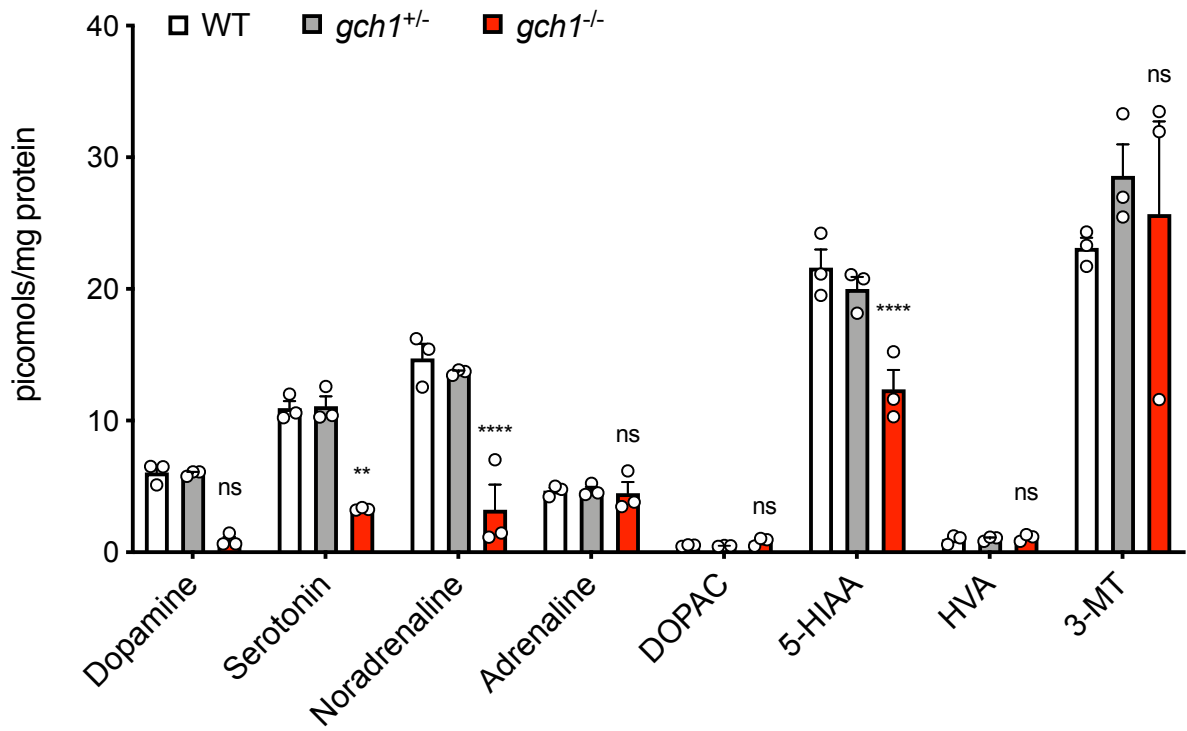


Figure 18: HPLC analysis of monoaminergic neurotransmitters and metabolites at 5 dpf. Levels of serotonin ($p=0.0047$) and noradrenaline ($p<0.0001$) are reduced in *gch1*^{-/-}. 5-HIAA was also reduced ($p = 0.0006$). 2-way ANOVA, Sidak's multiple comparison test, $n = 3$. "n" refers to a sample obtained from ~20 pooled larvae; each sample was obtained from an independent mating pair. Error bars represent SEM.

By 8 dpf, dopamine, serotonin and noradrenaline and adrenaline were all severely depleted, to 12.6% ($p < 0.0001$), 29.3% ($p < 0.0001$), 12.6% ($p < 0.0001$) and 33.8% ($p = 0.0062$) of WT levels respectively. Additionally, 3-MT, a primary metabolite of dopamine, was depleted to 10.8% of WT levels ($p < 0.0001$), however, HVA, the final breakdown product of dopamine, remained statistically unchanged at 49.4% of WT ($p = 0.8818$). DOPAC levels showed considerable variation in *gch1*^{-/-} larvae, and overall was non-significantly increased to 432% of WT levels ($p = 0.6211$). 5-HIAA showed a reduction, at 55.4% of WT levels ($p = 0.0239$, Figure 19).

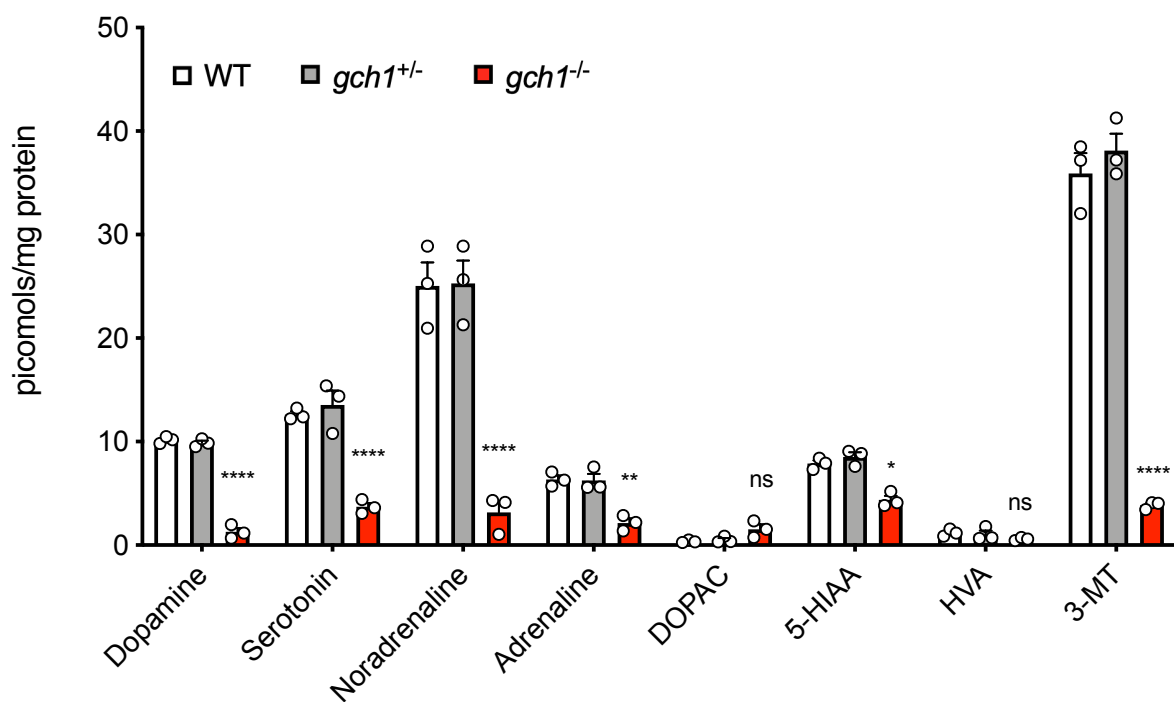


Figure 19: HPLC analysis of monoaminergic neurotransmitters and metabolites at 8 dpf. Adrenaline ($p=0.0062$), dopamine ($p<0.0001$) serotonin ($p<0.0001$) and noradrenaline ($p<0.0001$) are significantly depleted in *gch1*^{-/-}. 5-HIAA continued to show reduced levels in *gch1*^{-/-} ($p = 0.0239$), and 3-MT was also reduced ($p < 0.0001$). 2-way ANOVA, Sidak's multiple comparison test, $n = 3$. "n" refers to a sample obtained from ~20 pooled larvae; each sample was obtained from an independent mating pair. Error bars represent SEM.

In adult brain tissue, monoaminergic neurotransmitters in *gch1^{+/-}* samples remained largely unchanged from WT. Dopamine and serotonin were maintained at 90.9% ($p = 0.9778$) and 87.5% ($p = 0.4709$) of WT levels. Noradrenaline showed a modest but significant reduction, to 88% of WT levels ($p = 0.0015$, Figure 20), whereas adrenaline was undetectable. DOPAC, 5-HIAA, HVA and 3-MT were all statistically unchanged at 70.9% ($p > 0.9999$), 82.4% ($p = 0.9640$), 78.3% ($p > 0.9999$) and 77.6% ($p > 0.9999$) of WT levels.

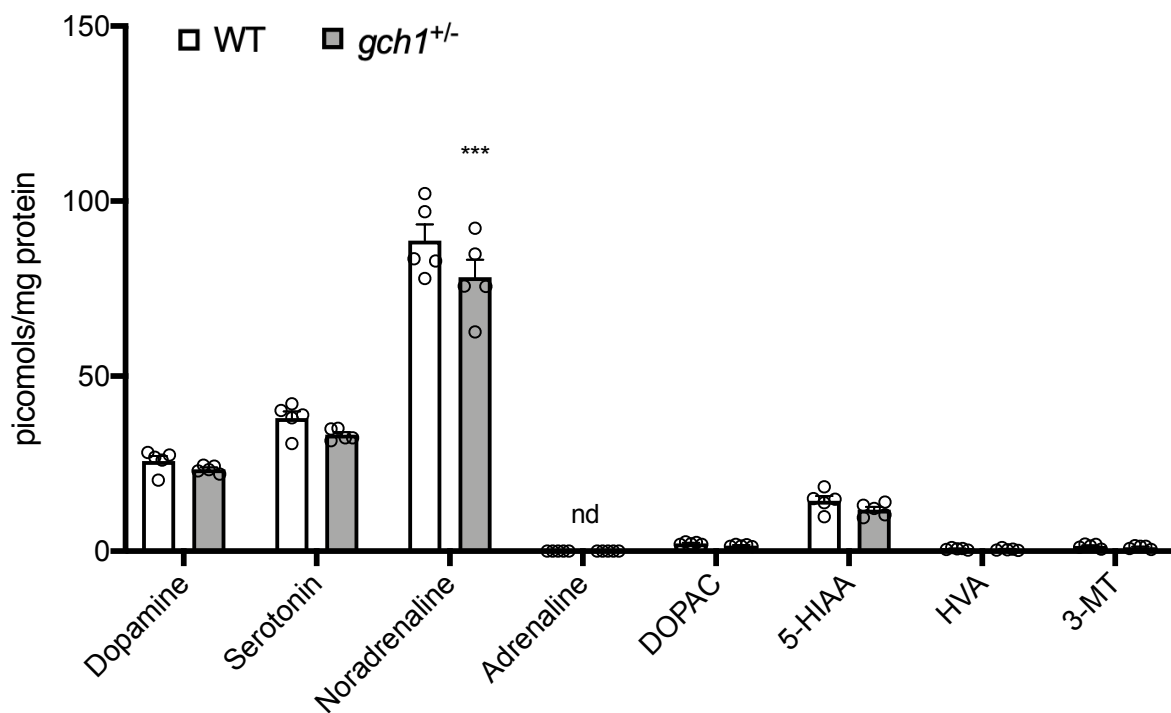


Figure 20: HPLC analysis of neurotransmitters and metabolites at 12 mpf. A modest but significant reduction in noradrenaline levels in *gch1^{+/-}* brain ($p = 0.0015$) compared to WT at 12 mpf, and no observable differences in any other monoaminergic neurotransmitter or metabolite. 2-way ANOVA with Sidak's multiple comparison test, $n = 5$. "n" refers to a single sample obtained from one brain; each sample was obtained from an independent mating pair. Error bars represent SEM.

The severe depletion of neurotransmitters in *gch1^{-/-}* as early as 5 dpf provides evidence that the 94bp deletion in *gch1* is sufficient to impair Gch1's enzymatic activity, having pathological consequences within the DA system.

3.2.2. Electrophysiological Assessment of DA Neurons

Given the severe reductions observed in dopamine levels, we postulated that the electrophysiological activity of the DA neurons would be impaired. Loose patch clamp recordings were performed on the diencephalic DA neurons at 4 dpf⁶ in order to assess the endogenous firing frequency. Larvae from a *gch1*^{+/-}; et-Vmat2-GFP incross, expressing GFP in the monoaminergic neuronal populations, were used to allow for visualisation of the neuron when forming the patch for recording. This technique is optimised at 4 dpf, a stage at which all DA tracts have been established in the developing fish and the larvae remain accessible for electrophysiological approaches. DC2 neurons from the ventral diencephalon were selected for patching, due to their conserved homology to the substantia nigra (Rink and Wullimann, 2002), and the ability to easily identify these neurons due to their large round soma.

We observed no alterations in either firing frequency ($p = 0.3436$, Figure 21A) nor in the interspike interval ($p = 0.9513$, Figure 21B) between WT, *gch1*^{+/-} or *gch1*^{-/-}, indicating that, until 4 dpf at least, DA neuronal firing is normal, contrary to our hypothesis. This result does, however, suggest that normal development of the neurons has occurred, and the basic electrophysiology is unchanged from WT.

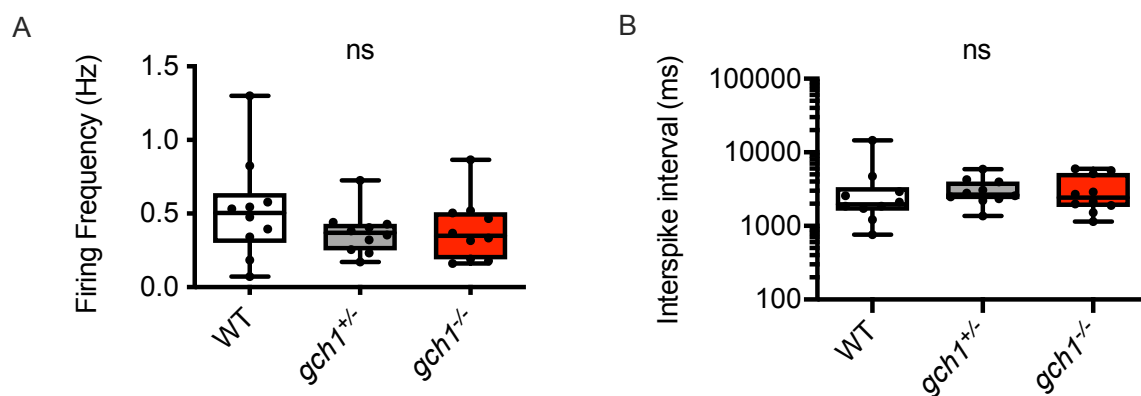


Figure 21: Electrophysiological assessment of DA neurons. Electrophysiology of the ventral diencephalic DA neurons reveals no change in firing frequency (A) or interspike interval (B) in *gch1*^{-/-} larvae at 4 dpf (WT $n = 11$, *gch1*^{-/-} $n = 10$, one way ANOVA). “n” refers to a reading from a single neuron – each from a separate larva. Larvae were obtained from multiple sets of independent mating pairs.

⁶ Electrophysiology performed by Neal Rimmer, University of Leicester

3.2.3. DA Neuron Counts

The identification of *GCH1* as a PD risk gene suggests that deficiency of GCH1 confers heightened risk of DA neuronal loss. To test this hypothesis in zebrafish, we sought to quantify DA neuron numbers to assess whether depletion of Gch1 may contribute to neuronal loss.

Our lab have previously used WISH for *th* to label and count the DC2 and DC4-5 DA neuron populations in a *pink1*^{-/-} zebrafish PD model, demonstrating reduced neuron counts as a result of *pink1* deficiency (Flinn et al., 2013). Here, we performed WISH as previously described to label the *th*⁺ cells in larvae from a *gch1*^{+/-} incross at 5 dpf, and subsequently counted the DC2 and DC4/5 neurons. No reduction in neuron counts was observed in *gch1*^{-/-} compared to WT siblings ($p = 0.9563$, Figure 22), and staining intensity and distribution appeared normal (Figure 23).

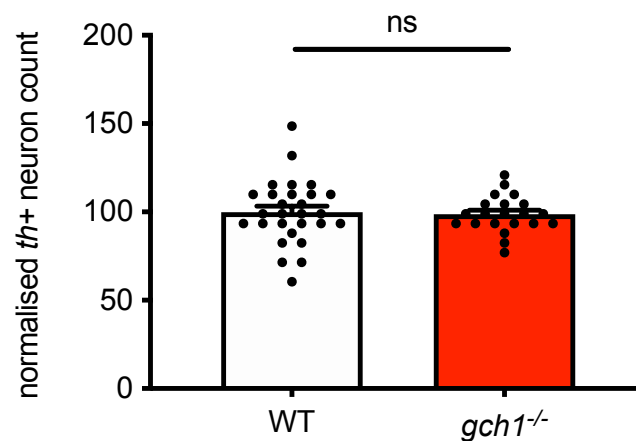


Figure 22: *th*⁺ neuron counts at 5 dpf. No change in the number of *th*⁺ neurons in *gch1*^{-/-} was observed. Counts are normalised to WT values. Unpaired, two-tailed t-test, WT $n = 28$, *gch1*^{-/-} $n = 21$. “*n*” refers to a single larva; samples were obtained from at least 3 independent sets of mating pairs. Error bars represent SEM.

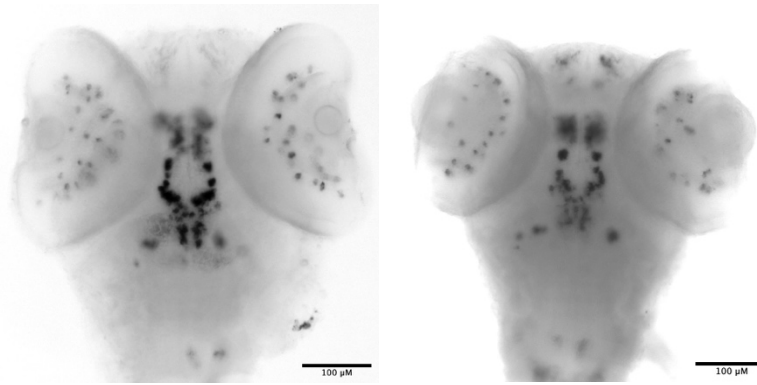


Figure 23: Representative th WISH image. *th+* WISH on WT (left) and *gch1*^{-/-} (right) larvae at 5 dpf shows similar staining localisation in both genotypes. Scale bar = 100µm.

To investigate whether *gch1*^{-/-} display neurodegeneration at a later stage, at which we see more overt phenotype and marked neurotransmitter reductions, we next performed neuron counts at 8 dpf. We utilised the *etVmat2*-GFP transgenic line, as mentioned above (section 3.2.2. *Electrophysiological Assessment of DA Neurons*), to label the DA populations, and counted the DC2 and DC4/5 groups of neurons (Figure 24). The DC2 and DC4/5 neuron groups in the *etVmat2*-GFP larvae can be found positioned ventrally in the brain, anterior to the distinctive raphe nuclei. DC2 and DC4/5 neuron numbers were again unaffected in *gch1*^{-/-} ($p = 0.0652$, Figure 25), indicating that, even when larvae have severely reduced levels of all monoaminergic neurotransmitters, the DA neurons are not showing evidence of degeneration from *gch1* deficiency alone.

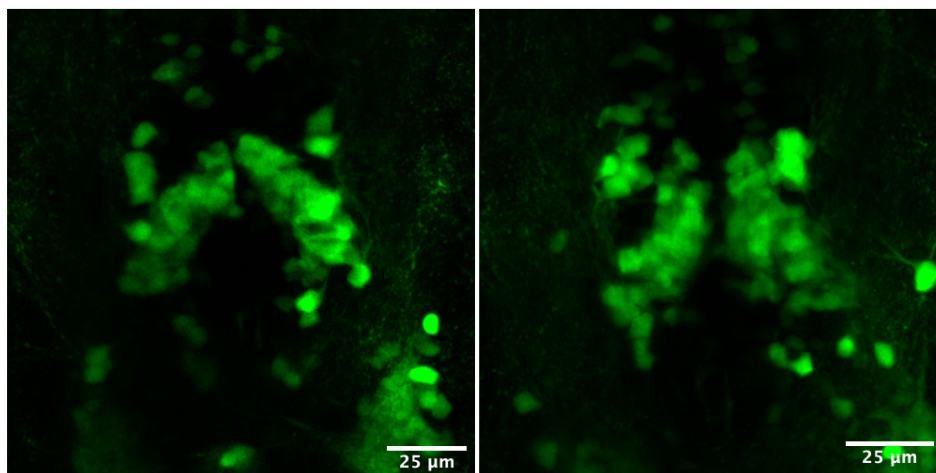


Figure 24: Representative *et-vmat2*;GFP image of DC2-DC4/5 neurons. A dorsal view of WT (left) and *gch1*^{-/-} (right) *et-vmat2*;GFP labelled ventral diencephalic DA neurons, DC2-DC5. Anterior-posterior from top to bottom of image. Scale bar = 25µm.

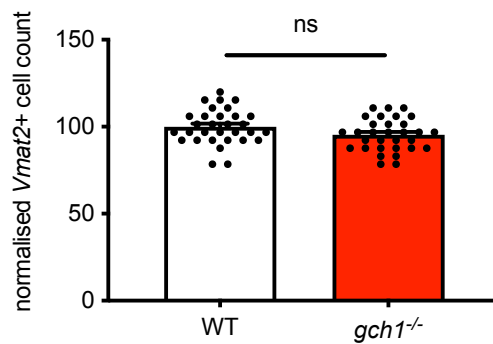


Figure 25: Vmat2+ neuron counts at 8 dpf. No change in number of Vmat2+ neurons was observed in *gch1*^{-/-}. Counts are normalised to WT values. Unpaired, two-tailed t-test, $p = 0.0652$, WT $n = 31$, *gch1*^{-/-} $n = 31$. “n” refers to a single larva; samples were obtained from at least 3 independent sets of mating pairs. Error bars represent SEM.

3.2.4. Neurotoxin Exposure

Genetic PD risk factors may interact with environmental risk factors, such as neurotoxins which act as mitochondrial inhibitors, to increase risk of developing PD. Mitochondrial dysfunction is a risk factor in sporadic and familial PD, and is a known mechanism of action in neurotoxin-induced PD models (Martinez and Greenamyre, 2012; Park et al., 2018; Trancikova et al., 2012). We explored the hypothesis that GCH1 deficiency exacerbates vulnerability of the DA neurons to neurotoxins. To test this hypothesis, we exposed larvae from a *gch1*^{-/-} incross to the classical PD neurotoxin 1-methyl-4-phenylpyridinium (MPP+), which acts as a mitochondrial Complex I inhibitor and has previously been used to model DA neuronal loss in larval zebrafish (Flinn et al., 2009); we proposed that *gch1*^{-/-} larvae would show exacerbated neuronal loss compared to their WT siblings when exposed to MPP+. At 2 dpf, larvae were immersed in 3mM MPP+ for 24h, and at 3 dpf were fixed and stained for *th* by WISH. Neuron counting, as described above, revealed a significant decrease in cell count between untreated and MPP+ exposed larvae, as predicted ($p < 0.0001$). However, the genotype had no effect upon susceptibility to MPP+, with WT and *gch1*^{-/-} larvae showing equivalent reductions in neuron count in response to MPP+ exposure ($p = 0.7863$, Figure 26)⁷. This result would suggest that GCH1 deficiency does not interact with mitochondrial toxins to exacerbate DA neuronal loss.

⁷ MPTP experiment performed by Siri Gowda

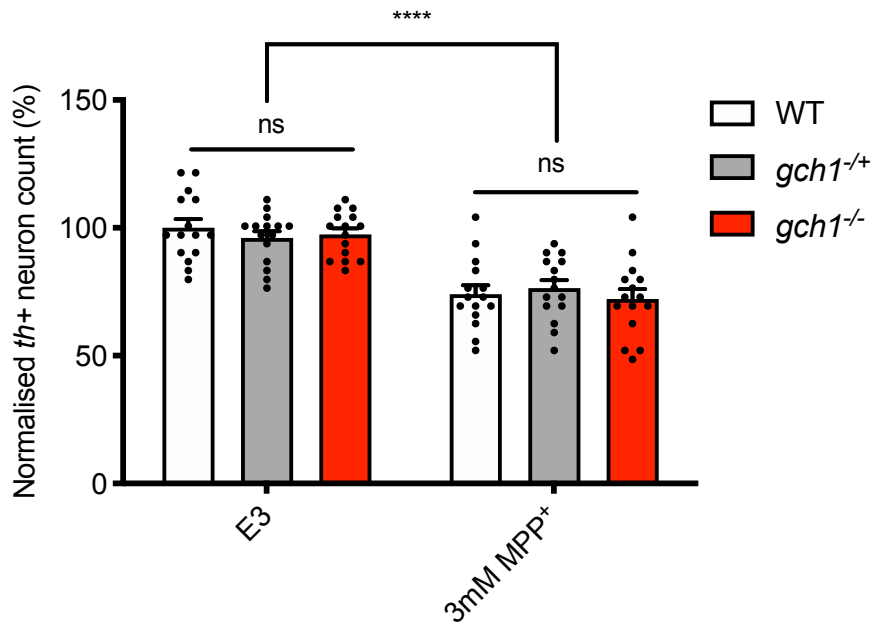


Figure 26: *th*⁺ counts in MPP⁺ treated larvae. No additional neuronal susceptibility to 24h 3mM MPP⁺ exposure was observed in *gch1*^{-/-} in comparison to WT ($p = 0.7863$). 2-way ANOVA with Tukey's multiple comparison test. $n = 15$ per group. "n" refers to a single larva; samples were obtained from at least 3 independent sets of mating pairs. Error bars represent SEM.

3.2.5. Tyrosine Hydroxylase Depletion in *gch1*^{-/-}

It has previously been demonstrated that deficiency of dopamine in PC12D cells, either by inhibition of aromatic l-amino acid decarboxylase (AADC) or inhibition of GCH1, leads to depletion of tyrosine hydroxylase via phosphorylation of Ser40 and subsequent degradation by the ubiquitin proteasome system (Kawahata et al., 2015). To identify whether Th depletion occurs *in vivo* in *gch1*^{-/-} larvae, we performed immunostaining for Th on cryosections of etVmat2-GFP 5 dpf larvae, in parallel with staining for Gch1 and Vmat2-GFP⁸. In WT cryosections, DC2 cells showed intense staining for Vmat2-GFP, Gch1 and Th (Figure 27). Consistent with Kawahata et al's finding, we observed reduced staining for Th in *gch1*^{-/-}, and no apparent staining for Gch1, in Vmat2-GFP positive DC2 cells, suggesting that tyrosine hydroxylase appears to be reduced in *gch1*^{-/-}.

⁸ Cryosectioning performed by Emma White; immunostaining performed jointly by the author and Emma White.

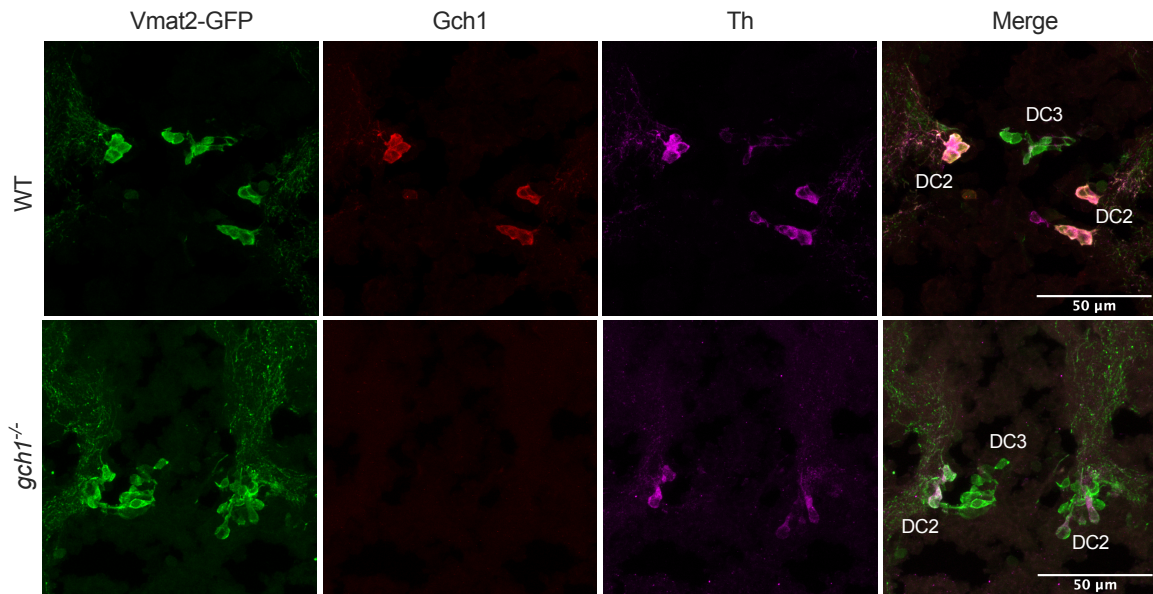


Figure 27: Reduced Th-immunofluorescence in *gch1*^{-/-} DA neurons. Diencephalic DA neurons of a WT zebrafish (upper panel) are positively immunolabelled by etVmat2-GFP, Gch1 and Th antibodies. *gch1*^{-/-} larvae (lower panel) are positively stained by etVmat2-GFP, however lack immunostaining for Gch1, and have minimal staining for Th at 5 dpf.

Kawahata et al described a post-translational mechanism of TH depletion. We sought to identify whether the reduction of Th levels in the *gch1*^{-/-} larvae was occurring at the transcriptional or the protein level, and additionally to validate the reduction in Th protein we had observed in cryosections. To address whether mRNA levels of *th* were affected, we performed qPCR for *th* at both 5 dpf and 8 dpf. We observed no change in *th* expression at 5 dpf ($p = 0.8568$, Figure 28A), and again observed no significant change in expression at 8 dpf ($p = 0.1951$, Figure 28B). We next sought to quantify protein levels of Th at these same stages. Western blot for Th demonstrated a trend towards reduced levels at 5 dpf (Figure 28C), but not a significant difference ($p = 0.1463$); at 8 dpf protein levels of Th were reduced to 45% of WT ($p = 0.0004$, Figure 28D). These results indicate that the reduction of Th levels cannot be attributed to DA cell death, nor to reduced transcription of *th* mRNA.

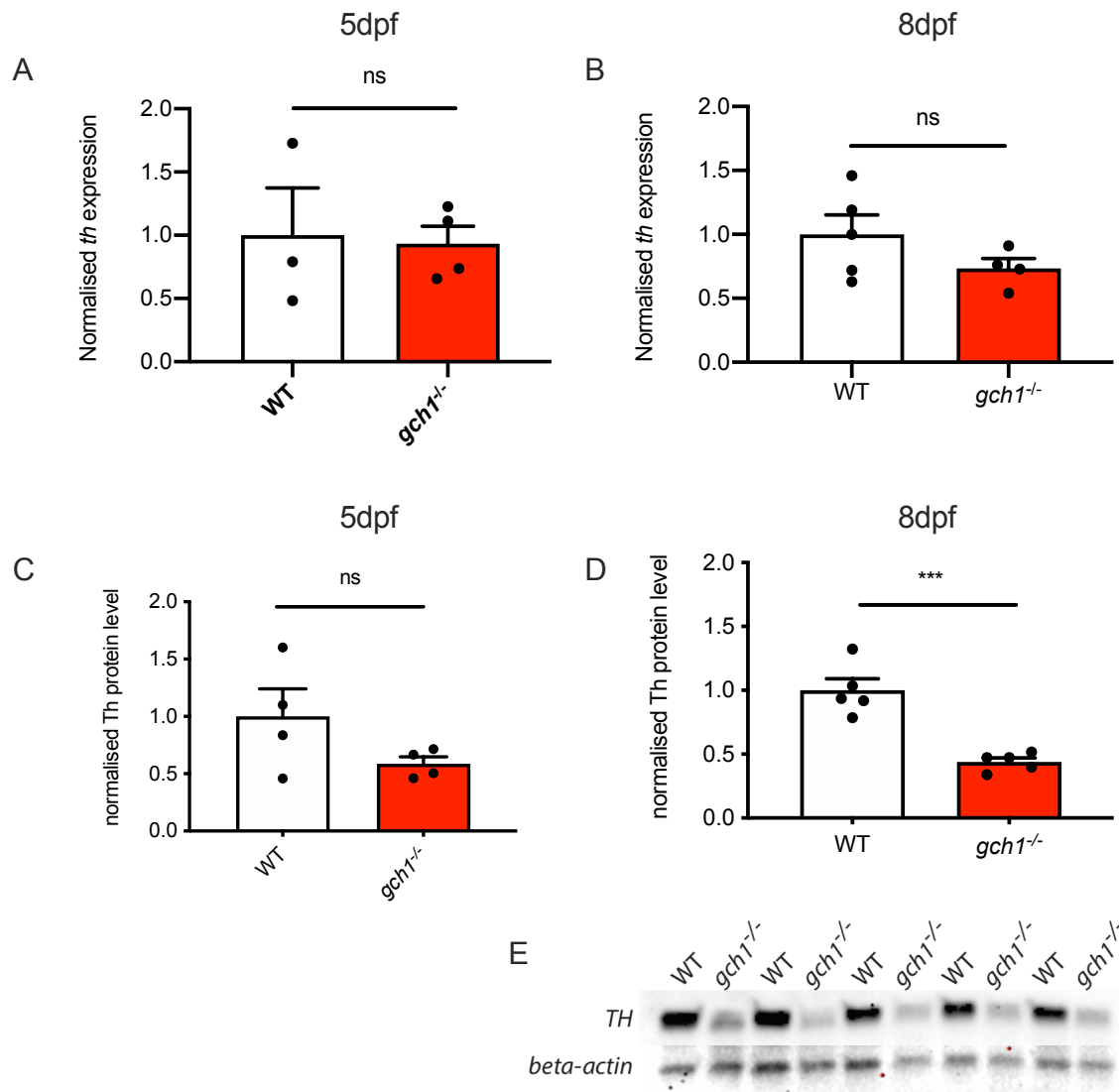


Figure 28: qPCR and Western blotting reveals depletion of Th protein in *gch1*^{-/-} at 8dpf. qPCR for *th* reveals no change in transcript levels between WT and *gch1*^{-/-} at A) 5 dpf ($p = 0.8568$, WT $n = 3$, *gch1*^{-/-} $n = 5$, unpaired t-test), or B) 8 dpf ($p = 0.1951$, WT $n = 5$, *gch1*^{-/-} $n = 4$, unpaired t-test). “n” refers to a pooled sample of heads of ~20 larvae; samples were obtained from at least 3 independent sets of mating pairs. Western blotting against Th shows no significant decrease in Th immunoreactivity in *gch1*^{-/-} larvae at C) 5 dpf ($p = 0.1463$, $n = 4$, unpaired t-test), but a 55% decrease in Th immunoreactivity is observed in *gch1*^{-/-} larvae at D) 8 dpf ($n = 5$, $p = 0.0004$, unpaired t-test). E) Western blot of alternating WT and *gch1*^{-/-} protein samples. Each sample was obtained from pooled heads from 15 individual larvae; each sample was obtained from independent sets of mating pairs. Error bars represent SEM.

3.3. Gene-gene interaction study

The common disease common variant model (CDCV) states that genetic variants, each of small effect, contribute to risk for polygenic disease, such as sporadic PD, in an additive manner. On a more complex level, interacting molecular mechanisms of genetic variants may also result in disease modifier effects, in which variants may interact to either augment or diminish the effects of other variants. PD phenotypes and risk genes can largely be categorised within a few highly conserved pathways, such as mitochondrial dysfunction, protein trafficking, neuroinflammation and lysosomal storage dysfunction. Furthermore, sporadic PD genes show strong enrichment in brain-derived tissue types, particularly in the substantia nigra (Nalls et al., 2019). GWAS and next generation sequencing have been instrumental in identifying common low-risk variants, many of which fall within few common pathways, but identifying genetic interactions which modify risk is challenging to study at a genome-wide level.

Using a targeted experimental approach to produce genetic crosses of known PD variants that may participate in the same pathway is a promising approach to identify new modifiers. Zebrafish provide a useful model for studying the effect of multiple mutations, due to the ease with which genetic crosses can be generated, and clutches of offspring containing all 4 genotypes (WT, mutant #1, mutant #2, double-mutant) can be obtained. As the offspring are obtained from healthy parents with heterozygous mutations of both genes (rather than homozygous mutations), inheritance of maternally contributed factors should not be problematic.

In order to identify whether other PD genes act as modifiers of *GCH1*, we produced genetic crosses of *gch1*^{+/-} to other stable mutant PD lines, and used readouts of DA neuron count and survival to assess phenotype⁹.

⁹ Gene-gene interaction experiment were performed jointly between Marcus Keatinge, Rebekah Grassby and the author

3.3.1. *gch1* ; *gba*

Variants in the *GBA* gene (encoding the lysosomal enzyme glucocerebrosidase [GCase]) are the most common genetic risk factor for PD (Nalls et al., 2019), but are also associated with Gaucher's Disease, a lysosomal storage disorder (Riboldi and Di Fonzo, 2019). Our group had previously established a *gba1*^{-/-} zebrafish model, which shows enzymatic GCase activity deficiency, sphingolipid accumulation, microglial activation by 4 dpf, sustained upregulation of miR-155 (a regulator of inflammation) and balance defects, with an endpoint phenotype around 3 months of age (Keatinge et al., 2015). Expression of *GCH1* is induced in states of inflammation, as demonstrated in cell culture models (Hattori et al., 1996; Huang et al., 2005; McNeill et al., 2018) and human vascular disease (Antoniades et al., 2011). The involvement of both *GCH1* and *GBA* in inflammation made *gba1* a promising candidate for a gene-gene interaction study. To determine if these risk factors interact genetically, we raised a *gch1*^{+/-} ; *gba1*^{+/-} double mutant zebrafish line and performed DA neuron counting and survival analysis on progeny from an incross of the double-heterozygous mutants. We hypothesised that double-homozygosity, or *gch1*-haploinsufficiency combined with *gba1*-homozygosity, would result in a more severe phenotype than in single mutants.

We performed WISH for *th* at 5 dpf and counted DA neurons of WT, *gch1*^{-/-}, *gba1*^{-/-} and *gch1*^{-/-} ; *gba1*^{-/-} larvae. We observed no difference in neuron counts across all genotypes (p = 0.9563, Figure 29), indicating that combined deficiency of these genes has no impact on DA neuron survival in larval stages. [No representative images of neuron staining are provided as the neuron counting method is performed on a manual stereomicroscope with no camera attachment].

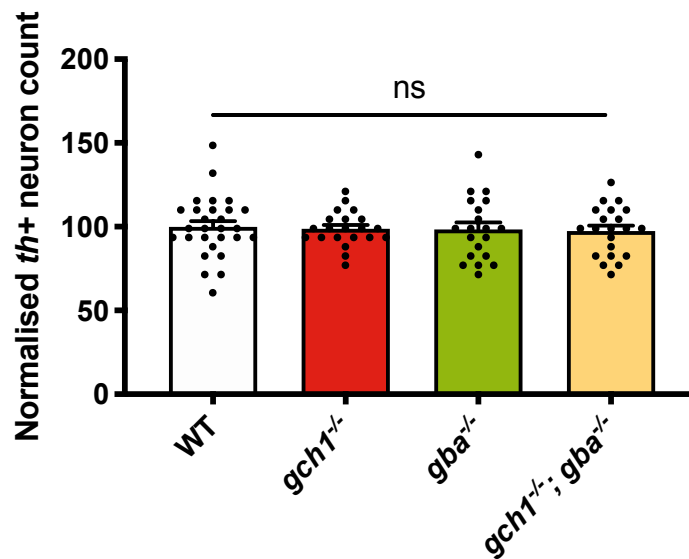


Figure 29: *gch1;gba1 th+* neuron counts, 5dpf. No difference was observed in neuron counts in either single or double homozygous *gch1;gba1* mutants in comparison to WT ($p = 0.9563$, one-way ANOVA, WT $n = 28$, *gch1*^{-/-} $n = 21$, *gba1*^{-/-} $n = 20$, *gch1*^{-/-}; *gba1*^{-/-} $n = 21$)

We additionally sought to assess whether double mutants had altered survival in comparison to *gch1*^{-/-} larvae. We performed genotyping of larvae from a double-heterozygous incross by tail-fin biopsy and PCR at 3 dpf, and divided larvae into groups of WT, *gch1*^{-/-}, *gba1*^{-/-} and *gch1*^{-/-}; *gba1*^{-/-}. Survival analysis of these groups demonstrated a median survival age of 10 dpf for *gch1*^{-/-} larvae and 11 dpf for *gch1*^{-/-}; *gba1*^{-/-}, with both groups showing complete lethality by 12 dpf (Figure 30); overall, survival was not statistically different between these 2 groups when assessed with a Log-rank test ($p = 0.1972$). WT and *gba1*^{-/-} larvae were maintained until 30 dpf, at which point they had 100% and 93.75% survival rates respectively, and the remaining fish were censored.

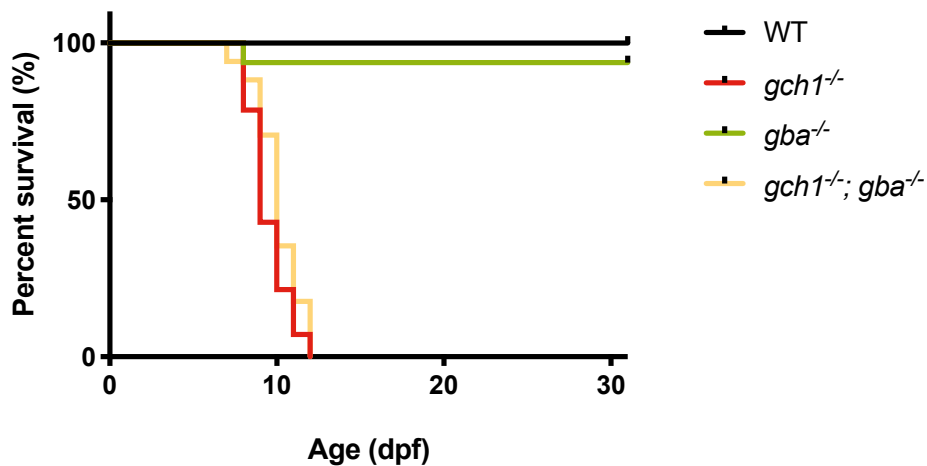


Figure 30: Survival curve of larvae from *gch1*^{+/-};*gba1*^{+/-} incross. *gba1*^{-/-} survival was not significantly different from WT. Survival was significantly reduced in *gch1*^{-/-} and *gch1*^{-/-}; *gba1*^{-/-} vs WT ($p < 0.0001$). Crucially, survival was not different between *gch1*^{-/-} and *gch1*^{-/-};*gba1*^{-/-} ($p = 0.1972$, Log-rank test, WT $n = 8$, *gch1*^{-/-} $n = 14$, *gba1*^{-/-} $n = 16$, *gch1*^{-/-}; *gba1*^{-/-} $n = 17$).

We also investigated the effects of *gch1* haploinsufficiency on *gba1*^{-/-} survival. As above, we performed tailfin biopsy at 3 dpf for genotyping and raised groups of WT, *gba1*^{-/-} and *gch1*^{+/-}; *gba1*^{-/-} fish. Fish were monitored daily, and culled at end-point, which was indicated by balance defects around 3 mpf, resulting in a “corkscrew” like swimming pattern, as previously described (Keatinge et al., 2015). Surprisingly, haploinsufficiency of *gch1* combined with *gba1*-homozygosity resulted in prolonged latency of phenotype onset, and improved survival in *gch1*^{+/-}; *gba1*^{-/-} fish in comparison to *gba1*^{-/-}. A median survival of 95 dpf was recorded for *gba1*^{-/-} and 109 dpf for *gch1*^{+/-}; *gba1*^{-/-} (Figure 31). *gba1*^{-/-} showed complete lethality by 122 dpf, and *gch1*^{+/-}; *gba1*^{-/-} at 150 dpf; curve comparison using the Log-rank test indicated that the difference was significant ($p = 0.0085$). WT and *gch1*^{+/-} fish had 100% survival at 150 dpf, and the experiment was ended at this point.

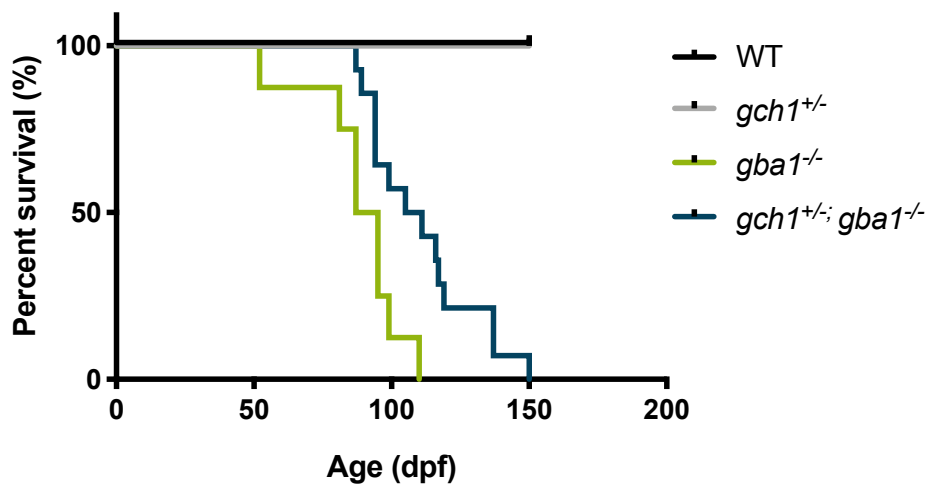


Figure 31: Survival curve of adult fish from a *gch1*^{+/-};*gba1*^{+/-} incross. *gch1*^{+/-} survival is unaffected compared to WT, while *gba1*^{-/-} and *gch1*^{+/-};*gba1*^{-/-} survival is significantly reduced from WT ($p < 0.0001$, Log-rank test). Additionally, an increase in survival was observed in *gch1*^{+/-};*gba1*^{-/-} in comparison to *gba1*^{-/-} ($p = 0.0085$, Log-rank test, WT $n = 9$, *gch1*^{+/-} $n = 10$, *gba1*^{-/-} $n = 8$, *gch1*^{+/-};*gba1*^{-/-} $n = 14$).

To summarise, our results here indicate that double-homozygosity for *gba1* and *gch1* was not sufficient to modify the phenotype of either mutant. However, in contrast to our hypothesis, haploinsufficiency of *gch1* combined with *gba1* homozygosity appears to prolong the healthspan of the fish, with a delay in the onset of balance defects.

3.4. RNAseq to Assess Transcriptional Changes in WT, *gch1*^{+/-} and *gch1*^{-/-} Larval Brain Samples

To unravel mechanisms leading to the phenotype and reduced survival in the *gch1* mutant in an unbiased manner, we performed RNAseq on larval brain samples at 8 dpf¹⁰. With the transcriptional data, we aimed to compare transcriptional changes across WT, heterozygous and homozygous samples to establish whether the apparently asymptomatic heterozygous samples show any overlap of differential gene expression with *gch1*^{-/-}, which may give an indication of pathological processes caused by haploinsufficiency of the gene. We additionally sought to use pathway analysis and gene ontology analysis to identify pathways and biological processes showing dysregulation in the mutant larvae. WT, *gch1*^{+/-} and *gch1*^{-/-} RNA samples were obtained from pooled brain samples of 4 independent biological clutches of ~20 larvae per sample, and whole transcriptome analysis was performed on these samples. Differential gene expression analysis was then performed on WT vs *gch1*^{+/-}, and WT vs *gch1*^{-/-}. Differential gene expression analysis was also performed on *gch1*^{+/-} vs *gch1*^{-/-}, however our research interest was how each mutant differed from WT, so we have not discussed or presented the *gch1*^{+/-} vs *gch1*^{-/-} data here.

¹⁰ Sample preparation was performed by Marcus Keatinge and Lisa Watson. Alignment of reads was performed by Wenbin Wei. Differential gene expression analysis, principal component analysis, pathway analysis and GO enrichment analysis was performed by Katjusa Koler. Analysis of the above data was performed by the author.

3.4.1. Principal component analysis

To assess the variance between WT, $gch1^{+/-}$ and $gch1^{-/-}$ transcriptomes, principal component analysis (PCA) was performed. Similar clustering of most WT and heterozygous samples was observed (Figure 32), indicating low variance between these samples, however, WT replicate 2 was identified as an outlier, and was therefore excluded from further analysis. $gch1^{-/-}$ showed clear separation from WT and $gch1^{+/-}$ samples on the first and second principal component, indicating high variance between the transcriptomes of these groups.



Figure 32: Principal component analysis of RNAseq data. PCA reveals low variance between WT and $gch1^{+/-}$ samples, and high variance of the $gch1^{-/-}$ samples on the 1st and 2nd principal component.

3.4.2. Differential gene expression analysis

Differential gene expression analysis was performed to compare gene-level differences between each genotype. Genes were classified as differentially expressed (DE) if they had a false-discovery rate (FDR) adjusted p value of <0.05, and a $|\log_2FC| > 1$. In *gch1^{+/-}* only 6 of 23457 genes were differentially expressed, all 6 of which showed upregulation (Table 3).

Table 3: Differentially expressed genes in the *gch1^{+/-}* vs WT dataset. FDR Adjusted p value <0.05, $|\log_2FC| > 1$

ensembl_gene_id	description	entrezgene_id	baseMean	log2FC	lfcSE	stat	pval	padj
ENSDARG0000009443	zgc:92137 [Source:ZFIN;Acc:ZDB-GENE-040801-179]	445049	92.7048	2.6495	0.5679	4.6654	0.0000	0.0184
ENSDARG0000038742	retinol binding protein 1, cellular, tandem duplicate 2 [Source:ZFIN;Acc:ZDB-GENE-070912-18]	100141334	32.7568	2.4169	0.5067	4.7702	0.0000	0.0147
ENSDARG0000104980	protein phosphatase with EF-hand domain 2a [Source:NCBI gene;Acc:100537120]	100537120	85.2062	1.3706	0.3094	4.4293	0.0000	0.0377
ENSDARG0000071347	aftiphilin b [Source:ZFIN;Acc:ZDB-GENE-060503-388]	100004990	189.7813	1.3605	0.1955	6.9573	0.0000	0.0000
ENSDARG0000079074	FERM and PDZ domain containing 1a [Source:ZFIN;Acc:ZDB-GENE-090313-137]	NA	117.8631	1.2098	0.2705	4.4722	0.0000	0.0370
ENSDARG0000086256	si:ch211-236p5.2 [Source:ZFIN;Acc:ZDB-GENE-081028-33]	561457	234.2560	1.0006	0.1722	5.8119	0.0000	0.0001

Interestingly, of the 6 differentially expressed (DE) genes in *gch1^{+/-}*, 3 are also present in the *gch1^{-/-}* DE data. The first of which is aftiphilin b (ENSDARG0000071347), an ortholog of human aftiphilin (*AFTPH*). *AFTPH* is primarily expressed in the brain, and is a component of neuronal clathrin machinery (Burman et al., 2005); *AFTPH* is important in regulating content release of secretory organelles in the trans-golgi network (Lui-Roberts et al., 2008).

Additionally, in both *gch1^{-/-}* and *gch1^{+/-}* we see upregulation of retinol binding protein 1, cellular, tandem duplicate 2 (ENSDARG0000038742), an ortholog of human retinol binding protein 1, which is a carrier protein involved in the transport of retinol from the liver to peripheral tissue. The third common DE gene was si:ch211-236p5.2 (ENSDARG0000086256), a homologue of human *NLRC5*; *NLRC5* is an IFN-gamma-inducible activator of MHC class I genes (Meissner et al., 2010), and is thus implicated in initiating and regulating adaptive immune responses. It is interesting that the few DE genes common to

both homozygous and heterozygous groups include genes with functions related to protein trafficking and immune response - 2 pathways common to many sporadic PD risk genes.

In *gch1*^{-/-} 456 of 23,457 genes were differentially expressed (Supplementary table 2, Appendix) 342 of which were upregulated and 114 were down-regulated (Figure 33). *gch1* was identified as a downregulated gene in the *gch1*^{-/-} data, with a log₂FC of -1.27, consistent with our qPCR data confirming reduced mRNA levels (See Figure 9).

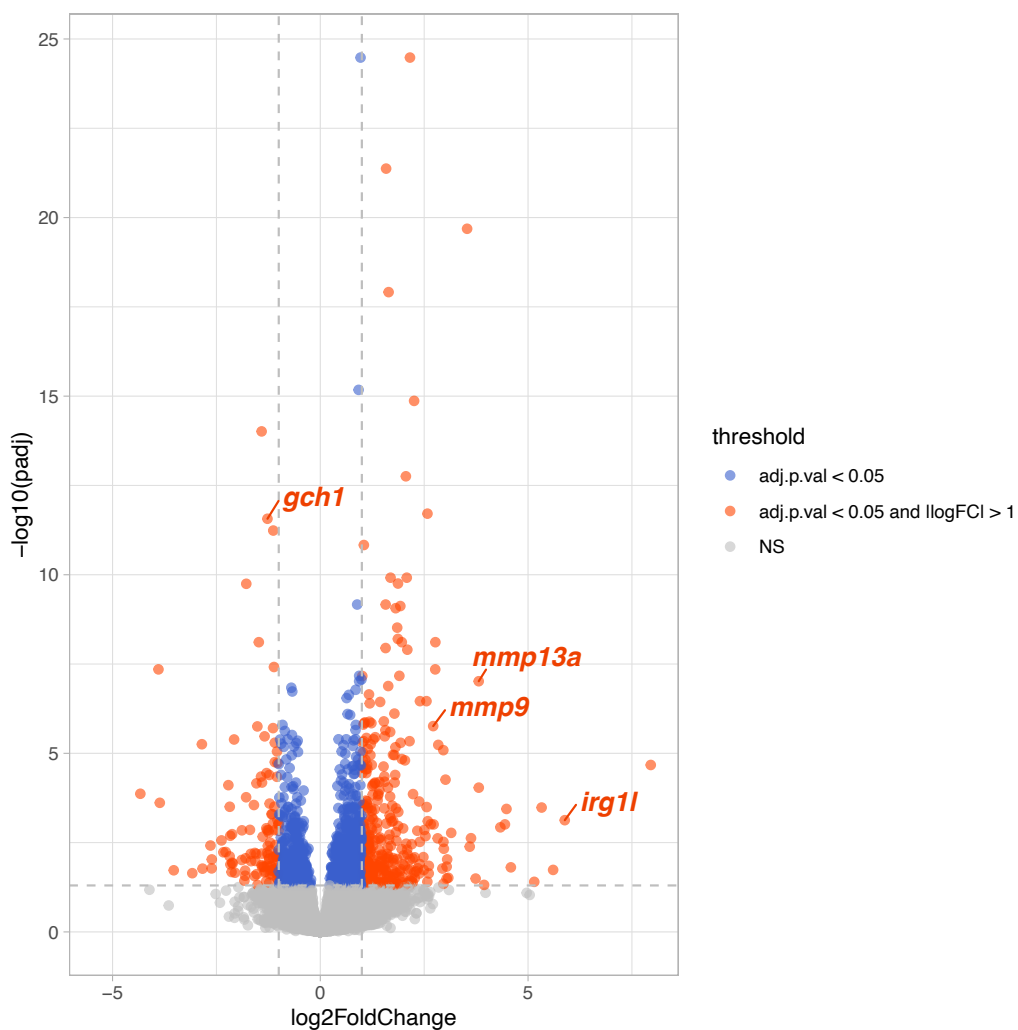


Figure 33: Volcano plot to illustrate DE genes in *gch1*^{-/-}. Upregulated and downregulated genes, with adjusted p value < 0.05 and $|\log_2FC| > 1$ are shown in red.

3.4.3. Pathway analysis

A novel pathway analysis approach was used to broadly analyse the complete transcriptome datasets for both *gch1^{+/-}* and *gch1^{-/-}* in comparison to the WT transcriptome. To summarise, transcripts were log-transformed and z-scaled to standardise values across the complete transcriptome dataset. Transcripts were then mapped to human orthologs or homologs, and assigned to pathways. Pathways were obtained from the Molecular Signature Database (MSigDB), and static modules were obtained from Pathprint (Altschuler et al., 2013). Static modules are “highly-connected modules from a functional-interaction network”, i.e. data-driven pathways, which are named according to the gene within the module with the most connections to other members. Each pathway was then summarised by a pathway-level expression score, which was calculated based on the top 50% of transcripts in a pathway, sorted by absolute t-statistic ($|t|$). Finally, differentially expressed pathways were analysed from pathway-level scores using limma (Ritchie et al., 2015). This method of analysis has the benefit of providing a more representative summary of the data, as individual genes within a pathway can show considerable variance even in biological samples with similar phenotype, however, orchestrated changes in expression of multiple genes within a pathway are likely to have more biological significance.

When analysing pathways, the following parameters were used to identify differentially expressed (DE) pathways: $\text{adj } p < 0.05$, $|\log_2\text{FC}| > 1$. Additionally, we excluded pathways with less than 50% gene conservation between human and zebrafish. Pathway analysis of the *gch1^{+/-}* data yielded no DE pathways. Contrastingly, 112 pathways were DE in *gch1^{-/-}* (Table 4), of which 64 were increased, and 48 decreased.

Table 4: Differentially expressed pathways in *gch1*^{-/-}. Pathways are ranked by log(Fold Change), from most increased to most decreased in expression. no_in_Hs refers to the total number of human (*Homo sapiens*) genes annotated under the corresponding pathway; no_in_data refers to the number of zebrafish orthologs/homologs of the human genes in the given pathway which were detected in the RNAseq. Conservation refers to the ratio of detected zebrafish transcripts in relation to the total number of human genes in the pathway. Pathways showing upregulation are highlighted in green; pathways showing downregulation are highlighted in red.

logFC	AveExpr	t	Pval	adjPval	pathway	no_in_Hs	no_in_data	conservation
1.7054	-1.22E-15	6.7376	0.0001	0.0151	REACTOME_ACTIVATION_OF_CHAPERONE_GENES_BY_ATF6_ALPHA	11	8	0.73
1.6868	-3.37E-17	5.9849	0.0002	0.0158	REACTOME_CYTOSOLIC_TRNA_AMINOACYLATION	24	24	1.00
1.6790	-1.19E-17	6.1962	0.0002	0.0151	EPRS_15_Static_Module	15	15	1.00
1.6781	-8.52E-16	6.1972	0.0002	0.0151	REACTOME_ACTIVATION_OF_CHAPERONES_BY_ATF6_ALPHA	13	10	0.77
1.6678	-2.07E-16	6.3330	0.0001	0.0151	REACTOME_AMINO_ACID_SYNTHESIS_AND_INTERCONVERSION_TRANSAMINATION	17	14	0.82
1.6304	-2.85E-17	5.5593	0.0004	0.0189	REACTOME_TRNA_AMINOACYLATION	42	40	0.95
1.6088	-2.85E-16	5.5883	0.0004	0.0189	MMP9_11_Static_Module	11	6	0.55
1.5980	1.90E-16	5.3229	0.0005	0.0189	BIOCARTA_EIF2_PATHWAY	11	10	0.91
1.5775	-5.25E-17	5.2335	0.0006	0.0189	BIOCARTA_RNA_PATHWAY	10	8	0.80
1.5621	-2.54E-16	7.1862	0.0001	0.0151	REACTOME_ACTIVATION_OF_GENES_BY_ATF4	26	22	0.85
1.5577	1.86E-16	7.4905	0.0000	0.0151	RAN_17_Static_Module	17	16	0.94
1.5491	-3.21E-16	6.7132	0.0001	0.0151	REACTOME_PERK_REGULATED_GENE_EXPRESSION	29	25	0.86
1.5403	1.35E-16	7.1908	0.0001	0.0151	REACTOME_AKT_PHOSPHORYLATES_TARGETS_IN_THE_CYTOSOL	12	10	0.83
1.5385	-1.74E-16	7.3157	0.0000	0.0151	REACTOME_OXYGEN_DEPENDENT_PROLINE_HYDROXYLATION_OF_HYPOXIA_INDUCIBLE_FACTOR_ALPHA	18	14	0.78
1.5085	9.17E-16	4.5419	0.0015	0.0239	BIOCARTA_EIF_PATHWAY	16	15	0.94
1.4870	1.01E-15	6.5168	0.0001	0.0151	HSP90AA1_18_Static_Module	18	16	0.89
1.4828	-1.70E-16	5.6337	0.0003	0.0189	KEGG_AMINOACYL_TRNA_BIOSYNTHESIS	41	39	0.95
1.4815	-7.01E-16	5.7699	0.0003	0.0187	REACTOME_ANTIGEN_PRESENTATION_FOLDING_ASSEMBLY_AND_PEPTIDE_LOADING_OF_CLASS_I_MHC	21	12	0.57
1.4804	5.27E-16	5.2042	0.0006	0.0189	BIOCARTA_NUCLEARRS_PATHWAY	15	8	0.53

1.4598	-3.57E-17	4.1778	0.0025	0.0261	BIOCARTA_RANKL_PATHWAY	14	9	0.64
1.4314	4.48E-16	4.1332	0.0026	0.0261	REACTOME_HDL_MEDIATED_LIPID_TRANSPORT	15	11	0.73
1.4155	-2.97E-16	5.3073	0.0005	0.0189	REACTOME_RNA_POL_III_TRANSCRIPTION_TERMINATION	19	17	0.89
1.3978	-3.01E-16	5.1794	0.0006	0.0189	REACTOME_RNA_POL_III_CHAIN_ELONGATION	17	16	0.94
1.3756	-3.45E-16	3.9945	0.0032	0.0280	BIOCARTA_IL22BP_PATHWAY	16	11	0.69
1.3754	2.67E-16	3.5849	0.0060	0.0381	ST_IL_13_PATHWAY	7	5	0.71
1.3727	2.54E-16	6.0893	0.0002	0.0154	REACTOME_AMINO_ACID_TRANSPORT_ACROSS_THE_PLASMA_MEMBRANE	31	26	0.84
1.3560	-8.72E-17	5.7978	0.0003	0.0187	EXOSC10_15_Static_Module	15	14	0.93
1.3493	1.03E-16	4.1609	0.0025	0.0261	KEGG_RENIN_ANGIOTENSIN_SYSTEM	17	10	0.59
1.3416	6.46E-16	5.5886	0.0004	0.0189	REACTOME_DOWNREGULATION_OF_ERBB2_ERBB3_SIGNALING	12	9	0.75
1.3239	8.05E-16	7.3649	0.0000	0.0151	BIOCARTA_SET_PATHWAY	11	8	0.73
1.2982	-2.38E-17	4.9755	0.0008	0.0202	REACTOME_GROWTH_HORMONE_RECEPTOR_SIGNALING	24	20	0.83
1.2910	-3.81E-16	5.2488	0.0006	0.0189	BIOCARTA_ARF_PATHWAY	17	14	0.82
1.2709	-1.96E-16	3.5157	0.0067	0.0401	BIOCARTA_IL10_PATHWAY	17	11	0.65
1.2461	1.54E-15	4.0832	0.0028	0.0267	REACTOME_MEMBRANE_BINDING_AND_TARGETTING_OF_GAG_PROTEINS	10	8	0.80
1.2207	-2.50E-16	3.6324	0.0056	0.0368	BIOCARTA_NFKB_PATHWAY	23	17	0.74
1.2176	1.28E-16	4.4594	0.0016	0.0243	REACTOME_MRNA_DECAY_BY_3_TO_5_EXORIBONUCLEASE	11	11	1.00
1.2155	-7.83E-17	4.9339	0.0008	0.0202	REACTOME_REGULATION_OF_HYPOXIA_INDUCIBLE_FACTOR_HIF_BY_OXYGEN	25	20	0.80
1.2071	-5.25E-16	3.6377	0.0056	0.0367	BIOCARTA_CD40_PATHWAY	15	11	0.73
1.2059	-1.10E-16	3.7967	0.0044	0.0325	REACTOME_ABACAVIR_TRANSPORT_AND_METABOLISM	10	6	0.60
1.2034	8.17E-16	6.1581	0.0002	0.0151	ESR1_24_Static_Module	24	21	0.88
1.1755	-2.93E-16	5.5293	0.0004	0.0189	PID_HIF1A_PATHWAY	19	18	0.95
1.1670	1.54E-15	4.7200	0.0011	0.0238	REACTOME_TRAF3_DEPENDENT_IRF_ACTIVATION_PATHWAY	14	9	0.64
1.1598	-3.19E-16	5.1334	0.0006	0.0189	KEGG_RNA_POLYMERASE	29	25	0.86
1.1417	-2.78E-17	4.2847	0.0021	0.0255	INS_35_Static_Module	35	30	0.86
1.1414	-1.65E-16	3.9853	0.0033	0.0281	REACTOME_SPHINGOLIPID_DE_NOVO_BIOSYNTHESIS	31	28	0.90

1.1389	5.15E-17	5.0518	0.0007	0.0196	REACTOME_DESTABILIZATION_OF_MRNA_BY_KSRP	17	14	0.82
1.1341	-8.19E-16	4.7008	0.0012	0.0238	BIOCARTA_P53HYPOXIA_PATHWAY	23	17	0.74
1.1341	2.06E-16	3.3172	0.0092	0.0455	REACTOME_REGULATION_OF_MRNA_STABILITY_BY_PROTEINS_THAT_BIND_AU_RICH_ELEMENTS	84	69	0.82
1.1227	-1.00E-16	4.6738	0.0012	0.0238	KEGG_PENTOSE_PHOSPHATE_PATHWAY	27	20	0.74
1.1194	-7.67E-16	4.3831	0.0018	0.0248	KEGG_PROTEIN_EXPORT	24	20	0.83
1.1164	-2.14E-16	4.3236	0.0020	0.0251	JUN_88_Static_Module	86	51	0.59
1.1145	1.96E-16	4.5710	0.0014	0.0238	BIOCARTA_IGF1MTOR_PATHWAY	20	17	0.85
1.1072	1.27E-16	4.6632	0.0012	0.0238	BIOCARTA_IL1R_PATHWAY	33	22	0.67
1.1062	2.40E-16	4.6416	0.0013	0.0238	BIOCARTA_TOLL_PATHWAY	37	26	0.70
1.0951	8.56E-16	4.1690	0.0025	0.0261	REACTOME_NEGATIVE_REGULATORS_OF_RIG_I_MDA5_SIGNALING	31	19	0.61
1.0612	4.36E-17	4.2565	0.0022	0.0258	BIOCARTA_HIF_PATHWAY	15	14	0.93
1.0595	6.34E-16	5.3922	0.0005	0.0189	PID_IL6_7_PATHWAY	47	35	0.74
1.0549	2.19E-16	4.3142	0.0020	0.0251	REACTOME_ENDOSOMAL_SORTING_COMPLEX_REQUIRED_FOR_TRANSPORT_ESCRT	27	22	0.81
1.0416	7.41E-16	5.5641	0.0004	0.0189	REACTOME_DOWNREGULATION_OF_TGF_BETA_RECEPTOR_SIGNALING	23	18	0.78
1.0405	7.93E-17	4.5148	0.0015	0.0242	REACTOME_PIP3_ACTIVATES_AKT_SIGNALING	29	23	0.79
1.0362	6.78E-16	5.0112	0.0008	0.0196	REACTOME_TGF_BETA_RECEPTOR_SIGNALING_ACTIVATES_SMADS	26	20	0.77
1.0195	1.96E-16	3.4946	0.0070	0.0403	SDC1_30_Static_Module	30	22	0.73
1.0174	8.72E-17	3.3419	0.0088	0.0453	REACTOME_METABOLISM_OF_RNA	330	219	0.66
1.0076	6.90E-16	3.7120	0.0050	0.0346	REACTOME_RIG_I_MDA5_MEDIATED_INDUCTION_OF_IFN_ALPHA_BETA_PATHWAYS	73	42	0.58
-1.0277	1.67E-16	-3.4892	0.0070	0.0404	REACTOME_GLUCAGON_TYPE_LIGAND_RECEPTORS	33	20	0.61
-1.0303	-8.25E-16	-4.2429	0.0022	0.0258	BIOCARTA_STATHMIN_PATHWAY	19	13	0.68
-1.0361	-2.58E-16	-4.6028	0.0013	0.0238	REACTOME_SHC_MEDIATED_CASCADE	28	20	0.71
-1.0427	-4.74E-16	-4.0692	0.0029	0.0269	REACTOME_ACTIVATION_OF_KAINATE_RECEPTORS_UPON GLUTAMATE_BINDING	31	22	0.71
-1.0496	-1.49E-17	-4.5958	0.0014	0.0238	REACTOME_NCAM_SIGNALING_FOR_NEURITE_OUT_GROWTH	64	55	0.86
-1.0555	-7.26E-16	-3.6170	0.0058	0.0370	PID_LPA4_PATHWAY	15	14	0.93
-1.0567	7.14E-16	-3.5045	0.0068	0.0401	KEGG_GLYCOSAMINOGLYCAN_BIOSYNTHESIS_HEPARAN_SULFATE	26	21	0.81

-1.0592	1.59E-17	-4.0336	0.0031	0.0272	REACTOME_INHIBITION_OF_INSULIN_SECRETION_BY_ADRENALINE_NORADRENALINE	25	18	0.72
-1.0593	5.67E-16	-5.2429	0.0006	0.0189	REACTOME_DOUBLE_STRAND_BREAK_REPAIR	24	19	0.79
-1.0711	-3.94E-16	-3.9396	0.0035	0.0295	REACTOME_N_GLYCAN_ANTENNAE_ELONGATION_IN_THE_MEDIAL_TRANS_GOLGI	18	17	0.94
-1.0855	1.11E-16	-6.0483	0.0002	0.0154	REACTOME_G1_S_SPECIFIC_TRANSCRIPTION	19	13	0.68
-1.0897	1.82E-16	-3.4088	0.0080	0.0430	NGF_31_Static_Module	31	24	0.77
-1.0936	-1.27E-16	-3.2625	0.0100	0.0487	REACTOME_POTASSIUM_CHANNELS	98	66	0.67
-1.0941	-3.59E-16	-4.6521	0.0013	0.0238	BIOCARTA_SHH_PATHWAY	16	15	0.94
-1.1032	-6.26E-16	-4.1336	0.0026	0.0261	REACTOME_INSULIN_SYNTHESIS_AND_PROCESSING	21	17	0.81
-1.1052	-7.93E-18	-4.0451	0.0030	0.0272	BIOCARTA_SKP2E2F_PATHWAY	10	7	0.70
-1.1280	-1.63E-16	-4.8847	0.0009	0.0210	REACTOME_FRS2_MEDIATED_CASCADE	36	28	0.78
-1.1281	-1.59E-17	-3.7485	0.0047	0.0335	KEGG_BASAL_CELL_CARCINOMA	55	50	0.91
-1.1295	2.50E-16	-4.1983	0.0024	0.0259	REACTOME_HS_GAG_BIOSYNTHESIS	31	22	0.71
-1.1526	5.63E-16	-4.5529	0.0014	0.0239	REACTOME_G0_AND_EARLY_G1	25	21	0.84
-1.1739	-4.80E-16	-5.1150	0.0007	0.0189	PID_WNT_SIGNALING_PATHWAY	28	24	0.86
-1.1773	-2.89E-16	-3.8163	0.0042	0.0320	REACTOME_INHIBITION_OF_VOLTAGE_GATED_CA2_CHANNELS_VIA_GBETA_GAMMA_SUBUNITS	25	17	0.68
-1.1917	-2.38E-16	-5.4665	0.0004	0.0189	REACTOME_NCAM1_INTERACTIONS	39	31	0.79
-1.2105	-2.54E-16	-3.4212	0.0078	0.0429	REACTOME_GABA_RECEPTOR_ACTIVATION	52	40	0.77
-1.2296	6.19E-16	-5.0115	0.0008	0.0196	REACTOME_HOMOLOGOUS_RECOMBINATION_REPAIR_OF_REPLICATION_INDEPENDENT_DOUBLE_STRAND_BREAKS	17	14	0.82
-1.2362	-6.42E-16	-4.0231	0.0031	0.0274	REACTOME_GABA_B_RECEPTOR_ACTIVATION	38	28	0.74
-1.2370	-7.02E-16	-3.5591	0.0063	0.0392	REACTOME_IONOTROPIC_ACTIVITY_OF_KAINATE_RECEPTORS	11	8	0.73
-1.2758	5.69E-16	-3.8008	0.0043	0.0325	RYR2_15_Static_Module	15	9	0.60
-1.2831	-4.28E-16	-3.3206	0.0091	0.0455	PID_REELIN_PATHWAY	29	26	0.90
-1.2835	-2.03E-15	-4.5403	0.0015	0.0239	REACTOME_SIGNALING_BY_FGFR3_MUTANTS	11	6	0.55
-1.2896	-7.14E-17	-5.3312	0.0005	0.0189	REACTOME_UNWINDING_OF_DNA	11	10	0.91
-1.3001	-2.10E-16	-3.6992	0.0051	0.0350	REACTOME_CASPASE_MEDIATED_CLEAVAGE_OF_CYTOSKELETAL_PROTEINS	13	10	0.77

-1.3093	-9.64E-16	-6.2841	0.0002	0.0151	REACTOME_FGFR_LIGAND_BINDING_AND_ACTIVATION	22	14	0.64
-1.3406	-4.68E-16	-5.1269	0.0007	0.0189	SA_FAS_SIGNALING	9	6	0.67
-1.3532	3.57E-17	-4.1648	0.0025	0.0261	OTX2_18_Static_Module	18	13	0.72
-1.3630	-1.15E-15	-5.1450	0.0006	0.0189	REACTOME_FGFR1_LIGAND_BINDING_AND_ACTIVATION	14	8	0.57
-1.3703	-6.34E-17	-5.0313	0.0007	0.0196	DVL1L1_17_Static_Module	17	12	0.71
-1.3935	-1.53E-15	-4.9248	0.0009	0.0202	REACTOME_SIGNALING_BY_ACTIVATED_POINT_MUTANTS_OF_FGFR1	11	6	0.55
-1.3935	-1.53E-15	-4.9248	0.0009	0.0202	REACTOME_FGFR4_LIGAND_BINDING_AND_ACTIVATION	12	6	0.50
-1.3993	1.51E-16	-6.9780	0.0001	0.0151	REACTOME_CDC6_ASSOCIATION_WITH_THE_ORC_ORIGIN_COMPLEX	11	9	0.82
-1.4069	7.06E-16	-3.7390	0.0048	0.0336	REACTOME_ROLE_OF_SECOND_MESSENGERS_IN_NETRIN1_SIGNALING	11	9	0.82
-1.4096	8.33E-16	-4.4589	0.0016	0.0243	RB1_11_Static_Module	11	8	0.73
-1.4171	-1.01E-15	-5.6346	0.0003	0.0189	REACTOME_ACTIVATED_POINT_MUTANTS_OF_FGFR2	16	10	0.63
-1.4325	-1.25E-15	-3.7590	0.0046	0.0335	SPTAN1_10_Static_Module	10	8	0.80
-1.4333	-6.86E-16	-3.7027	0.0050	0.0350	REACTOME_CRMP5_IN_SEMA3A_SIGNALING	14	14	1.00
-1.4378	4.76E-17	-5.2235	0.0006	0.0189	REACTOME_E2F_ENABLED_INHIBITION_OF_PRE_REPLICATION_COMPLEX_FORMATION	10	10	1.00
-1.4534	-1.24E-15	-5.3900	0.0005	0.0189	REACTOME_FGFR2C_LIGAND_BINDING_AND_ACTIVATION	12	7	0.58
-1.4682	8.66E-16	-5.3106	0.0005	0.0189	NRP1_11_Static_Module	9	9	1.00

Upregulated pathways in gch1^{-/-}

Upregulated pathways included tRNA aminoacylation, a static module centred on *mmp9*, HDL-mediated lipid transport, and regulation of hypoxia inducible factor alpha, among many others.

tRNA aminoacylation was a pathway that showed the most substantial upregulation in *gch1^{-/-}*, with the majority of the cytoplasmic aminoacyl tRNA synthetases (ARSs) showing significant upregulation in the mutant. While the primary role of ARSs is charging amino acids to their cognate tRNAs for protein synthesis, the ARS family have a wide range of non-canonical roles, including involvement in inflammatory response, angiogenesis and apoptosis (Yao and Fox, 2013). Additionally, mutation of several of the individual ARS genes is implicated in different subtypes of Charcot-Marie Tooth Syndrome, a heterogenous group of inherited neuropathies, which are characterised by progressive degeneration of sensory neuron and motor function, as a result of demyelination or axonal degeneration (Timmerman et al., 2014). To our knowledge, upregulation of the majority of tRNAs simultaneously hasn't been described in any pathologies or disease models, so drawing conclusions about this upregulation is challenging. While it may indicate increased levels of protein synthesis, it may also be a non-specific form of stress response.

Upregulation of matrix metalloprotease 9 (*mmp9*) and other matrix metalloproteases in this static module was of interest, due to the roles of matrix metalloproteases in both Parkinson's Disease and in neuroinflammation (Brkic et al., 2015). Within this static module, *mmp9*, *mmp13a* and *mmp14b* were all upregulated. *mmp9* and *mmp13a* are known to be infection-inducible transcripts in zebrafish, with ~20-fold increases in expression following *Listeria monocytogenes* infection (Shan et al., 2016). Furthermore, in mammalian MPTP-induced PD models, sustained upregulation of MMP9 is associated with microglial activation and DA cell death (Lorenzl et al., 2004, Annese et al., 2015). Upregulation of *mmp9* and other MMPs may thus be indicative of neuroinflammation and microglial activation in *gch1^{-/-}* larvae.

*Downregulated pathways in *gch1*^{-/-}*

The most downregulated pathway observed in *gch1*^{-/-} was a static module centred around neuropilin 1, a coreceptor to a tyrosine kinase receptor for both vascular endothelial growth factor and semaphorin; neuropilin 1 has roles in angiogenesis, axon guidance and cell survival (Schwarz and Ruhrberg, 2010). Other neuronal guidance-related pathways were also detected as downregulated, including CRMPs in SEMA3A signalling (Schmidt and Strittmatter, 2007), the Reelin signalling pathway (Rice and Curran, 2001), second messengers in netrin-1 signalling (Boyer and Gupton, 2018), and NCAM signalling for neurite outgrowth.

Several pathways involved in neurotransmission were also downregulated. Of these, GABA A and GABA B receptor activation, and ionotropic activation of kainite receptors were all significant. Dopamine, acetylcholine and norepinephrine release pathways were initially identified as significantly downregulated, however, did not reach significance when the pathway analysis pipeline was amended for the final time ($p = 0.055$). Inhibition of insulin secretion by adrenaline and noradrenaline was also downregulated, which was of interest for validation of the pathway analysis pipeline, given our finding of dramatically reduced levels of the aforementioned neurotransmitters (See figure 12-13).

We additionally detected downregulation of numerous pathways related to FGFR ligand signalling. FGFR signalling has roles in growth, cell proliferation, cell survival, angiogenesis and differentiation, however, dysregulation of FGFR pathways is also implicated in numerous cancers (Zhou et al., 2016). In addition, we detected downregulation of multiple pathways involved in cell cycle regulation – dysregulation of which is often cancer-linked (Stewart et al., 2003). Downregulated cell cycle pathways included CDC6 association with the ORC origin complex, G0 and early G1, and G1-S specific transcription, and DNA repair pathways, such as homologous recombination repair of replication-independent double strand breaks. The basal cell carcinoma KEGG pathway was additionally downregulated, indicating that some cancer-like transcriptional changes are occurring in *gch1*^{-/-}

3.4.4. Gene Ontology enrichment analysis

As an additional method of examining the transcriptional data, we performed gene ontology (GO) enrichment analysis to observe the biological processes (BP) showing dysregulation in *gch1*^{-/-}. We performed separate analyses for upregulated transcripts and downregulated transcripts, to identify the directionality by which biological processes are affected. Terms were considered to be significantly up/downregulated if adj p < 0.05.

Downregulated GO biological processes

GO enrichment analysis of the downregulated transcripts in *gch1*^{-/-} returned results that were almost exclusively related to cell cycle (Table 5, Figure 34), consistent with pathway analysis identifying multiple cell cycle regulation pathways. Few terms were also related to negative regulation of protein processing.

Table 5: GO enrichment analysis of downregulated transcripts in *gch1*^{-/-}.

ID	Description	GeneRatio	BgRatio	pvalue	p.adjust	qvalue	Count
GO:0000278	mitotic cell cycle	18/91	474/17011	5.39E-11	3.75E-08	3.40E-08	18
GO:0000226	microtubule cytoskeleton organization	13/91	314/17011	1.19E-08	4.14E-06	3.75E-06	13
GO:0007017	microtubule-based process	15/91	467/17011	2.46E-08	5.20E-06	4.72E-06	15
GO:0022402	cell cycle process	15/91	474/17011	2.99E-08	5.20E-06	4.72E-06	15
GO:1903047	mitotic cell cycle process	11/91	273/17011	2.26E-07	3.15E-05	2.86E-05	11
GO:1902850	microtubule cytoskeleton organization involved in mitosis	6/91	62/17011	9.58E-07	0.0001	0.0001	6
GO:0051301	cell division	8/91	215/17011	1.98E-05	0.0020	0.0018	8
GO:0008608	attachment of spindle microtubules to kinetochore	3/91	13/17011	4.07E-05	0.0034	0.0031	3
GO:0098813	nuclear chromosome segregation	6/91	120/17011	4.44E-05	0.0034	0.0031	6
GO:0007052	mitotic spindle organization	4/91	42/17011	7.34E-05	0.0051	0.0046	4
GO:0007051	spindle organization	5/91	83/17011	8.19E-05	0.0052	0.0047	5
GO:0007059	chromosome segregation	6/91	149/17011	0.0001	0.0086	0.0078	6
GO:0140014	mitotic nuclear division	5/91	106/17011	0.0003	0.0139	0.0126	5
GO:0044772	mitotic cell cycle phase transition	5/91	115/17011	0.0004	0.0188	0.0171	5
GO:0051726	regulation of cell cycle	9/91	435/17011	0.0005	0.0232	0.0210	9
GO:0044770	cell cycle phase transition	5/91	125/17011	0.0006	0.0232	0.0210	5
GO:0000070	mitotic sister chromatid segregation	4/91	71/17011	0.0006	0.0232	0.0210	4
GO:0051983	regulation of chromosome segregation	3/91	38/17011	0.0011	0.0422	0.0383	3
GO:0000280	nuclear division	5/91	150/17011	0.0013	0.0437	0.0397	5

GO:0051304	chromosome separation	3/91	41/17011	0.0014	0.0437	0.0397	3
GO:0000819	sister chromatid segregation	4/91	92/17011	0.0015	0.0437	0.0397	4
GO:0007076	mitotic chromosome condensation	2/91	11/17011	0.0015	0.0437	0.0397	2
GO:0010955	negative regulation of protein processing	2/91	11/17011	0.0015	0.0437	0.0397	2
GO:1903318	negative regulation of protein maturation	2/91	11/17011	0.0015	0.0437	0.0397	2
GO:0010564	regulation of cell cycle process	5/91	161/17011	0.0017	0.0465	0.0422	5
GO:0070613	regulation of protein processing	2/91	12/17011	0.0018	0.0465	0.0422	2
GO:1903317	regulation of protein maturation	2/91	12/17011	0.0018	0.0465	0.0422	2

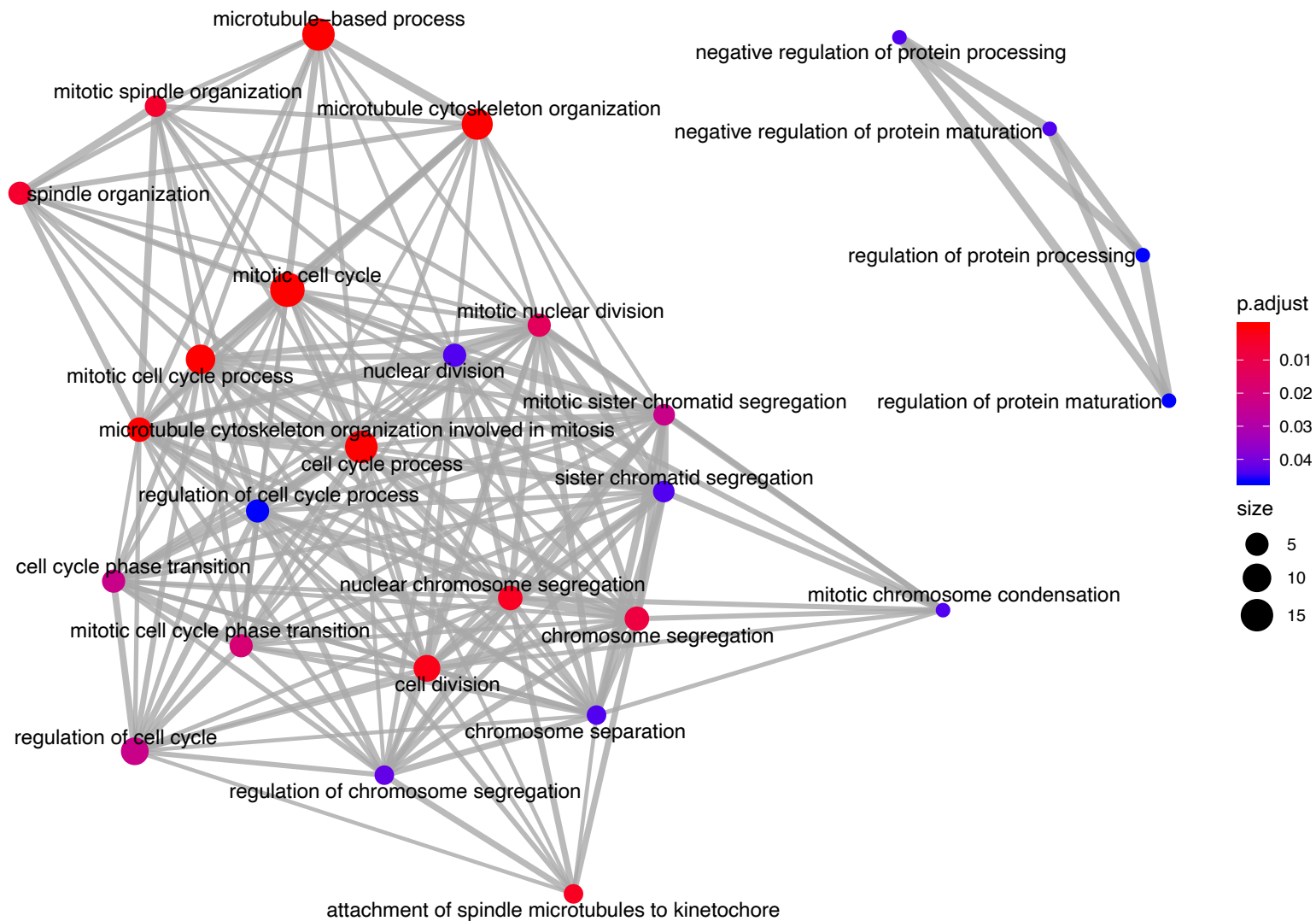


Figure 34: GO term clusters of downregulated genes in *gch1*^{-/-} reveals marked dysregulation of cell cycle-associated genes. Gene set enrichment analysis from *gch1*^{-/-} was analysed for GO term (biological process) enrichment vs WT control. Each node represents a gene set, and connections to linked nodes indicate similarity. Size of node represents number of genes within the gene set. GO terms of adj *p* < 0.05 are shown. The majority of downregulated transcripts are involved in cell-cycle regulation, in addition to few GO term clusters associated with protein processing.

Upregulated GO biological processes

The GO analysis of upregulated transcripts returned BP descriptions which could largely be categorised into 5 groups: organic acid biosynthetic process, stress/defence response, protein translation / tRNA aminoacylation, metabolism, and regulation of phosphorylation / kinase activity. In total, 40 GO terms were enriched (Table 6, Figure 35).

The increased expression of transcripts involved in both metabolic process and stress/defence response is consistent with recent findings in *Gch1*-KO murine macrophages, which demonstrate metabolic remodelling in the tricarboxylic acid (TCA) cycle, resulting in itaconate and succinate accumulation (Bailey et al., 2019). This metabolic remodelling was demonstrated to result in inflammatory macrophage activation, thus also providing a link between metabolism and immune activation.

We also detected large alterations in stress response genes, including *irg1l*, which showed a striking increase in expression of 5.88 log₂FC (~59.05 FC, adj p < 0.0001). *irg1l* has previously been shown to be upregulated in bacterially-infected or wounded zebrafish (Hall et al., 2014). Hall et al. demonstrated that *irg1l* promotes fatty acid uptake into the mitochondria, which then undergoes beta-oxidation to fuel production of mROS, which subsequently contributes to macrophage recruitment via *mmp9*-mediated extracellular matrix breakdown. mROS production has previously been identified as the key contributor to increased superoxide production in *Gch1*-depleted murine endothelial cells (Bailey et al., 2017), hence, we proposed that upregulation of *irg1l* may account for this elevated superoxide production. Furthermore, given that we have also identified upregulation of *mmp9*, amongst other matrix metalloproteases, upregulation of this pathway was of particular interest.

Table 6: GO enrichment analysis of upregulated transcripts in *gch1*^{-/-}. Upregulated biological processes largely fell into the following groups: organic acid biosynthetic process (green), stress/defense response (orange), protein translation / tRNA aminoacylation (red), metabolism (blue), and regulation of phosphorylation / kinase activity (purple).

ID	Description	GeneRatio	BgRatio	pvalue	p.adjust	qvalue	Count
GO:0006520	cellular amino acid metabolic process	19/245	225/17011	6.77E-10	9.10E-07	8.02E-07	19
GO:0006418	tRNA aminoacylation for protein translation	9/245	40/17011	4.27E-09	2.87E-06	2.53E-06	9
GO:0043038	amino acid activation	9/245	44/17011	1.05E-08	3.54E-06	3.12E-06	9
GO:0043039	tRNA aminoacylation	9/245	44/17011	1.05E-08	3.54E-06	3.12E-06	9
GO:0043171	peptide catabolic process	5/245	20/17011	7.73E-06	0.0021	0.0018	5
GO:0046942	carboxylic acid transport	10/245	128/17011	1.64E-05	0.0036	0.0032	10
GO:0015849	organic acid transport	10/245	130/17011	1.88E-05	0.0036	0.0032	10
GO:0015711	organic anion transport	12/245	200/17011	3.41E-05	0.0057	0.0051	12
GO:0046686	response to cadmium ion	4/245	15/17011	5.06E-05	0.0076	0.0067	4
GO:0006986	response to unfolded protein	5/245	38/17011	0.0002	0.0249	0.0220	5
GO:0051247	positive regulation of protein metabolic process	17/245	436/17011	0.0002	0.0249	0.0220	17
GO:0043405	regulation of MAP kinase activity	7/245	85/17011	0.0002	0.0251	0.0221	7
GO:0006399	tRNA metabolic process	9/245	148/17011	0.0003	0.0307	0.0271	9
GO:0032270	positive regulation of cellular protein metabolic process	16/245	414/17011	0.0003	0.0332	0.0292	16
GO:0006000	fructose metabolic process	3/245	11/17011	0.0004	0.0371	0.0327	3
GO:1901605	alpha-amino acid metabolic process	9/245	157/17011	0.0005	0.0371	0.0327	9
GO:0006820	anion transport	13/245	303/17011	0.0005	0.0371	0.0327	13
GO:0032147	activation of protein kinase activity	7/245	97/17011	0.0005	0.0377	0.0332	7

GO:0046394	carboxylic acid biosynthetic process	10/245	199/17011	0.0006	0.0421	0.0371	10
GO:0042558	pteridine-containing compound metabolic process	4/245	28/17011	0.0007	0.0421	0.0371	4
GO:0016053	organic acid biosynthetic process	10/245	201/17011	0.0007	0.0421	0.0371	10
GO:0019220	regulation of phosphate metabolic process	16/245	443/17011	0.0007	0.0421	0.0371	16
GO:0051174	regulation of phosphorus metabolic process	16/245	443/17011	0.0007	0.0421	0.0371	16
GO:0006458	'de novo' protein folding	4/245	29/17011	0.0008	0.0421	0.0371	4
GO:0010562	positive regulation of phosphorus metabolic process	12/245	283/17011	0.0009	0.0431	0.0380	12
GO:0045937	positive regulation of phosphate metabolic process	12/245	283/17011	0.0009	0.0431	0.0380	12
GO:0006952	defense response	14/245	365/17011	0.0009	0.0431	0.0380	14
GO:0006865	amino acid transport	5/245	53/17011	0.0010	0.0435	0.0383	5
GO:0007259	JAK-STAT cascade	4/245	31/17011	0.0010	0.0435	0.0383	4
GO:0097696	STAT cascade	4/245	31/17011	0.0010	0.0435	0.0383	4
GO:0044283	small molecule biosynthetic process	14/245	372/17011	0.0010	0.0435	0.0383	14
GO:0035966	response to topologically incorrect protein	5/245	54/17011	0.0011	0.0435	0.0383	5
GO:0042325	regulation of phosphorylation	15/245	416/17011	0.0011	0.0435	0.0383	15
GO:0046653	tetrahydrofolate metabolic process	3/245	15/17011	0.0012	0.0462	0.0407	3
GO:0009408	response to heat	4/245	33/17011	0.0012	0.0462	0.0407	4
GO:0034620	cellular response to unfolded protein	4/245	33/17011	0.0012	0.0462	0.0407	4
GO:0043549	regulation of kinase activity	10/245	219/17011	0.0013	0.0478	0.0422	10
GO:1902475	L-alpha-amino acid transmembrane transport	3/245	16/17011	0.0014	0.0496	0.0437	3
GO:2001243	negative regulation of intrinsic apoptotic signaling pathway	3/245	16/17011	0.0014	0.0496	0.0437	3

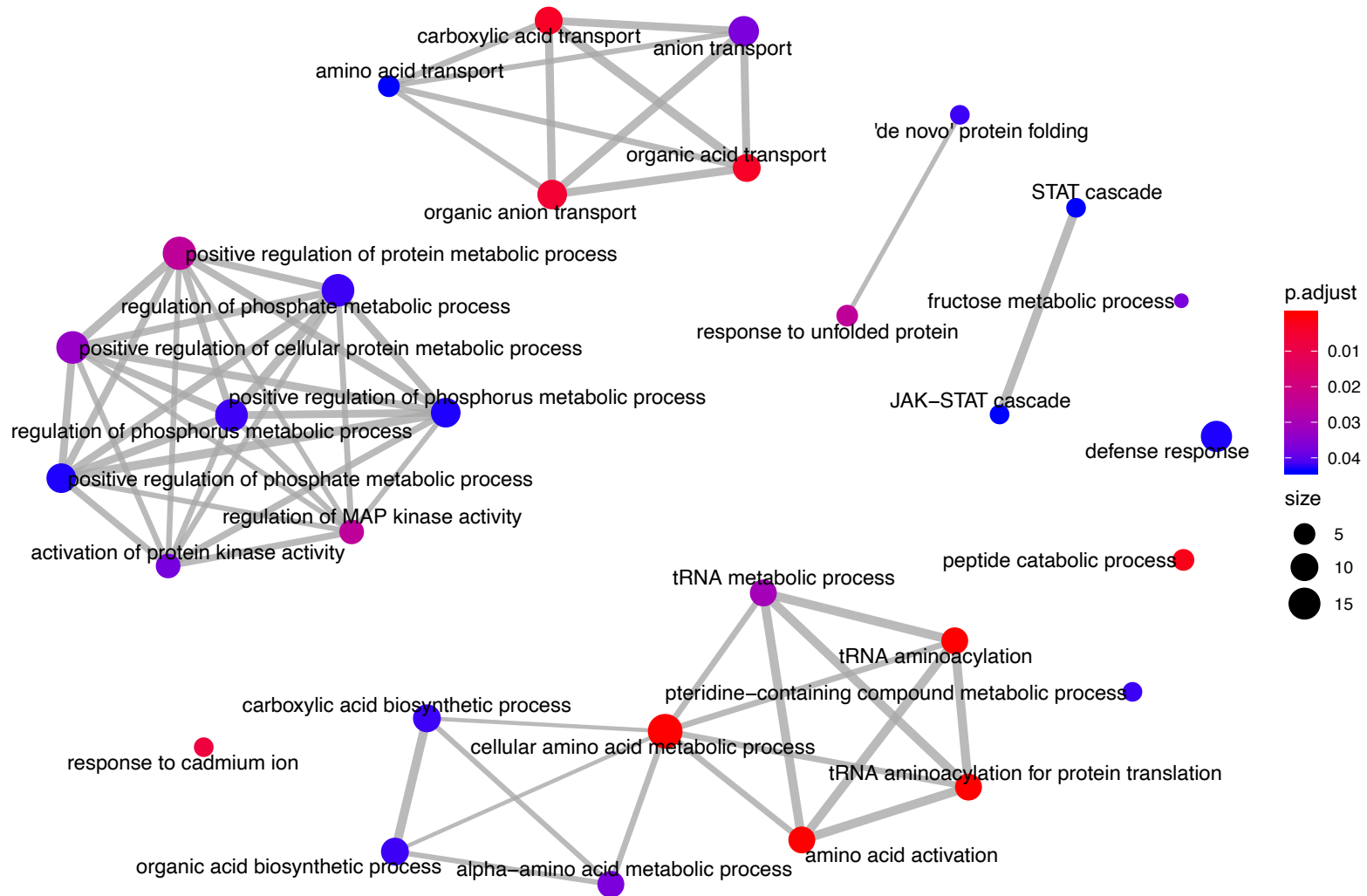


Figure 35: GO term clusters of upregulated genes in *gch1*^{-/-}. Gene set enrichment analysis from *gch1*^{-/-} was analysed for GO term (biological process) enrichment vs WT control. Each node represents a gene set, and connections to linked nodes indicate similarity. Size of node represents number of genes within the gene set. GO terms of adj *p* < 0.05 are shown. The majority of the upregulated GO terms could be grouped into clusters of the following: organic acid biosynthetic process, stress/defence response, protein translation / tRNA aminoacylation, metabolism, and regulation of phosphorylation / kinase activity.

3.4.5. Validation of upregulation of *irg1l*

The identification of *irg1l* as one of the most dramatically upregulated transcripts was of interest due to its involvement in inflammation, and potential to produce mROS and superoxides. To validate that this transcript shows the same magnitude of increased expression as observed in the RNAseq, we performed qPCR as an additional method to corroborate this result. We also sought to identify at what stage *irg1l* shows upregulation, in order to establish when inflammatory changes may be occurring in *gch1*^{-/-} larval development. We performed qPCR for *irg1l* on *gch1*^{-/-} and WT larvae at 3, 5 and 8 dpf. qPCR at 3 dpf showed no change in expression ($p = 0.9716$), however, by 5 dpf, a modest increase of 3.2-fold was observed in *gch1*^{-/-} ($p = 0.0340$, Figure 36). By 8 dpf, expression was increased 55.9-fold ($p = 0.0414$), consistent with the changes observed in the RNAseq data at this timepoint.

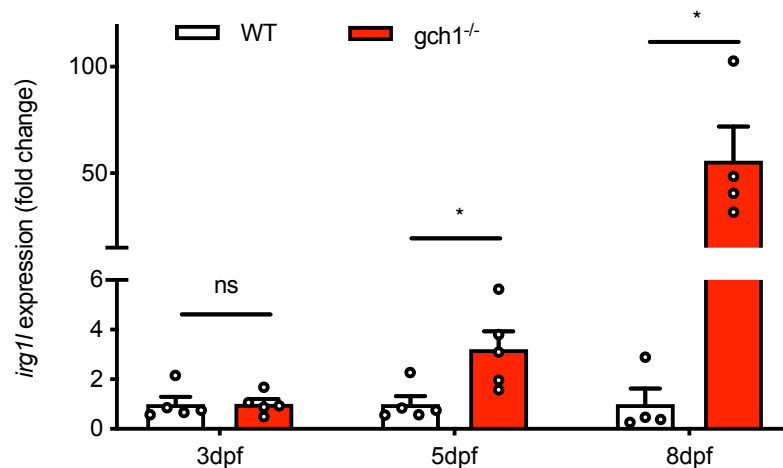


Figure 36: qPCR to quantify *irg1l* expression levels at 3, 5 and 8 dpf in *gch1*^{-/-} larvae. At 3 dpf no difference is observed ($p = 0.9716$, $n = 5$). At 5 dpf, *irg1l* is upregulated 3.2-fold ($p = 0.0340$, $n = 5$). At 8 dpf, *irg1l* is upregulated 55.9-fold ($p = 0.0414$, $n = 4$, Welch's 2-tailed t-test). Expression is normalized to WT. *ef1a* was used as a reference gene.

3.5. Microglial analysis

Microglia become activated in response to triggers such as tissue damage, infection or neurodegeneration. Upon activation, microglia undergo morphological changes, transcriptional changes and behavioural changes. Morphologically, microglia transition from a quiescent, ramified state to an amoeboid morphology (Karperien et al., 2013), accompanied by increased motility to the site of damage or infection.

We proposed that *gch1*^{-/-} would show signs of microglial activation, given our findings of increased expression of stress response genes in our GO enrichment analysis (Section 4.4). Furthermore, previous research in *Gch1*^{-/-} models has demonstrated altered inflammatory macrophage response (Bailey et al., 2019; McNeill et al., 2015, 2018).

As microglia become activated, they are known to show increased proliferative capacity (Kreutzberg, 1996; Li et al., 2013; Remington et al., 2007) and a change in morphology from a ramified to an amoeboid shape. We thus aimed to develop a method which would summarise the morphological status of the microglia, in addition to quantifying the number of microglia per fish.

Few markers are able to differentiate microglia from macrophages, due to their shared lineage and functional similarity. For example, *mpeg1*;mCherry is a commonly used zebrafish transgenic line for labelling macrophages, but is unable to differentiate between macrophages and microglia. However, α -4c4 is a mouse monoclonal antibody highly specific to microglia, without labelling additional cell types in the brain (Becker and Becker, 2001; Chia et al., 2018; Ohnmacht et al., 2016; Tsarouchas et al., 2018). We sought to validate this as a microglial marker and use it for characterisation of the phenotype of *gch1*^{-/-} microglia.

3.5.1. Validating microglial specific staining with α -4c4

To verify the validity of using a 4c4 antibody to stain microglia, we initially performed 4c4 immunostaining on *mpeg1*;mCherry larvae to observe the distribution of 4c4 staining in comparison to the macrophage reporter. 4c4 staining was restricted to the CNS, whereas *mpeg1*;mCherry was observed in all 4c4+ cells, in addition to peripheral macrophages. No

4c4 signal was detected in mpeg-negative cells (Figure 37). Hence, we concluded that 4c4 is a valid marker for microglia. Microglia were observed to show localisation mostly to the regions of the optic tectum with high density of neuronal cell bodies, i.e. along the midline, and anterior to the optic tectum-cerebellum boundary. Distribution throughout the telencephalon was observed, and few microglia were also observed in the cerebellum.

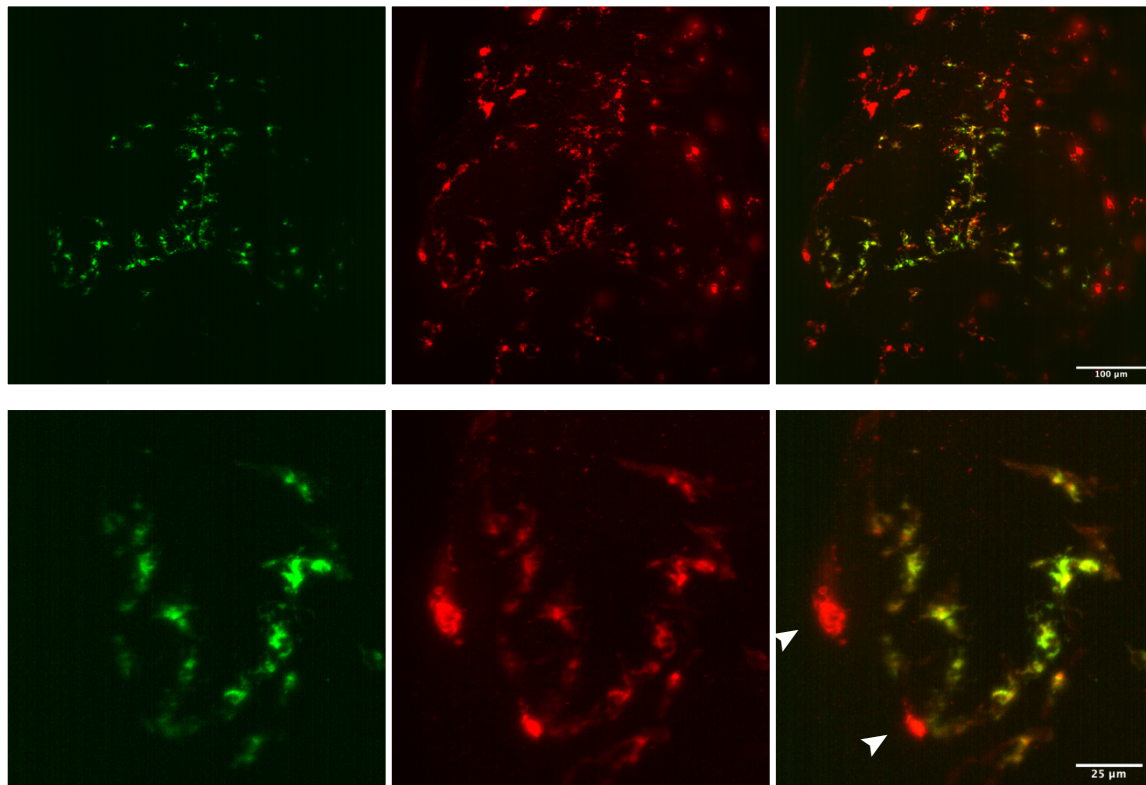


Figure 37: Comparison of microglial specificity of mpeg-mCherry and 4c4 immunostain. Co-immunostaining of mpeg-mCherry larvae (red) with anti-4c4 (green) demonstrates that all 4c4+ cells are mpeg+, while some peripheral mpeg+ cells are 4c4-negative. Upper panel shows dorsal view of zebrafish brain, scale bar = 100 μ m. Lower panel depicts a cluster of microglia (4c4+, mpeg+), and 2 macrophage cells (arrow, mpeg+, 4c4-negative). scale bar = 25 μ m.

3.5.2. High throughput imaging of 4c4-stained larvae for microglial analysis

We used the Perkin Elmer Opera Phenix high-throughput confocal imaging system to image 4c4-immunostained larvae at 8 dpf. The Opera Phenix is a plate-based imaging system, which enabled us to mount up to 96 samples in a plate for each imaging session. Once mounted, samples could be automatically detected based on user-defined parameters, allowing for largely automated imaging of the larvae with a fast turnover. The images produced by the Opera Phenix with a 20X optical lens produced images with a depth of field clear enough to count microglia throughout the whole brain, and assess morphology in the

majority of these cells. We thus performed counting of the microglia across WT, *gch1*^{+/-} and *gch1*^{-/-}. We additionally opted to perform a simplified method of quantifying microglial activation, in which we simply counted the number of completely amoeboid cell types, as previously described (Chia et al., 2018), and calculated the percentage of cells showing amoeboid morphology.

Quantification of microglial number per fish revealed no change in number by genotype, indicating that microglia are not proliferating in *gch1*^{-/-} (Figure 38).

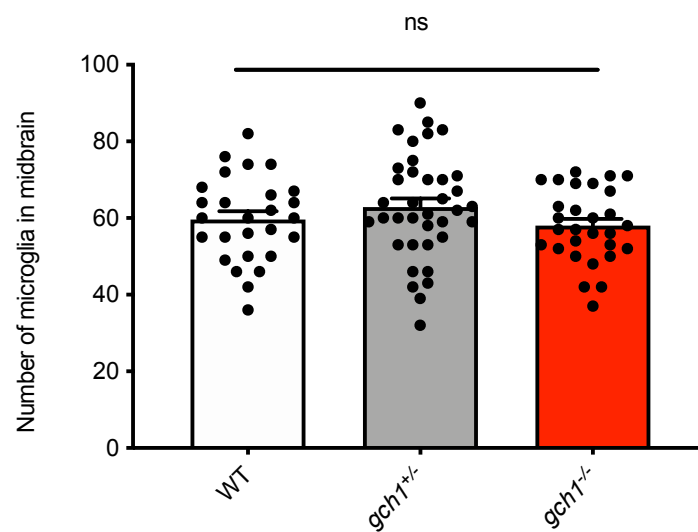


Figure 38: Microglial counts, 8dpf. Quantification of the number of microglia in the midbrain reveals no difference between *gch1*^{-/-} and WT (WT *n* = 27, *gch1*^{+/-} *n* = 37, *gch1*^{-/-} *n* = 29, one-way ANOVA).

Analysis of the percentage of microglia in the brain exhibiting amoeboid morphology, however, did show an increase in the percentage of amoeboid cells in *gch1*^{-/-} vs WT (Figure 39). Interestingly, *gch1*^{-/-} larvae still demonstrated high levels of heterogeneity in their activation state, with the majority of larvae showing similar levels of activation to WT, while some *gch1*^{-/-} showed heightened levels of amoeboid numbers.

3.5.3. Functional assessment of microglial activity by quantifying phagocytic efficiency of zymosan engulfment

Having established that microglia show increased numbers of amoeboid cells, we also sought to assess whether microglia are functionally more active in *gch1*^{-/-} than WT. We opted to use zymosan to induce sterile inflammation in the brain and promote microglial phagocytic activity. Zymosan is an immunogenic yeast cell wall particle, commonly used to induce sterile inflammation in animal models. It is most commonly used to induce short-term, self-resolving peritonitis in mammalian models, including mice (Rao et al., 1994), rats (Zagorski and Wahl, 1997), and rabbits (Forrest et al., 1986), however, its use has also been documented for modelling traumatic brain injury in adult zebrafish (Kyritsis et al., 2012). Additionally, it has been used in adult zebrafish to stimulate an immune response and aid the regeneration of dopaminergic cells following ablation (Caldwell et al., 2019). Macrophages respond to zymosan by phagocytosing the immunogenic particles, and as a result, measurement of phagocytosis of fluorescein-conjugated zymosan has been established as a useful method to determine macrophage phagocytic activity (Suzuki et al., 1988). We injected a fluorescently-tagged zymosan preparation into the optic tectum at 5 dpf to stimulate activation of microglia and induce phagocytic engulfment of the zymosan particles. We subsequently fixed and immunostained samples with anti-4c4 at 6h post-injection, enabling us to visualise phagocytosed particles of zymosan (Figure 41).



Figure 41: Zymosan engulfment by microglia, representative image. Immunostaining of the zymosan-injected larvae shows zymosan (cyan) phagocytosed by microglia (4c4). Scale bar = 50 μ m.

Analysis of the phagocytosed particles (assessed by scrolling through 3D immunofluorescent images of microglia and zymosan) revealed a significant increase in the phagocytic activity of *gch1*^{-/-} microglia in comparison to WT or *gch1*^{+/-} ($p = 0.0279$, Figure 42), indicating that *gch1*^{-/-} microglia are more responsive to immune insult and are capable of clearing foreign cells with increased efficiency.

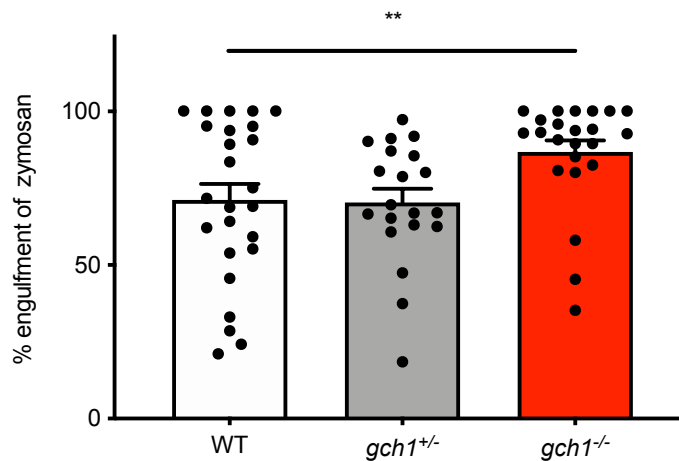


Figure 42: Quantification of phagocytic engulfment of zymosan. Phagocytic efficiency is elevated in *gch1*^{-/-}, with 86.8% of zymosan phagocytosed 6h post-injection, compared to 71.1% in WT ($p = 0.0096$, WT $n = 25$, *gch1*^{+/-} $n = 20$, *gch1*^{-/-} $n = 23$, Kruskal-Wallis test). "n" refers to an individual larva; larvae were obtained from at least 3 sets of independent mating pairs. Error bars show SEM.

In addition to analysing phagocytic activity, we assessed microglial number in response to zymosan injection, to observe whether zymosan would induce proliferation in comparison to a PBS control injection. We observed no difference in number of microglia between different genotypes (consistent with previous observations performed at 8 dpf), nor did we observe alterations in microglial count between zymosan and PBS controls (Figure 43), suggesting that zymosan does not induce proliferation of the microglia.

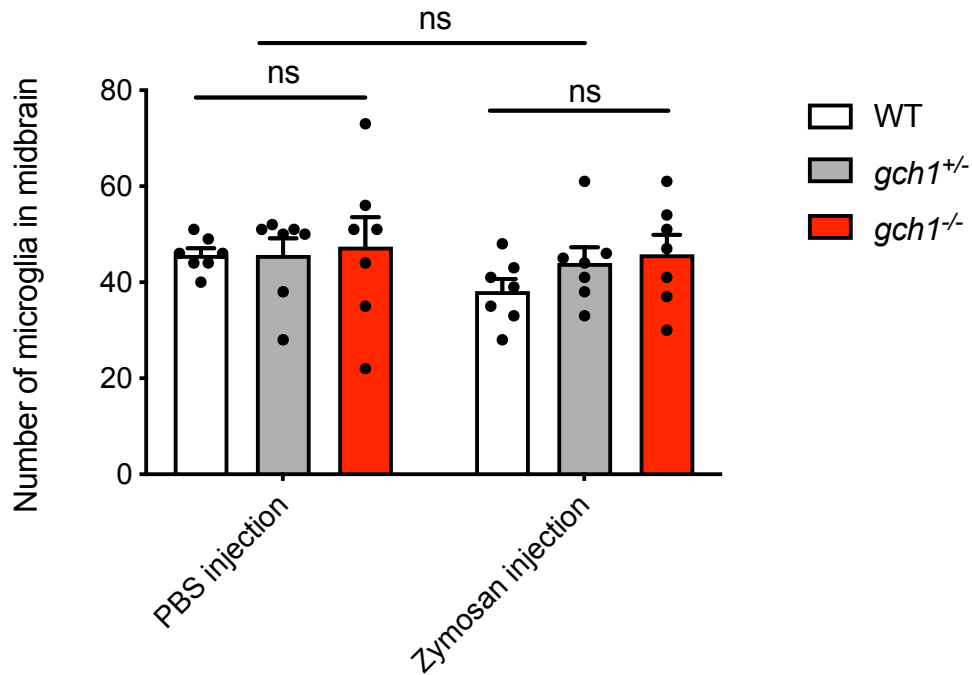


Figure 43: Counting of microglia in zymosan- vs PBS-injected samples. Microglial number was not affected by genotype or by injection-type ($n = 7$ per group, 2-way ANOVA)

We additionally assessed the percentage of microglia demonstrating amoeboid morphology in response to zymosan injection or PBS injection at 5 dpf. Genotype conferred no changes in the percentage of amoeboid cells at this 5dpf timepoint ($p = 0.6158$), in contrast to our finding of microglial activation at 8dpf (Figure 39). However, injection of zymosan resulted in significantly more cells exhibiting amoeboid morphology than the PBS controls ($p < 0.0001$, Figure 44).

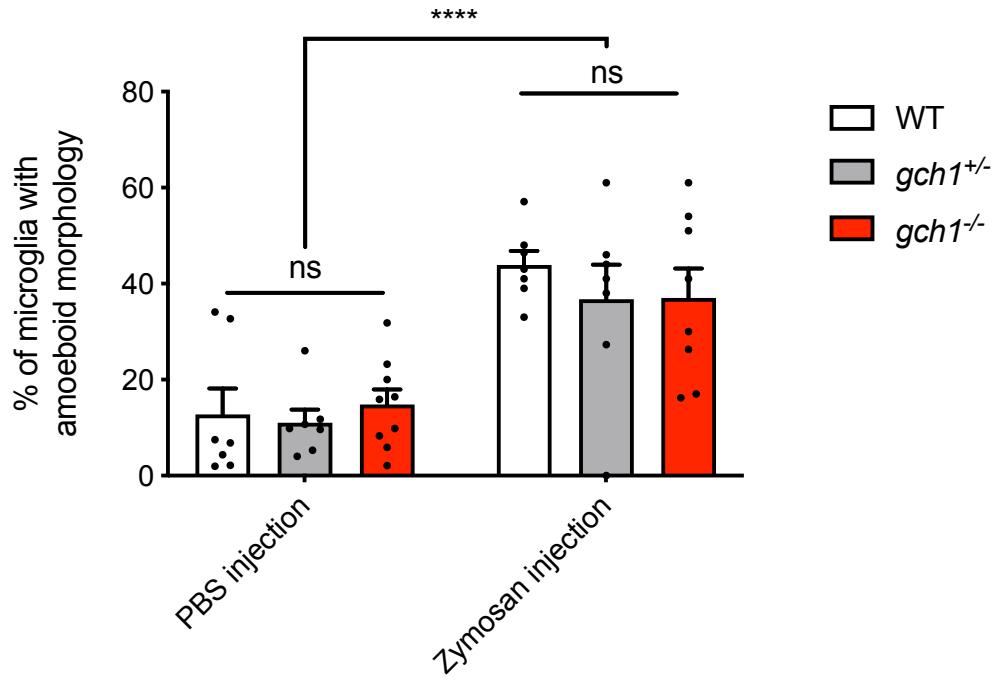


Figure 44: Microglial activation in response to zymosan injection. Analysis of % of microglia with amoeboid morphology revealed no difference by genotype ($p = 0.6158$), however, zymosan injection resulted in a higher percentage of amoeboid microglia than PBS injection ($p < 0.0001$, $n = 7$ per group, 2-way ANOVA).

3.6. Effect of targeted drug treatments on *gch1*^{-/-} survival

We sought to use our findings from RNAseq data and observations from previous experiments to guide our choice of therapeutic options for treating *gch1*^{-/-} larvae. We did this with the aim of identifying whether certain drugs would rescue the hypoactive movement phenotype, or prolong the survival of *gch1*^{-/-}; we hoped that finding drugs that could modify survival would also give insight into the mechanism leading to mortality. To assess the effect of each drug on the overall health of the fish, we used survival as a readout; larvae were culled if showing signs of infirmity, which was primarily assessed by behavioural response to a tail-fin touch, which would normally evoke an escape response in a healthy fish. Larvae showing a weak response to touch were culled (i.e. this was considered a “death” in terms of survival analysis).

In order to optimise drug doses for each treatment, we performed drug toxicity trials on WT larvae, and selected the highest tolerated dose in order to avoid non-specific toxicity of drugs. The highest tolerate dose was subsequently use for treatment on *gch1*^{-/-} to assess the effect on survival.

3.6.1. Sepiapterin treatment fails to modify survival in *gch1*^{-/-}

Our initial aim was to supplement BH4 production in *gch1*^{-/-}, with the expectation that this would rescue BH4 levels and other downstream factors, including dopamine, serotonin, noradrenaline and adrenaline levels. However, BH4 supplementation itself is challenging, as the substance is easily oxidised. Sepiapterin, or 2-amino-6-[-2-hydroxypropanoyl]-7,8-dihydro-1H-pteridin-4-one, is a more stable molecule, and can be metabolised into tetrahydrobiopterin via the salvage pathway. Additionally, sepiapterin is more permeable, allowing transport of the substance across cell membranes (Smith et al., 2019). Sepiapterin has been tested in a Phase I clinical trial (Smith et al., 2019), with no serious adverse effects reported; results indicated that sepiapterin was rapidly converted to BH4 and was able to increase plasma BH4 levels to 1.7-1.8-fold, or more in fasted subjects, with no long term accumulation of the drug in blood plasma.

We performed a dose toxicity assessment from 1-5 dpf in WT larvae, with doses of 1mM, 500 μ M, 100 μ M, and a DMSO-only control; 0.5% DMSO was used in each treatment, to aid permeability of the drug. 6 fish per treatment were maintained in individual wells of a 96-well plate, and media was changed daily. A 33% drop off in survival was observed at 2 dpf in 1mM-treated larvae, and a 17% drop in survival was observed at 2 dpf in 100 μ M and 500 μ M-treated larvae (Figure 45). Overall, no groups showed a significant change in survival ($p = 0.5125$), likely because the experiment was underpowered. However, we opted to perform future experiments with a 100 μ M dose of the drug, due to limited availability of the substance.

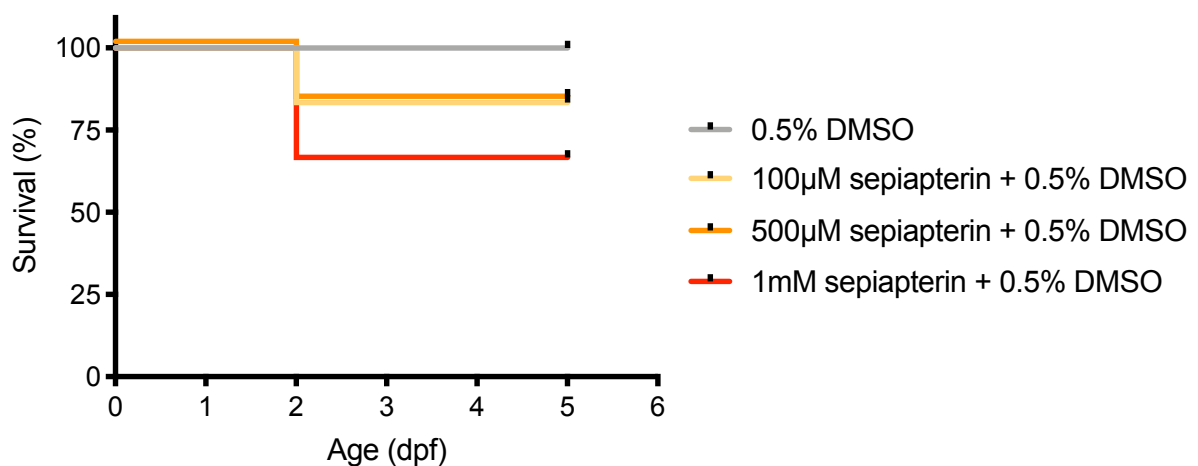


Figure 45 Sepiapterin toxicity assessment. A range of concentrations from 100 μ M to 1mM were trialled on WT larvae to assess toxicity. No difference was observed between survival of any groups ($p = 0.5125$, $n = 6$ per group, Mantel-Cox Log-rank test).

To assess the effect of sepiapterin on survival of *gch1*^{-/-}, larvae were maintained in 96-well plates, with 100 μ M sepiapterin applied from 1 dpf, and larvae were genotyped by fin-biopsy at 3 dpf. Only WT and *gch1*^{-/-} larvae were maintained after this time. At 5 dpf, larvae were transferred to 24-well plates. Sepiapterin conferred no effect on survival of *gch1*^{-/-} ($p = 0.0813$), with a median survival time of 11 dpf in both treated and untreated larvae (Figure 46). However, it should also be noted that treated and untreated WT larvae showed significantly different survival curves ($p = 0.0298$), with sepiapterin-treated larvae showing a drop-off in survival from 12 dpf, and only 22% remaining healthy at 13 dpf. Untreated larvae also showed a slight drop off at 13 dpf, with 67% remaining healthy. Reduced survival in the WT groups indicates husbandry issues with this experiment, possibly as a result of keeping

fish in relatively small plates over 10 dpf. Despite husbandry issues, it seems clear that sepiapterin was not conferring any benefit to *gch1*^{-/-} larvae.

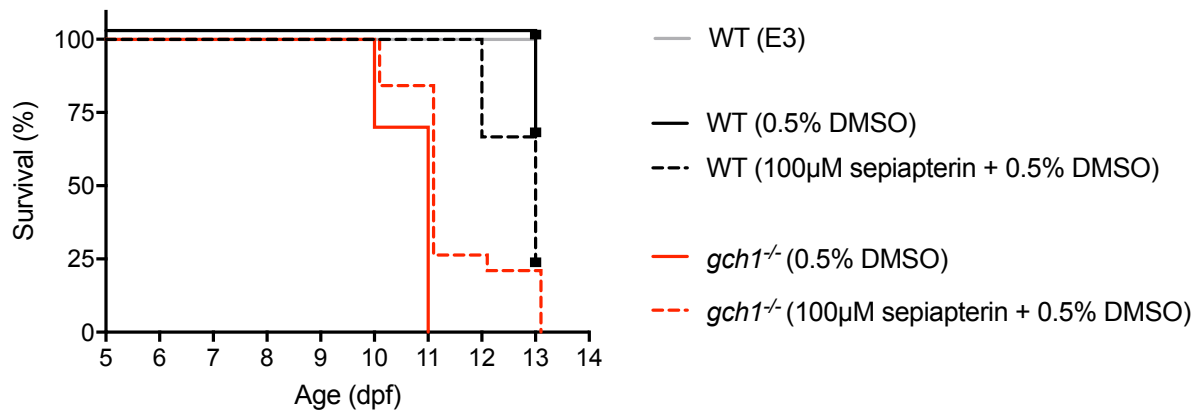


Figure 46: *Sepiapterin treatment.* Treatment of *gch1*^{-/-} with 100 µM sepiapterin from 1 dpf conferred no survival advantage over DMSO control ($p = 0.0813$, *gch1*^{-/-} DMSO $n = 10$, *gch1*^{-/-} sepiapterin-treated $n = 19$, Mantel-Cox Log-rank test). *Sepiapterin-treated WT* showed a significant reduction in survival compared to DMSO-treated WT ($p = 0.0298$, WT DMSO $n = 11$, WT sepiapterin-treated $n = 9$).

3. 6.2. L-DOPA treatment prolongs survival but does not ameliorate hypoactive motor phenotype

We have already demonstrated that deletion of *gch1* results in drastically reduced levels of catecholamines, and additionally reduced levels of Th protein levels. Given that AADC catalyses dopamine from L-DOPA, without the requirement for Th, we proposed that treatment of *gch1*^{-/-} with L-DOPA should theoretically rescue dopamine levels, in addition to raising adrenaline and noradrenaline levels, which use dopamine as a precursor, and should thus improve survival and movement behaviour.

Toxicity testing of a range of concentrations up to 1 mM revealed no difference in the survival of WT larvae when treated from 1-12 dpf ($p = 0.4085$, Figure 47). We thus opted to use a dose of 1 mM for future experiments.

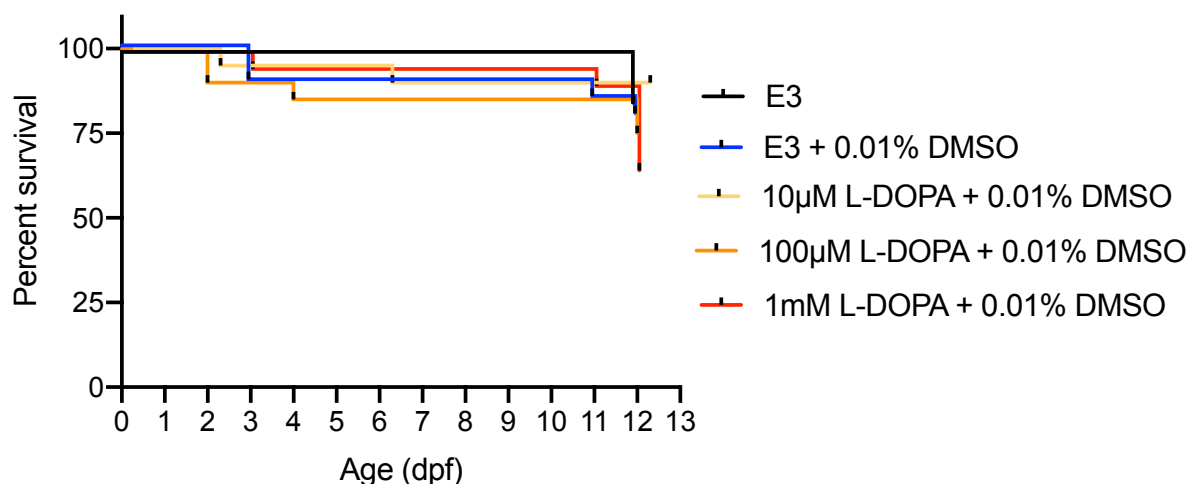


Figure 47: L-DOPA toxicity test. Doses from 10 µM to 1 mM L-DOPA from 1-12 dpf resulted in no changes in survival between groups ($p = 0.4085$, $n = 20$ per group, Mantel-Cox Log-rank test)

We initially assessed survival of *gch1*^{-/-} when treated with L-DOPA. Survival was observed over 2 separate experiments blinded to genotype, each with 3 independent clutches of larvae. Each clutch was separated into 2 petri-dishes, with a maximum of 50 larvae per plate. At 1 dpf treatment was applied to one plate, or a DMSO control solution applied to the other. Survival was monitored from 5 dpf onwards, due to the absence of a *gch1*^{-/-} phenotype until this time, and due to non-specific lethality sometimes occurring during early stages of development. Larvae were culled if displaying a weak (or complete lack of)

response to touch. Median survival time increased from 8 dpf to 10 dpf in the treated *gch1*^{-/-} larvae ($p = 0.0002$), indicating a partial rescue, however, it was evident that *gch1*^{-/-} larvae still showed reduced survival in comparison to their WT sibs ($p < 0.0001$, Figure 48). L-DOPA had no effect on survival of WT larvae in comparison to E3 treatment, however, the DMSO-control group showed modestly reduced survival compared to E3-treated ($p = 0.0040$) and L-DOPA treated WT ($p = 0.0048$).

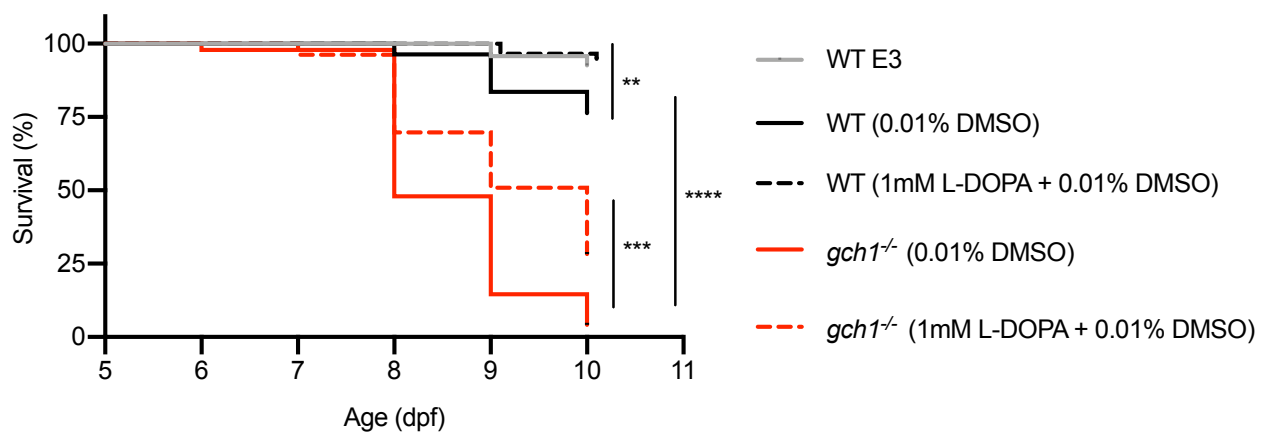


Figure 48: Survival analysis of L-DOPA-treated *gch1*^{-/-}. Treatment of *gch1*^{-/-} with 1mM L-DOPA improved survival in comparison to DMSO control ($p = 0.0002$, *gch1*^{-/-} DMSO $n = 48$, *gch1*^{-/-} L-DOPA $n = 53$, Mantel-Cox Log-rank test), and improved median survival time from 8 dpf to 10 dpf. L-DOPA-treated WT showed no change in survival vs E3-treated WT, however, DMSO-treated WT showed a reduction in survival compared to E3-treated WT and L-DOPA treated WT ($p = 0.0040$ and 0.0048 respectively, WT DMSO $n = 55$, WT L-DOPA $n = 58$, WT E3 $n = 95$). Both *gch1*^{-/-} groups had reduced survival compared to WT groups ($p < 0.0001$, Mantel-Cox Log-Rank test). Results were obtained over 2 separate experiments.

We subsequently assessed movement of larvae at 8 dpf, to identify whether treatment with L-DOPA would improve the hypoactivity phenotype in *gch1*^{-/-}. Larvae were treated with 1mM L-DOPA from 1 dpf onwards, and movement was analysed at 8 dpf. Larvae were subjected to 5 min cycles of light and dark, and distance travelled within each 5 min period was quantified. Treatment of WT larvae with L-DOPA resulted in no change in movement behaviour ($p = 0.6828$), indicating that the selected dose of L-DOPA was not resulting in toxicity in WT larvae. Treatment of *gch1*^{-/-} larvae showed no significant improvement in activity (Figure 49-Figure 50), with a non-significant increase in distance travelled from 445mm to 540mm on average for each 5 minute interval ($p = 0.0665$). Movement of treated and untreated *gch1*^{-/-} was significantly lower than WT levels ($p < 0.0001$), with untreated

WT travelling on average 889 mm over a 5 minute period, indicating that supplementation of L-DOPA was insufficient to rescue behavioural defects.

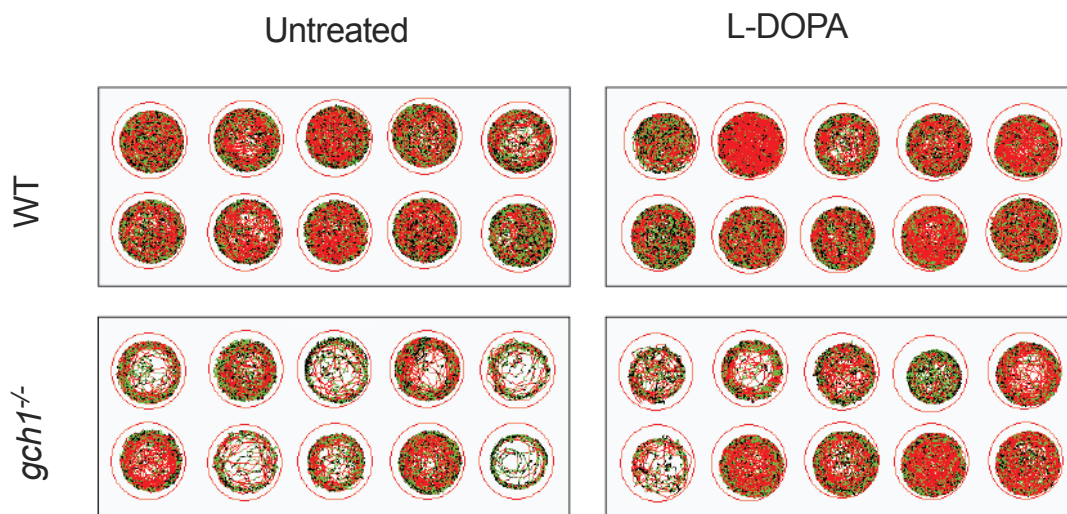


Figure 49: Representative movement trace from L-DOPA treatment. Traces were obtained from the first 5 minute period of behavioural tracking of L-DOPA treated *gch1*^{-/-} and WT larvae at 8 dpf.

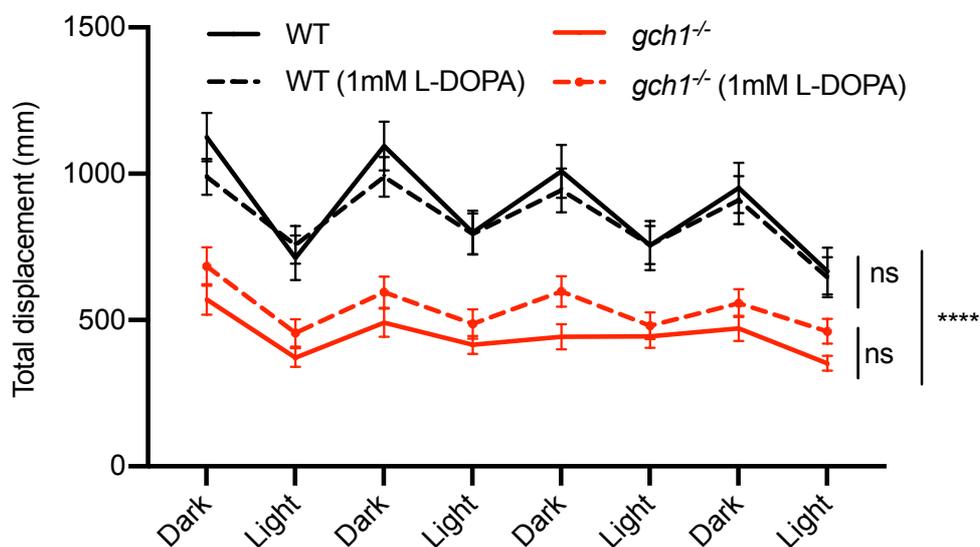


Figure 50: Movement analysis of L-DOPA-treated larvae from a *gch1*^{+/-} incross at 8 dpf. L-DOPA treated WT larvae ($n = 32$) showed equivalent movement for each 5 minute bout as untreated WT ($n = 35$, $p = 0.6828$). L-DOPA-treated *gch1*^{-/-} ($n = 37$) failed to show increased movement in comparison to DMSO-control *gch1*^{-/-} ($n = 38$, $p = 0.0665$). Both treated and untreated *gch1*^{-/-} larvae show markedly reduced movement in comparison to their WT sibs ($p < 0.0001$). (2-way ANOVA with 8 repeated measures; Bonferroni adjusted p -value significance threshold = 0.0125). Results were obtained over >2 separate experiments.

3. 6.3. Etomoxir treatment has no effect on *gch1*^{-/-} survival

We hypothesised that increased fatty acid metabolism due to upregulation of *irg1l*, and the downstream effects in the mitochondria including mROS production, may be contributing to lethality in *gch1*^{-/-}. Etomoxir acts as an inhibitor of carnitine palmitoyltransferase I (CPT1), and has previously been used in zebrafish to inhibit uptake of fatty acids into the mitochondria via the Cpt1a transporter (Hall et al., 2014). We proposed that treatment of *gch1*^{-/-} with etomoxir may improve the survival by inhibiting the downstream effects of *irg1l*.

Previous experiments in zebrafish have utilised etomoxir at a dose of 100 μ M and 10 μ M, however, only for 1-2h treatment periods (Hall et al., 2014). To determine a suitable dose for a prolonged treatment, we performed a toxicity assessment from 5 dpf to 10 dpf in WT larvae. Treatment from 5 dpf was selected due to upregulation of *irg1l* only occurring from this stage onwards. Doses of 1 μ M and 10 μ M were tested with 1% DMSO, alongside DMSO and E3 controls. 100% toxicity was observed at 7 dpf in the 10 μ M treatment group ($p < 0.0001$), whereas 1 μ M showed no signs of toxicity (Figure 51), hence, we opted to use 1 μ M etomoxir for treatment of *gch1*^{-/-} larvae.

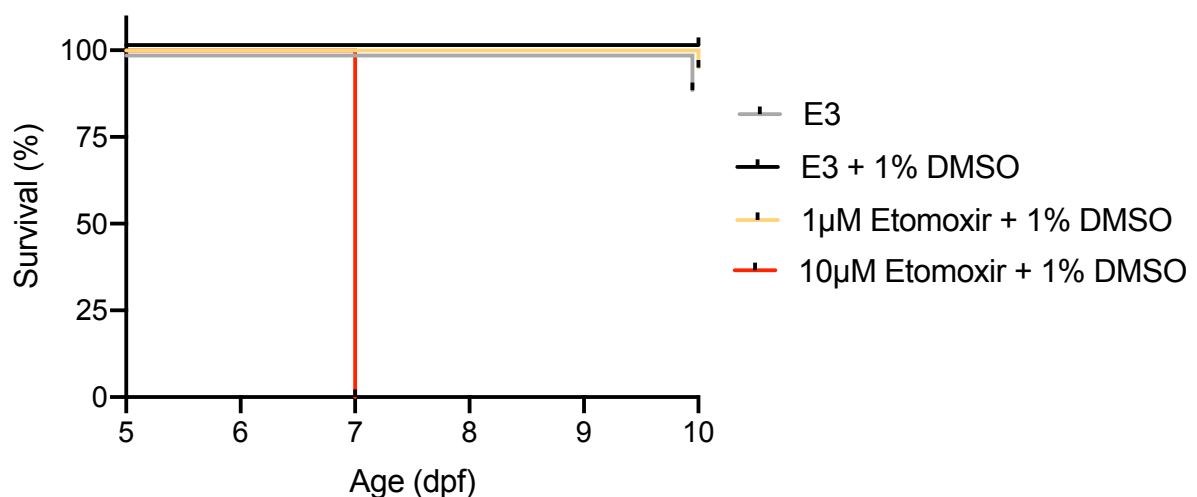


Figure 51: Etomoxir toxicity assessment #1. Doses from 1 μ M and 10 μ M etomoxir from 5-10 dpf resulted in 100% toxicity in the 10 μ M-treated group at 7 dpf ($p < 0.0001$). Treatment with 1 μ M etomoxir resulted in no toxicity ($n = 20$ per group, Mantel-Cox Log-rank test).

Treatment of *gch1*^{-/-} with 1 μ M etomoxir from 5 dpf failed to improve survival ($p = 0.9989$, Figure 52); additionally, we saw a large decrease in the survival of etomoxir-treated and DMSO-treated WT from 10 dpf onwards, indicating that treatment with 1% DMSO after this time point is causing toxicity which we had previously not recognised from toxicity trials.

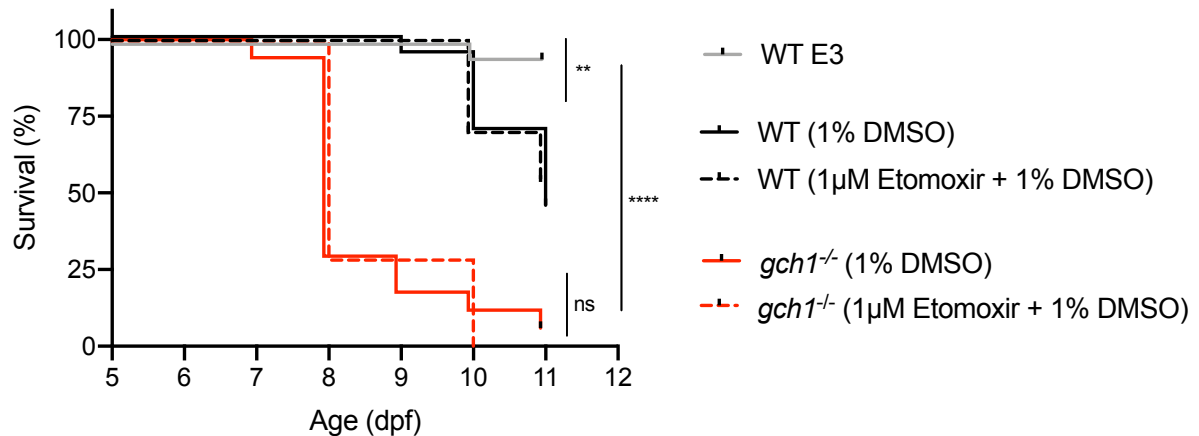


Figure 52: Survival analysis of 1 μ M etomoxir-treated *gch1*^{-/-}. Treatment of *gch1*^{-/-} with 1 μ M etomoxir ($n = 14$) conferred no survival advantage over DMSO control treatment ($p = 0.9989$, $n = 17$, Mantel-Cox Log-Rank test). Both *gch1*^{-/-} groups showed significantly decreased survival vs WT etomoxir-treated and DMSO-treated groups ($p < 0.0001$, WT DMSO $n = 20$, WT etomoxir $n = 20$). Treatment of WT with 1% DMSO or 1 μ M etomoxir conferred lower survival compared to E3-only treatment $n = 20$; ($p = 0.0008$, $p = 0.0036$ respectively, Mantel-Cox Log-Rank test).

We subsequently repeated toxicity trials for etomoxir, this time including an intermediate dose of 5 μ M to identify if larvae could tolerate a higher dose. We additionally reduced DMSO concentration in line with previous research suggesting that 0.01% DMSO is an optimal dose for minimising toxicity of the drug (Chen et al., 2011). Due to the drug being dissolved initially in DMSO, 0.025% DMSO was the lowest attainable concentration for the 10 μ M treatment, while the 1 μ M and 5 μ M groups were adjusted to 0.01% DMSO. We observed almost 100% toxicity of the 10 μ M etomoxir group at 8 dpf ($p < 0.0001$, Figure 53), whereas the 5 μ M group showed high survival until 12 dpf, at which point survival dropped below 50%, showing reduced survival vs E3-treated larvae ($p = 0.0026$). Husbandry issues, even in untreated WT, are a common issue when fish are maintained in low volumes of media past 10 dpf, hence, from this point we opted to perform treatment experiments only up to 10 dpf. We selected the 5 μ M dose for an additional treatment on *gch1*^{-/-} larvae between 5-10 dpf, based on a lack of toxicity until around 12 dpf.

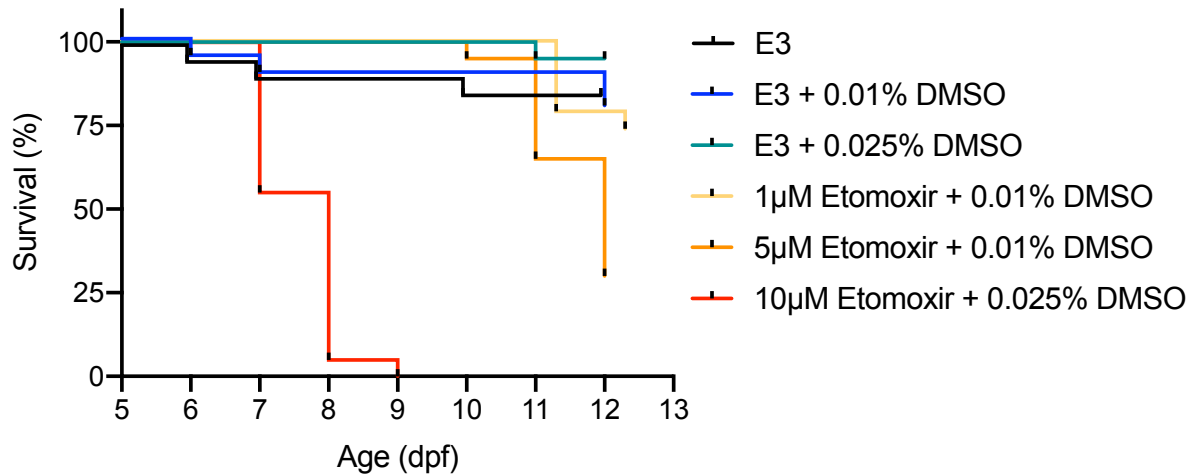


Figure 53: Etomoxir toxicity assessment #2. Etomoxir doses of 1 μ M, 5 μ M and 10 μ M were tested from 5-12 dpf. Toxicity was observed in the 10 μ M-treated group, with reduced survival compared to E3 and DMSO controls ($p < 0.0001$), with median survival of 8 dpf. Treatment with 5 μ M showed median survival time of 12 dpf, which was significantly lower than DMSO control ($p = 0.0033$) and E3 control ($p = 0.0026$). Treatment with 1 μ M etomoxir resulted in comparable survival to E3 ($p = 0.5059$), and DMSO controls ($p = 0.6822$, $n = 20$ per group, Mantel-Cox Log-rank test).

Again, treatment of *gch1*^{-/-} with 5 μ M etomoxir had no effect on survival ($p = 0.8084$, Figure 54). Both untreated and etomoxir-treated *gch1*^{-/-} had a median survival time of 8 dpf. 19% of untreated *gch1*^{-/-} were surviving at 10 dpf, and 7.7% of *gch1*^{-/-} surviving in the etomoxir-treated group. 100% survival was observed in the WT E3 control group and in the WT 0.01% DMSO group, however, the etomoxir-treated WT group showed 87% survival by 10 dpf, which was lower than the E3-treated group ($p = 0.0069$) suggesting that toxicity of the drug was causing reduced survival. Given that the majority of *gch1*^{-/-} larvae showed mortality prior to this toxicity arising, we can probably conclude that etomoxir treatment did not confer any survival advantage.

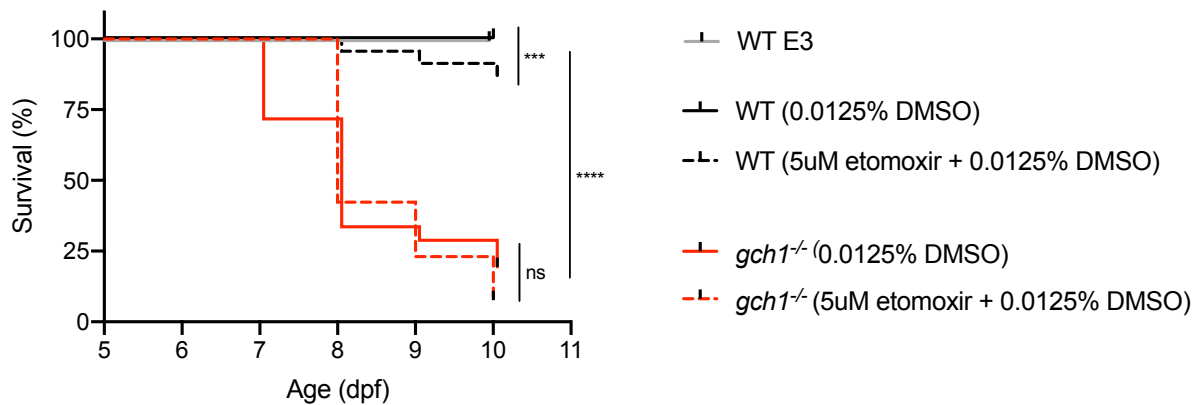


Figure 54: Survival analysis of 5 μM etomoxir-treated *gch1*^{-/-}. Treatment of *gch1*^{-/-} larvae with 5 μM etomoxir conferred no survival advantage compared to control treatment. Survival curves between DMSO control-treated *gch1*^{-/-} ($n = 21$) and 5 μM etomoxir-treated *gch1*^{-/-} ($n = 26$) showed no difference in survival ($p = 0.8084$). Etomoxir-treated WT larvae ($n = 23$) had reduced survival compared to E3-treated WT ($n = 50$, $p = 0.0090$) but not compared to DMSO-treated WT ($n = 23$, $p = 0.0764$). Both *gch1*^{-/-} groups displayed reduced survival compared to WT groups ($p < 0.0001$, Mantel-Cox Log Rank test).

3. 6.4. L-N⁶-(1-Iminoethyl)lysine treatment has no effect on *gch1*^{-/-} survival

Deficiency of BH4 can lead to uncoupling of NOS and production of superoxide. We hypothesised that superoxide production from iNOS was contributing to impaired survival in *gch1*^{-/-}. To address this hypothesis, we sought to inhibit iNOS, using L-N⁶-(1-Iminoethyl)lysine (L-NIL), a moderately selective inhibitor for iNOS (Boer et al., 2000), which has previously been used for treatment of zebrafish (Elks et al., 2013).

We initially performed a toxicity assessment from 1-5 dpf, to determine the toxicity of a wide range of doses, from 7 μM to 700 μM ¹¹ (Figure 55). The highest dose, 700 μM , resulted in complete lethality within 24h of exposure, with 100% of larvae dying at 2 dpf ($p < 0.0001$). 140 μM resulted in toxicity at 5 dpf, with only 40% remaining at this time; survival was significantly lower than E3 treated WT ($p = 0.0034$).

¹¹ The unusual choice of doses can be attributed to initially being informed of the incorrect molecular weight for this drug, which was subsequently amended following the experiment. Initially a dose response curve was designed for doses between 10 μM to 1 mM. When the dose calculations were amended after calculating the correct molecular weight, the dose curve ranged from 7 μM to 700 μM .

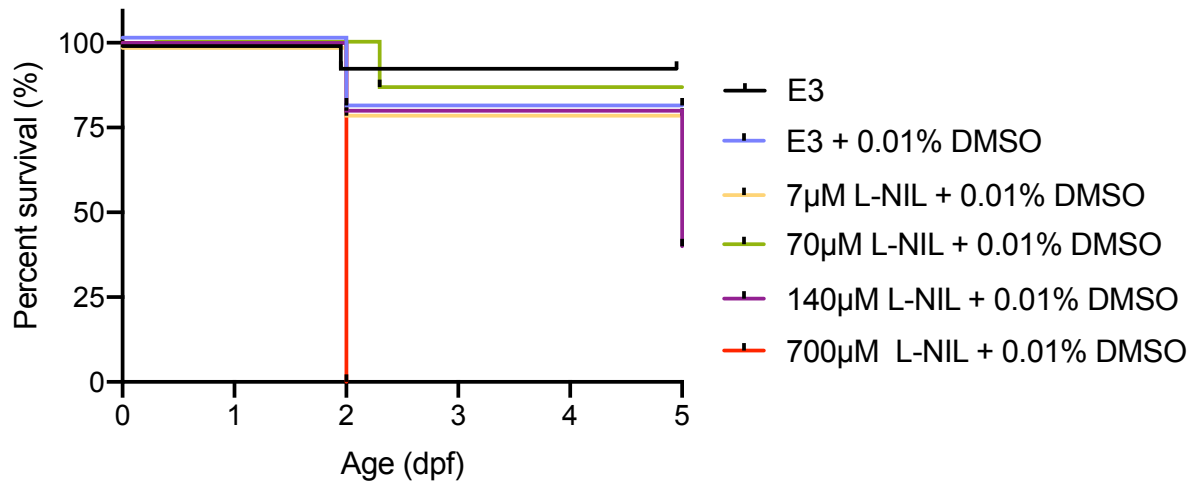


Figure 55: L-NIL toxicity assessment #1. Testing toxicity of doses from 7-700 µM from 1-5 dpf. 700 µM caused 100% toxicity within 24h of treatment, and 140 µM resulted in toxicity at 5 dpf, with only 40% survival.

We then performed a 1-10 dpf dose curve to test a closer range of concentrations below 140 µM; 7, 35 and 70 µM doses were tested (Figure 56). None of the groups showed significantly diminished survival, however, at the highest dose, 70 µM, some potential but non-significant toxicity appeared at 9 and 10 dpf, with 20% of larvae succumbing at this late timepoint ($p=0.3251$). We thus opted to use the 35 µM dose for treatment of *gch1^{-/-}*.

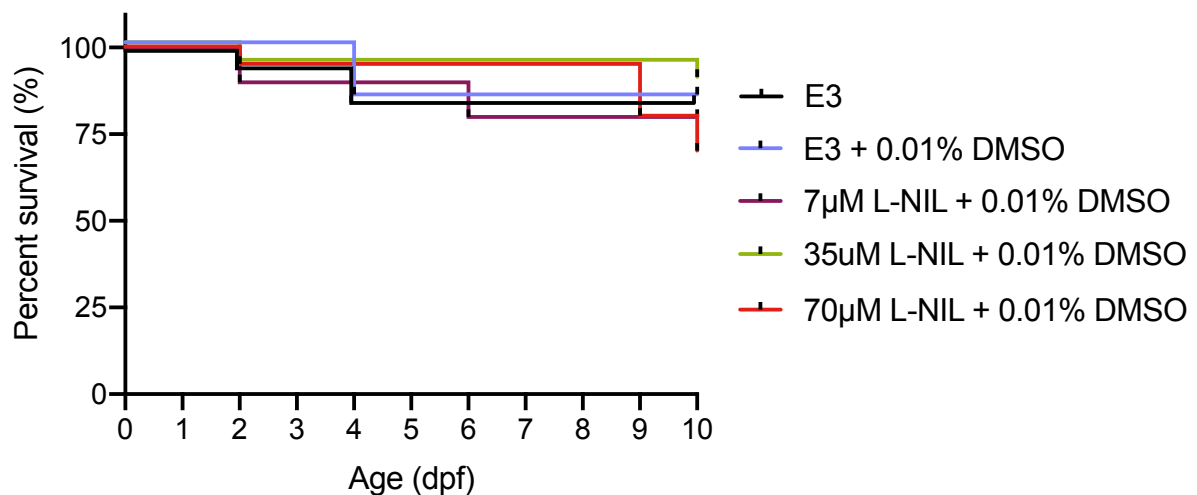


Figure 56: L-NIL toxicity assessment #2. Toxicity assessment to test doses from 7-70 µM, from 1-10 dpf. No difference was observed in survival of groups ($n = 20$ per group, Mantel-Cox Log-Rank test).

We performed treatment of *gch1^{-/-}* with 35µM L-NIL over 2 independent experiments, each with 3 separate clutches of fish. Contrary to our hypothesis, L-NIL treatment conferred no

survival advantage to *gch1*^{-/-} larvae. Both treated and untreated *gch1*^{-/-} larvae showed a gradual decline in survival from 6 dpf to 10 dpf, with a median survival time of 9 dpf. 37.5% of L-NIL treated *gch1*^{-/-}, and 23.5% of untreated *gch1*^{-/-}, were surviving at 10 dpf ($p = 0.7115$, Figure 57). All WT groups showed almost 100% survival ($p = 0.7009$). This result suggests that superoxide production from iNOS is not a contributing factor to *gch1*^{-/-} mortality.

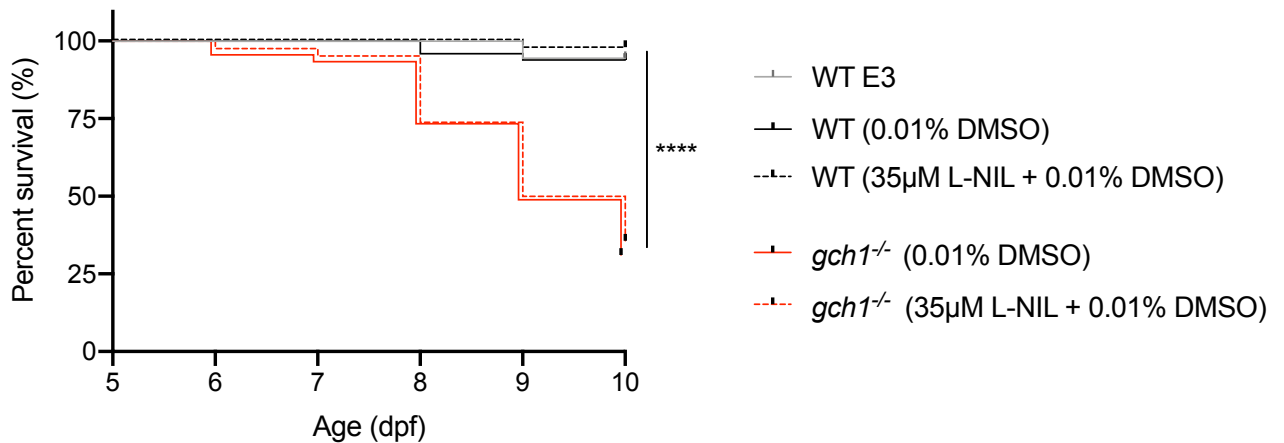


Figure 57: Survival analysis of L-NIL-treated *gch1*^{-/-}. Treatment of *gch1*^{-/-} with 35µM L-NIL ($n = 42$) conferred no survival advantage over control treatment ($p = 0.7115$, $n = 45$, Mantel-Cox Log-Rank test). Both *gch1*^{-/-} groups showed significantly decreased survival vs WT groups ($p < 0.0001$, WT DMSO $n = 49$, WT L-NIL $n = 40$, Mantel-Cox Log-Rank test).

3.6.5. Nitric oxide donor, Sodium Nitroprusside, prolongs median survival of *gch1*^{-/-}

Deficiency of BH₄ results in uncoupling of NOS, thus preventing normal production of nitric oxide. We proposed that lack of nitric oxide may be a contributing factor to lethality in *gch1*^{-/-}. We sought to supplement nitric oxide in *gch1*^{-/-} by treating with sodium nitroprusside (SNP), a chemical donor of nitric oxide, which is a commonly used drug to treat acute cases of hypertension via brief intravenous delivery.

We performed a toxicity assessment from 1-10 dpf, using 10 μM, 50 μM and 100 μM SNP. SNP is light-sensitive, and can be transformed from a brown to a blue colour, caused by reduction of the ferric ion to ferrous ion (Gordon and Kittleson, 2008); when protected from light, SNP solution is reportedly stable for 24h, hence, we maintained larvae in a light-protected box during treatment, and refreshed the media every 24h. Death of up to 25% of larvae was observed in groups before 5 dpf in a non-dose-dependent manner, however, after 5 dpf, no further death was observed (Figure 58). We proposed that any observed deaths were due to developmental anomalies, as the untreated E3-only group demonstrated the most pronounced decrease in survival. Overall, no groups showed significantly different survival curves ($p = 0.1218$). We thus opted to use the highest dose, 100μM, for further experiments.

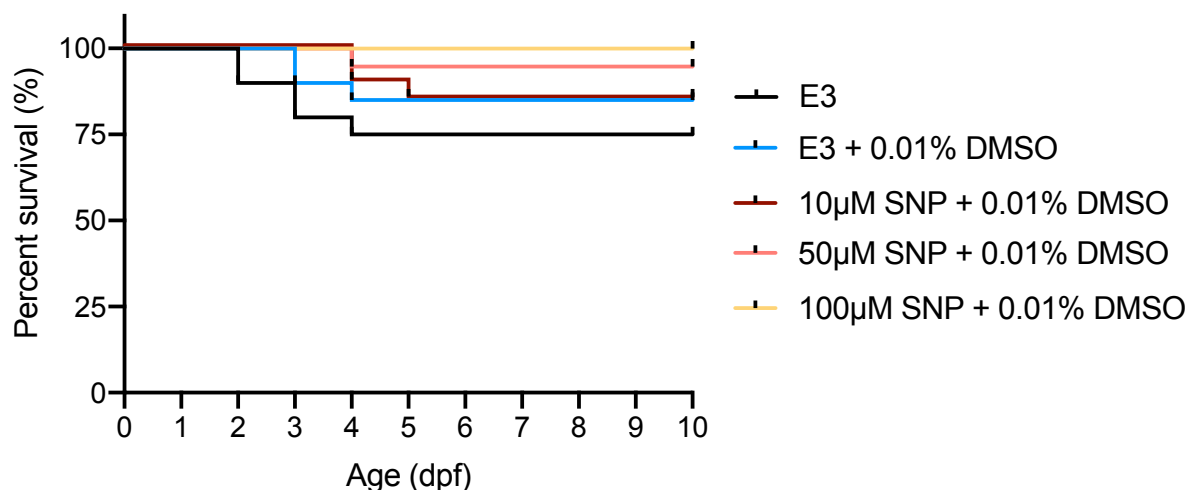


Figure 58: SNP toxicity assessment. Toxicity testing of doses from 10-100μM SNP on WT larvae revealed no apparent toxicity at the highest dose between 1-10 dpf. No groups showed statistically different survival curves ($p = 0.1218$, $n=20$ per group, Mantel-Cox Log-Rank test).

Treatment of *gch1*^{-/-} with SNP was performed over 2 independent experiments, each with 3 individual clutches of larvae, blinded to genotype. Untreated *gch1*^{-/-} larvae showed a gradual decline in survival from 6 to 10 dpf, with a median survival time of 8 dpf. SNP-treated *gch1*^{-/-} showed a prolonged survival ($p = 0.0027$), with decline occurring from 8 dpf, and a median survival of 10 dpf. 50% of SNP-treated *gch1*^{-/-} were surviving at 10 dpf, in contrast to 26.2% of untreated *gch1*^{-/-}. 92.9% and 98.2% of DMSO and SNP-treated WT, respectively, were surviving at 10 dpf, thus SNP treatment did not affect WT survival ($p = 0.1816$, Figure 59). This result indicates that supplementation of NO is sufficient to prolong survival in *gch1*^{-/-}, although a decline in health is still apparent.

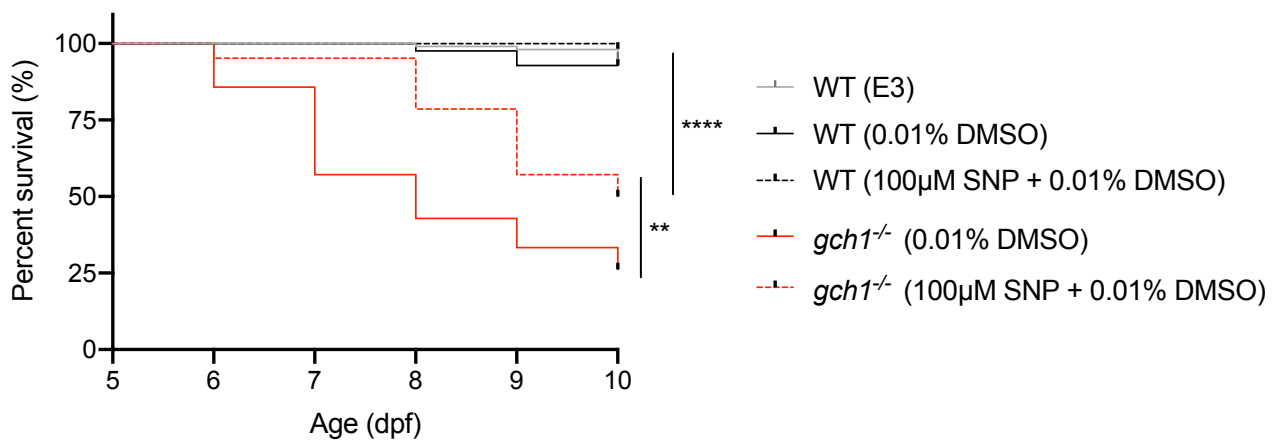


Figure 59: Survival analysis of SNP-treated *gch1*^{-/-}. Median survival of *gch1*^{-/-} larvae was prolonged from 8 dpf in untreated *gch1*^{-/-} ($n = 42$) to 10 dpf when treated with SNP ($n = 42$, $p = 0.0027$, Mantel-Cox Log-Rank test), however, SNP-treated *gch1*^{-/-} showed reduced survival in comparison to all WT controls ($p < 0.0001$, $n = 42$, Mantel-Cox Log-Rank test). Results were obtained over 2 separate experiments.

Chapter 4. Discussion

4.1. Key findings

The core aims of this project were to establish a zebrafish line to model GCH1 deficiency and characterise how deficiency of GCH1 may contribute to increased PD risk. We were successful in establishing a homozygous mutant which recapitulates monoaminergic neurotransmitter deficits and movement deficits, consistent with deficits observed in cases of DRD and PD with autosomal dominant heterozygous GCH1 mutations. We subsequently performed analyses of the ventral diencephalic DA neurons, and identified no evidence of dopaminergic neuronal cell death, however, we observed reductions in total Th protein in the brain. We additionally studied whether Gch1 deficiency in zebrafish may act to exacerbate risk in combination with additional genetic or environmental risk factors for PD, but found no evidence to suggest this to be the case. RNAseq was used to identify dysregulated pathways and transcripts which may contribute to pathology, and we identified upregulation of immune-related pathways and metabolic processes. We used morphological and functional activity assays to assess microglial activation in *gch1*^{-/-} larvae, and identified increased microglial activity, indicative of neuroinflammation. Finally, we tested drug candidates for phenotype-modifying effects in *gch1*^{-/-}, and observed improved survival as a result of supplementation of L-DOPA or supplementation of NO. In summary, we identified 2 major mechanisms which may contribute to PD in cases of GCH1 deficiency: tyrosine hydroxylase depletion, and neuroinflammation.

4.2. DA Neuron Characterisation

4.2.1. HPLC analysis of neurotransmitter levels

Consistent with our hypothesis that loss of function of *gch1* would have a direct effect on neurotransmitter levels, we observed significant reductions in all monoaminergic neurotransmitters by 8 dpf. Reductions in the serotonin metabolite, 5-HIAA, and the dopamine metabolite, 3-MT, were also observed, but the dopamine metabolites DOPAC and HVA remained unchanged. The reduction in neurotransmitter levels provides evidence that the mutation in *gch1* results in loss of function, given the requirement for Gch1 in the synthesis of BH4, and the subsequent requirement for BH4 as a cofactor for dopamine and serotonin metabolism. Furthermore, the finding of decreased dopamine is consistent with reports from patients with GCH1-deficient DRD, who display reduced dopamine content in

nigrostriatal cells (Furukawa et al., 1999; Rajput et al., 1994), and also display reduced neopterin levels (Furukawa et al., 1996). Reduced levels of HVA are also reported in cases of *TH*-deficient DRD (Antelmi et al., 2015), in contrast to our findings (in which reductions in HVA were statistically not significant), however, closer scrutiny of our results suggests that HVA levels may be reduced in *gch1*^{-/-}, but the experiment was underpowered to detect this.

Levels of monoaminergic neurotransmitters other than dopamine are not widely reported in cases of GCH1-deficient DRD, but given the widely reported reductions in BH4 levels (Assmann et al., 2003; Furukawa et al., 1999), it would be expected that levels of serotonin, adrenaline and noradrenaline (which all require BH4 as a cofactor for synthesis) are also affected, but do not result in such obvious manifestations as dopamine deficiency. The phenotypic description of *GCH1*-deficient DRD includes serotonin-related non-motor symptoms, such as depression and anxiety. A literature-based study investigating non-motor symptoms (NMS) in DRD cases revealed that a sizeable number of cases display depression (34%, n = 70), anxiety (19%) and obsessive-compulsive disorder (9%) (Tadic et al., 2012). Despite the considerable proportion of cases displaying NMS, the status of brain serotonin levels in cases is relatively uncharacterised (Antelmi et al., 2015; Furukawa et al., 2016); Furukawa and co-authors investigated serotonin markers in the putamen in one case of *GCH1*-deficient DRD and reported normal levels of serotonin (79% of control levels) and tryptophan hydroxylase (118% of control levels), despite marked decrease in dopamine levels (8% of control levels) and tyrosine hydroxylase (1.5% of control levels). Several mechanisms have been suggested for the contrasting levels of serotonin and dopamine in these cases: 1) the varying susceptibility of aromatic amino acid hydroxylases to BH4 deficiency may be due to differing substrate concentration requirements for enzymatic activity; 2) differences in tissue-specific expression of GCH1; 3) protein stability of aromatic amino acid hydroxylases under conditions of reduced BH4 availability (Furukawa and Kish, 1999). A reasonable explanation for severely reduced serotonin levels in the *gch1*^{-/-} zebrafish, in contrast to normal levels in GCH1-deficient DRD, may be that BH4 levels in the zebrafish are completely ablated, whereas very low level of BH4 activity is sufficient for serotonin production in DRD patients. Further investigation of the non-motor effects of serotonin deficiency in the *gch1*^{-/-} zebrafish would be an interesting research avenue to explore, for example into the effects on circadian rhythm and sleep disturbance.

Additionally, behavioural assays can be utilised to identify whether these fish demonstrate behaviours associated with anxiety.

Our finding of reduced neurotransmitter levels is also consistent with the *Gch1*-KO mouse model, which demonstrated depleted BH4 and L-DOPA levels (Douglas et al., 2015). The authors also performed an untargeted metabolomic screen, in addition to a targeted metabolomic screen to assess BH4-related compounds, and surprisingly did not observe any disturbances in metabolism. The authors did not assess levels of dopamine, serotonin, noradrenaline or adrenaline in the targeted screen, but did include phenylalanine and tyrosine, neither of which were affected; phenylalanine, and the phenylalanine to tyrosine ratio, would be expected to be perturbed in severe cases of severe GCH1 deficiency, as BH4 is required as a cofactor for conversion of phenylalanine to tyrosine.

In several homozygous and compound heterozygous *GCH1* mutation cases, hyperphenylalanemia (HPA) and phenylketonuria (PKU) has been reported (Table 7). HPA and PKU (a more severe increase in blood phenylalanine levels) are more commonly a result of phenylalanine hydroxylase deficiency (Williams et al., 2008), but can also occur as a result of severe GCH1 deficiency. If untreated, HPA is neurotoxic and can lead to severe developmental delays. Screening for high phenylalanine levels is therefore performed in newborn screening tests, from a blood spot from a heel prick test. In GCH1-deficient HPA/PKU cases, screening of blood serum reveals high levels of phenylalanine, and urinary pteridine screening reveals low levels of neopterin, biopterin, dopamine and serotonin (Table 7); GCH1 activity assays on liver biopsy tissue can subsequently be used to diagnose GCH1 deficiency. While typical PKU/HPA cases can be treated with low-phenylalanine diets, GCH1-deficient cases can be treated with BH4 in addition to neurotransmitter replacement therapy. Therapy typically results in improvement of motor symptoms and prevention of further developmental delays.

Table 7: Reports of hyperphenylalanemia as a result of homozygous or compound-heterozygous GCH1 mutations

Paper	Symptoms	Screening results	Treatment	Following treatment	GCH1 mutation
(Niederwieser et al., 1984)	retardation of development, muscular hypotonia of trunk and extremities, convulsions, hyperthermia in absence of infection	At 4 y/o. 1270 µmol/L serum phenylalanine. v low urinary excretion of neopterin and biopterin, dopamine and serotonin. v low CSF levels of HVA, 5-HIAA, neopterin and biopterin. No detectable GCH1 activity from liver biopsy.	BH4, L-Dopa, Benserazide, 5-hydroxytryptophan	BH4 treatment improved muscle tone, hyperthermic fever and nystagmus. Increased malanisation of hair.	Not described. Likely autosomal recessive (consanguineous parents).
(Naylor et al., 1987)	Asymptomatic at diagnosis. Slightly increased muscle tone around hips.	Positive result for PKU at neonatal screening (1250 µmol/L Phe plasma level). Urinary pteridine screen revealed v low neopterin and biopterin, but normal ratio. Low CSF levels of 5-HIAA and 5HT. GCH1 activity levels <4% of control levels from liver tissue biopsy.	Phe-restricted diet.	More evidence of hypotonia and episodes of seizure-like activity. GCH1 deficiency was subsequently diagnosed.	Not described.
(Blau et al., 1995)	Negative at newborn PKU screening. Phenotype arising at 5 m/o: developmental delay, generalized hypotonia, clonic movements, and tendon reflexes in the upper limbs	Slight hypotonia but negative PKU test at newborn screening. 418 µmol/L plasma Phe at 5 m/o. Undetectable urinary biopterin and neopterin. Absence of GCH1 activity in liver biopsy.	BH4 and neurotransmitter replacement therapy from 9 m/o	After 1 month of treatment a reduction in the intention tremors and dystonic movements observed, but axial hypotonia persisted. At 15 m/o slight axial hypotonia persisted, but the intention tremors and the dystonic movements had completely disappeared.	M211I/M211I
(Bandmann et al., 1998)	Feeding problems, postural talipes	Blood Phe 3.5 mmol/L at neonatal screening. Normal CSF levels of 5-HIAA, and low levels of HVA < 1y/o; 5-HIAA decreased after 1 year. No detectable urinary biopterin or neopterin. No detectable GCH1 activity from liver biopsy.	BH4, levodopa, carbidopa, and 5-hydroxytryptophan	Satisfactory growth. Age-appropriate early development. Learning difficulties, dystonic movement when tired or upset at 5 y/o	M211 V/M211 V
(Sato et al., 2014)	asymptomatic at newborn screening	phenylalanine 1273 µmol/L at 5 d/o. Low serum and urinary biopterin and neopterin. Low CSF levels of 5-HIAA and HVA.	BH4 and L-dopa/carbidopa at 1 m/o, later with addition of 5-HTP at 5 m/o	Phenylalanine levels normalized following BH4 administration. Slight dystonia but no obvious developmental delay at 10 m/o	R184H/R235 W
(Gowda et al., 2019)	Delayed milestones, episodic noisy breathing from 2 m/o. Stiffening of limbs with up-rolling of eyes from 4 m/o. Increased sweating from 6 m/o.	9 m/o. Elevated phenylalanine 302.32 mmol/L	L-dopa/carbidopa supplementation, 5HT supplements and dietary phenylalanine restriction	Improvement in irritability, dystonic episodes and up-rolling of eyes	C703G/ C703G

Monoaminergic neurotransmitter levels in *gch1*^{+/-} adult brain samples were normal, suggesting that haploinsufficiency of *gch1* does not have a direct effect on dopamine synthesis. This may be due to samples being collected in fish at 12 mpf, which is perhaps not representative of an aged phenotype. Given that age is the biggest risk factor in developing PD, a dopamine-deficient phenotype may only be observed in haploinsufficient cases at older age. However, we have observed general health and monitored swimming behaviour in adult heterozygous fish until 30 mpf, and observed no overt phenotype, indicating that even in aged *gch1*^{+/-} fish, there is insufficient evidence of a PD phenotype arising.

Suitability of the *gch1*^{-/-} zebrafish for modelling autosomal dominant GCH1 deficiency

The results of the HPLC-based neurotransmitter analysis have importantly given insight to the effect of the *gch1* mutation on enzymatic activity, in the absence of a direct measure of Gch1 protein levels or activity. By comparing neurotransmitter levels between the zebrafish *gch1* genotypes and GCH1-mutation carriers, we can assess the suitability of the zebrafish mutant to model GCH1-deficient PD and DRD.

We established that heterozygotes don't display any gross imbalances in neurotransmitter levels at 12 mpf, suggesting that Gch1 enzyme activity is sufficient to maintain normal neurotransmitter levels, thus the *gch1*^{+/-} zebrafish is not suitable for modelling PD. Homozygous *gch1* KO appears to lead to complete loss of gene function, nonsense-mediated decay of the mRNA product, and thus the mutant protein is only produced at minimal levels (if at all, although this has not been quantified); this results in severely depleted dopamine levels in the *gch1*^{-/-} fish, consistent with observations in autosomal-dominant (AD) *GCH1* mutation carriers. The *gch1*^{-/-} fish also have depleted serotonin levels, which are more severe than serotonin reductions observed in AD-*GCH1* mutation carriers. The key difference between the *gch1* zebrafish mutant and AD-*GCH1* point mutations is that the zebrafish mutation results in complete loss of Gch1 protein, whereas AD-*GCH1* point mutations lead to the production of a non-functional protein product, which will act in a dominant negative manner. As a homodecamer, GCH1 proteins will be formed of both WT and mutant subunits, and the mutant protein acts to reduce the enzyme activity of the WT protein. As a result, GCH1 enzyme activity is reduced to <50%, despite the presence of a functional copy of the gene.

To summarise, the *gch1*^{-/-} zebrafish is therefore a better model of GCH1-deficiency than *gch1*^{+/-}, however, a knock-in model imitating a *GCH1* mutation with a dominant-negative effect would be a more accurate model.

4.2.2. Electrophysiology

Electrophysiology of the DC4 neurons in *gch1*^{-/-} revealed no changes in neuronal firing activity, contrary to our hypothesis. A major limitation of this experiment is that the technique is optimised at 4dpf (and cannot be performed at a later timepoint), which is prior to the appearance of an overt phenotype in *gch1*^{-/-} and is not in line with timepoints used for other experiments, such as the HPLC data described above. HPLC analysis at 5dpf did not show a significant decrease in dopamine levels, however, dopamine did appear to be reduced, and the HPLC analysis was likely underpowered. Lack of an electrophysiological phenotype may be attributed to lack of a dopamine deficiency at 4dpf, but we have insufficient evidence to conclude this.

4.2.3. Dopaminergic neuronal cell counts

Menacci et al. proposed that lack of DA innervation of neurons may result in apoptotic cell death (Menacci et al., 2014). We performed cell counts of the DA neurons of the ventral diencephalon in *gch1*^{-/-} and observed no reductions in cell numbers in comparison to WT sibs, even at 8dpf when dopamine levels are severely reduced, and fish were close to an endpoint phenotype. This finding contradicts the proposed mechanism, suggesting that dopamine deficiency is not sufficient to result in a decrease in dopaminergic neuron numbers. However, our model does not imitate haploinsufficiency in combination with the effects of aging, due to the lethality of the phenotype, therefore, dopamine deficiency may interact with other factors, to contribute to DA denervation. Additionally, our method fails to identify whether neurons may be dying and regenerating; this could be achieved by performing time-lapse analysis of a transgenic *etVmat2-GFP;mpeg1-mCherry* line (labelling the monoaminergic neuron populations and the microglia); in the event of neuronal death, one would expect to observe the microglia to engulf the dying neurons.

The involvement of dopamine, or dopamine deficiency, in contributing to DA neurodegeneration remains contentious. In contradiction to the hypothesis stated above, it has been postulated that dopamine contributes to the disease process, and that oxidation of dopamine is a mechanism that contributes to cell death by producing toxic species (reviewed by Mor et al., 2019). Oxidative deamination of dopamine by monoamine oxidase (MAO) generates 3,4-dihydroxyphenylacetaldehyde (DOPAL), a documented neurotoxin (Lamensdorf et al., 2000), and hydrogen peroxide as a by-product. Hydrogen peroxide is especially membrane-permeable, thus enabling it to enter surrounding neurons, where it reacts with Fe^{2+} to form hydroxyl radical (Nagatsu and Sawada, 2006). Elevated expression of glial MAO-B expression has been demonstrated to lead to PD pathology and locomotor deficits in mice, supporting the theory that metabolism of dopamine can contribute to DA neurodegeneration (Mallajosyula et al., 2008).

A recent clinical study on dopamine supplementation in PD cases suggests that treatment with L-DOPA has no disease-modifying effects, providing evidence in contradiction to both of the above hypotheses (Verschuur et al., 2019). Patients with early-onset PD were randomly assigned either an 80-week treatment of levodopa and carbidopa, or 40 weeks of placebo treatment followed by 40 weeks of treatment with levodopa and carbidopa. The primary outcome for the trial was the difference in disease severity between baseline and week 80, on which, early start vs delayed start treatment had no significant effect on disease severity. Furthermore, treatment did not affect symptom progression within the first 40 weeks. This suggests that dopamine supplementation has no protective effect on survival of the DA neurons, nor does it have a detrimental effect via metabolism-related toxicity.

Another recent publication provides insight into the potential mechanism by which *GCH1* mutation can lead to PD development, as a result of dopamine deficiency unmasking subclinical levels of nigral degeneration (Shin et al., 2020). The study describes a Korean woman with a novel *GCH1* variant presenting with PD symptoms at age 47, and follows the progression of the disease over 11 years from onset. DAT imaging throughout the course of disease progression displayed some nigral neurodegeneration, but not enough to account for the severity of symptoms; it was therefore concluded that Parkinsonism in this case was

a result of dopamine deficiency as a result of GCH1 biochemical deficiency, in addition to subclinical levels of neurodegeneration. As a result, the authors propose that it would be expected that carriers of the mutation would expect to show earlier onset than is typical for PD, in addition to more benign disease course, treatment with a relatively low L-DOPA concentration, and later development of motor complications. Indeed, these assumptions were corroborated shortly thereafter by a 2-cohort case-control study, which concluded that deleterious *GCH1* variants contribute to PD risk and earlier age of onset (Pan et al., 2020). Cases with *GCH1* variants were found to manifest symptoms earlier than other PD cases, and this was then validated in a meta-analysis of 6 studies, demonstrating a 6.4 year-earlier age at onset. In addition, *GCH1*-cases had milder motor and fatigue symptoms, consistent with Shin et al.'s (2020) assumptions. These recent findings are consistent with our observations in *gch1*^{-/-} zebrafish, which display biochemical neurotransmitter deficits, however, do not display evidence of nigral degeneration.

It still remains unclear why *GCH1*-mutation carriers who develop DRD in childhood do not tend to develop PD in later life, while some mutation carriers are asymptomatic for DRD, but will develop PD and show nigrostriatal degeneration in older age. Childhood-onset DRD cases likely have lower dopamine turnover and lower striatal dopamine levels, resulting in the early onset phenotype, and it may be that this deficiency of dopamine is actually protective of neurodegeneration. This would be consistent with our finding in the *gch1*^{-/-} larvae, which show similar reduction in dopamine levels to DRD cases, and do not show DA degeneration – however this model does not take into account the long-term effects of aging. Neuron counting of the same populations in the aged *gch1*^{+/-} fish would elucidate whether degeneration may occur in cases of heterozygosity, which have unchanged dopamine levels when we have assessed biochemistry at 12 mpf.

4.2.4. MPP+ treatment

We tested the hypothesis that GCH1 deficiency in combination with environmental factors may contribute to increased PD risk. We found that treatment with the classical PD neurotoxin MPP+ contributed to DA cell death, but Gch1 deficiency did not confer increased susceptibility to MPP+, with equivalent neuron counts in WT and *gch1*^{-/-}.

Interestingly, treatment with MPTP has been shown to have a diminished effect in nNOS and iNOS-KO mice, which show decreased susceptibility to MPP⁺-induced neurodegeneration (Liberatore et al., 1999; Przedborski et al., 1996; Ryan et al., 2014b). NOS-KO models show depleted NO production, like GCH1-KO models, however, they lack the superoxide-producing capacity of NOS, which GCH1-KO models retain.

The MPTP derivative MPP⁺ is selectively uptaken by DAT into the DA neurons, where it inhibits Complex I of the mitochondrial electron transport chain, leading to exacerbated oxidative stress through a number of mechanisms (Figure 60). The major mechanism is via an increase in ROS production directly from the electron transport chain. In addition, complex I inhibition leads to activation of iNOS (Dehmer et al., 2000), which, particularly in highly oxidising conditions, can contribute to superoxide generation and downstream peroxynitrite production, when iNOS becomes uncoupled. Finally, inhibition of complex I results in decreased ATP production, leading to reduction in cellular GTP, and reduced BH4 production (Ryan et al., 2014b); this reduction in BH4 levels further exacerbates NOS uncoupling, leading to excessive superoxide production. As a result, inhibition or inactivation of iNOS has been demonstrated to protect against MPTP-induced neurodegeneration in both mouse and cell models.

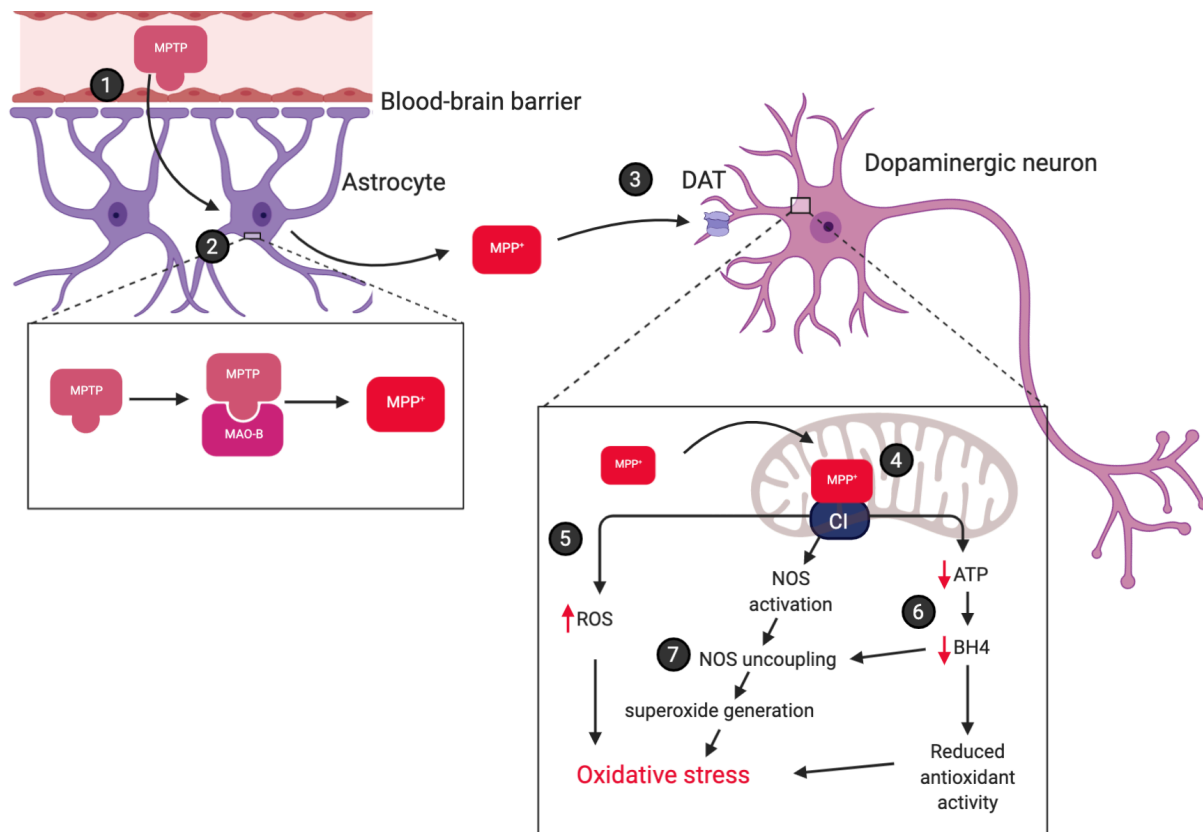


Figure 60: MPTP neurotoxicity mechanism. 1) MPTP passes through the blood brain barrier. 2) MPTP is taken up by astrocytes, and converted to MPP⁺. 3) MPP⁺ is selectively uptaken by DAT into the DA neurons, where it enters the mitochondria (4), and inhibits CI of the electron transport chain. Inhibition of CI results leads oxidative stress via increased ROS production (5), in addition to reduced cellular BH4 (6), causing both reduced antioxidant activity, in addition to leading to superoxide production via NOS uncoupling (7). Figure produced by myself, with the use of Biorender.

Loss of function of Gch1 in our zebrafish model, unlike loss of function nNOS or iNOS, does not appear to either exacerbate or attenuate DA cell death when treated with MPTP. In nNOS- and iNOS-KO, a protective effect is observed by removing the superoxide-contributing effects of NOS, whereas, in *gch1*^{-/-}, NOS is present, but would be expected to be uncoupled even in unstimulated conditions. Furthermore, the diminished BH4 production observed in MPTP-treatment (Ryan et al., 2014b) would be expected to have no additional effect on *gch1*^{-/-} larvae, as BH4 levels are expected to be already depleted. Finally, Complex I appears to already be a major contributor of ROS in a Gch1 knockdown murine endothelial model (Bailey et al., 2017), therefore basal levels of ROS are expected to be already elevated.

The major limitation of this experiment is that it was performed at an early stage, with 24h MPTP exposure at 2 dpf, and neuron counts at 3 dpf. The inconsistency of this with other characterisation means we do not know whether larvae show significant biochemical changes at this age; moreover, maternal transfer of WT *gch1*^{-/-} mRNA may be sufficient at this age for maintaining BH4 levels. Therefore, while the result suggests MPTP does not affect *gch1*^{-/-} any more than WT, we cannot definitively conclude that Gch1-deficiency does, or does not, interact with exogenous factors to contribute to PD.

4.2.5. Tyrosine hydroxylase depletion

We identified significant depletion of Th protein in the *gch1*^{-/-} mutants at 8dpf. This was despite apparently normal *th* mRNA expression levels. Regulation of TH activity in cases of GCH1 deficiency has previously been reported in *Drosophila Punch* (GCH1) mutants (Krishnakumar et al., 2000). TH and GCH1 were identified as directly interacting binding partners, thus implicating GCH1-deficiency in TH regulation via an additional mechanism to BH4 depletion. In several different *Punch* mutant haplotypes, TH activity was found to be substantially reduced, however, Western blotting to assess protein levels of TH observed no marked changes in TH abundance. The physical association between GCH1 and TH has since been validated, and shown to be regulated by phosphorylation (Bowling et al., 2008). As a result of the interaction, GCH1 activity is enhanced, and GCH1 is protected from feedback inhibition by BH4, thus ensuring BH4 levels are sufficiently high for maximal TH activity. Additionally, TH activity was found to be directly enhanced by the interaction with GCH1. Under optimal BH4 concentration, the maximal velocity of TH alone was observed to be 1.06; when TH was physically associated with GCH1, a V_{max} value of 1.23 was observed.

More recently, research in PC12D cells has revealed that severe reductions in dopamine or BH4 results in proteasomal degradation of TH (Kawahata et al., 2015). Inhibition of GCH1 by treatment with 3-Deoxy-D-arabino-2-heptulosonic acid 7-phosphate (DAHP), or inhibition of AADC to prevent L-DOPA to dopamine conversion, resulted in phosphorylation of TH at serine-40. This phosphorylation was mediated via the dopamine D2-autoreceptor, which regulates cAMP-dependent protein kinase, which is known to phosphorylate TH serine-40 (Campbell et al., 1986). p40-TH was then identified to be ubiquitinated and degraded by proteasomal degradation. Serine-40 is conserved in zebrafish, and phosphorylation of this

residue has been observed in adult zebrafish by our collaborators (Semenova, S., 2020, private communication, 29 March). This mechanism is likely resulting in the degradation of Th in *gch1*^{-/-}, which could be validated by further experimentation utilising proteasomal inhibitors, and Western blot to assess levels of the Th:phospho-Th ratio.

It is possible this mechanism may result in subtle decreases of TH abundance in cases of *GCH1* haploinsufficiency. However, we observed no reduction in Th protein in heterozygous larvae by in pilot Western blot at 5dpf (data not shown); additionally, we did not undertake analysis of *gch1* mRNA levels or Gch1 protein levels in heterozygous mutants, so it is unknown whether gene dosage affects Gch1 protein levels in the *gch1*^{+/-} fish. If haploinsufficiency does have an effect on Gch1 protein levels, further work in aged heterozygotes may elucidate whether Th depletion is involved in haploinsufficient cases.

Severely depleted levels of tyrosine hydroxylase protein have been described in few cases of *GCH1*-DRD (Furukawa et al., 1999, 2016), which report levels as low as 1.5% of controls, but have not been reported in *GCH1*-PD cases. We propose that reduced dopamine levels in familial *GCH1* mutation carriers could result in decreased TH levels, leading to a self-perpetuating decline in dopamine levels, contributing to development of parkinsonism.

4.3. Gene-gene interactions

We performed gene-gene interaction studies to test the hypothesis that *gch1*-deficiency contributes to an additive or modifying effect on PD risk, in combination with other sporadic PD genes. Several genetic interactions in PD have been identified previously, which act within the same pathways. Most notable are *PINK1* and Parkin (*PARK2*), which, in *Drosophila*, have been demonstrated to have similar muscle wastage and male sterility phenotypes; overexpression of parkin is sufficient to ameliorate this phenotype in *pink1*, however, double KO of both genes results in a muscle phenotype equivalent to that seen in the individual mutants, due to their involvement in the same pathway (Clark et al., 2006; Park et al., 2006). Other genetic modifiers in PD include *PARK2* and *LRRK2* (Smith et al., 2005), *SNCA* and *ATP13A2* (Gitler et al., 2009), *GBA* and *SNCA* (Mazzulli et al., 2011), and *GBA* and *SMPD1* (Keatinge et al., 2019), and there are likely many modifiers yet to be identified in novel sporadic PD risk loci.

Methods for identifying new genetic modifiers of disease can involve genotype-phenotype correlations, linkage studies, and functional genomics approaches, however, due to the low penetrance of sporadic PD risk loci, and the highly polygenic nature of PD, the first and second of these approaches are impractical. Furthermore, potential modifiers identified by either of these mechanisms require validation for the mechanism of action in a model system. Performing genetic interaction studies in zebrafish is a useful approach, due to the ease of generating genetic crosses. We used a targeted approach to identify potential genetic modifiers, by selecting PD genes which act in pathways or mechanisms that are likely to be affected by loss of *gch1* function.

When selecting candidate genes for gene-gene interaction studies, we cross-examined the *gch1*^{-/-} RNAseq data against our library of PD zebrafish mutants to identify whether any of our available mutant lines may show dysregulation in *gch1*^{-/-}. None of the genes for which we have stable mutant lines showed dysregulation in *gch1*^{-/-}. We selected *gba1* as a promising candidate to study, due to previous research demonstrating microglial activation in this mutant, and *gch1*^{-/-} also showing signs of inflammatory response in the RNAseq data.

In the *gch1*^{-/-}; *gba1*^{-/-} interaction study, we observed no difference in DA neuron count, which is perhaps unsurprising, given that neither *gch1*^{-/-} nor *gba1*^{-/-} display DA degeneration at 5dpf. *gba1*^{-/-} have previously been shown to exhibit degeneration of the DA neurons of the caudal hypothalamus and posterior tuberculum at 12 wpf (Keatinge et al., 2015) – significantly later than the 5 dpf timepoint we assessed. Lack of a phenotype in the double mutants may be attributed to the differing timepoints of a pathogenic phenotype arising in either of the single mutants, as the endpoint phenotypes differ from 12 dpf in *gch1*^{-/-} to 12 wpf in *gba1*^{-/-}. However, both *gch1*^{-/-} and *gba1*^{-/-} demonstrate microglial activation in larval stages (8dpf and 4dpf respectively); assessing a readout of microglial activation in the double mutants would be a more suitable method to assess whether deficiency of both of these genes may lead to exacerbated neuroinflammation. This could be a promising avenue of further work.

We additionally assessed the effect of haploinsufficiency of *gch1* in combination with homozygous *gba1* mutants, to determine whether deficiency of both genes would affect survival. Surprisingly, the *gch1^{+/-};gba1^{-/-}* survival curve was significantly extended in comparison to *gba1^{-/-}*. Haploinsufficiency of *gch1* therefore appears to ameliorate the endpoint phenotype of *gba1^{-/-}*, however, it is unclear what the mechanism for this may be. Before any further work to investigate this, it would be important to repeat this experiment with a larger number of fish, and with blinded conditions to avoid bias. During this experiment, fish of each genotype were maintained in separate tanks and in differing densities, which may have introduced bias, in addition to differing conditions such as food availability.

4.4. RNAseq and microglial activation

We used RNAseq as an unbiased method to detect transcriptional changes in brains from *gch1^{-/-}* and *gch1^{+/-}* at 8 dpf. We detected minimal changes in the *gch1^{+/-}* data, with only 6 genes showing differential expression vs WT - 3 of which were also DE in the *gch1^{-/-}* data. The finding of so few DE genes in the heterozygous sample suggests that there is limited evidence of pathological processes occurring.

As expected, the transcriptional changes in *gch1^{-/-}* were significantly greater than in the heterozygous sample, with 456 DE expressed genes. Pathway analysis and gene ontology analysis identified upregulation of pathways and biological processes related to tRNA aminoacylation, *mmp9* signalling, defence response, lipid transport, *hif1a* regulation, regulation of kinase activity, and metabolic processes. We also observed downregulation of neurite outgrowth, neurotransmission, cell cycle regulation, and FGFR signalling.

In the context of recent findings in cellular *GCH1* models, alterations in metabolic processes, lipid transport, defence response, and *mmp9* signalling were of particular interest. Metabolic remodelling to mediate inflammatory response has been noted in *Gch1*-KO murine macrophages when stimulated with mycobacterial infection (McNeill et al., 2018); *Gch1* macrophage-KO mice were identified to show improved infection responsiveness in comparison to WT controls. McNeill and co-authors performed gene expression analysis of infected GCH1-deficient macrophages, and identified upregulated expression of genes

involved in inflammatory response and lipid metabolism, and downregulated expression of genes involved in cell cycle regulation, consistent with our RNAseq findings. Interestingly, GO terms related to tRNA aminoacylation and cellular metabolism were downregulated in the *Gch1*-KO macrophages, whereas we identified these processes to be upregulated in *gch1*^{-/-}. However, our model differs in that it displays these transcriptional changes in unstimulated larvae, whereas the mouse model only demonstrates these transcriptional changes under immune insult, suggesting that *gch1*^{-/-} larvae develop endogenous neuroinflammation. Further characterisation including qPCR for pro- and anti-inflammatory cytokines would be important to gain further insight into the neuroinflammatory phenotype in *gch1*^{-/-}.

In parallel to analysis of the *Gch1* macrophage-KO mouse, McNeill and co-authors (2018) performed analysis of infection-responsiveness in iNOS-KO mice, which, like *Gch1*-KO, have ablated NO producing-capability, however, the *Gch1*-KO retains additional functions of iNOS. They identified that, in contrast to the enhanced infection-responsiveness of GCH1-deficient mice, iNOS-KO resulted in increased bacterial burden and required early experiment termination at a humane-endpoint. The authors compared gene-set enrichment analysis between the 2 models, to identify transcriptional changes which may explain the alterations in infection-responsiveness. Metabolic changes were unique to GCH1-deficient macrophages, and not identified in iNOS-deficient macrophages, suggesting that iNOS-mediated ROS production, or other NO-independent mechanisms of iNOS, are responsible for altered metabolism. tRNA processing and aminoacylation was affected in both *Gch1*- and iNOS-KO macrophages. This may be because iNOS interacts with proteins with metabolic and ribosomal functions (Foster et al., 2013); loss of function of *Gch1* may impair these protein interactions, potentially through reduced stability of iNOS mRNA due to low levels of BH4 (Linscheid et al., 1998), or altered iNOS activity due to deficient BH4 levels. Therefore, altered iNOS activity due to loss of function of either iNOS or *Gch1* is likely the underlying mechanism leading to dysregulation of tRNA synthetases.

In follow-up to this publication, the authors performed an in-depth analysis of metabolic changes in inflammatory GCH1-deficient and iNOS-deficient macrophages (Bailey et al.,

2019). LPS+IFN γ was used to stimulate an inflammatory response in macrophages. Bailey et al. identified that NO regulates the tricarboxylic acid (TCA) cycle in inflammatory macrophages, leading to accumulation of itaconate in conditions of inflammation; itaconate accumulation was exacerbated in the absence of NO. Itaconate accumulation has been previously linked to elevated Immuno-responsive Gene I (*Irg1*) expression, which is highly upregulated in states of inflammation (Michelucci et al., 2013). The gene encodes Aconitate Decarboxylase, a mitochondrial enzyme that produces itaconate via the decarboxylation of cis-aconitate. *Irg1* expression correlates with levels of itaconate, and silencing of the gene results in diminished antimicrobial activity (Michelucci et al., 2013). Bailey and co-authors identified elevated mRNA expression of *Irg1* in *Gch1*- and iNOS-KO inflammatory macrophages vs WT, similar to our findings in *gch1*^{-/-} larvae, which showed elevated expression of the zebrafish homolog of *Irg1*, *irg1l*. However, in contrast to our result, *Irg1* gene expression was unaffected in *Gch1*-deficient unstimulated (i.e. non-inflammatory cells) vs WT unstimulated cells. When they examined protein levels of Irg1, by both mass spectrometry and Western blot, they identified ~200-fold abundance in inflammatory cells, scaled to WT unstimulated cells, however there was no difference between WT and *Gch1*-deficient cells. Instead of *Irg1* regulating glycolytic metabolism, the authors identified isocitrate dehydrogenase 1 (IDH1) and 2 (IDH2) activity to be the regulator of cellular citrate and itaconate levels. Repression of IDH1 and IDH2 activity was observed in inflammatory WT cells, but not in NO-depleted cells, and this was concluded to be the determinant of metabolic alterations.

We were unable to perform immunostaining or Western blot for *irg1l* due to a lack of availability of an antibody with zebrafish reactivity, therefore the Irg1l protein levels in the *gch1*^{-/-} larvae remain uncharacterised. However, the marked increase in mRNA levels indicates presence of inflammation in *gch1*^{-/-}. *irg1l* upregulation in zebrafish has been previously identified in response to immersion or injection of the pathogen *Edwardsiella tarda* (van Soest et al., 2011). In *E. tarda* immersion-infected embryos, *irg1l* mRNA expression levels were induced between 10 and 50-fold, with low but variable mortality, and induced between 4- and 140-fold in *E. tarda*-injected embryos, which showed reproducible mortality across samples. Expression analysis in 5 individual immersion-infected embryos demonstrated that *irg1l* expression was elevated in all embryos, but was

only highly induced in one embryo; an obvious induction of *il1b* and *mmp9* was only observed in the embryo with high *irg1l* expression, indicating that *irg1l* may act as a rapid response factor, and leads to induction of *il1b* and *mmp9* expression.

An in-depth investigation into the *irg1l* signal transduction pathway in zebrafish has revealed that *irg1l* increases beta-oxidation-fuelled mROS production, which contributes to *mmp9* transcriptional induction, resulting in enhanced macrophage recruitment (Hall et al., 2014). In this model, *Salmonella enterica* serovar Typhimurium was injected into the hindbrain ventricle of embryos at 2dpf, which resulted in an induction of *irg1l* expression in the epithelial cells overlying the injection site. Induction of expression was found to be downstream of macrophage Myd88 signalling, but was upstream of *mmp9* expression. The authors demonstrated that *irg1l* is required for elevated mROS production, which is fuelled by increased uptake of fatty acids into the mitochondria in epithelial cells in inflammatory states. mROS acts as a transcriptional regulator of MMPs (Nelson and Melendez, 2004; Svineng et al., 2008), thus contributing to *mmp9* transcription, which acts as a signalling molecule to recruit macrophages to the site of inflammation. Morpholino-mediated knockdown of *irg1l* in zebrafish resulted in elevated bacterial burden and reduced survival when infected with *Salmonella* (Hall et al., 2014), implicating this as an important signalling pathway for the clearance of infection.

In addition to its role in macrophage recruitment, upregulation of matrix metalloproteases has been implicated in PD in several animal models. In an MPTP-induced PD mouse model, upregulation of MMP9 has been reported within 3h of MPTP injection to the striatum (Lorenzl et al., 2004). In MPTP-mouse and macaque models, upregulation of MMP9 has been demonstrated to promote glial activation and neuroinflammation; sustained inflammation and upregulation of MMP9 was shown to exacerbate DA neuronal death in macaques. Conversely, knockout of MMP9 in mice resulted in reduced microglial activation and a decrease in the loss of DA neurons and fibres (Annese et al., 2015). Upregulation of *mmp9* in *gch1*^{-/-} may therefore be responsible for the increase in microglial activation we observed. Therapeutic modulation of MMP9 has thus been proposed as a strategy to curb inflammation and reduce striatal degeneration in PD, and it would be interesting to observe the effect of *mmp9* inhibition or knockout on the *gch1*^{-/-} phenotype.

To summarise, from our transcriptional analysis, we observed increased expression of *myd88*, *irg1l*, and *mmp9* from brain RNA samples, and lipid synthesis and transport pathways were upregulated, providing considerable evidence of activation of the *irg1l* pathway in *gch1*^{-/-}. However, it is still unclear from our research what is stimulating this inflammatory activation. Furthermore, we were unable to pinpoint where expression of *irg1l* is localised; RNAseq data shows that expression is from brain tissue, and not epithelial, however, WISH staining for *irg1l* to demonstrate localisation was unsuccessful in our hands. The observation of *irg1l* expression contributing to enhanced leukocyte recruitment and enhanced bacterial clearance provides a potential mechanism for our finding of enhanced phagocytic activity in zymosan-injected *gch1*^{-/-} larvae. This could be validated by qPCR to identify if *irg1l* and *mmp9* are elevated in *gch1*^{-/-} zymosan-injected larvae vs WT, in addition to performing the zymosan assay in *irg1l*-deficient *gch1*^{-/-} larvae to observe whether loss of *irg1l* activity normalises the phagocytic activity in *gch1*^{-/-}.

4.5. Microglial characterisation

Microglia are a resident myeloid-derived macrophage population in the brain, essential for processes in development such as synaptic pruning, and essential throughout life for induction and resolution of inflammation, neural tissue remodelling and regeneration, debris clearance, angiogenesis, and matrix remodelling. Microglia derive from erythro-myeloid progenitor cells that populate the brain during early development, then continue to self-renew throughout adulthood (Prinz et al., 2017). As the resident immune cells of the brain, microglia play a fundamental role in protecting neurons from tissue damage and infection. In their healthy, “resting” state, microglia are actually highly dynamic, with long thin ramified processes which branch outwards to constantly survey the surrounding environment. The rapid extension and retraction of microglial processes makes them the fastest moving structure within the CNS, and injury to the brain results in immediate response by the microglia, as observed by 2-photon microscopy in mammalian brains (Davalos et al., 2005; Nimmerjahn et al., 2005).

The classical activation state of microglia is often termed “M1” and refers to the pro-inflammatory response of microglia to stimuli, in which microglia rapidly respond to cells

displaying damage-associated molecular patterns (DAMPs, e.g. misfolded proteins or ATP released from dying cells) or pathogen-associated molecular patterns (PAMPs, e.g. foreign molecules, LPS) by promoting a respiratory burst, characterised by production of reactive oxygen species, reactive nitrogen species, and pro-inflammatory cytokines such as IL-1 β and TNF α .

In addition to M1 microglia, a secondary “alternatively activated” state, termed M2 polarisation exists at the opposite end of the spectrum, which is characterised by anti-inflammatory activity to resolve the inflammation mediated by M1 macrophages. The M2 state can be promoted by multiple ligands, including IL-4, IL-13, glucocorticoids, IL-10, and Ig complexes (Mantovani et al., 2002). Additionally, peripheral monocytes may infiltrate the CNS to the site of inflammation, and these monocytes often exhibit an M2-like state, as observed by the expression of IL-10 (Shechter and Schwartz, 2013). The M1 and M2 states represent two simplified summaries of macrophage activation status, whereas, in reality, macrophages likely occupy a broad spectrum of activation states which are challenging to characterise under such discrete classification.

Despite the importance of microglial activation in mounting responses to CNS damage or infection, chronic activation of these cells can exacerbate tissue damage by over-producing pro-inflammatory cytokines. Chronic activation of microglia is a key hallmark of both neuroinflammation and PD pathology. Microglial activation within the substantia nigra has been identified via PET imaging studies and in postmortem histology of PD brains (Doorn et al., 2014; Langston et al., 1999; Stokholm et al., 2017) and, in some cases, widespread microglial activation is observed throughout the brain (Gerhard et al., 2006). Furthermore, activation of microglia and neuroinflammation has been reported in numerous neurotoxin-induced animal models of PD (Barcia et al., 2004; Kurkowska-Jastrzębska et al., 1999; Manocha et al., 2017; Ojha et al., 2016; Smeyne et al., 2016; Walsh et al., 2011; Wu et al., 2002), and in some genetic animal models of PD (Keatinge et al., 2015; Su et al., 2008; Watson et al., 2012).

To assess whether *gch1*^{-/-} larvae displayed microglial activation, we performed a simplified binary analysis of microglial activation, by categorising a cell as either “activated” or “not

activated”; this method provided us with a percentage value of activation, in addition to providing microglial cell counts. The results suggested that the majority of *gch1*^{-/-} larvae showed a similar percentage of “activated” cells as WT, however, some individual larvae with very high levels of activation increased the overall mean, pushing the result to significance. Due to the subjectivity of this method, the result is difficult to interpret, and assessment of these images with an automated image analysis to provide more objective characterisation of the cell morphology is part of ongoing work.

In addition to characterising morphological status, we performed a functional microglial activity assay, by injecting zymosan into the optic tectum and assessing phagocytic engulfment by microglia. We identified elevated phagocytic engulfment of zymosan particles in the *gch1*^{-/-} larvae at 5 dpf, indicating that resolution of inflammation is enhanced in Gch1-deficient larvae. This result supports the finding that *Gch1* macrophage-KO mice have increased clearance of Mycobacterial bacterial burden (McNeill et al., 2018).

In summary, we found *gch1*^{-/-} microglia to show signs of activation, as assessed by morphological observations and a functional activity assay. This finding provides evidence of neuroinflammation, corroborating recent findings of enhanced inflammatory response in GCH1-deficient murine models (Bailey et al., 2019; McNeill et al., 2018). Furthermore, the finding of microglial activation in the absence of exogenously induced inflammation, provides evidence that GCH1-deficiency contributes to chronic neuroinflammation, which over time may lead to increased susceptibility to dopaminergic degeneration.

4.6. Drug treatments

Finding novel therapeutics to halt disease progression in PD is of key importance, due to the lack of disease-modifying treatments currently available. Characterisation of genetic determinants of PD is essential to understand the underlying mechanisms behind disease progression in different genetic subtypes of disease; this approach may lead to targeted treatments in stratified patient populations. We sought to test therapeutics for their ability to modify the *gch1*^{-/-} phenotype, based on knowledge of pathomechanisms in *gch1*^{-/-} from our findings and from existing literature.

4.6.1. Sepiapterin

Treatment with sepiapterin has previously been shown to supplement BH4 levels in *Gch1*-KO mice, and prolong survival when administered with L-DOPA (Douglas et al., 2015). Additionally, treatment of *Gch1*-KD murine endothelial cells with sepiapterin has been shown to rescue cellular BH4 levels and abolish elevated superoxide production observed in GCH1-deficient cells (Bailey et al., 2017). We thus proposed that sepiapterin treatment may supplement BH4 levels and rescue survival in *gch1*^{-/-} larvae.

We observed no improvement in survival when *gch1*^{-/-} larvae were treated with sepiapterin at a concentration of 100 µM from 1 dpf onwards. We did not perform analysis of BH4 levels or neurotransmitter levels following treatment, so it is unclear whether the dosage was sufficient to elevate BH4 levels or rescue neurotransmitter metabolism. However, from the murine *Gch1*-KO model, it is clear that supplementation of sepiapterin is insufficient to completely rescue mice from embryonic lethality, therefore our result is consistent with this. Furthermore, sepiapterin may be insufficient to rescue dopamine levels if Th levels are already depleted.

4.6.2. L-DOPA

We hypothesised that treatment with L-DOPA could improve survival and motor deficits in *gch1*^{-/-} by directly supplementing dopamine production, bypassing the requirement for Th. This would theoretically also supplement adrenaline and noradrenaline levels, which use dopamine as a precursor, however, serotonin levels would not be expected to be improved. Treatment with 1 mM L-DOPA improved survival (judged by a healthy touch-evoked escape response), with an increase in median survival from 8 dpf to 10 dpf. However, analysis of swimming activity, stimulated by alternating light and dark cycles, revealed no significant improvement in behaviour at 8dpf. This may be attributed to low serotonin levels; serotonin is known to modulate anxiety behaviour and light-dark responsiveness (Herculano and Maximino, 2014). This result may suggest that deficits in swimming behaviour in *gch1*^{-/-} are due, at least in part, to serotonin deficiency, rather than dopamine deficiency. This

speculation could be tested in future by supplementing larvae with both L-DOPA and 5-HT treatment.

4.6.3. Etomoxir

Findings from our RNAseq revealed highly elevated levels of the *irg1l* transcript, which has previously been shown to enhance fatty-acid beta oxidation in the mitochondria, leading to elevated mROS production (Hall et al., 2014). Additionally, mROS production has been identified as the major source of ROS in Gch1-depleted murine endothelial cells (Bailey et al., 2017). The drug etomoxir is a small-molecule inhibitor of fatty acid oxidation, which acts via irreversible inhibition of the CPT1 mitochondrial membrane transporter. Etomoxir has previously been used in zebrafish over short exposure periods, and was demonstrated to diminish uptake of fatty acids into the mitochondria (Hall et al., 2014), attenuating mROS production. We proposed that inhibiting fatty acid uptake into the mitochondria by treatment with etomoxir would lead to enhanced survival by diminishing mROS production. However, we observed no effect of etomoxir on *gch1*^{-/-} survival at either 1 or 5µM. Doses above this were highly toxic, therefore, we would propose the given dose would be likely to have target activation. However, the drug is also shown to have off-target effects of mitochondrial complex I inhibition when inhibiting fatty acid oxidation by 90% or more (Yao et al., 2018), thus potentially negating the desired effect of inhibiting ROS production. Increased oxidative stress has been observed in etomoxir-treated glioblastoma cells, and it has been suggested that fatty-acid oxidation derived NADPH is in fact protective against oxidative stress (Pike et al., 2011). The off-target effects and unclear mechanisms of action of etomoxir on mitochondrial ROS production thus make our results challenging to interpret. Instead, treatment with a ROS scavenger, or general antioxidant may give a simpler indication of whether ROS-induced cytotoxicity is a causative factor in *gch1*^{-/-} lethality.

4.6.4. L-NIL

Uncoupling of NOS isoforms due to BH4 deficiency results in superoxide production instead of NO production. L-NIL has previously been characterised as a moderately selective iNOS inhibitor. To test the hypothesis that iNOS-mediated superoxide production contributes to

lethality in *gch1*^{-/-}, we treated larvae with L-NIL and assessed survival. We observed no effect on survival in *gch1*^{-/-}, contrary to our original hypothesis.

Previous findings from *Gch1*-KD murine endothelial cells showed mildly attenuated ROS production when cells were treated with L-NAME (Bailey et al., 2017) – a non-specific NOS inhibitor. More recently, the authors have demonstrated that “NO-independent roles of iNOS” are responsible for enhanced inflammatory macrophage activation and infection-response in *Gch1*-KO macrophages (Bailey et al., 2019); it is unknown whether this is via iNOS-mediated superoxide production, or via protein-protein interactions of iNOS with other targets. While our results may suggest that iNOS-derived superoxide production is not contributing to lethality in *gch1*^{-/-}, interpreting this result is problematic due to lack of evidence of efficacy of the drug in this treatment. A positive control, or evidence of target activation, would be necessary in order to draw any conclusions from this experiment.

4.6.5. Sodium nitroprusside

To test the hypothesis that lack of NO signalling may contribute to lethality in *gch1*^{-/-} larvae, we treated larvae with SNP, a NO donor. We found that SNP treatment extended median survival from 8 dpf to 10 dpf in *gch1*^{-/-}, indicating that lethality in *gch1*^{-/-} may be partially attributed to lack of NO production. NO is a signalling molecule with roles in regulating a diverse array of biological processes, including vascular tone and blood pressure, inflammatory response, and neurotransmission (Tuteja et al., 2004).

NO signalling has recently been linked to increased TH enzyme activity via S-nitrosylation (Wang et al., 2017). In HEK293T cells expressing recombinant TH, treatment of cells with an NO donor resulted in reversible S-nitrosylation and increased enzymatic activity of TH. This finding was subsequently validated in mouse striatal tissue. Our finding of prolonged lifespan in *gch1*^{-/-} may therefore be linked to augmented Th activity.

Additionally, NO signalling has been implicated in regulation of mitochondrial complex I subunit abundance in *Gch1*-KO and iNOS-KO murine macrophage models (Bailey et al., 2019). In “inflammatory” (i.e. LPS-stimulated) WT cells, elevated NO production resulted in decreases in abundance of mitochondrial CI proteins, limiting the metabolic rate of

mitochondria. Supplementation of NO in *gch1*^{-/-} may therefore be acting to decrease mitochondrial CI abundance, and thereby decreasing mitochondrial ROS production.

4.7. Concluding summary

The favoured hypothesis for PD susceptibility in *GCH1* mutation carriers was previously that lack of dopamine signalling could directly predispose to nigral degeneration (Mencacci et al., 2014). Our findings here strongly argue against this hypothesis, with almost complete loss of dopamine resulting in no observed reduction of the SNpc-like DA neurons in the zebrafish. Instead, we propose that dopamine deficiency and depletion of TH reduces the threshold for DA neuron degeneration, resulting in onset of PD symptoms prior to extensive neuronal death. Post-mortem histopathological analyses specifically of *GCH1*-PD brains would further elucidate whether *GCH1* deficiency in cases results in increases in phospho-TH and TH depletion, and the extent of degeneration in the SNpc. Since this project was completed, a clinical case study and a 2-cohort case control study have both provided evidence which supports our conclusion that biochemical dopamine deficiencies unmask subclinical levels of SNpc degeneration, leading to early age of disease onset (Pan et al., 2020; Shin et al., 2020). In addition, we propose that in cases of *GCH1* deficiency, chronic low-level neuroinflammation and/or exacerbated inflammatory response in cases of acute inflammation exacerbates neuronal tissue damage by chronic exposure to pro-inflammatory mediators. Our findings of microglial activation and increased expression of inflammation-linked genes suggests that targeted therapeutics, such as non-steroidal anti-inflammatories or MMP inhibitors, may have a beneficial effect in preventing disease onset in familial *GCH1*-mutation carriers.

4.8. Future outlook

Our work has enabled the investigation of the effects of loss of function of *gch1* on the dopaminergic populations in the zebrafish, however, this has led to new research questions that would make a promising avenue for further work. Crucially, no models exist to recapitulate the effects of autosomal-dominant pathogenic *GCH1* mutations, which show severe biochemical deficits but still maintain low levels of *GCH1* activity; this could be modelled in zebrafish by a knock-in mutant with a known pathogenic dominant-negative

mutation. This mutant would be expected to be homozygous lethal, but to show marked neurotransmitter deficits in the heterozygous fish, enabling characterisation of an aged phenotype. Possible experimental routes may investigate whether these mutants would exhibit exacerbated neuroinflammation and oxidative stress, and whether this may lead to worsened neurodegeneration in the aged fish. Analysis of TH levels in this hypothetical model may also reveal whether TH depletion is a contributing factor in the development of PD in *GCH1* mutation carriers.

Bibliography

Allen, M.T., and Levy, L.S. (2013). Parkinson's disease and pesticide exposure--a new assessment. *Crit. Rev. Toxicol.* 43, 515–534.

Altschuler, G.M., Hofmann, O., Kalatskaya, I., Payne, R., Ho Sui, S.J., Saxena, U., Krivtsov, A. V, Armstrong, S.A., Cai, T., Stein, L., et al. (2013). Pathprinting: An integrative approach to understand the functional basis of disease. *Genome Med.* 5, 68.

Annese, V., Herrero, M.T., Di Pentima, M., Gomez, A., Lombardi, L., Ros, C.M., De Pablos, V., Fernandez-Villalba, E., and De Stefano, M.E. (2015). Metalloproteinase-9 contributes to inflammatory glia activation and nigro-striatal pathway degeneration in both mouse and monkey models of 1-methyl-4-phenyl-1,2,3,6-tetrahydropyridine (MPTP)-induced Parkinsonism. *Brain Struct. Funct.* 220, 703–727.

Antelmi, E., Stamelou, M., Liguori, R., and Bhatia, K.P. (2015). Nonmotor Symptoms in Dopa-Responsive Dystonia. *Mov. Disord. Clin. Pract.* 2, 347–356.

Antoniades, C., Shirodaria, C., Van Assche, T., Cunnington, C., Tegeder, I., Lotsch, J., Guzik, T.J., Leeson, P., Diesch, J., Tousoulis, D., et al. (2008). GCH1 haplotype determines vascular and plasma biopterin availability in coronary artery disease effects on vascular superoxide production and endothelial function. *J. Am. Coll. Cardiol.* 52, 158–165.

Antoniades, C., Cunnington, C., Antonopoulos, A., Neville, M., Margaritis, M., Demosthenous, M., Bendall, J., Hale, A., Cerrato, R., Tousoulis, D., et al. (2011). Induction of vascular GTP-cyclohydrolase I and endogenous tetrahydrobiopterin synthesis protect against inflammation-induced endothelial dysfunction in human atherosclerosis. *Circulation* 124, 1860–1870.

Ara, J., Przedborski, S., Naini, A.B., Jackson-Lewis, V., Trifiletti, R.R., Horwitz, J., and Ischiropoulos, H. (1998). Inactivation of tyrosine hydroxylase by nitration following exposure

to peroxynitrite and 1-methyl-4-phenyl-1,2,3,6-tetrahydropyridine (MPTP). *Proc. Natl. Acad. Sci.* *95*, 7659 LP – 7663.

Ascherio, A., Weisskopf, M.G., O'Reilly, E.J., McCullough, M.L., Calle, E.E., Rodriguez, C., and Thun, M.J. (2004). Coffee consumption, gender, and Parkinson's disease mortality in the cancer prevention study II cohort: the modifying effects of estrogen. *Am. J. Epidemiol.* *160*, 977–984.

Ascherio, A., Chen, H., Weisskopf, M.G., O'Reilly, E., McCullough, M.L., Calle, E.E., Schwarzschild, M.A., and Thun, M.J. (2006). Pesticide exposure and risk for Parkinson's disease. *Ann. Neurol.* *60*, 197–203.

Assmann, B., Surtees, R., and Hoffmann, G.F. (2003). Approach to the diagnosis of neurotransmitter diseases exemplified by the differential diagnosis of childhood-onset dystonia. *Ann. Neurol.* *54*, S18–S24.

Bailey, J., Shaw, A., Fischer, R., Ryan, B.J., Kessler, B.M., McCullagh, J., Wade-Martins, R., Channon, K.M., and Crabtree, M.J. (2017). A novel role for endothelial tetrahydrobiopterin in mitochondrial redox balance. *Free Radic. Biol. Med.* *104*, 214–225.

Bailey, J.D., Diotallevi, M., Nicol, T., McNeill, E., Shaw, A., Chuaiphichai, S., Hale, A., Starr, A., Nandi, M., Stylianou, E., et al. (2019). Nitric Oxide Modulates Metabolic Remodeling in Inflammatory Macrophages through TCA Cycle Regulation and Itaconate Accumulation. *Cell Rep.* *28*, 218–230.

Bandmann, O., Valente, E.M., Holmans, P., Surtees, R.A.H., Walters, J.H., Wevers, R.A., Marsden, C.D., and Wood, N.W. (1998). Dopa-responsive dystonia: A clinical and molecular genetic study. *Ann. Neurol.* *44*, 649–656.

Barcia, C., Sanchez Bahillo, A., Fernandez-Villalba, E., Bautista, V., Poza Y Poza, M., Fernandez-Barreiro, A., Hirsch, E.C., and Herrero, M.-T. (2004). Evidence of active microglia in substantia nigra pars compacta of parkinsonian monkeys 1 year after MPTP exposure. *Glia* *46*, 402–409.

Becker, T., and Becker, C.G. (2001). Regenerating descending axons preferentially reroute to

the gray matter in the presence of a general macrophage/microglial reaction caudal to a spinal transection in adult zebrafish. *J. Comp. Neurol.* **433**, 131–147.

Beckman, J.S., and Koppenol, W.H. (1996). Nitric oxide, superoxide, and peroxynitrite: the good, the bad, and ugly. *Am. J. Physiol.* **271**, C1424-37.

Blau, N., Ichinose, H., Nagatsu, T., Heizmann, C.W., Zacchello, F., and Burlina, A.B. (1995). A missense mutation in a patient with guanosine triphosphate cyclohydrolase I deficiency missed in the newborn screening program. *J. Pediatr.* **126**, 401–405.

Blechman, J., Borodovsky, N., Eisenberg, M., Nabel-Rosen, H., Grimm, J., and Levkowitz, G. (2007). Specification of hypothalamic neurons by dual regulation of the homeodomain protein Orthopedia. *Development* **134**, 4417–4426.

Bode, V.C., McDonald, J.D., Guenet, J.L., and Simon, D. (1988). hph-1: a mouse mutant with hereditary hyperphenylalaninemia induced by ethylnitrosourea mutagenesis. *Genetics* **118**, 299–305.

Boer, R., Ulrich, W.R., Klein, T., Mirau, B., Haas, S., and Baur, I. (2000). The inhibitory potency and selectivity of arginine substrate site nitric-oxide synthase inhibitors is solely determined by their affinity toward the different isoenzymes. *Mol. Pharmacol.* **58**, 1026–1034.

Bowling, K.M., Huang, Z., Xu, D., Ferdousy, F., Funderburk, C.D., Karnik, N., Neckameyer, W., and O'Donnell, J.M. (2008). Direct binding of GTP cyclohydrolase and tyrosine hydroxylase: Regulatory interactions between key enzymes in dopamine biosynthesis. *J. Biol. Chem.* **283**, 31449–31459.

Boyer, N.P., and Gupton, S.L. (2018). Revisiting Netrin-1: One Who Guides (Axons) . *Front. Cell. Neurosci.* **12**, 221.

Braak, H., Del Tredici, K., Rub, U., de Vos, R.A.I., Jansen Steur, E.N.H., and Braak, E. (2003a). Staging of brain pathology related to sporadic Parkinson's disease. *Neurobiol. Aging* **24**, 197–211.

Braak, H., Rub, U., Gai, W.P., and Del Tredici, K. (2003b). Idiopathic Parkinson's disease: possible routes by which vulnerable neuronal types may be subject to neuroinvasion by an unknown pathogen. *J. Neural Transm.* *110*, 517–536.

Breuer, M., Guglielmi, L., Zielonka, M., Hemberger, V., Kölker, S., Okun, J.G., Hoffmann, G.F., Carl, M., Sauer, S.W., and Opladen, T. (2019). QDPR homologues in *Danio rerio* regulate melanin synthesis, early gliogenesis, and glutamine homeostasis. *PLoS One* *14*, e0215162.

Brkic, M., Balusu, S., Libert, C., and Vandenbroucke, R.E. (2015). Friends or Foes: Matrix Metalloproteinases and Their Multifaceted Roles in Neurodegenerative Diseases. *Mediators Inflamm.* *2015*, 620581.

Brune, B., Dimmeler, S., Molina y Vedia, L., and Lapetina, E.G. (1994). Nitric oxide: a signal for ADP-ribosylation of proteins. *Life Sci.* *54*, 61–70.

Burman, J.L., Wasiak, S., Ritter, B., de Heuvel, E., and McPherson, P.S. (2005). Aftiphilin is a component of the clathrin machinery in neurons. *FEBS Lett.* *579*, 2177–2184.

Burns, R.S., Chiueh, C.C., Markey, S.P., Ebert, M.H., Jacobowitz, D.M., and Kopin, I.J. (1983). A primate model of parkinsonism: selective destruction of dopaminergic neurons in the pars compacta of the substantia nigra by N-methyl-4-phenyl-1,2,3,6-tetrahydropyridine. *Proc. Natl. Acad. Sci. U. S. A.* *80*, 4546–4550.

Caldwell, L.J., Davies, N.O., Cavone, L., Mysiak, K.S., Semenova, S.A., Panula, P., Armstrong, J.D., Becker, C.G., and Becker, T. (2019). Regeneration of Dopaminergic Neurons in Adult Zebrafish Depends on Immune System Activation and Differs for Distinct Populations. *J. Neurosci.* *39*, 4694 LP – 4713.

Campbell, D.G., Hardie, D.G., and Vulliet, P.R. (1986). Identification of four phosphorylation sites in the N-terminal region of tyrosine hydroxylase. *J. Biol. Chem.* *261*, 10489–10492.

Cario, C.L., Farrell, T.C., Milanese, C., and Burton, E.A. (2011). Automated measurement of zebrafish larval movement. *J. Physiol.* *589*, 3703–3708.

Chen, H., Zhang, S.M., Schwarzschild, M.A., Hernan, M.A., and Ascherio, A. (2005a). Physical

activity and the risk of Parkinson disease. *Neurology* 64, 664–669.

Chen, H., Jacobs, E., Schwarzschild, M.A., McCullough, M.L., Calle, E.E., Thun, M.J., and Ascherio, A. (2005b). Nonsteroidal antiinflammatory drug use and the risk for Parkinson's disease. *Ann. Neurol.* 58, 963–967.

Chen, H., Mosley, T.H., Alonso, A., and Huang, X. (2009). Plasma urate and Parkinson's disease in the Atherosclerosis Risk in Communities (ARIC) study. *Am. J. Epidemiol.* 169, 1064–1069.

Chen, H., Huang, X., Guo, X., Mailman, R.B., Park, Y., Kamel, F., Umbach, D.M., Xu, Q., Hollenbeck, A., Schatzkin, A., et al. (2010). Smoking duration, intensity, and risk of Parkinson disease. *Neurology* 74, 878–884.

Chen, T.-H., Wang, Y.-H., and Wu, Y.-H. (2011). Developmental exposures to ethanol or dimethylsulfoxide at low concentrations alter locomotor activity in larval zebrafish: Implications for behavioral toxicity bioassays. *Aquat. Toxicol.* 102, 162–166.

Chia, K., Mazzolini, J., Mione, M., and Sieger, D. (2018). Tumor initiating cells induce Cxcr4-mediated infiltration of pro-tumoral macrophages into the brain. *Elife* 7.

Chiba, K., Trevor, A., and Castagnoli, N.J. (1984). Metabolism of the neurotoxic tertiary amine, MPTP, by brain monoamine oxidase. *Biochem. Biophys. Res. Commun.* 120, 574–578.

Clark, I.E., Dodson, M.W., Jiang, C., Cao, J.H., Huh, J.R., Seol, J.H., Yoo, S.J., Hay, B.A., and Guo, M. (2006). *Drosophila pink1* is required for mitochondrial function and interacts genetically with parkin. *Nature* 441, 1162–1166.

Collins, J.E., White, S., Searle, S.M.J., and Stemple, D.L. (2012). Incorporating RNA-seq data into the zebrafish Ensembl genebuild. *Genome Res.* 22, 2067–2078.

Contestabile, A. (2008). Regulation of transcription factors by nitric oxide in neurons and in neural-derived tumor cells. *Prog. Neurobiol.* 84, 317–328.

Costello, S., Cockburn, M., Bronstein, J., Zhang, X., and Ritz, B. (2009). Parkinson's disease and residential exposure to maneb and paraquat from agricultural applications in the central valley of California. *Am. J. Epidemiol.* *169*, 919–926.

Crabtree, M.J., and Channon, K.M. (2011). Synthesis and recycling of tetrahydrobiopterin in endothelial function and vascular disease. *Nitric Oxide Biol. Chem.* *25*, 81–88.

Crabtree, M., Smith, C., Lam, G., Goligorsky, M., and Gross, S. (2008). Ratio of 5,6,7,8-tetrahydrobiopterin to 7,8-dihydrobiopterin in endothelial cells determines glucose-elicited changes in NO vs. superoxide production by eNOS. *Am. J. Physiol.* *294*, H1530.

Crabtree, M.J., Tatham, A.L., Al-Wakeel, Y., Warrick, N., Hale, A.B., Cai, S., Channon, K.M., and Alp, N.J. (2009). Quantitative Regulation of Intracellular Endothelial Nitric-oxide Synthase (eNOS) Coupling by Both Tetrahydrobiopterin-eNOS Stoichiometry and Biopterin Redox Status: INSIGHTS FROM CELLS WITH TET-REGULATED GTP CYCLOHYDROLASE I EXPRESSION. *J. Biol. Chem.* *284*, 1136–1144.

Crow, J.P., and Ischiropoulos, H. (1996). Detection and quantitation of nitrotyrosine residues in proteins: in vivo marker of peroxynitrite. *Methods Enzymol.* *269*, 185–194.

Dauer, W., and Przedborski, S. (2003). Parkinson's Disease: Mechanisms and Models. *Neuron* *39*, 889–909.

Davalos, D., Grutzendler, J., Yang, G., Kim, J. V, Zuo, Y., Jung, S., Littman, D.R., Dustin, M.L., and Gan, W.-B. (2005). ATP mediates rapid microglial response to local brain injury in vivo. *Nat. Neurosci.* *8*, 752–758.

Dehmer, T., Lindenau, J., Haid, S., Dichgans, J., and Schulz, J.B. (2000). Deficiency of inducible nitric oxide synthase protects against MPTP toxicity in vivo. *J. Neurochem.* *74*, 2213–2216.

Dickson, D.W., Braak, H., Duda, J.E., Duyckaerts, C., Gasser, T., Halliday, G.M., Hardy, J., Leverenz, J.B., Del Tredici, K., Wszolek, Z.K., et al. (2009). Neuropathological assessment of Parkinson's disease: refining the diagnostic criteria. *Lancet. Neurol.* *8*, 1150–1157.

Djaldetti, R., Ziv, I., and Melamed, E. (2006). The mystery of motor asymmetry in Parkinson's disease. *Lancet Neurol.* 5, 796–802.

Doorn, K.J., Moors, T., Drukarch, B., van de Berg, W.D., Lucassen, P.J., and van Dam, A.-M. (2014). Microglial phenotypes and toll-like receptor 2 in the substantia nigra and hippocampus of incidental Lewy body disease cases and Parkinson's disease patients. *Acta Neuropathol. Commun.* 2, 90.

Dorsey, E.R., Constantinescu, R., Thompson, J.P., Biglan, K.M., Holloway, R.G., Kieburtz, K., Marshall, F.J., Ravina, B.M., Schifitto, G., Siderowf, A., et al. (2007). Projected number of people with Parkinson disease in the most populous nations, 2005 through 2030. *Neurology* 68, 384–386.

Douglas, G., Hale, A.B., Crabtree, M.J., Ryan, B.J., Hansler, A., Watschinger, K., Gross, S.S., Lygate, C.A., Alp, N.J., and Channon, K.M. (2015). A requirement for Gch1 and tetrahydrobiopterin in embryonic development. *Dev. Biol.* 399, 129–138.

Du, J., Teng, R.-J., Lawrence, M., Guan, T., Xu, H., Ge, Y., and Shi, Y. (2012). The Protein Partners of GTP Cyclohydrolase I in Rat Organs. *PLoS One* 7, e33991.

Durinck, S., Spellman, P.T., Birney, E., and Huber, W. (2009). Mapping identifiers for the integration of genomic datasets with the R/Bioconductor package biomaRt. *Nat. Protoc.* 4, 1184–1191.

Ehrlich, J., Sankoff, D., and Nadeau, J.H. (1997). Synteny Conservation and Chromosome Rearrangements During Mammalian Evolution. *Genetics* 147, 289 LP – 296.

Elks, P.M., Brizee, S., van der Vaart, M., Walmsley, S.R., van Eeden, F.J., Renshaw, S.A., and Meijer, A.H. (2013). Hypoxia inducible factor signaling modulates susceptibility to mycobacterial infection via a nitric oxide dependent mechanism. *PLoS Pathog.* 9, e1003789–e1003789.

Fang, F., Chen, H., Feldman, A.L., Kamel, F., Ye, W., and Wirdefeldt, K. (2012). Head injury and Parkinson's disease: a population-based study. *Mov. Disord.* 27, 1632–1635.

Farrer, M., Wavrant-De Vrieze, F., Crook, R., Boles, L., Perez-Tur, J., Hardy, J., Johnson, W.G., Steele, J., Maraganore, D., Gwinn, K., et al. (1998). Low frequency of alpha-synuclein mutations in familial Parkinson's disease. *Ann. Neurol.* *43*, 394–397.

Federico, A., and Monti, S. (2020). hypeR: an R package for geneset enrichment workflows. *Bioinformatics* *15*, 1307–1308.

Flinn, L., Mortiboys, H., Volkmann, K., Kster, R.W., Ingham, P.W., and Bandmann, O. (2009). Complex I deficiency and dopaminergic neuronal cell loss in parkin-deficient zebrafish (*Danio rerio*). *Brain* *132*, 1613–23.

Flinn, L.J., Keatinge, M., Bretau, S., Mortiboys, H., Matsui, H., De Felice, E., Woodroof, H.I., Brown, L., McTighe, A., Soellner, R., et al. (2013). TigarB causes mitochondrial dysfunction and neuronal loss in PINK1 deficiency. *Ann. Neurol.* *74*, 837–847.

Forrest, M.J., Jose, P.J., and Williams, T.J. (1986). Kinetics of the generation and action of chemical mediators in zymosan-induced inflammation of the rabbit peritoneal cavity. *Br. J. Pharmacol.* *89*, 719–730.

Förstermann, U., and Sessa, W.C. (2012). Nitric oxide synthases: regulation and function. *Eur. Heart J.* *33*, 829–837d.

Foster, M.W., Thompson, J.W., Forrester, M.T., Sha, Y., McMahon, T.J., Bowles, D.E., Moseley, M.A., and Marshall, H.E. (2013). Proteomic analysis of the NOS2 interactome in human airway epithelial cells. *Nitric Oxide Biol. Chem.* *34*, 37–46.

Furukawa, Y., and Kish, S.J. (1999). Dopa-responsive dystonia: recent advances and remaining issues to be addressed. *Mov. Disord.* *14*, 709–715.

Furukawa, Y., and Kish, S.J. (2014). Parkinsonism in GTP cyclohydrolase 1-deficient DOPA-responsive dystonia. *Brain* *138*, e351–e351.

Furukawa, Y., Shimadzu, M., Rajput, A.H., Shimizu, Y., Tagawa, T., Mori, H., Yokochi, M., Narabayashi, H., Hornykiewicz, O., Mizuno, Y., et al. (1996). GTP-cyclohydrolase I gene mutations in hereditary progressive and dopa-responsive dystonia. *Ann. Neurol.* *39*, 609–

617.

Furukawa, Y., Nygaard, T.G., Güttlich, M., Rajput, A.H., Pifl, C., DiStefano, L., Chang, L.J., Price, K., Shimadzu, M., Hornykiewicz, O., et al. (1999). Striatal biopterin and tyrosine hydroxylase protein reduction in dopa- responsive dystonia. *Neurology* 53, 1032–1041.

Furukawa, Y., Rajput, A.H., Tong, J., Tomizawa, Y., Hornykiewicz, O., and Kish, S.J. (2016). A marked contrast between serotonergic and dopaminergic changes in dopa-responsive dystonia. *Neurology* 87, 1060–1061.

Gao, J., Liu, R., Zhao, E., Huang, X., Nalls, M.A., Singleton, A.B., and Chen, H. (2015). Head injury, potential interaction with genes, and risk for Parkinson's disease. *Parkinsonism Relat. Disord.* 21, 292–296.

Gao, X., Chen, H., Schwarzschild, M.A., and Ascherio, A. (2011). Use of ibuprofen and risk of Parkinson disease. *Neurology* 76, 863–869.

Gao, X., O'Reilly, E.J., Schwarzschild, M.A., and Ascherio, A. (2016). Prospective study of plasma urate and risk of Parkinson disease in men and women. *Neurology* 86, 520–526.

Garcia-Ruiz, P.J., Chaudhuri, K.R., and Martinez-Martin, P. (2014). Non-motor symptoms of Parkinson's disease A review...from the past. *J. Neurol. Sci.* 338, 30–33.

Geller, D.A., Di Silvio, M., Billiar, T.R., and Hatakeyama, K. (2000). GTP cyclohydrolase I is coinduced in hepatocytes stimulated to produce nitric oxide. *Biochem. Biophys. Res. Commun.* 276, 633–641.

Gerhard, A., Pavese, N., Hotton, G., Turkheimer, F., Es, M., Hammers, A., Eggert, K., Oertel, W., Banati, R.B., and Brooks, D.J. (2006). In vivo imaging of microglial activation with [11C](R)-PK11195 PET in idiopathic Parkinson's disease. *Neurobiol. Dis.* 21, 404–412.

Giasson, B.I., Duda, J.E., Murray, I. V, Chen, Q., Souza, J.M., Hurtig, H.I., Ischiropoulos, H., Trojanowski, J.Q., and Lee, V.M. (2000). Oxidative damage linked to neurodegeneration by selective alpha-synuclein nitration in synucleinopathy lesions. *Science* 290, 985–989.

Gitler, A.D., Chesi, A., Geddie, M.L., Strathearn, K.E., Hamamichi, S., Hill, K.J., Caldwell, K.A., Caldwell, G.A., Cooper, A.A., Rochet, J.C., et al. (2009). α -Synuclein is part of a diverse and highly conserved interaction network that includes PARK9 and manganese toxicity. *Nat. Genet.*

Gordon, S.G., and Kittleson, M.D. (2008). Chapter 17 - Drugs used in the management of heart disease and cardiac arrhythmias. In *Small Animal Clinical Pharmacology (Second Edition)*, J.E. MADDISON, S.W. PAGE, and D.B.B.T.-S.A.C.P. (Second E. CHURCH, eds. (Edinburgh: W.B. Saunders), pp. 380–457.

Gowda, V., Nagarajan, B., Srinivasan, V., and Benakappa, A. (2019). A Novel GCH1 Mutation in An Indian Child with GTP Cyclohydrolase Deficiency. *Indian J. Pediatr.* *86*, 752–753.

Gutlich, M., Ziegler, I., Witter, K., Hemmens, B., Hultner, L., Mcdonald, J.D., Werner, T., Rodl, W., and Bacher, A. (1994). Molecular Characterization of HPH-1: A Mouse Mutant Deficient in GTP Cyclohydrolase I Activity. *Biochem. Biophys. Res. Commun.* *203*, 1675–1681.

Haavik, J., and Flatmark, T. (1987). Isolation and characterization of tetrahydropterin oxidation products generated in the tyrosine 3-monooxygenase (tyrosine hydroxylase) reaction. *Eur. J. Biochem.* *168*, 21–26.

Haaxma, C.A., Bloem, B.R., Borm, G.F., Oyen, W.J.G., Leenders, K.L., Eshuis, S., Booij, J., Dluzen, D.E., and Horstink, M.W.I.M. (2007). Gender differences in Parkinson's disease. *J. Neurol. Neurosurg. Psychiatry* *78*, 819–824.

Hall, C.J., Boyle, R.H., Sun, X., Wicker, S.M., Misa, J.P., Krissansen, G.W., Print, C.G., Crosier, K.E., and Crosier, P.S. (2014). Epidermal cells help coordinate leukocyte migration during inflammation through fatty acid-fuelled matrix metalloproteinase production. *Nat. Commun.* *5*, 1–17.

Hasegawa, K., Stoessl, A.J., Yokoyama, T., Kowa, H., Wszolek, Z.K., and Yagishita, S. (2009). Familial parkinsonism: Study of original Sagamihara PARK8 (I2020T) kindred with variable clinicopathologic outcomes. *Parkinsonism Relat. Disord.* *15*, 300–306.

Hattori, Y., Nakanishi, N., Kasai, K., Murakami, Y., and Shimoda, S. (1996).

Tetrahydrobiopterin and GTP cyclohydrolase I in a rat model of endotoxic shock: relation to nitric oxide synthesis. *Exp. Physiol.* *81*, 665–671.

Hemminki, K., Försti, A., and Bermejo, J.L. (2008). The “common disease-common variant” hypothesis and familial risks. *PLoS One* *3*, e2504–e2504.

Herculano, A.M., and Maximino, C. (2014). Serotonergic modulation of zebrafish behavior: Towards a paradox. *Prog. Neuro-Psychopharmacology Biol. Psychiatry* *55*, 50–66.

Hirayama, K., Lentz, S.I., and Kapatos, G. (1993). Tetrahydrobiopterin cofactor biosynthesis: GTP cyclohydrolase I mRNA expression in rat brain and superior cervical ganglia. *J. Neurochem.* *61*, 1006–1014.

Hirsch, L., Jette, N., Frolkis, A., Steeves, T., and Pringsheim, T. (2016). The Incidence of Parkinson’s Disease: A Systematic Review and Meta-Analysis. *Neuroepidemiology* *46*, 292–300.

Howe, K., Clark, M.D., Torroja, C.F., Torrance, J., Berthelot, C., Muffato, M., Collins, J.E., Humphray, S., McLaren, K., Matthews, L., et al. (2013). The zebrafish reference genome sequence and its relationship to the human genome. *Nature* *496*, 498–503.

Hruscha, A., Krawitz, P., Rechenberg, A., Heinrich, V., Hecht, J., Haass, C., and Schmid, B. (2013). Efficient CRISPR/Cas9 genome editing with low off-target effects in zebrafish. *Dev.* *140*, 4982–4987.

Huang, A., Zhang, Y.-Y., Chen, K., Hatakeyama, K., and Keaney, J.F.J. (2005). Cytokine-stimulated GTP cyclohydrolase I expression in endothelial cells requires coordinated activation of nuclear factor-kappaB and Stat1/Stat3. *Circ. Res.* *96*, 164–171.

Hughes, A.J., Daniel, S.E., Ben-Shlomo, Y., and Lees, A.J. (2002). The accuracy of diagnosis of parkinsonian syndromes in a specialist movement disorder service. *Brain* *125*, 861–870.

Hussein, D., Starr, A., Heikal, L., McNeill, E., Channon, K.M., Brown, P.R., Sutton, B.J., McDonnell, J.M., and Nandi, M. (2015). Validating the GTP-cyclohydrolase 1-feedback regulatory complex as a therapeutic target using biophysical and in vivo approaches. *Br. J.*

Pharmacol. *172*, 4146–4157.

Hwang, S. (2012). Comparison and evaluation of pathway-level aggregation methods of gene expression data. *BMC Genomics* *13*, S26.

Hwu, W., Chiou, Y., Lai, S., and Lee, Y. (2000). Dopa-Responsive Dystonia Is Induced by a Dominant-Negative Mechanism. *Ann. Neurol.* *48*, 609–613.

Hyland, K., Gunasekara, R.S., Munk-martin, T.L., Arnold, L.A., and Engle, T. (2003). The HPH-1 Mouse : A Model for Dominantly Inherited GTP-Cyclohydrolase Deficiency. 46–48.

Inoue, D., and Wittbrodt, J. (2011). One for all-a highly efficient and versatile method for fluorescent immunostaining in fish embryos. *PLoS One* *6*.

Ischiropoulos, H., and al-Mehdi, A.B. (1995). Peroxynitrite-mediated oxidative protein modifications. *FEBS Lett.* *364*, 279–282.

Jay, M., De Faveri, F., and McDearmid, J.R. (2015). Firing dynamics and modulatory actions of supraspinal dopaminergic neurons during zebrafish locomotor behavior. *Curr. Biol.* *25*, 435–444.

Jeon, B.S. (1997). Dopa-responsive dystonia: A syndrome of selective nigrostriatal dopaminergic deficiency. *J. Korean Med. Sci.* *12*, 269–279.

Jeon, B.S., Jeong, J.-M., Park, S.-S., Kim, J.-M., Chang, Y.-S., Song, H.-C., Kim, K.-M., Yoon, K.-Y., Lee, M.-C., and Lee, S.-B. (1998). Dopamine transporter density measured by [¹²³I]β-CIT single-photon emission computed tomography is normal in dopa-responsive dystonia. *Ann. Neurol.* *43*, 792–800.

Jin, R.C., and Loscalzo, J. (2010). Vascular Nitric Oxide: Formation and Function. *J. Blood Med.* *2010*, 147–162.

Johannessen, J.N., Chiueh, C.C., Bacon, J.P., Garrick, N.A., Burns, R.S., Weise, V.K., Kopin, I.J., Parisi, J.E., and Markey, S.P. (1989). Effects of 1-methyl-4-phenyl-1,2,3,6-tetrahydropyridine in the dog: effect of pargyline pretreatment. *J. Neurochem.* *53*, 582–589.

Johansen, K.K., Torp, S.H., Farrer, M.J., Gustavsson, E.K., and Aasly, J.O. (2018). A Case of Parkinson's Disease with No Lewy Body Pathology due to a Homozygous Exon Deletion in Parkin. *Case Rep. Neurol. Med.* 2018, 6838965.

Karperien, A., Ahammer, H., and Jelinek, H.F. (2013). Quantitating the subtleties of microglial morphology with fractal analysis. *Front. Cell. Neurosci.* 7, 3.

Kaufman, S. (1991). Some metabolic relationships between biopterin and folate: Implications for the "methyl trap hypothesis." *Neurochem. Res.* 16, 1031–1036.

Kaufman, D.M., and Milstein, M.J. (2013). Chapter 18 - Involuntary Movement Disorders. D.M. Kaufman, and M.J.B.T.-K.C.N. for P. (Seventh E. Milstein, eds. (Philadelphia: W.B. Saunders), pp. 397–453.

Kawahata, I., Ohtaku, S., Tomioka, Y., Ichinose, H., and Yamakuni, T. (2015). Dopamine or biopterin deficiency potentiates phosphorylation at 40Ser and ubiquitination of tyrosine hydroxylase to be degraded by the ubiquitin proteasome system. *Biochem. Biophys. Res. Commun.* 465, 53–58.

Keatinge, M., Bui, H., Menke, A., Chen, Y.C., Sokol, A.M., Bai, Q., Ellett, F., Da Costa, M., Burke, D., Gegg, M., et al. (2015). Glucocerebrosidase 1 deficient *Danio rerio* mirror key pathological aspects of human Gaucher disease and provide evidence of early microglial activation preceding alpha-synuclein-independent neuronal cell death. *Hum. Mol. Genet.* 24, 6640–6666.

Keatinge, M., Gegg, M.E., Watson, L., Mortiboys, H., Bui, H., van Rens, A., Lefeber, D.J., MacDonald, R.B., Schapira, A.H. V, and Bandmann, O. (2019). Loss of acid sphingomyelinase ameliorates disease progression in a vertebrate model of Glucocerebrosidase deficiency. *BioRxiv* 702340.

Kimmel, C.B., Ballard, W.W., Kimmel, S.R., Ullmann, B., and Schilling, T.F. (1995). Stages of embryonic development of the zebrafish. *Dev. Dyn.* 203, 253–310.

Klein, C., and Westenberger, A. (2012). Genetics of Parkinson's Disease. *Cold Spring Harb. Perspect. Med.* 2.

- Kofman, O. (1971). Treatment of Parkinson's disease with L-dopa: a current appraisal. *Can. Med. Assoc. J.* *104*, 483–487.
- Kreutzberg, G.W. (1996). Microglia: a sensor for pathological events in the CNS. *Trends Neurosci.* *19*, 312–318.
- Krishnakumar, S., Burton, D., Rasco, J., Chen, X., and O'Donnell, J. (2000). Functional interactions between GTP cyclohydrolase I and tyrosine hydroxylase in *Drosophila*. *J. Neurogenet.* *14*, 1–23.
- Kuriyama, K., and Ohkuma, S. (1995). Role of nitric oxide in central synaptic transmission: effects on neurotransmitter release. *Jpn. J. Pharmacol.* *69*, 1–8.
- Kurkowska-Jastrzębska, I., Wrońska, A., Kohutnicka, M., Członkowski, A., and Członkowska, A. (1999). The Inflammatory Reaction Following 1-Methyl-4-phenyl-1,2,3,6-tetrahydropyridine Intoxication in Mouse. *Exp. Neurol.* *156*, 50–61.
- Kyritsis, N., Kizil, C., Zocher, S., Kroehne, V., Kaslin, J., Freudenreich, D., Iltzsche, A., and Brand, M. (2012). Acute Inflammation Initiates the Regenerative Response in the Adult Zebrafish Brain. *Science* (80-.). *338*, 1353 LP – 1356.
- Lam, C.S., Korzh, V., and Strahle, U. (2005). Zebrafish embryos are susceptible to the dopaminergic neurotoxin MPTP. *Eur. J. Neurosci.* *21*, 1758–1762.
- Lambert, A.M., Bonkowsky, J.L., and Masino, M.A. (2012). The Conserved Dopaminergic Diencephalospinal Tract Mediates Vertebrate Locomotor Development in Zebrafish Larvae. *J. Neurosci.* *32*, 13488 LP – 13500.
- Lamensdorf, I., Eisenhofer, G., Harvey-White, J., Hayakawa, Y., Kirk, K., and Kopin, I.J. (2000). Metabolic stress in PC12 cells induces the formation of the endogenous dopaminergic neurotoxin, 3,4-dihydroxyphenylacetaldehyde. *J. Neurosci. Res.* *60*, 552–558.
- Langston, J.W., Ballard, P., Tetrud, J.W., and Irwin, I. (1983). Chronic Parkinsonism in humans due to a product of meperidine-analog synthesis. *Science* *219*, 979–980.

- Langston, J.W., Forno, L.S., Tetrud, J., Reeves, A.G., Kaplan, J.A., and Karluk, D. (1999). Evidence of active nerve cell degeneration in the substantia nigra of humans years after 1-methyl-4-phenyl-1,2,3,6-tetrahydropyridine exposure. *Ann. Neurol.* *46*, 598–605.
- Li, T., Pang, S., Yu, Y., Wu, X., Guo, J., and Zhang, S. (2013). Proliferation of parenchymal microglia is the main source of microgliosis after ischaemic stroke. *Brain* *136*, 3578–3588.
- Liberatore, G.T., Jackson-Lewis, V., Vukosavic, S., Mandir, a S., Vila, M., McAuliffe, W.G., Dawson, V.L., Dawson, T.M., and Przedborski, S. (1999). Inducible nitric oxide synthase stimulates dopaminergic neurodegeneration in the MPTP model of Parkinson disease. *Nat. Med.* *5*, 1403–1409.
- Liew, Z., Wang, A., Bronstein, J., and Ritz, B. (2014). Job exposure matrix (JEM)-derived estimates of lifetime occupational pesticide exposure and the risk of Parkinson's disease. *Arch. Environ. Occup. Health* *69*, 241–251.
- Lindsay, K.W., Bone, I., and Fuller, G. (2010). Section IV - Localised neurological disease and its management. In *Neurology and Neurosurgery Illustrated*, K.W. Lindsay, I. Bone, and G.B.T.-N. and N.I. (Fifth E. Fuller, eds. (Content Repository Only!)), pp. 389–427.
- Linscheid, P., Schaffner, A., and Schoedon, G. (1998). Modulation of inducible nitric oxide synthase mRNA stability by tetrahydrobiopterin in vascular smooth muscle cells. *Biochem. Biophys. Res. Commun.* *243*, 137–141.
- Liu, R., Guo, X., Park, Y., Huang, X., Sinha, R., Freedman, N.D., Hollenbeck, A.R., Blair, A., and Chen, H. (2012). Caffeine intake, smoking, and risk of Parkinson disease in men and women. *Am. J. Epidemiol.* *175*, 1200–1207.
- Livak, K.J., and Schmittgen, T.D. (2001). Analysis of Relative Gene Expression Data Using Real-Time Quantitative PCR and the $2^{-\Delta\Delta CT}$ Method. *Methods* *25*, 402–408.
- Lorenzl, S., Calingasan, N., Yang, L., Albers, D.S., Shugama, S., Gregorio, J., Krell, H.W., Chirichigno, J., Joh, T., and Beal, M.F. (2004). Matrix Metalloproteinase-9 Is Elevated in 1-Methyl-4-Phenyl-1,2,3,6-Tetrahydropyridine-Induced Parkinsonism in Mice. *NeuroMolecular Med.* *5*, 119–131.

- Love, M.I., Huber, W., and Anders, S. (2014). Moderated estimation of fold change and dispersion for RNA-seq data with DESeq2. *Genome Biol.* *15*, 550.
- Lui-Roberts, W.W.Y., Ferraro, F., Nightingale, T.D., and Cutler, D.F. (2008). Aftiphilin and gamma-synergin are required for secretagogue sensitivity of Weibel-Palade bodies in endothelial cells. *Mol. Biol. Cell* *19*, 5072–5081.
- Macleod, A.D., Taylor, K.S.M., and Counsell, C.E. (2014). Mortality in Parkinson's disease: a systematic review and meta-analysis. *Mov. Disord.* *29*, 1615–1622.
- Mallajosyula, J.K., Kaur, D., Chinta, S.J., Rajagopalan, S., Rane, A., Nicholls, D.G., Di Monte, D.A., Macarthur, H., and Andersen, J.K. (2008). MAO-B elevation in mouse brain astrocytes results in Parkinson's pathology. *PLoS One* *3*, e1616.
- Manocha, G.D., Floden, A.M., Puig, K.L., Nagamoto-Combs, K., Scherzer, C.R., and Combs, C.K. (2017). Defining the contribution of neuroinflammation to Parkinson's disease in humanized immune system mice. *Mol. Neurodegener.* *12*, 17.
- Manolio, T.A., Collins, F.S., Cox, N.J., Goldstein, D.B., Hindorff, L.A., Hunter, D.J., McCarthy, M.I., Ramos, E.M., Cardon, L.R., Chakravarti, A., et al. (2009). Finding the missing heritability of complex diseases. *Nature* *461*, 747–753.
- Mantovani, A., Sozzani, S., Locati, M., Allavena, P., and Sica, A. (2002). Macrophage polarization: tumor-associated macrophages as a paradigm for polarized M2 mononuclear phagocytes. *Trends Immunol.* *23*, 549–555.
- Martinez, T.N., and Greenamyre, J.T. (2012). Toxin models of mitochondrial dysfunction in Parkinson's disease. *Antioxid. Redox Signal.* *16*, 920–934.
- Mazzulli, J.R., Xu, Y.-H., Sun, Y., Knight, A.L., McLean, P.J., Caldwell, G.A., Sidransky, E., Grabowski, G.A., and Krainc, D. (2011). Gaucher disease glucocerebrosidase and alpha-synuclein form a bidirectional pathogenic loop in synucleinopathies. *Cell* *146*, 37–52.
- McCarthy, M.I., Abecasis, G.R., Cardon, L.R., Goldstein, D.B., Little, J., Ioannidis, J.P.A., and Hirschhorn, J.N. (2008). Genome-wide association studies for complex traits: consensus,

uncertainty and challenges. *Nat. Rev. Genet.* *9*, 356–369.

McNeill, E., Crabtree, M.J., Sahgal, N., Patel, J., Chuaiphichai, S., Iqbal, A.J., Hale, A.B., Greaves, D.R., and Channon, K.M. (2015). Regulation of iNOS function and cellular redox state by macrophage Gch1 reveals specific requirements for tetrahydrobiopterin in NRF2 activation. *Free Radic. Biol. Med.* *79*, 206–216.

McNeill, E., Stylianou, E., Crabtree, M.J., Harrington-Kandt, R., Kolb, A.-L., Diotallevi, M., Hale, A.B., Bettencourt, P., Tanner, R., O’Shea, M.K., et al. (2018). Regulation of mycobacterial infection by macrophage Gch1 and tetrahydrobiopterin. *Nat. Commun.* *9*, 5409.

Meissner, T.B., Li, A., Biswas, A., Lee, K.-H., Liu, Y.-J., Bayir, E., Iliopoulos, D., van den Elsen, P.J., and Kobayashi, K.S. (2010). NLR family member NLRC5 is a transcriptional regulator of MHC class I genes. *Proc. Natl. Acad. Sci. U. S. A.* *107*, 13794–13799.

Mencacci, N.E., Isaias, I.U., Reich, M.M., Ganos, C., Plagnol, V., Polke, J.M., Bras, J., Hersheson, J., Stamelou, M., Pittman, A.M., et al. (2014). Parkinson’s disease in GTP cyclohydrolase 1 mutation carriers. *Brain* *137*, 2480–2492.

Michelucci, A., Cordes, T., Ghelfi, J., Pailot, A., Reiling, N., Goldmann, O., Binz, T., Wegner, A., Tallam, A., Rausell, A., et al. (2013). Immune-responsive gene 1 protein links metabolism to immunity by catalyzing itaconic acid production. *Proc. Natl. Acad. Sci. U. S. A.* *110*, 7820–7825.

Milstien, S., and Katusic, Z. (1999). Oxidation of tetrahydrobiopterin by peroxynitrite: implications for vascular endothelial function. *Biochem. Biophys. Res. Commun.* *263*, 681–684.

Montioli, R., Voltattorni, C.B., and Bertoldi, M. (2016). Parkinson’s Disease: Recent Updates in the Identification of Human Dopa Decarboxylase Inhibitors. *Curr. Drug Metab.* *17*, 513–518.

Mor, D.E., Daniels, M.J., and Ischiropoulos, H. (2019). The usual suspects, dopamine and alpha-synuclein, conspire to cause neurodegeneration. *Mov. Disord.* *34*, 167–179.

Muller, T. (2015). Catechol-O-methyltransferase inhibitors in Parkinson's disease. *Drugs* 75, 157–174.

Munoz, E., Oliva, R., Obach, V., Marti, M.J., Pastor, P., Ballesta, F., and Tolosa, E. (1997). Identification of Spanish familial Parkinson's disease and screening for the Ala53Thr mutation of the alpha-synuclein gene in early onset patients. *Neurosci. Lett.* 235, 57–60.

Murray, J., Taylor, S.W., Zhang, B., Ghosh, S.S., and Capaldi, R.A. (2003). Oxidative damage to mitochondrial complex I due to peroxynitrite: identification of reactive tyrosines by mass spectrometry. *J. Biol. Chem.* 278, 37223–37230.

Nagatsu, T., and Ichinose, H. (1999). Regulation of pteridine-requiring enzymes by the cofactor tetrahydrobiopterin. *Mol. Neurobiol.* 19, 79–96.

Nagatsu, T., and Sawada, M. (2006). Molecular mechanism of the relation of monoamine oxidase B and its inhibitors to Parkinson's disease: possible implications of glial cells. *J. Neural Transm. Suppl.* 53–65.

Nair, V.D., Olanow, C.W., and Sealfon, S.C. (2003). Activation of phosphoinositide 3-kinase by D2 receptor prevents apoptosis in dopaminergic cell lines. *Biochem. J.* 373, 25 LP – 32.

Nalls, M.A., Pankratz, N., Lill, C.M., Do, C.B., Hernandez, D.G., Saad, M., Destefano, A.L., Kara, E., Bras, J., Sharma, M., et al. (2014). Large-scale meta-analysis of genome-wide association data identifies six new risk loci for Parkinson's disease. *Nat. Publ. Gr.* 46, 989–993.

Nalls, M.A., Blauwendraat, C., Vallerga, C.L., Heilbron, K., Bandres-Ciga, S., Chang, D., Tan, M., Kia, D.A., Noyce, A.J., Xue, A., et al. (2019). Identification of novel risk loci, causal insights, and heritable risk for Parkinson's disease: a meta-analysis of genome-wide association studies. *Lancet Neurol.* 18, 1091–1102.

Nasser, A., Bjerrum, O.J., Heegaard, A.-M., Møller, A.T., Larsen, M., Dalbøge, L.S., Dupont, E., Jensen, T.S., and Møller, L.B. (2013). Impaired behavioural pain responses in hph-1 mice with inherited deficiency in GTP cyclohydrolase 1 in models of inflammatory pain. *Mol. Pain* 9, 5.

Naylor, E.W., Ennis, D., Davidson, A.G., Wong, L.T., Applegarth, D.A., and Niederwieser, A. (1987). Guanosine triphosphate cyclohydrolase I deficiency: early diagnosis by routine urine pteridine screening. *Pediatrics* 79, 374–378.

Nelson, K.K., and Melendez, J.A. (2004). Mitochondrial redox control of matrix metalloproteinases. *Free Radic. Biol. Med.* 37, 768–784.

Niederwieser, A., Blau, N., Wang, M., Joller, P., Atarés, M., and Cardesa-Garcia, J. (1984). GTP cyclohydrolase I deficiency, a new enzyme defect causing hyperphenylalaninemia with neopterin, biopterin, dopamine, and serotonin deficiencies and muscular hypotonia. *Eur. J. Pediatr.* 141, 208–214.

Nimmerjahn, A., Kirchhoff, F., and Helmchen, F. (2005). Resting microglial cells are highly dynamic surveillants of brain parenchyma in vivo. *Science* 308, 1314–1318.

Ohnmacht, J., Yang, Y., Maurer, G.W., Barreiro-Iglesias, A., Tsarouchas, T.M., Wehner, D., Sieger, D., Becker, C.G., and Becker, T. (2016). Spinal motor neurons are regenerated after mechanical lesion and genetic ablation in larval zebrafish. *Development* 143, 1464–1474.

Ojha, S., Javed, H., Azimullah, S., and Haque, M.E. (2016). beta-Caryophyllene, a phytocannabinoid attenuates oxidative stress, neuroinflammation, glial activation, and salvages dopaminergic neurons in a rat model of Parkinson disease. *Mol. Cell. Biochem.* 418, 59–70.

Pan, H.X., Zhao, Y.W., Mei, J.P., Fang, Z.H., Wang, Y., Zhou, X., Zhou, Y.J., Zhang, R., Zhang, K.L., Jiang, L., et al. (2020). GCH1 variants contribute to the risk and earlier age-at-onset of Parkinson's disease: A two-cohort case-control study. *Transl. Neurodegener.* 9.

Pandey, S., and Srivanitchapoom, P. (2017). Levodopa-induced Dyskinesia: Clinical Features, Pathophysiology, and Medical Management. *Ann. Indian Acad. Neurol.* 20, 190–198.

Park, J.-S., Davis, R.L., and Sue, C.M. (2018). Mitochondrial Dysfunction in Parkinson's Disease: New Mechanistic Insights and Therapeutic Perspectives. *Curr. Neurol. Neurosci. Rep.* 18, 21.

Park, J., Lee, S.B., Lee, S., Kim, Y., Song, S., Kim, S., Bae, E., Kim, J., Shong, M., Kim, J.-M., et al. (2006). Mitochondrial dysfunction in *Drosophila* PINK1 mutants is complemented by parkin. *Nature* *441*, 1157–1161.

Pastor, C.M., Williams, D., Yoneyama, T., Hatakeyama, K., Singleton, S., Naylor, E., and Billiar, T.R. (1996). Competition for tetrahydrobiopterin between phenylalanine hydroxylase and nitric oxide synthase in rat liver. *J. Biol. Chem.* *271*, 24534–24538.

Patro, R., Duggal, G., Love, M.I., Irizarry, R.A., and Kingsford, C. (2017). Salmon provides fast and bias-aware quantification of transcript expression. *Nat. Methods* *14*, 417–419.

Pelletier, I., Bally-Cuif, L., and Ziegler, I. (2001). Cloning and developmental expression of zebrafish GTP cyclohydrolase I. *Mech. Dev.* *109*, 99–103.

Pike, L.S., Smift, A.L., Croteau, N.J., Ferrick, D.A., and Wu, M. (2011). Inhibition of fatty acid oxidation by etomoxir impairs NADPH production and increases reactive oxygen species resulting in ATP depletion and cell death in human glioblastoma cells. *Biochim. Biophys. Acta* *1807*, 726–734.

Poewe, W. (2008). Non-motor symptoms in Parkinson's disease. *Eur. J. Neurol.* *15*, 14–20.

Polymeropoulos, M.H., Higgins, J.J., Golbe, L.I., Johnson, W.G., Ide, S.E., Di Iorio, G., Sanges, G., Stenroos, E.S., Pho, L.T., Schaffer, A.A., et al. (1996). Mapping of a gene for Parkinson's disease to chromosome 4q21-q23. *Science* *274*, 1197–1199.

Polymeropoulos, M.H., Lavedan, C., Leroy, E., Ide, S.E., Dehejia, A., Dutra, A., Pike, B., Root, H., Rubenstein, J., Boyer, R., et al. (1997). Mutation in the alpha-synuclein gene identified in families with Parkinson's disease. *Science* *276*, 2045–2047.

Postlethwait, J.H., Woods, I.G., Ngo-Hazelett, P., Yan, Y.L., Kelly, P.D., Chu, F., Huang, H., Hill-Force, A., and Talbot, W.S. (2000). Zebrafish comparative genomics and the origins of vertebrate chromosomes. *Genome Res.* *10*, 1890–1902.

Postuma, R.B., Berg, D., Stern, M., Poewe, W., Olanow, C.W., Oertel, W., Obeso, J., Marek, K., Litvan, I., Lang, A.E., et al. (2015). MDS clinical diagnostic criteria for Parkinson's disease.

Mov. Disord. 30, 1591–1601.

Prinz, M., Erny, D., and Hagemeyer, N. (2017). Ontogeny and homeostasis of CNS myeloid cells. *Nat. Immunol.* 18, 385–392.

Pritchard, J.K. (2001). Are rare variants responsible for susceptibility to complex diseases? *Am. J. Hum. Genet.* 69, 124–137.

Przedborski, S., Jackson-Lewis, V., Yokoyama, R., Shibata, T., Dawson, V.L., and Dawson, T.M. (1996). Role of neuronal nitric oxide in 1-methyl-4-phenyl-1,2,3,6-tetrahydropyridine (MPTP)-induced dopaminergic neurotoxicity. *Proc. Natl. Acad. Sci. U. S. A.* 93, 4565–4571.

Przedborski, S., Jackson-Lewis, V., Djaldetti, R., Liberatore, G., Vila, M., Vukosavic, S., and Almer, G. (2000). The parkinsonian toxin MPTP: action and mechanism. *Restor. Neurol. Neurosci.* 16, 135–142.

Puschmann, A., Jiménez-Ferrer, I., Lundblad-Andersson, E., Mårtensson, E., Hansson, O., Odin, P., Widner, H., Brolin, K., Mzezewa, R., Kristensen, J., et al. (2019). Low prevalence of known pathogenic mutations in dominant PD genes: A Swedish multicenter study. *Parkinsonism Relat. Disord.* 66, 158–165.

Rajput, A.H., Gibb, W.R., Zhong, X.H., Shannak, K.S., Kish, S., Chang, L.G., and Hornykiewicz, O. (1994). Dopa-responsive dystonia: pathological and biochemical observations in a case. *Ann. Neurol.* 35, 396–402.

Rao, T.S., Currie, J.L., Shaffer, A.F., and Isakson, P.C. (1994). In vivo characterization of zymosan-induced mouse peritoneal inflammation. *J. Pharmacol. Exp. Ther.* 269, 917 LP – 925.

Rebrin, I., Bailey, S.W., Boerth, S.R., Ardell, M.D., and Ayling, J.E. (1995). Catalytic characterization of 4a-hydroxytetrahydropterin dehydratase. *Biochemistry* 34, 5801–5810.

Remington, L.T., Babcock, A.A., Zehntner, S.P., and Owens, T. (2007). Microglial recruitment, activation, and proliferation in response to primary demyelination. *Am. J. Pathol.* 170, 1713–1724.

Rengmark, A., Pihlstrøm, L., Linder, J., Forsgren, L., and Toft, M. (2016). Low frequency of GCH1 and TH mutations in Parkinson's disease. *Park. Relat. Disord.* 29, 109–111.

Riboldi, G.M., and Di Fonzo, A.B. (2019). GBA, Gaucher Disease, and Parkinson's Disease: From Genetic to Clinic to New Therapeutic Approaches. *Cells* 8, 364.

Rice, D.S., and Curran, T. (2001). Role of the reelin signaling pathway in central nervous system development. *Annu. Rev. Neurosci.* 24, 1005–1039.

Rink, E., and Wullimann, M.F. (2001). The teleostean (zebrafish) dopaminergic system ascending to the subpallium (striatum) is located in the basal diencephalon (posterior tuberculum). *Brain Res.* 889, 316–330.

Rink, E., and Wullimann, M.F. (2002). Development of the catecholaminergic system in the early zebrafish brain: An immunohistochemical study. *Dev. Brain Res.* 137, 89–100.

Ritchie, M.E., Phipson, B., Wu, D., Hu, Y., Law, C.W., Shi, W., and Smyth, G.K. (2015). limma powers differential expression analyses for RNA-sequencing and microarray studies. *Nucleic Acids Res.* 43, e47.

Ritz, B., Lee, P.-C., Lassen, C.F., and Arah, O.A. (2014). Parkinson disease and smoking revisited: ease of quitting is an early sign of the disease. *Neurology* 83, 1396–1402.

Robinson, M.D., McCarthy, D.J., and Smyth, G.K. (2010). edgeR: a Bioconductor package for differential expression analysis of digital gene expression data. *Bioinformatics* 26, 139–140.

Ryan, B.J., Crabtree, M.J., Channon, K.M., and Wade-Martins, R. (2014a). Parkinson's disease in GTP cyclohydrolase 1 mutation carriers. *Brain* 138, e348–e348.

Ryan, B.J., Lourenço-venda, L.L., Crabtree, M.J., Hale, A.B., Channon, K.M., and Wade-Martins, R. (2014b). α -Synuclein and mitochondrial bioenergetics regulate tetrahydrobiopterin levels in a human dopaminergic model of Parkinson disease. *Free Radic. Biol. Med.* 67, 58–68.

Sato, H., Uematsu, M., Endo, W., Nakayama, T., Kobayashi, T., Hino-Fukuyo, N., Sakamoto,

O., Shintaku, H., and Kure, S. (2014). Early replacement therapy in a first Japanese case with autosomal recessive guanosine triphosphate cyclohydrolase I deficiency with a novel point mutation. *Brain Dev.* 36, 268–271.

Schinelli, S., Zuddas, A., Kopin, I.J., Barker, J.L., and di Porzio, U. (1988). 1-Methyl-4-phenyl-1,2,3,6-tetrahydropyridine metabolism and 1-methyl-4-phenylpyridinium uptake in dissociated cell cultures from the embryonic mesencephalon. *J. Neurochem.* 50, 1900–1907.

Schmidt, E.F., and Strittmatter, S.M. (2007). The CRMP family of proteins and their role in Sema3A signaling. *Adv. Exp. Med. Biol.* 600, 1–11.

Schwarz, Q., and Ruhrberg, C. (2010). Neuropilin, you gotta let me know: should I stay or should I go? *Cell Adh. Migr.* 4, 61–66.

Scott, W.K., Stajich, J.M., Yamaoka, L.H., Speer, M.C., Vance, J.M., Roses, A.D., and Pericak-Vance, M.A. (1997). Genetic Complexity and Parkinson's Disease. *Science* (80-). 277, 387 LP – 390.

Scott, W.K., Yamaoka, L.H., Stajich, J.M., Scott, B.L., Vance, J.M., Roses, A.D., Pericak-Vance, M.A., Watts, R.L., Nance, M., Hubble, J., et al. (1999). The α -synuclein gene is not a major risk factor in familial Parkinson disease. *Neurogenetics* 2, 191–192.

Shan, Y., Zhang, Y., Zhuo, X., Li, X., Peng, J., and Fang, W. (2016). Matrix metalloproteinase-9 plays a role in protecting zebrafish from lethal infection with *Listeria monocytogenes* by enhancing macrophage migration. *Fish Shellfish Immunol.* 54, 179–187.

Shechter, R., and Schwartz, M. (2013). Harnessing monocyte-derived macrophages to control central nervous system pathologies: no longer 'if' but 'how.' *J. Pathol.* 229, 332–346.

Shi, W., Meininger, C.J., Haynes, T.E., Hatakeyama, K., and Wu, G. (2004). Regulation of tetrahydrobiopterin synthesis and bioavailability in endothelial cells. *Cell Biochem. Biophys.* 41, 415–434.

Shin, J.H., Lee, W.-W., Lee, J.-Y., Kim, H.-J., and Jeon, B. (2020). GCH-1 genetic variant may cause Parkinsonism by unmasking the subclinical nigral pathology. *J. Neurol.* 267, 1952–

1959.

Smeets, W.J., and Gonzalez, A. (2000). Catecholamine systems in the brain of vertebrates: new perspectives through a comparative approach. *Brain Res. Brain Res. Rev.* *33*, 308–379.

Smeyne, R.J., Breckenridge, C.B., Beck, M., Jiao, Y., Butt, M.T., Wolf, J.C., Zadory, D., Minnema, D.J., Sturgess, N.C., Travis, K.Z., et al. (2016). Assessment of the Effects of MPTP and Paraquat on Dopaminergic Neurons and Microglia in the Substantia Nigra Pars Compacta of C57BL/6 Mice. *PLoS One* *11*, e0164094.

Smith, N., Longo, N., Levert, K., Hyland, K., and Blau, N. (2019). Phase I clinical evaluation of CNSA-001 (sepiapterin), a novel pharmacological treatment for phenylketonuria and tetrahydrobiopterin deficiencies, in healthy volunteers. *Mol. Genet. Metab.* *126*, 406–412.

Smith, W.W., Pei, Z., Jiang, H., Moore, D.J., Liang, Y., West, A.B., Dawson, V.L., Dawson, T.M., and Ross, C.A. (2005). Leucine-rich repeat kinase 2 (LRRK2) interacts with parkin, and mutant LRRK2 induces neuronal degeneration. *Proc. Natl. Acad. Sci. U. S. A.*

Snow, B.J., Nygaard, T.G., Takahashi, H., and Calne, D.B. (1993). Positron emission tomographic studies of dopa-responsive dystonia and early-onset idiopathic parkinsonism. *Ann. Neurol.* *34*, 733–738.

van Soest, J.J., Stockhammer, O.W., Ordas, A., Bloemberg, G. V, Spaik, H.P., and Meijer, A.H. (2011). Comparison of static immersion and intravenous injection systems for exposure of zebrafish embryos to the natural pathogen *Edwardsiella tarda*. *BMC Immunol.* *12*, 58.

Stewart, Z.A., Westfall, M.D., and Pietenpol, J.A. (2003). Cell-cycle dysregulation and anticancer therapy. *Trends Pharmacol. Sci.* *24*, 139–145.

Stokholm, M.G., Iranzo, A., Ostergaard, K., Serradell, M., Otto, M., Svendsen, K.B., Garrido, A., Vilas, D., Borghammer, P., Santamaria, J., et al. (2017). Assessment of neuroinflammation in patients with idiopathic rapid-eye-movement sleep behaviour disorder: a case-control study. *Lancet. Neurol.* *16*, 789–796.

Su, X., Maguire-Zeiss, K.A., Giuliano, R., Prifti, L., Venkatesh, K., and Federoff, H.J. (2008).

Synuclein activates microglia in a model of Parkinson's disease. *Neurobiol. Aging* 29, 1690–1701.

Subramanian, A., Tamayo, P., Mootha, V.K., Mukherjee, S., Ebert, B.L., Gillette, M.A., Paulovich, A., Pomeroy, S.L., Golub, T.R., Lander, E.S., et al. (2005). Gene set enrichment analysis: A knowledge-based approach for interpreting genome-wide expression profiles. *Proc. Natl. Acad. Sci.* 102, 15545–15550.

Suzuki, I., Tanaka, H., Adachi, Y., and Yadomae, T. (1988). Rapid Measurement of Phagocytosis by Macrophages. *Chem. Pharm. Bull. (Tokyo)*. 36, 4871–4875.

Svineng, G., Ravuri, C., Rikardsen, O., Huseby, N.-E., and Winberg, J.-O. (2008). The role of reactive oxygen species in integrin and matrix metalloproteinase expression and function. *Connect. Tissue Res.* 49, 197–202.

Tadic, V., Kasten, M., Brüggemann, N., Stiller, S., Hagenah, J., and Klein, C. (2012). Dopa-Responsive Dystonia Revisited: Diagnostic Delay, Residual Signs, and Nonmotor Signs. *Arch. Neurol.* 69, 1558–1562.

Tanner, C.M., Kamel, F., Ross, G.W., Hoppin, J.A., Goldman, S.M., Korell, M., Marras, C., Bhudhikanok, G.S., Kasten, M., Chade, A.R., et al. (2011). Rotenone, paraquat, and Parkinson's disease. *Environ. Health Perspect.* 119, 866–872.

Tay, T.L., Ronneberger, O., Ryu, S., Nitschke, R., and Driever, W. (2011). Comprehensive catecholaminergic projectome analysis reveals single-neuron integration of zebrafish ascending and descending dopaminergic systems. *Nat. Commun.* 2, 171.

Thisse, C., and Thisse, B. (2008). High-resolution in situ hybridization to whole-mount zebrafish embryos. *Nat. Protoc.* 3, 59–69.

Thomas, B., and Beal, M.F. (2007). Parkinson's disease. *Hum. Mol. Genet.* 16 *Spec No*, R183–94.

Timmerman, V., Strickland, A. V, and Zuchner, S. (2014). Genetics of Charcot-Marie-Tooth (CMT) Disease within the Frame of the Human Genome Project Success. *Genes (Basel)*. 5,

13–32.

Tolosa, E., Wenning, G., and Poewe, W. (2006). The diagnosis of Parkinson's disease. *Lancet Neurol.* *5*, 75–86.

Trancikova, A., Tsika, E., and Moore, D.J. (2012). Mitochondrial dysfunction in genetic animal models of Parkinson's disease. *Antioxid. Redox Signal.* *16*, 896–919.

Tsarouchas, T.M., Wehner, D., Cavone, L., Munir, T., Keatinge, M., Lambertus, M., Underhill, A., Barrett, T., Kassapis, E., Ogryzko, N., et al. (2018). Dynamic control of proinflammatory cytokines Il-1beta and Tnf-alpha by macrophages in zebrafish spinal cord regeneration. *Nat. Commun.* *9*, 4670.

Tuteja, N., Chandra, M., Tuteja, R., and Misra, M.K. (2004). Nitric Oxide as a Unique Bioactive Signaling Messenger in Physiology and Pathophysiology. *J. Biomed. Biotechnol.* *2004*, 227–237.

Tysnes, O.-B., and Storstein, A. (2017). Epidemiology of Parkinson's disease. *J. Neural Transm.* *124*, 901–905.

Vaarmann, A., Kovac, S., Holmstrom, K.M., Gandhi, S., and Abramov, A.Y. (2013). Dopamine protects neurons against glutamate-induced excitotoxicity. *Cell Death Dis* *4*, e455.

Vasquez-Vivar, J., Kalyanaraman, B., and Martasek, P. (2003). The role of tetrahydrobiopterin in superoxide generation from eNOS: enzymology and physiological implications. *Free Radic. Res.* *37*, 121–127.

Vásquez-Vivar, J., Kalyanaraman, B., Martásek, P., Hogg, N., Masters, B.S.S., Karoui, H., Tordo, P., and Kirkwood A. Pritchard, J. (1998). Superoxide generation by endothelial nitric oxide synthase: The influence of cofactors. *Proc. Natl. Acad. Sci. U. S. A.* *95*, 9220.

Verschuur, C.V.M., Suwijn, S.R., Boel, J.A., Post, B., Bloem, B.R., van Hilten, J.J., van Laar, T., Tissingh, G., Munts, A.G., Deuschl, G., et al. (2019). Randomized Delayed-Start Trial of Levodopa in Parkinson's Disease. *N. Engl. J. Med.* *380*, 315–324.

Walsh, S., Finn, D.P., and Dowd, E. (2011). Time-course of nigrostriatal neurodegeneration and neuroinflammation in the 6-hydroxydopamine-induced axonal and terminal lesion models of Parkinson's disease in the rat. *Neuroscience* 175, 251–261.

Wang, S., Zhang, J., Theel, S., Barb, J.J., Munson, P.J., and Danner, R.L. (2006). Nitric oxide activation of Erk1/2 regulates the stability and translation of mRNA transcripts containing CU-rich elements. *Nucleic Acids Res.* 34, 3044–3056.

Wang, Y., Sung, C.C., and Chung, K.K.K. (2017). Novel enhancement mechanism of tyrosine hydroxylase enzymatic activity by nitric oxide through S-nitrosylation. *Sci. Rep.* 7, 44154.

Watson, M.B., Richter, F., Lee, S.K., Gabby, L., Wu, J., Masliah, E., Effros, R.B., and Chesselet, M.-F. (2012). Regionally-specific microglial activation in young mice over-expressing human wildtype alpha-synuclein. *Exp. Neurol.* 237, 318–334.

Williams-Gray, C.H., Mason, S.L., Evans, J.R., Foltynie, T., Brayne, C., Robbins, T.W., and Barker, R.A. (2013). The CamPaIGN study of Parkinson's disease: 10-year outlook in an incident population-based cohort. *J. Neurol. Neurosurg. Psychiatry* 84, 1258–1264.

Williams, R.A., Mamotte, C.D.S., and Burnett, J.R. (2008). Phenylketonuria: an inborn error of phenylalanine metabolism. *Clin. Biochem. Rev.* 29, 31–41.

Wu, D.C., Jackson-Lewis, V., Vila, M., Tieu, K., Teismann, P., Vadseth, C., Choi, D.-K., Ischiropoulos, H., and Przedborski, S. (2002). Blockade of microglial activation is neuroprotective in the 1-methyl-4-phenyl-1,2,3,6-tetrahydropyridine mouse model of Parkinson disease. *J. Neurosci.* 22, 1763–1771.

Xu, Q., Park, Y., Huang, X., Hollenbeck, A., Blair, A., Schatzkin, A., and Chen, H. (2010). Physical activities and future risk of Parkinson disease. *Neurology* 75, 341–348.

Yao, P., and Fox, P.L. (2013). Aminoacyl-tRNA synthetases in medicine and disease. *EMBO Mol. Med.* 5, 332–343.

Yao, C.-H., Liu, G.-Y., Wang, R., Moon, S.H., Gross, R.W., and Patti, G.J. (2018). Identifying off-target effects of etomoxir reveals that carnitine palmitoyltransferase I is essential for

cancer cell proliferation independent of β -oxidation. *PLOS Biol.* *16*, e2003782.

Yoneyama, T., and Hatakeyama, K. (1998). Decameric GTP cyclohydrolase I forms complexes with two pentameric GTP cyclohydrolase I feedback regulatory proteins in the presence of phenylalanine or of a combination of tetrahydrobiopterin and GTP. *J. Biol. Chem.* *273*, 20102–20108.

Zagorski, J., and Wahl, S.M. (1997). Inhibition of acute peritoneal inflammation in rats by a cytokine-induced neutrophil chemoattractant receptor antagonist. *J. Immunol.* *159*, 1059 LP – 1062.

Zeng, X.-S., Jia, J.-J., Kwon, Y., Wang, S.-D., and Bai, J. (2014). The role of thioredoxin-1 in suppression of endoplasmic reticulum stress in Parkinson disease. *Free Radic. Biol. Med.* *67*, 10–18.

Zeng, X.-S., Geng, W.-S., and Jia, J.-J. (2018). Neurotoxin-Induced Animal Models of Parkinson Disease: Pathogenic Mechanism and Assessment. *ASN Neuro* *10*.

Zhou, W.-Y., Zheng, H., Du, X.-L., and Yang, J.-L. (2016). Characterization of FGFR signaling pathway as therapeutic targets for sarcoma patients. *Cancer Biol. Med.* *13*, 260–268.

Supplementary table 1: list of PD risk loci (Nalls et al., 2019), their nearest gene in the human genome, and the zebrafish ortholog(s) of each gene.

SNP	Nearest Gene	zf ortholog of nearest gene	additional orthologs		
rs147288664	<i>HRNR</i>	<i>n/a</i>			
rs114138760	<i>PMVK</i>	<i>pmvk</i>			
rs35749011	<i>KRTCAP2</i>	<i>krtcap2</i>			
rs76763715	<i>GBAP1</i>	<i>n/a</i>			
rs143756968	<i>ASH1L</i>	<i>ash1l</i>			
rs35643925	<i>SEMA4A</i>	<i>sema3aa</i>	<i>si:ch211-129c21.1</i>	<i>sema3h</i>	<i>sema4e</i>
rs6658353	<i>FCGR2A</i>	<i>zgc:154125</i>	<i>si:ch1073-66l23.1</i>		
rs11578699	<i>VAMP4</i>	<i>vamp4</i>			
rs823118	<i>NUCKS1</i>	<i>nucks1a</i>	<i>nucks1b</i>		
rs11557080	<i>RAB29</i>	<i>n/a</i>			
rs4653767	<i>ITPKB</i>	<i>itpkb</i>			
rs10797576	<i>SIPA1L2</i>	<i>sipa1l2</i>			
rs76116224	<i>KCNS3</i>	<i>kcns3a</i>			
rs2042477	<i>KCNIP3</i>	<i>kcnip3b</i>			
rs11683001	<i>MAP4K4</i>	<i>map4k4</i>			
rs4954162	<i>TMEM163</i>	<i>tmem163a</i>			
rs57891859	<i>TMEM163</i>	<i>tmem163b</i>			
rs1474055	<i>STK39</i>	<i>stk39</i>			
rs73038319	<i>SATB1</i>	<i>satb1b</i>			
rs6808178	<i>LINC00693</i>	<i>n/a</i>			
rs12497850	<i>IP6K2</i>	<i>ip6k2a</i>	<i>ip6k2b</i>		
rs55961674	<i>KPNA1</i>	<i>kpna1</i>			
rs11707416	<i>MED12L</i>	<i>n/a</i>			
rs1450522	<i>SPTSSB</i>	<i>sptssb</i>			
rs10513789	<i>MCCC1</i>	<i>mccc1</i>			
rs873786	<i>GAK</i>	<i>gak</i>			
rs34311866	<i>TMEM175</i>	<i>tmem175</i>			
rs4698412	<i>BST1</i>	<i>n/a</i>			
rs34025766	<i>LCORL</i>	<i>lcorl</i>			
rs6825004	<i>SCARB2</i>	<i>scarb2c</i>			
rs4101061	<i>FAM47E</i>	<i>n/a</i>			
rs6854006	<i>FAM47E-STBD1</i>	<i>stbd1</i>			
rs356228	<i>SNCA</i>	<i>n/a</i>			

rs356182	SNCA	n/a			
rs5019538	SNCA	n/a			
rs356203	SNCA	n/a			
rs13117519	CAMK2D	camk2d1			
rs62333164	CLCN3	clcn3			
rs1867598	ELOVL7	elovl7a	elovl7b		
rs26431	PAM	pam			
rs6875262	ZNF608	n/a			
rs11950533	C5orf24	si:ch1073-44g3.1	zgc:77058		
rs4140646	LOC100131289	n/a			
rs9261484	TRIM40	n/a			
rs9267659	SLC44A4	slc44a4			
rs112485576	HLA-DRB5	n/a			
rs12528068	RIMS1	rims1a			
rs997368	FYN	fyna	fynb		
rs75859381	RPS12	rps12			
rs199351	GPNMB	gpnmb			
rs76949143	GS1-124K5.11	n/a			
rs1293298	CTSB	ctsb			
rs620513	FGF20	fgf20a	fgf20b		
rs2280104	BIN3	bin3			
rs2086641	FAM49B	n/a			
rs13294100	SH3GL2	sh3gl2a	sh3gl2b		
rs10756907	SH3GL2	sh3gl2a	sh3gl2b		
rs6476434	UBAP2	ubap2b	ubap2a		
rs896435	ITGA8	itga8			
rs10748818	GBF1	gbf1			
rs72840788	BAG3	bag3			
rs117896735	INPP5F	inpp5f			
rs7938782	RNF141	rnf141			
rs12283611	DLG2	dlg2			
rs3802920	IGSF9B	igsf9bb			
rs181609621	FGD4	fgd4b	fgd4a		
rs148163066	PKP2	pkp2			
rs183981418	ALG10	alg10			
rs180751015	ALG10	n/a			
rs76904798	LRRK2	lrrk2			

rs28903073	LRRK2	n/a		
rs34637584	LRRK2	n/a		
rs117073808	LRRK2	n/a		
rs141128804	CNTN1	cntn1b		
rs139571909	CNTN1	cntn1a		
rs145918020	CNTN1	n/a		
rs186111791	CNTN1	n/a		
rs187043470	PDZRN4	pdzrn4		
rs138017112	GXYLT1	gxylt1b		
rs144755950	GXYLT1	CABZ01072254.1		
rs7134559	SCAF11	scaf11		
rs10847864	HIP1R	hip1ra	hip1rb	
rs11610045	FBRSL1	si:dkey-33o22.1	fbrsl1	
rs9568188	CAB39L	cab39l		
rs4771268	MBNL2	mbnl2		
rs12147950	MIPOL1	mipol1		
rs11158026	GCH1	gch1		
rs3742785	RPS6KL1	rps6kl1		
rs979812	GALC	galcb	galca	
rs2251086	VPS13C	vps13c		
rs6497339	SYT17	syt17		
rs2904880	CD19	n/a		
rs11150601	SETD1A	n/a		
rs6500328	NOD2	nod2		
rs3104783	CASC16	n/a		
rs10221156	CHD9	chd9		
rs200564078	CNOT1	cnot1		
rs12600861	CHRNA1	chrnb1l	chrnb1	
rs12951632	RETREG3	n/a		
rs2269906	UBTF	ubtf		
rs850738	FAM171A2	fam171a2a	fam171a2b	
rs17686238	MAP3K14	arf2b	map3k14a	
rs62053943	CRHR1	crhr1		
rs9912362	CRHR1	n/a		
rs117615688	CRHR1	n/a		
rs7221167	MAPT-AS1	n/a		
rs7225002	KANSL1	kansl1b	kansl1a	

rs199453	<i>NSF</i>	<i>nsfa</i>	<i>nsfb</i>		
rs11658976	<i>WNT3</i>	<i>wnt3</i>			
rs61169879	<i>BRIP1</i>	<i>brip1</i>			
rs666463	<i>DNAH17</i>	<i>n/a</i>			
rs1941685	<i>ASXL3</i>	<i>n/a</i>			
rs12456492	<i>RIT2</i>	<i>n/a</i>			
rs8087969	<i>MEX3C</i>	<i>n/a</i>			
rs55818311	<i>SPPL2B</i>	<i>sppl2</i>			
rs2295545	<i>DDRKG1</i>	<i>n/a*</i> (<i>a ddrkg1</i> gene exists in zebrafish, however, is not listed as an ortholog in ensembl [ENSDARG00000037172])			
rs77351827	<i>CRLS1</i>	<i>crls1</i>			
rs2248244	<i>DYRK1A</i>	<i>dyrk1ab</i>	<i>dyrk1aa</i>		

Appendix

Supplementary table 2: DE genes in *gch1*^{-/-} vs WT. $|\log_2FC| > 1$, FDR adj $p < 0.05$. Genes are ranked by fold change (FC), from most upregulated to most downregulated. baseMean = mean of normalized counts of all samples. lfcSE = \log_2FC standard error.

ensembl_gene_id	description	entrezgene_							-log10	
		id	baseMean	FC	log ₂ FC	lfcSE	stat	pvalue	padj	(FDRpval)
ENSDARG00000073820	zgc:174917 [Source:ZFIN;Acc:ZDB-GENE-070928-42]	565650	18.0375	247.8927	7.9536	1.5071	5.2772	0.0000	0.0000	4.6735
ENSDARG00000062788	immunoresponsive gene 1, like [Source:ZFIN;Acc:ZDB-GENE-061103-301]	562007	75.7298	59.0532	5.8839	1.3333	4.4130	0.0000	0.0007	3.1279
ENSDARG00000012366	fructose-1,6-bisphosphatase 2 [Source:ZFIN;Acc:ZDB-GENE-040822-23]	445505	55.0836	48.6305	5.6038	1.6854	3.3248	0.0009	0.0184	1.7358
ENSDARG00000077169	si:ch211-153b23.4 [Source:ZFIN;Acc:ZDB-GENE-030131-7332]	335392	49.2386	40.1437	5.3271	1.1506	4.6298	0.0000	0.0003	3.4818
ENSDARG00000095930	myosin, heavy chain a [Source:ZFIN;Acc:ZDB-GENE-060531-50] myosin, heavy polypeptide 1.3, skeletal muscle [Source:ZFIN;Acc:ZDB-GENE-	100149148	29.0532	35.4915	5.1494	1.7174	2.9984	0.0027	0.0397	1.4017
ENSDARG00000067997	070705-74] low density lipoprotein receptor-related protein 2b [Source:ZFIN;Acc:ZDB-GENE-	100008070	815.4419	24.0357	4.5871	1.3526	3.3913	0.0007	0.0156	1.8076
ENSDARG00000007906	111115-1] transmembrane and immunoglobulin domain containing 1 [Source:ZFIN;Acc:ZDB-	101886177	26.9992	22.3323	4.4811	0.9740	4.6008	0.0000	0.0004	3.4426
ENSDARG00000007040	GENE-080303-6]	559127	12.6041	21.7696	4.4442	1.0258	4.3323	0.0000	0.0010	3.0101
ENSDARG00000089399	transmembrane protein 176l.2 [Source:ZFIN;Acc:ZDB-GENE-080829-12] heat shock protein, alpha-crystallin-related, 9 [Source:ZFIN;Acc:ZDB-GENE-080214-	NA	29.7523	20.1709	4.3342	1.0129	4.2789	0.0000	0.0012	2.9278
ENSDARG000000078674	6]	100137108	40.8296	15.3700	3.9420	1.3563	2.9064	0.0037	0.0483	1.3164
ENSDARG000000086374	ISG15 ubiquitin like modifier [Source:ZFIN;Acc:ZDB-GENE-021211-1]	558956	25.7413	14.0678	3.8143	0.7725	4.9374	0.0000	0.0001	4.0387
ENSDARG00000012395	matrix metalloproteinase 13a [Source:ZFIN;Acc:ZDB-GENE-031202-2]	387293	43.4977	14.0562	3.8131	0.5976	6.3807	0.0000	0.0000	7.0180
ENSDARG00000068088	transcobalamin beta a [Source:ZFIN;Acc:ZDB-GENE-060531-123]	566714	50.7592	13.3492	3.7387	1.2117	3.0856	0.0020	0.0321	1.4933
ENSDARG00000057064	glutamyl aminopeptidase [Source:ZFIN;Acc:ZDB-GENE-050309-218]	504088	28.3957	12.3586	3.6274	0.8919	4.0669	0.0000	0.0024	2.6236
ENSDARG00000079647	mucin 13b, cell surface associated [Source:ZFIN;Acc:ZDB-GENE-080220-61]	799648	64.8860	12.0971	3.5966	0.9241	3.8921	0.0001	0.0041	2.3861

ensembl_gene_id	description	entrezgene_							-log10	
		id	baseMean	FC	log2FC	lfcSE	stat	pvalue	padj	(FDRpval)
ENSDARG00000091234	si:ch73-335l21.4 [Source:ZFIN;Acc:ZDB-GENE-160728-105] placenta associated 8, tandem duplicate 1 [Source:ZFIN;Acc:ZDB-GENE-050809-124]	100000332	105.5515	11.5806	3.5336	0.3489	10.1274	0.0000	0.0000	19.6862
ENSDARG00000043729	alanyl (membrane) aminopeptidase b [Source:ZFIN;Acc:ZDB-GENE-030131-1253] heat shock cognate 70-kd protein, tandem duplicate 3 [Source:ZFIN;Acc:ZDB-GENE-110713-1]	791783	25.1437	8.8825	3.1510	0.7559	4.1683	0.0000	0.0017	2.7731
ENSDARG00000103878	si:dkey-239b22.1 [Source:ZFIN;Acc:ZDB-GENE-131119-12]	322533	156.0282	8.4606	3.0808	0.9912	3.1082	0.0019	0.0305	1.5155
ENSDARG00000021924	cathepsin L.1 [Source:ZFIN;Acc:ZDB-GENE-040718-61]	30671	129.9412	8.3041	3.0538	0.8490	3.5972	0.0003	0.0093	2.0295
ENSDARG00000031588	NA	100330672	480.4197	8.2447	3.0435	0.9850	3.0899	0.0020	0.0318	1.4972
ENSDARG00000003902	heat shock cognate 70-kd protein, tandem duplicate 2 [Source:ZFIN;Acc:ZDB-GENE-110713-1]	436641	159.5978	8.2386	3.0424	0.8915	3.4127	0.0006	0.0149	1.8274
ENSDARG00000097289	NA	NA	22.4917	8.0787	3.0141	0.5951	5.0645	0.0000	0.0001	4.2630
ENSDARG00000093365	chloride channel accessory 1 [Source:ZFIN;Acc:ZDB-GENE-030131-6221]	NA	18.7350	7.8601	2.9745	0.7729	3.8487	0.0001	0.0047	2.3283
ENSDARG00000092362	si:dkey-23n7.10 [Source:ZFIN;Acc:ZDB-GENE-141222-64]	100535101	131.3063	7.8055	2.9645	0.7422	3.9944	0.0001	0.0030	2.5206
ENSDARG00000016290	wu:fb59d01 [Source:ZFIN;Acc:ZDB-GENE-030131-1098]	334289	13.7379	7.7934	2.9623	1.0078	2.9393	0.0033	0.0451	1.3458
ENSDARG00000104129	activating transcription factor 3 [Source:ZFIN;Acc:ZDB-GENE-040426-728]	100333689	37.8270	7.7887	2.9614	0.5394	5.4901	0.0000	0.0000	5.0878
ENSDARG00000089361	HtrA serine peptidase 2 [Source:HGNC Symbol;Acc:HGNC:14348]	322379	19.1159	7.6696	2.9392	0.8747	3.3601	0.0008	0.0168	1.7743
ENSDARG00000007823	CCAAT enhancer binding protein beta [Source:ZFIN;Acc:ZDB-GENE-020111-3]	393939	436.9279	7.1569	2.8393	0.5104	5.5632	0.0000	0.0000	5.2361
ENSDARG00000093005	GTP binding protein 2b [Source:ZFIN;Acc:ZDB-GENE-050208-373] heat shock cognate 70-kd protein, tandem duplicate 1 [Source:ZFIN;Acc:ZDB-GENE-990415-91]	NA	21.3279	7.0867	2.8251	0.6954	4.0627	0.0000	0.0024	2.6190
ENSDARG00000042725	matrix metalloproteinase 9 [Source:ZFIN;Acc:ZDB-GENE-040426-2132]	140814	230.5730	6.8200	2.7698	0.4065	6.8136	0.0000	0.0000	8.1112
ENSDARG00000102651	interleukin 11a [Source:ZFIN;Acc:ZDB-GENE-051019-1]	570143	156.8787	6.8043	2.7664	0.4241	6.5226	0.0000	0.0000	7.3498
ENSDARG00000029688	alpha-kinase 3b [Source:ZFIN;Acc:ZDB-GENE-121101-3]	100126123	63.8438	6.6246	2.7278	0.6298	4.3311	0.0000	0.0010	3.0092
ENSDARG00000042816	CD59 glycoprotein-like [Source:NCBI gene;Acc:103910140] E74-like factor 3 (ets domain transcription factor, epithelial-specific)	406397	109.8574	6.5768	2.7174	0.4654	5.8385	0.0000	0.0000	5.7614
ENSDARG00000037859	[Source:ZFIN;Acc:ZDB-GENE-030131-8760]	570404	27.9684	6.3200	2.6599	0.6136	4.3352	0.0000	0.0010	3.0131
ENSDARG00000105630		100534893	16.9207	6.1169	2.6128	0.7607	3.4348	0.0006	0.0141	1.8494
ENSDARG00000101479		103910140	11.9085	6.1052	2.6100	0.8087	3.2274	0.0012	0.0230	1.6380
ENSDARG00000077982		560869	102.8303	6.0096	2.5873	0.5887	4.3951	0.0000	0.0008	3.1000

ensembl_gene_id	description	entrezgene_							-log10	
		id	baseMean	FC	log ₂ FC	lfcSE	stat	pvalue	padj	(FDRpval)
ENSDARG00000070012	sestrin 2 [Source:ZFIN;Acc:ZDB-GENE-070108-1]	100149745	110.4477	5.9778	2.5796	0.3213	8.0283	0.0000	0.0000	11.7100
ENSDARG00000106172	NA	NA	177.6941	5.9647	2.5765	0.8581	3.0024	0.0027	0.0394	1.4048
ENSDARG00000077201	myosin VIIb [Source:ZFIN;Acc:ZDB-GENE-070912-482]	566034	39.2087	5.9008	2.5609	0.5521	4.6383	0.0000	0.0003	3.4957
ENSDARG00000090337	PPARG related coactivator 1 [Source:ZFIN;Acc:ZDB-GENE-030131-9858] glycolipid transfer protein domain containing 2 [Source:ZFIN;Acc:ZDB-GENE-	100002463	62.8657	5.8817	2.5562	0.4161	6.1434	0.0000	0.0000	6.4603
ENSDARG00000067889	060526-346]	565337	13.9590	5.7836	2.5320	0.6163	4.1081	0.0000	0.0021	2.6802
ENSDARG00000097157	si:ch211-207n23.2 [Source:ZFIN;Acc:ZDB-GENE-131121-310]	559783	85.9731	5.6702	2.5034	0.5923	4.2267	0.0000	0.0014	2.8537
ENSDARG00000055723	heat shock cognate 70-kd protein, like [Source:ZFIN;Acc:ZDB-GENE-050321-1]	560210	167.8237	5.6208	2.4908	0.7493	3.3240	0.0009	0.0184	1.7350
ENSDARG00000037425	S100 calcium binding protein A10a [Source:ZFIN;Acc:ZDB-GENE-041010-35]	449788	47.2758	5.5862	2.4819	0.6789	3.6556	0.0003	0.0080	2.0944
ENSDARG00000007377	ornithine decarboxylase 1 [Source:ZFIN;Acc:ZDB-GENE-010816-1]	114426	174.7346	5.2739	2.3989	0.3904	6.1452	0.0000	0.0000	6.4603
ENSDARG00000074642	NA	NA	24.7637	5.2595	2.3949	0.5996	3.9940	0.0001	0.0030	2.5206
ENSDARG00000057706	si:ch211-137i24.10 [Source:ZFIN;Acc:ZDB-GENE-060526-34]	565274	28.5279	5.2463	2.3913	0.6857	3.4875	0.0005	0.0126	1.9009
ENSDARG00000004748	zgc:100868 [Source:ZFIN;Acc:ZDB-GENE-040801-33] stearoyl-CoA desaturase (delta-9-desaturase) [Source:ZFIN;Acc:ZDB-GENE-031106-	554458	461.8269	5.2145	2.3825	0.7391	3.2235	0.0013	0.0232	1.6345
ENSDARG00000033662	3]	386661	50.7220	5.2021	2.3791	0.5029	4.7303	0.0000	0.0002	3.6510
ENSDARG00000078552	grainyhead-like transcription factor 3 [Source:ZFIN;Acc:ZDB-GENE-030131-9854]	794613	37.7050	5.0856	2.3464	0.6967	3.3678	0.0008	0.0165	1.7835
ENSDARG00000075045	chemokine (C-X-C motif) ligand 18b [Source:ZFIN;Acc:ZDB-GENE-090313-165]	795785	21.0780	5.0465	2.3353	0.5551	4.2066	0.0000	0.0015	2.8311
ENSDARG00000031757	transmembrane channel-like 4 [Source:ZFIN;Acc:ZDB-GENE-030131-7489]	100333974	12.7175	4.9626	2.3111	0.7035	3.2850	0.0010	0.0202	1.6951
ENSDARG00000099581	NA	NA	38.0090	4.8375	2.2743	0.7338	3.0993	0.0019	0.0312	1.5063
ENSDARG00000102375	si:ch211-204c21.1 [Source:ZFIN;Acc:ZDB-GENE-030429-35] heat shock protein 90, alpha (cytosolic), class A member 1, tandem duplicate 1	NA	15.7663	4.8307	2.2722	0.6222	3.6518	0.0003	0.0082	2.0886
ENSDARG00000010478	[Source:ZFIN;Acc:ZDB-GENE-990415-94]	30591	61.0429	4.8161	2.2679	0.6952	3.2622	0.0011	0.0213	1.6713
ENSDARG00000000551	solute carrier family 1 member 4 [Source:ZFIN;Acc:ZDB-GENE-030616-566] growth arrest and DNA-damage-inducible, alpha, a [Source:ZFIN;Acc:ZDB-GENE-	368885	590.3677	4.7837	2.2581	0.2533	8.9164	0.0000	0.0000	14.8672
ENSDARG00000043581	040426-1501]	393548	67.1625	4.6986	2.2322	0.4607	4.8452	0.0000	0.0001	3.8581
ENSDARG00000014916	solute carrier family 10 member 2 [Source:ZFIN;Acc:ZDB-GENE-040426-1328]	393329	14.0702	4.6751	2.2250	0.7461	2.9823	0.0029	0.0409	1.3887
ENSDARG00000002509	zgc:153911 [Source:ZFIN;Acc:ZDB-GENE-061013-174]	768172	17.2569	4.6727	2.2243	0.6142	3.6212	0.0003	0.0089	2.0526

ensembl_gene_id	description	entrezgene_							-log10	
		id	baseMean	FC	log2FC	lfcSE	stat	pvalue	padj	(FDRpval)
ENSDARG00000088040	si:dkeyp-27c8.2 [Source:ZFIN;Acc:ZDB-GENE-090311-51]	557652	18.9159	4.5975	2.2009	0.5576	3.9468	0.0001	0.0035	2.4554
ENSDARG00000013871	solute carrier family 5 member 1 [Source:ZFIN;Acc:ZDB-GENE-040426-1524]	393654	56.2320	4.5960	2.2004	0.7138	3.0825	0.0021	0.0324	1.4895
ENSDARG00000093347	si:ch211-239f4.6 [Source:ZFIN;Acc:ZDB-GENE-061009-18]	799879	26.6835	4.5762	2.1941	0.7272	3.0173	0.0026	0.0380	1.4206
ENSDARG00000089697	nuclear factor, erythroid 2-like 2b [Source:ZFIN;Acc:ZDB-GENE-120320-3]	100873093	268.5438	4.5008	2.1702	0.6494	3.3418	0.0008	0.0175	1.7563
ENSDARG00000071347	aftiphilin b [Source:ZFIN;Acc:ZDB-GENE-060503-388]	100004990	189.7813	4.4651	2.1587	0.1921	11.2346	0.0000	0.0000	24.4794
ENSDARG00000016081	claudin 15-like a [Source:ZFIN;Acc:ZDB-GENE-010328-12]	81591	28.3858	4.4638	2.1583	0.5995	3.6004	0.0003	0.0093	2.0322
ENSDARG00000021046	rhomboid domain containing 1 [Source:ZFIN;Acc:ZDB-GENE-050417-85]	550277	79.7136	4.4332	2.1483	0.3822	5.6208	0.0000	0.0000	5.3399
ENSDARG00000005565	ectonucleoside triphosphate diphosphohydrolase 8 [Source:ZFIN;Acc:ZDB-GENE-040724-142]	436652	30.1931	4.4259	2.1460	0.7064	3.0380	0.0024	0.0363	1.4406
ENSDARG00000097539	si:ch211-39f2.3 [Source:ZFIN;Acc:ZDB-GENE-131126-52]	110437733	21.7037	4.3981	2.1369	0.7396	2.8892	0.0039	0.0499	1.3019
ENSDARG00000079227	pleckstrin homology domain containing, family 5 member 1 [Source:ZFIN;Acc:ZDB-GENE-080204-50]	100136845	29.2307	4.3344	2.1158	0.7120	2.9717	0.0030	0.0417	1.3795
ENSDARG00000103727	transferrin receptor 2 [Source:ZFIN;Acc:ZDB-GENE-041220-3]	494476	19.9357	4.3112	2.1081	0.6329	3.3310	0.0009	0.0181	1.7432
ENSDARG00000100185	ELOVL fatty acid elongase 7b [Source:ZFIN;Acc:ZDB-GENE-030131-5485]	NA	21.1085	4.2912	2.1014	0.7099	2.9602	0.0031	0.0431	1.3658
ENSDARG00000075926	immunoglobulin like and fibronectin type III domain containing 1, tandem duplicate 2 [Source:ZFIN;Acc:ZDB-GENE-130530-789]	NA	18.6084	4.2901	2.1010	0.5642	3.7240	0.0002	0.0067	2.1746
ENSDARG00000068128	protein phosphatase 1, regulatory subunit 15B [Source:ZFIN;Acc:ZDB-GENE-030829-40]	571470	205.4372	4.2719	2.0949	0.3116	6.7230	0.0000	0.0000	7.9016
ENSDARG00000098206	peptidyl-tRNA hydrolase 1 homolog [Source:ZFIN;Acc:ZDB-GENE-050306-33]	503752	37.8415	4.2590	2.0905	0.5461	3.8284	0.0001	0.0050	2.3037
ENSDARG00000036376	claudin 7a [Source:ZFIN;Acc:ZDB-GENE-040718-29]	436612	171.1426	4.2329	2.0816	0.2792	7.4558	0.0000	0.0000	9.9172
ENSDARG00000098761	regulator of G protein signaling 2 [Source:ZFIN;Acc:ZDB-GENE-040718-410]	436935	20.8215	4.1935	2.0681	0.5227	3.9563	0.0001	0.0034	2.4689
ENSDARG00000101135	si:dkey-85k7.7 [Source:ZFIN;Acc:ZDB-GENE-040128-7]	NA	1206.7552	4.1708	2.0603	0.2473	8.3312	0.0000	0.0000	12.7559
ENSDARG00000013711	zgc:77486 [Source:ZFIN;Acc:ZDB-GENE-040426-2056]	335278	56.4168	4.1050	2.0374	0.3812	5.3452	0.0000	0.0000	4.8023
ENSDARG00000053131	interleukin-1 receptor-associated kinase 3 [Source:ZFIN;Acc:ZDB-GENE-060503-710]	567444	16.2269	4.0873	2.0312	0.5904	3.4402	0.0006	0.0140	1.8532
ENSDARG00000003219	bridging integrator 2a [Source:ZFIN;Acc:ZDB-GENE-041114-126]	492780	42.9490	4.0699	2.0250	0.7000	2.8929	0.0038	0.0496	1.3047
ENSDARG00000068586	cadherin related family member 2 [Source:NCBI gene;Acc:100536704]	100536704	40.8837	4.0188	2.0068	0.5431	3.6949	0.0002	0.0072	2.1406

ensembl_gene_id	description	entrezgene_							-log10	
		id	baseMean	FC	log ₂ FC	lfcSE	stat	pvalue	padj	(FDRpval)
ENSDARG00000044441	si:ch73-194h10.2 [Source:ZFIN;Acc:ZDB-GENE-100921-21] filamin C, gamma a (actin binding protein 280) [Source:ZFIN;Acc:ZDB-GENE-	108190403	66.5837	3.9821	1.9935	0.4685	4.2550	0.0000	0.0013	2.8975
ENSDARG00000018566	070503-1] phosphatidylinositol transfer protein, alpha a [Source:ZFIN;Acc:ZDB-GENE-040426-	100048921	45.7104	3.9717	1.9898	0.5725	3.4756	0.0005	0.0129	1.8896
ENSDARG00000039490	744]	393909	46.6646	3.9369	1.9771	0.6303	3.1369	0.0017	0.0284	1.5473
ENSDARG00000094316	si:rp71-80o10.4 [Source:ZFIN;Acc:ZDB-GENE-090313-413]	100307105	68.0407	3.8991	1.9631	0.3657	5.3675	0.0000	0.0000	4.8402
ENSDARG00000060246	solute carrier family 16 member 6b [Source:ZFIN;Acc:ZDB-GENE-110208-3]	561766	433.9272	3.8964	1.9621	0.2882	6.8085	0.0000	0.0000	8.1112
ENSDARG00000069027	adrenomedullin b [Source:ZFIN;Acc:ZDB-GENE-120221-6] ATPase Na ⁺ /K ⁺ transporting subunit alpha 1a, tandem duplicate 3	570100	16.3515	3.8917	1.9604	0.5105	3.8400	0.0001	0.0048	2.3164
ENSDARG00000039131	[Source:ZFIN;Acc:ZDB-GENE-001212-3] ribosomal protein S6 kinase b, polypeptide 1a [Source:ZFIN;Acc:ZDB-GENE-091113-	64614	65.0952	3.8794	1.9558	0.6538	2.9916	0.0028	0.0402	1.3958
ENSDARG00000018399	52]	562242	111.8313	3.8211	1.9340	0.3456	5.5963	0.0000	0.0000	5.2940
ENSDARG00000034577	si:dkey-23o4.6 [Source:ZFIN;Acc:ZDB-GENE-100922-3]	561542	41.8181	3.8120	1.9306	0.5772	3.3447	0.0008	0.0174	1.7595
ENSDARG00000035913	tyrosyl-tRNA synthetase [Source:ZFIN;Acc:ZDB-GENE-030425-2]	368235	219.9992	3.8016	1.9266	0.2688	7.1675	0.0000	0.0000	9.1230
ENSDARG00000087832	BCL3 transcription coactivator [Source:ZFIN;Acc:ZDB-GENE-061013-1]	565656	12.4533	3.7782	1.9177	0.5841	3.2834	0.0010	0.0202	1.6939
ENSDARG00000068851	ring finger protein 183 [Source:ZFIN;Acc:ZDB-GENE-060929-1090]	767730	40.4168	3.7425	1.9040	0.6108	3.1170	0.0018	0.0300	1.5235
ENSDARG00000015355	FOS-like antigen 1a [Source:ZFIN;Acc:ZDB-GENE-061207-7] 3-hydroxy-3-methylglutaryl-CoA reductase a [Source:ZFIN;Acc:ZDB-GENE-040401-	564241	219.0524	3.7408	1.9034	0.2951	6.4497	0.0000	0.0000	7.1693
ENSDARG00000052734	2]	559054	70.2248	3.6752	1.8778	0.4126	4.5510	0.0000	0.0004	3.3577
ENSDARG00000068515	chitin synthase 1 [Source:ZFIN;Acc:ZDB-GENE-030131-1188]	322468	85.4566	3.6652	1.8739	0.4355	4.3032	0.0000	0.0011	2.9644
ENSDARG00000010641	solute carrier family 20 member 1b [Source:ZFIN;Acc:ZDB-GENE-030131-260]	321541	1254.5873	3.6563	1.8704	0.2530	7.3934	0.0000	0.0000	9.7532
ENSDARG00000013250	threonyl-tRNA synthetase [Source:ZFIN;Acc:ZDB-GENE-041010-218] transient receptor potential cation channel, subfamily M, member 4a	449661	502.5263	3.6504	1.8681	0.2727	6.8514	0.0000	0.0000	8.2025
ENSDARG00000059993	[Source:ZFIN;Acc:ZDB-GENE-090302-3]	100004946	43.0251	3.6503	1.8680	0.6354	2.9400	0.0033	0.0451	1.3459
ENSDARG00000102377	solute carrier family 6 member 16b [Source:ZFIN;Acc:ZDB-GENE-070424-95]	567809	129.7665	3.6087	1.8515	0.2660	6.9610	0.0000	0.0000	8.5186
ENSDARG00000030616	nuclear factor, erythroid 2-like 1a [Source:ZFIN;Acc:ZDB-GENE-040630-5]	405781	83.4724	3.6058	1.8503	0.5125	3.6104	0.0003	0.0091	2.0417
ENSDARG00000099351	insulin-like growth factor binding protein 1a [Source:ZFIN;Acc:ZDB-GENE-021231-1]	317638	654.3139	3.5836	1.8414	0.5679	3.2425	0.0012	0.0222	1.6536

ensembl_gene_id	description	entrezgene_							-log10	
		id	baseMean	FC	log ₂ FC	lfcSE	stat	pvalue	padj	(FDRpval)
ENSDARG00000013050	ATP-binding cassette, sub-family C (CFTR/MRP), member 12 [Source:ZFIN;Acc:ZDB-GENE-050517-25]	568482	28.8978	3.5628	1.8330	0.4565	4.0157	0.0001	0.0028	2.5532
ENSDARG00000016188	strawberry notch homolog 2 [Source:HGNC Symbol;Acc:HGNC:29158]	100002292	337.6051	3.5389	1.8233	0.3952	4.6134	0.0000	0.0003	3.4594
ENSDARG00000052045	gamma-glutamyltransferase 5a [Source:ZFIN;Acc:ZDB-GENE-080226-1]	569734	60.6419	3.5336	1.8211	0.4355	4.1821	0.0000	0.0016	2.7932
ENSDARG00000099073	si:zfos-741a10.4 [Source:ZFIN;Acc:ZDB-GENE-141222-65]	NA	13.3843	3.5282	1.8189	0.6098	2.9827	0.0029	0.0408	1.3889
ENSDARG00000053467	GTP binding protein 1 [Source:ZFIN;Acc:ZDB-GENE-030909-12]	378721	860.9983	3.5164	1.8141	0.2540	7.1418	0.0000	0.0000	9.0629
ENSDARG00000054814	protein tyrosine phosphatase 4A3b [Source:ZFIN;Acc:ZDB-GENE-030131-2635]	567691	617.6750	3.5023	1.8083	0.3272	5.5264	0.0000	0.0000	5.1682
ENSDARG00000102758	gamma-glutamyl hydrolase [Source:NCBI gene;Acc:553228]	553228	16.5673	3.4981	1.8066	0.5566	3.2459	0.0012	0.0220	1.6568
ENSDARG00000001953	6-phosphofructo-2-kinase/fructose-2,6-biphosphatase 3 [Source:ZFIN;Acc:ZDB-GENE-040426-2724]	554477	481.9403	3.4882	1.8025	0.3515	5.1281	0.0000	0.0000	4.3939
ENSDARG00000022303	HIG1 hypoxia inducible domain family, member 1A [Source:ZFIN;Acc:ZDB-GENE-030826-15]	373084	353.2617	3.4577	1.7898	0.3563	5.0227	0.0000	0.0001	4.1816
ENSDARG00000098949	mesothelin a [Source:ZFIN;Acc:ZDB-GENE-120727-9]	NA	59.9107	3.4543	1.7884	0.6065	2.9487	0.0032	0.0442	1.3542
ENSDARG00000078172	prostaglandin F2 receptor inhibitor [Source:NCBI gene;Acc:101883373]	101883373	270.0795	3.4463	1.7850	0.3295	5.4175	0.0000	0.0000	4.9490
ENSDARG00000016200	tribbles pseudokinase 3 [Source:ZFIN;Acc:ZDB-GENE-040426-2609]	405805	650.6569	3.4444	1.7843	0.2971	6.0047	0.0000	0.0000	6.1126
ENSDARG00000063539	solute carrier family 25 member 15a [Source:ZFIN;Acc:ZDB-GENE-070112-1072]	791156	22.7024	3.4186	1.7734	0.6140	2.8882	0.0039	0.0500	1.3011
ENSDARG00000041083	alanyl (membrane) aminopeptidase a [Source:ZFIN;Acc:ZDB-GENE-030131-4781]	558452	42.8266	3.4064	1.7683	0.4942	3.5783	0.0003	0.0098	2.0105
ENSDARG00000029290	syntaxin 11b, tandem duplicate 1 [Source:ZFIN;Acc:ZDB-GENE-040426-1893]	393836	35.2411	3.4037	1.7671	0.5522	3.2001	0.0014	0.0244	1.6120
ENSDARG00000076251	interferon regulatory factor 3 [Source:ZFIN;Acc:ZDB-GENE-071120-7]	564854	17.8300	3.3743	1.7546	0.4828	3.6341	0.0003	0.0086	2.0662
ENSDARG00000105424	si:rp71-46j2.7 [Source:ZFIN;Acc:ZDB-GENE-160113-120]	368429	98.4994	3.3729	1.7540	0.3985	4.4011	0.0000	0.0008	3.1088
ENSDARG00000092671	par-3 family cell polarity regulator beta a [Source:ZFIN;Acc:ZDB-GENE-080225-12]	100149472	63.8513	3.3685	1.7521	0.5603	3.1274	0.0018	0.0291	1.5358
ENSDARG00000007412	solute carrier family 2 member 1b [Source:ZFIN;Acc:ZDB-GENE-090915-1]	100321338	134.9862	3.3653	1.7507	0.3228	5.4241	0.0000	0.0000	4.9567
ENSDARG00000003313	eps8 like 1b [Source:ZFIN;Acc:ZDB-GENE-050506-143]	553062	30.0512	3.3619	1.7493	0.4976	3.5151	0.0004	0.0117	1.9335
ENSDARG00000042874	pleckstrin homology-like domain, family A, member 2 [Source:ZFIN;Acc:ZDB-GENE-050522-73]	553622	31.8641	3.3563	1.7469	0.5929	2.9463	0.0032	0.0444	1.3523
ENSDARG00000024540	tetraspanin 36 [Source:ZFIN;Acc:ZDB-GENE-040718-248]	437021	294.0892	3.3531	1.7455	0.5262	3.3169	0.0009	0.0188	1.7266
ENSDARG00000091111	si:ch211-15b10.6 [Source:ZFIN;Acc:ZDB-GENE-160728-113]	560548	277.8493	3.3213	1.7318	0.3713	4.6637	0.0000	0.0003	3.5350

ensembl_gene_id	description	entrezgene_							-log10	
		id	baseMean	FC	log ₂ FC	lfcSE	stat	pvalue	padj	(FDRpval)
ENSDARG00000102580	ras-related protein Rab-39A-like [Source:NCBI gene;Acc:100330257]	100330257	47.8807	3.2974	1.7213	0.3925	4.3855	0.0000	0.0008	3.0857
ENSDARG00000103615	si:dkey-31j3.11 [Source:ZFIN;Acc:ZDB-GENE-141216-100]	NA	11.3461	3.2750	1.7115	0.5912	2.8951	0.0038	0.0494	1.3063
ENSDARG00000076472	ovo-like zinc finger 1a [Source:ZFIN;Acc:ZDB-GENE-031010-37] DnaJ heat shock protein family (Hsp40) member B9b [Source:ZFIN;Acc:ZDB-GENE-	792456	16.9439	3.2629	1.7062	0.5609	3.0419	0.0024	0.0360	1.4439
ENSDARG00000016886	050522-76]	554091	27.7062	3.2484	1.6997	0.4346	3.9112	0.0001	0.0039	2.4110
ENSDARG00000070972	si:ch211-81a5.8 [Source:ZFIN;Acc:ZDB-GENE-060503-138]	560648	75.6237	3.2361	1.6943	0.3809	4.4477	0.0000	0.0007	3.1864
ENSDARG00000035622	X-box binding protein 1 [Source:ZFIN;Acc:ZDB-GENE-011210-2] 5-methyltetrahydrofolate-homocysteine methyltransferase [Source:ZFIN;Acc:ZDB-	140614	1133.4431	3.2296	1.6914	0.2270	7.4519	0.0000	0.0000	9.9172
ENSDARG00000104906	GENE-031001-5]	378847	52.1377	3.2088	1.6820	0.2920	5.7595	0.0000	0.0000	5.5983
ENSDARG00000045051	solute carrier family 16 member 3 [Source:ZFIN;Acc:ZDB-GENE-030131-5487]	327276	354.4827	3.2061	1.6808	0.3498	4.8050	0.0000	0.0002	3.7894
ENSDARG00000099424	lecithin-cholesterol acyltransferase [Source:ZFIN;Acc:ZDB-GENE-010716-3] phosphodiesterase 6A, cGMP-specific, rod, alpha [Source:ZFIN;Acc:ZDB-GENE-	793137	106.0944	3.1816	1.6697	0.3713	4.4965	0.0000	0.0005	3.2617
ENSDARG00000000380	030616-42]	368410	62.4068	3.1732	1.6659	0.4027	4.1366	0.0000	0.0019	2.7212
ENSDARG00000062662	leiomodrin 3 (fetal) [Source:ZFIN;Acc:ZDB-GENE-090313-353]	100149390	26.5011	3.1584	1.6592	0.5261	3.1538	0.0016	0.0272	1.5652
ENSDARG00000100887	si:dkey-11f4.20 [Source:ZFIN;Acc:ZDB-GENE-070912-359]	100322456	62.4226	3.1542	1.6573	0.4099	4.0435	0.0001	0.0026	2.5909
ENSDARG00000086256	si:ch211-236p5.2 [Source:ZFIN;Acc:ZDB-GENE-081028-33]	561457	234.2560	3.1260	1.6443	0.1696	9.6971	0.0000	0.0000	17.9121
ENSDARG00000041051	MID1 interacting protein 1a [Source:ZFIN;Acc:ZDB-GENE-990415-81]	30600	103.4585	3.1173	1.6403	0.4475	3.6656	0.0002	0.0078	2.1066
ENSDARG00000059805	solute carrier family 25 member 38a [Source:ZFIN;Acc:ZDB-GENE-060929-320]	767662	35.2947	3.1120	1.6378	0.4652	3.5208	0.0004	0.0115	1.9410
ENSDARG00000036028	arrestin domain containing 3b [Source:ZFIN;Acc:ZDB-GENE-040912-182]	447866	1973.9514	3.1064	1.6352	0.2585	6.3258	0.0000	0.0000	6.8834
ENSDARG00000099186	solute carrier family 1 member 5 [Source:ZFIN;Acc:ZDB-GENE-070501-4]	100002129	696.2830	3.0918	1.6284	0.3298	4.9371	0.0000	0.0001	4.0387
ENSDARG00000045180	actin alpha 2, smooth muscle [Source:ZFIN;Acc:ZDB-GENE-030131-1229] DNA-damage regulated autophagy modulator 1 [Source:ZFIN;Acc:ZDB-GENE-	322509	103.8154	3.0881	1.6267	0.5448	2.9861	0.0028	0.0406	1.3913
ENSDARG00000045561	041010-147]	450028	19.6468	3.0790	1.6225	0.4191	3.8709	0.0001	0.0044	2.3564
ENSDARG00000053853	solute carrier family 13 member 2 [Source:ZFIN;Acc:ZDB-GENE-040426-2389] retinol binding protein 1, cellular, tandem duplicate 2 [Source:ZFIN;Acc:ZDB-GENE-	406537	93.2141	3.0759	1.6210	0.5167	3.1372	0.0017	0.0283	1.5475
ENSDARG00000038742	070912-18]	100141334	32.7568	3.0747	1.6204	0.5134	3.1563	0.0016	0.0271	1.5663

ensembl_gene_id	description	entrezgene_					-log10				
		id	baseMean	FC	log2FC	lfcSE	stat	pvalue	padj	(FDRpval)	
ENSDARG00000041394	DnaJ heat shock protein family (Hsp40) member B1b [Source:ZFIN;Acc:ZDB-GENE-030131-5455]	327244	62.9590	3.0587	1.6129	0.4320	3.7340	0.0002	0.0065	2.1862	
ENSDARG00000028163	proteoglycan 4b [Source:ZFIN;Acc:ZDB-GENE-041014-324]	553377	159.6389	3.0454	1.6066	0.4427	3.6290	0.0003	0.0087	2.0609	
ENSDARG00000059294	macrophage receptor with collagenous structure [Source:ZFIN;Acc:ZDB-GENE-120514-2]	571584	26.8818	3.0095	1.5895	0.5431	2.9270	0.0034	0.0463	1.3346	
ENSDARG00000043586	Fas cell surface death receptor [Source:ZFIN;Acc:ZDB-GENE-061019-2]	768248	29.0475	3.0068	1.5882	0.3654	4.3463	0.0000	0.0009	3.0335	
ENSDARG00000060494	glutamyl-prolyl-tRNA synthetase [Source:ZFIN;Acc:ZDB-GENE-030131-638]	562037	1414.3925	2.9984	1.5842	0.1505	10.5271	0.0000	0.0000	21.3707	
ENSDARG00000094792	twinfilin actin-binding protein 2a [Source:ZFIN;Acc:ZDB-GENE-030131-7638]	100310784	134.0514	2.9899	1.5801	0.4813	3.2828	0.0010	0.0203	1.6935	
ENSDARG00000059247	transmembrane protein 54a [Source:ZFIN;Acc:ZDB-GENE-040426-1304]	393318	57.5230	2.9830	1.5768	0.4766	3.3085	0.0009	0.0191	1.7185	
ENSDARG00000103799	lysyl-tRNA synthetase [Source:ZFIN;Acc:ZDB-GENE-021115-8]	280647	691.2093	2.9759	1.5733	0.2188	7.1913	0.0000	0.0000	9.1659	
ENSDARG00000010316	glutamyl-tRNA synthetase [Source:ZFIN;Acc:ZDB-GENE-040426-1011]	394188	136.8113	2.9731	1.5720	0.2331	6.7436	0.0000	0.0000	7.9473	
ENSDARG00000002298	ankyrin repeat domain 22 [Source:ZFIN;Acc:ZDB-GENE-040426-1120]	393244	29.5778	2.9713	1.5711	0.4328	3.6298	0.0003	0.0087	2.0609	
ENSDARG00000100564	SIL1 nucleotide exchange factor [Source:ZFIN;Acc:ZDB-GENE-160113-49]	568308	115.1198	2.9631	1.5671	0.2709	5.7843	0.0000	0.0000	5.6489	
ENSDARG00000104659		NA	16.4879	2.9398	1.5557	0.5179	3.0036	0.0027	0.0393	1.4059	
ENSDARG00000013670	hypoxia up-regulated 1 [Source:ZFIN;Acc:ZDB-GENE-030131-5344]	327133	273.0024	2.9303	1.5511	0.2719	5.7056	0.0000	0.0000	5.4747	
ENSDARG00000098646	methylenetetrahydrofolate dehydrogenase (NADP+ dependent) 2,										
ENSDARG00000098646	methenyltetrahydrofolate cyclohydrolase [Source:ZFIN;Acc:ZDB-GENE-040704-20]	100004977	167.9326	2.9232	1.5476	0.3073	5.0358	0.0000	0.0001	4.2036	
ENSDARG00000057121	complement component 7b [Source:ZFIN;Acc:ZDB-GENE-021120-1]	570832	357.8316	2.9150	1.5435	0.3021	5.1085	0.0000	0.0000	4.3517	
ENSDARG00000009266	UEV and lactate/malate dehydrogenase domains [Source:ZFIN;Acc:ZDB-GENE-040801-138]	445225	22.3651	2.9139	1.5429	0.4574	3.3737	0.0007	0.0163	1.7889	
ENSDARG00000026611	suppressor of cytokine signaling 3b [Source:ZFIN;Acc:ZDB-GENE-040426-2528]	406596	218.5784	2.9100	1.5410	0.3341	4.6125	0.0000	0.0003	3.4594	
ENSDARG00000089307	phorbol-12-myristate-13-acetate-induced protein 1 [Source:ZFIN;Acc:ZDB-GENE-070119-3]	751765	44.3517	2.8948	1.5334	0.4434	3.4582	0.0005	0.0135	1.8688	
ENSDARG00000045842	zgc:113263 [Source:ZFIN;Acc:ZDB-GENE-050306-34]	503753	702.4659	2.8872	1.5297	0.2587	5.9129	0.0000	0.0000	5.8944	
ENSDARG00000070434	ras homolog family member V [Source:ZFIN;Acc:ZDB-GENE-031002-10]	100005849	20.0108	2.8740	1.5231	0.4879	3.1218	0.0018	0.0295	1.5295	
ENSDARG00000027744	growth arrest and DNA-damage-inducible, beta a [Source:ZFIN;Acc:ZDB-GENE-040426-1971]	406304	445.1772	2.8736	1.5228	0.2900	5.2516	0.0000	0.0000	4.6304	

ensembl_gene_id	description	entrezgene_							-log10	
		id	baseMean	FC	log ₂ FC	lfcSE	stat	pvalue	padj	(FDRpval)
ENSDARG00000069295	BCL6A transcription repressor b [Source:ZFIN;Acc:ZDB-GENE-030131-7523]	100001936	80.0886	2.8520	1.5120	0.4441	3.4046	0.0007	0.0152	1.8192
ENSDARG00000040064	acid phosphatase 6, lysophosphatidic [Source:ZFIN;Acc:ZDB-GENE-050208-290]	558758	23.1251	2.8408	1.5063	0.4504	3.3444	0.0008	0.0174	1.7595
ENSDARG00000076221	ferritin, heavy polypeptide-like 28 [Source:ZFIN;Acc:ZDB-GENE-030131-7540]	100006523	66.8668	2.8339	1.5028	0.4998	3.0065	0.0026	0.0390	1.4090
ENSDARG00000056367	MPV17 mitochondrial membrane protein-like 2 [Source:ZFIN;Acc:ZDB-GENE-040718-306]	436840	44.6752	2.8296	1.5006	0.5110	2.9366	0.0033	0.0454	1.3433
ENSDARG00000020952	si:ch211-214j8.1 [Source:ZFIN;Acc:ZDB-GENE-060526-100]	100000223	46.2972	2.8150	1.4931	0.4043	3.6929	0.0002	0.0073	2.1395
ENSDARG00000090401	apoptosis facilitator Bcl-2-like protein 14 [Source:NCBI gene;Acc:101885512]	101885512	20.0892	2.8149	1.4931	0.4498	3.3197	0.0009	0.0186	1.7302
ENSDARG00000037121	methionine adenosyltransferase II, alpha b [Source:ZFIN;Acc:ZDB-GENE-050327-6]	791612	193.7923	2.7771	1.4736	0.3965	3.7167	0.0002	0.0068	2.1677
ENSDARG00000061120	solute carrier family 43 member 2b [Source:ZFIN;Acc:ZDB-GENE-041212-6]	494042	187.1812	2.7761	1.4731	0.4140	3.5582	0.0004	0.0104	1.9837
ENSDARG00000075121	heparin-binding EGF-like growth factor a [Source:ZFIN;Acc:ZDB-GENE-080204-119]	797938	81.6328	2.7636	1.4665	0.3640	4.0295	0.0001	0.0027	2.5703
ENSDARG00000040284	si:dkey-79d12.5 [Source:ZFIN;Acc:ZDB-GENE-131127-429]	100538016	237.8941	2.7154	1.4412	0.2350	6.1321	0.0000	0.0000	6.4387
ENSDARG00000102482	zgc:165573 [Source:ZFIN;Acc:ZDB-GENE-070615-27]	100073329	59.0520	2.7106	1.4386	0.3527	4.0793	0.0000	0.0023	2.6429
ENSDARG00000091003	interleukin 34 [Source:ZFIN;Acc:ZDB-GENE-050419-150]	560193	16.5230	2.7092	1.4379	0.4810	2.9895	0.0028	0.0404	1.3938
ENSDARG00000076238	GRAM domain containing 1c [Source:ZFIN;Acc:ZDB-GENE-050506-88]	563054	33.6738	2.7049	1.4356	0.4830	2.9721	0.0030	0.0417	1.3796
ENSDARG00000099002	cAMP responsive element binding protein 5a [Source:ZFIN;Acc:ZDB-GENE-120827-2]	101886947	29.8435	2.6951	1.4304	0.4038	3.5422	0.0004	0.0108	1.9667
ENSDARG00000056795	serpin peptidase inhibitor, clade E (nexin, plasminogen activator inhibitor type 1), member 1 [Source:ZFIN;Acc:ZDB-GENE-070912-60]	100136840	38.4888	2.6915	1.4284	0.4347	3.2858	0.0010	0.0202	1.6951
ENSDARG00000044754	gonadotropin-releasing hormone 2 [Source:ZFIN;Acc:ZDB-GENE-030516-1]	353222	41.7548	2.6854	1.4251	0.3730	3.8207	0.0001	0.0051	2.2935
ENSDARG00000016733	phosphoserine aminotransferase 1 [Source:ZFIN;Acc:ZDB-GENE-030131-5723]	327512	288.6714	2.6812	1.4229	0.2827	5.0323	0.0000	0.0001	4.1985
ENSDARG00000104687	solute carrier family 16 member 9b [Source:ZFIN;Acc:ZDB-GENE-040801-69]	445158	516.4638	2.6811	1.4228	0.2905	4.8974	0.0000	0.0001	3.9586
ENSDARG00000094210	ferritin, heavy polypeptide-like 31 [Source:ZFIN;Acc:ZDB-GENE-050522-428]	553552	123.7546	2.6642	1.4137	0.4767	2.9656	0.0030	0.0424	1.3722
ENSDARG00000042934	cellular communication network factor 2a [Source:ZFIN;Acc:ZDB-GENE-030131-102]	321449	230.8661	2.6580	1.4104	0.4077	3.4589	0.0005	0.0135	1.8694
ENSDARG00000012369	retinol dehydrogenase 10b [Source:ZFIN;Acc:ZDB-GENE-030909-7]	378722	39.5449	2.6562	1.4094	0.3477	4.0538	0.0001	0.0025	2.6078
ENSDARG00000028731	signal transducer and activator of transcription 4 [Source:ZFIN;Acc:ZDB-GENE-030616-264]	368519	32.9172	2.6367	1.3988	0.4739	2.9515	0.0032	0.0439	1.3572

ensembl_gene_id	description	entrezgene_							-log10	
		id	baseMean	FC	log ₂ FC	lfcSE	stat	pvalue	padj	(FDRpval)
ENSDARG00000013926	solute carrier family 16 member 9a [Source:ZFIN;Acc:ZDB-GENE-040426-1364]	795588	205.6533	2.6349	1.3977	0.2882	4.8501	0.0000	0.0001	3.8640
ENSDARG00000023287	hydroxysteroid (17-beta) dehydrogenase 3 [Source:ZFIN;Acc:ZDB-GENE-040426-1339]	393335	47.2809	2.6201	1.3896	0.2881	4.8231	0.0000	0.0002	3.8170
ENSDARG00000070426	ChaC, cation transport regulator homolog 1 (E. coli) [Source:ZFIN;Acc:ZDB-GENE-030131-1957]	563855	2142.4096	2.6188	1.3889	0.4035	3.4425	0.0006	0.0140	1.8553
ENSDARG00000088584	si:ch73-352p18.4 [Source:ZFIN;Acc:ZDB-GENE-110411-101]	100535246	27.6502	2.6091	1.3836	0.4694	2.9475	0.0032	0.0443	1.3531
ENSDARG00000038027	nucleolar protein 12 [Source:ZFIN;Acc:ZDB-GENE-040426-1035]	393260	79.7408	2.6037	1.3806	0.2906	4.7515	0.0000	0.0002	3.6854
ENSDARG00000105889	NA	NA	71.4906	2.5831	1.3691	0.3719	3.6813	0.0002	0.0075	2.1254
ENSDARG00000034707	finTRIM family, member 85 [Source:ZFIN;Acc:ZDB-GENE-070705-22]	569616	39.2765	2.5816	1.3683	0.3134	4.3666	0.0000	0.0009	3.0549
ENSDARG00000071082	prolyl 4-hydroxylase, alpha polypeptide I b [Source:ZFIN;Acc:ZDB-GENE-030131-4089]	100003675	50.4521	2.5729	1.3634	0.3208	4.2503	0.0000	0.0013	2.8914
ENSDARG00000015263	adrenomedullin a [Source:ZFIN;Acc:ZDB-GENE-120221-5]	556502	36.6876	2.5460	1.3482	0.3973	3.3931	0.0007	0.0155	1.8090
ENSDARG00000045141	aquaporin 8a, tandem duplicate 1 [Source:ZFIN;Acc:ZDB-GENE-040912-106]	447923	30.0326	2.5338	1.3413	0.4612	2.9085	0.0036	0.0481	1.3182
ENSDARG00000077407	si:dkey-184p18.2 [Source:ZFIN;Acc:ZDB-GENE-060503-55]	768134	96.7072	2.5291	1.3386	0.4145	3.2294	0.0012	0.0229	1.6399
ENSDARG00000055784	protein tyrosine phosphatase non-receptor type 3 [Source:ZFIN;Acc:ZDB-GENE-030131-2934]	407635	119.2736	2.5197	1.3333	0.3826	3.4845	0.0005	0.0126	1.8980
ENSDARG00000033735	neutrophil cytosolic factor 1 [Source:ZFIN;Acc:ZDB-GENE-031006-6]	378966	18.2556	2.5059	1.3253	0.4507	2.9403	0.0033	0.0451	1.3460
ENSDARG00000008388	matrix metalloproteinase 14b (membrane-inserted) [Source:ZFIN;Acc:ZDB-GENE-030901-2]	566945	402.9948	2.5022	1.3232	0.2325	5.6919	0.0000	0.0000	5.4510
ENSDARG00000093019	si:dkey-83k24.5 [Source:ZFIN;Acc:ZDB-GENE-081104-440]	NA	116.8084	2.4948	1.3189	0.3884	3.3958	0.0007	0.0154	1.8112
ENSDARG00000031795	ATP-binding cassette, sub-family F (GCN20), member 1 [Source:ZFIN;Acc:ZDB-GENE-050517-31]	406467	316.6051	2.4928	1.3178	0.2624	5.0213	0.0000	0.0001	4.1816
ENSDARG00000078002	si:dkey-13n15.11 [Source:ZFIN;Acc:ZDB-GENE-070705-295]	562819	42.3471	2.4926	1.3177	0.3886	3.3908	0.0007	0.0156	1.8074
ENSDARG00000074378	JunB proto-oncogene, AP-1 transcription factor subunit a [Source:ZFIN;Acc:ZDB-GENE-040426-2172]	407086	154.9501	2.4908	1.3166	0.2631	5.0051	0.0000	0.0001	4.1566
ENSDARG00000071116	endonuclease/exonuclease/phosphatase family domain containing 1 [Source:ZFIN;Acc:ZDB-GENE-040426-1831]	402965	100.8109	2.4892	1.3157	0.3271	4.0224	0.0001	0.0027	2.5614

ensembl_gene_id	description	entrezgene_					-log10				
		id	baseMean	FC	log ₂ FC	lfcSE	stat	pvalue	padj	(FDRpval)	
ENSDARG00000054543	SAM domain, SH3 domain and nuclear localisation signals 1a [Source:ZFIN;Acc:ZDB-GENE-030131-8639]	336695	119.5121	2.4868	1.3143	0.3900	3.3696	0.0008	0.0164	1.7853	
ENSDARG00000102076	serine peptidase inhibitor, Kazal type 2, tandem duplicate 1 [Source:ZFIN;Acc:ZDB-GENE-070112-972]	565497	34.6731	2.4820	1.3115	0.4349	3.0159	0.0026	0.0380	1.4205	
ENSDARG00000054304	homeobox and leucine zipper encoding a [Source:ZFIN;Acc:ZDB-GENE-030616-592]	368671	112.0680	2.4775	1.3089	0.2852	4.5901	0.0000	0.0004	3.4259	
ENSDARG00000100815	serine and arginine rich splicing factor 3a [Source:ZFIN;Acc:ZDB-GENE-030616-631]	368925	129.8225	2.4569	1.2968	0.4486	2.8906	0.0038	0.0497	1.3033	
ENSDARG00000044125	thioredoxin [Source:ZFIN;Acc:ZDB-GENE-040718-162]	436734	125.8503	2.4436	1.2890	0.4242	3.0388	0.0024	0.0362	1.4408	
ENSDARG00000086418	si:ch211-236p5.3 [Source:ZFIN;Acc:ZDB-GENE-081028-31]	100002266	401.8600	2.4275	1.2795	0.2262	5.6567	0.0000	0.0000	5.3930	
ENSDARG00000070452	store-operated calcium entry-associated regulatory factor [Source:ZFIN;Acc:ZDB-GENE-060929-208]	767649	153.9330	2.4220	1.2762	0.2556	4.9936	0.0000	0.0001	4.1353	
ENSDARG00000061549	forkhead box O1 b [Source:ZFIN;Acc:ZDB-GENE-080425-3]	567969	23.7523	2.4218	1.2761	0.3858	3.3077	0.0009	0.0191	1.7182	
ENSDARG00000074287	serine palmitoyltransferase, long chain base subunit 2b [Source:ZFIN;Acc:ZDB-GENE-080305-8]	557286	329.6437	2.4194	1.2747	0.2878	4.4295	0.0000	0.0007	3.1545	
ENSDARG00000070794	growth regulating estrogen receptor binding 1 [Source:ZFIN;Acc:ZDB-GENE-070112-332]	791135	197.2849	2.4157	1.2724	0.3251	3.9145	0.0001	0.0038	2.4152	
ENSDARG00000026229	prion protein a [Source:ZFIN;Acc:ZDB-GENE-041217-6]	494129	77.0780	2.4100	1.2690	0.4017	3.1594	0.0016	0.0270	1.5693	
ENSDARG00000042548	tpd52 like 1 [Source:ZFIN;Acc:ZDB-GENE-050522-121]	553769	58.0452	2.4057	1.2664	0.3991	3.1736	0.0015	0.0262	1.5821	
ENSDARG00000008732	zgc:66479 [Source:ZFIN;Acc:ZDB-GENE-031030-10]	327541	43.1431	2.4039	1.2654	0.3524	3.5908	0.0003	0.0094	2.0251	
ENSDARG00000038025	chromobox homolog 7a [Source:ZFIN;Acc:ZDB-GENE-050417-400]	550551	2007.1214	2.3985	1.2622	0.2609	4.8384	0.0000	0.0001	3.8457	
ENSDARG00000052279	oxidative stress induced growth inhibitor 1 [Source:ZFIN;Acc:ZDB-GENE-040426-864]	393155	177.0215	2.3949	1.2600	0.4168	3.0233	0.0025	0.0375	1.4258	
ENSDARG00000007955	isoleucyl-tRNA synthetase [Source:ZFIN;Acc:ZDB-GENE-030131-6325]	334393	347.4498	2.3771	1.2492	0.2516	4.9657	0.0000	0.0001	4.0845	
ENSDARG00000069681	polycomb group ring finger 6 [Source:ZFIN;Acc:ZDB-GENE-060526-178]	555238	20.8548	2.3759	1.2485	0.3845	3.2473	0.0012	0.0220	1.6580	
ENSDARG00000059035	P450 (cytochrome) oxidoreductase b [Source:ZFIN;Acc:ZDB-GENE-030131-5767]	327556	1010.3814	2.3754	1.2482	0.2952	4.2278	0.0000	0.0014	2.8546	
ENSDARG00000026090	ADP-ribose/CDP-alcohol diphosphatase, manganese-dependent [Source:ZFIN;Acc:ZDB-GENE-040426-1406]	393393	31.8468	2.3734	1.2469	0.3893	3.2027	0.0014	0.0243	1.6142	
ENSDARG00000096389	SRY-box transcription factor 4a [Source:ZFIN;Acc:ZDB-GENE-030131-8290]	NA	21.0698	2.3728	1.2466	0.4108	3.0346	0.0024	0.0365	1.4380	

ensembl_gene_id	description	entrezgene_					-log10				
		id	baseMean	FC	log ₂ FC	lfcSE	stat	pvalue	padj	(FDRpval)	
ENSDARG00000015164	MAPK interacting serine/threonine kinase 2b [Source:ZFIN;Acc:ZDB-GENE-030829-2]	373121	6178.1299	2.3639	1.2412	0.2719	4.5647	0.0000	0.0004	3.3824	
ENSDARG00000056200	ATP-binding cassette, sub-family B (MDR/TAP), member 9 [Source:ZFIN;Acc:ZDB-GENE-050517-12]	570148	90.7515	2.3601	1.2389	0.2346	5.2808	0.0000	0.0000	4.6747	
ENSDARG00000079497	transcriptional and immune response regulator a [Source:ZFIN;Acc:ZDB-GENE-050320-36]	541345	132.3649	2.3571	1.2370	0.2773	4.4617	0.0000	0.0006	3.2097	
ENSDARG00000069142	alanyl-tRNA synthetase [Source:ZFIN;Acc:ZDB-GENE-030131-3663]	324940	1194.8241	2.3450	1.2296	0.2090	5.8829	0.0000	0.0000	5.8432	
ENSDARG00000041951	selenoprotein O1 [Source:ZFIN;Acc:ZDB-GENE-030131-4485]	558648	358.7883	2.3426	1.2281	0.2875	4.2712	0.0000	0.0012	2.9145	
ENSDARG00000029695	phosphoglycolate phosphatase [Source:ZFIN;Acc:ZDB-GENE-030131-6240]	792824	88.4728	2.3406	1.2268	0.3791	3.2362	0.0012	0.0225	1.6482	
ENSDARG00000045075	transmembrane protein 106A [Source:ZFIN;Acc:ZDB-GENE-030131-5129]	407612	105.0781	2.3291	1.2198	0.3186	3.8289	0.0001	0.0050	2.3037	
ENSDARG00000023028	carnitine deficiency-associated gene expressed in ventricle 3 [Source:ZFIN;Acc:ZDB-GENE-030131-6034]	334102	476.2347	2.3287	1.2195	0.2637	4.6251	0.0000	0.0003	3.4760	
ENSDARG00000093201	si:dkey-112e17.1 [Source:ZFIN;Acc:ZDB-GENE-060526-193]	NA	121.9718	2.3183	1.2131	0.2176	5.5739	0.0000	0.0000	5.2542	
ENSDARG00000103720	zgc:162730 [Source:ZFIN;Acc:ZDB-GENE-030131-6366]	564559	275.2873	2.3152	1.2111	0.3549	3.4129	0.0006	0.0149	1.8274	
ENSDARG00000034396	methionyl-tRNA synthetase [Source:ZFIN;Acc:ZDB-GENE-030219-83]	338183	313.6399	2.3070	1.2060	0.2226	5.4184	0.0000	0.0000	4.9490	
ENSDARG00000041108	cathepsin H [Source:ZFIN;Acc:ZDB-GENE-030131-3539]	324818	54.6542	2.2987	1.2008	0.3253	3.6919	0.0002	0.0073	2.1384	
ENSDARG00000101894	serine/threonine kinase 10 [Source:ZFIN;Acc:ZDB-GENE-040426-1136]	394108	89.7423	2.2934	1.1975	0.3465	3.4560	0.0005	0.0136	1.8674	
ENSDARG00000100872	OTU deubiquitinase 1 [Source:ZFIN;Acc:ZDB-GENE-170421-2]	100537398	40.4201	2.2851	1.1923	0.3162	3.7708	0.0002	0.0059	2.2296	
ENSDARG00000020645	solute carrier family 7 member 3a [Source:ZFIN;Acc:ZDB-GENE-041114-206]	492363	1342.5872	2.2812	1.1898	0.1946	6.1139	0.0000	0.0000	6.3984	
ENSDARG00000086848	ATPase family AAA domain containing 3 [Source:ZFIN;Acc:ZDB-GENE-040426-1826]	403004	53.7235	2.2804	1.1893	0.2694	4.4139	0.0000	0.0007	3.1280	
ENSDARG00000070110	opsin 5 [Source:ZFIN;Acc:ZDB-GENE-041001-179]	564181	34.2277	2.2791	1.1884	0.3081	3.8568	0.0001	0.0046	2.3367	
ENSDARG00000004840	Ras association domain family member 1 [Source:ZFIN;Acc:ZDB-GENE-040912-14]	447811	114.4543	2.2758	1.1863	0.2877	4.1234	0.0000	0.0020	2.6999	
ENSDARG00000059906	syndecan 4 [Source:ZFIN;Acc:ZDB-GENE-061111-1]	568593	815.7884	2.2726	1.1844	0.2902	4.0809	0.0000	0.0023	2.6430	
ENSDARG00000058206	si:ch211-153b23.5 [Source:ZFIN;Acc:ZDB-GENE-030131-9744]	321177	166.1232	2.2705	1.1830	0.2003	5.9067	0.0000	0.0000	5.8863	
ENSDARG00000035890	alpha-L-fucosidase 1, tandem duplicate 1 [Source:ZFIN;Acc:ZDB-GENE-030131-7434]	335494	219.2301	2.2615	1.1772	0.3953	2.9780	0.0029	0.0413	1.3841	
ENSDARG00000002213	inversin [Source:ZFIN;Acc:ZDB-GENE-020507-2]	245946	55.0791	2.2613	1.1772	0.2950	3.9899	0.0001	0.0030	2.5179	

ensembl_gene_id	description	entrezgene_					-log10			
		id	baseMean	FC	log ₂ FC	lfcSE	stat	pvalue	padj	(FDRpval)
ENSDARG00000070230	aldehyde dehydrogenase 1 family, member L2 [Source:ZFIN;Acc:ZDB-GENE-100426-6]	100333269	109.5272	2.2608	1.1768	0.2847	4.1342	0.0000	0.0019	2.7178
ENSDARG00000026322	dehydrogenase/reductase (SDR family) member 13a, tandem duplicate 1 [Source:ZFIN;Acc:ZDB-GENE-041114-58]	492491	272.7450	2.2593	1.1759	0.2993	3.9284	0.0001	0.0037	2.4299
ENSDARG00000019417	growth arrest and DNA-damage-inducible, gamma a [Source:ZFIN;Acc:ZDB-GENE-040426-1882]	402991	205.3153	2.2537	1.1723	0.1883	6.2263	0.0000	0.0000	6.6491
ENSDARG00000105104	si:dkey-223p19.1 [Source:ZFIN;Acc:ZDB-GENE-120215-140]	NA	123.8168	2.2435	1.1657	0.3307	3.5247	0.0004	0.0113	1.9451
ENSDARG00000071021	3'-phosphoadenosine 5'-phosphosulfate synthase 2a [Source:ZFIN;Acc:ZDB-GENE-061110-85]	777719	122.6562	2.2356	1.1606	0.3567	3.2536	0.0011	0.0216	1.6646
ENSDARG00000056160	heat shock 60 protein 1 [Source:ZFIN;Acc:ZDB-GENE-021206-1]	282676	1487.7229	2.2344	1.1599	0.2978	3.8952	0.0001	0.0041	2.3898
ENSDARG00000015803	Smith-Magenis syndrome chromosome region, candidate 8b [Source:ZFIN;Acc:ZDB-GENE-061122-1]	407723	43.0101	2.2302	1.1572	0.3270	3.5385	0.0004	0.0109	1.9630
ENSDARG00000034568	fat storage inducing transmembrane protein 2 [Source:ZFIN;Acc:ZDB-GENE-050508-5]	552928	75.6942	2.2261	1.1545	0.2881	4.0070	0.0001	0.0029	2.5404
ENSDARG00000104938	FtsJ RNA 2'-O-methyltransferase 3 [Source:ZFIN;Acc:ZDB-GENE-030131-9828]	321247	116.0999	2.2156	1.1477	0.2486	4.6164	0.0000	0.0003	3.4635
ENSDARG00000029075	6-phosphofructo-2-kinase/fructose-2,6-biphosphatase 4b [Source:ZFIN;Acc:ZDB-GENE-031031-4]	386663	886.9921	2.2154	1.1475	0.2996	3.8309	0.0001	0.0049	2.3055
ENSDARG00000104555	SH2 domain containing 3Cb [Source:ZFIN;Acc:ZDB-GENE-040426-1052]	394051	215.6345	2.2143	1.1468	0.3250	3.5287	0.0004	0.0112	1.9499
ENSDARG00000012199	glutamic pyruvate transaminase (alanine aminotransferase) 2 [Source:ZFIN;Acc:ZDB-GENE-030729-8]	799963	240.2995	2.2102	1.1442	0.2078	5.5068	0.0000	0.0000	5.1244
ENSDARG00000045254	zmp:0000000624 [Source:ZFIN;Acc:ZDB-GENE-130530-627]	567594	69.3768	2.2099	1.1440	0.3523	3.2475	0.0012	0.0220	1.6580
ENSDARG00000012390	potassium channel, subfamily K, member 5b [Source:ZFIN;Acc:ZDB-GENE-040426-1297]	393606	44.0352	2.1992	1.1370	0.3747	3.0348	0.0024	0.0365	1.4380
ENSDARG00000035858	calponin 2 [Source:ZFIN;Acc:ZDB-GENE-030131-542]	406658	192.0737	2.1985	1.1365	0.3196	3.5564	0.0004	0.0104	1.9835
ENSDARG00000078425	ornithine aminotransferase [Source:ZFIN;Acc:ZDB-GENE-110411-148]	572518	322.7957	2.1947	1.1340	0.2173	5.2190	0.0000	0.0000	4.5638
ENSDARG00000104538	transmembrane protein 184a [Source:ZFIN;Acc:ZDB-GENE-040426-2925]	406841	62.7155	2.1889	1.1302	0.3505	3.2249	0.0013	0.0231	1.6359
ENSDARG00000008765	transmembrane p24 trafficking protein 5 [Source:ZFIN;Acc:ZDB-GENE-040426-1302]	393374	41.2059	2.1882	1.1297	0.3048	3.7066	0.0002	0.0070	2.1535

ensembl_gene_id	description	entrezgene_							-log10	
		id	baseMean	FC	log ₂ FC	lfcSE	stat	pvalue	padj	(FDRpval)
ENSDARG0000007836	cathepsin La [Source:ZFIN;Acc:ZDB-GENE-030131-106]	321453	2135.8527	2.1869	1.1289	0.2764	4.0845	0.0000	0.0023	2.6468
ENSDARG00000059070	glycyl-tRNA synthetase [Source:ZFIN;Acc:ZDB-GENE-030131-9174]	337230	599.7881	2.1866	1.1287	0.2384	4.7354	0.0000	0.0002	3.6575
ENSDARG00000020847	ATPase H+ transporting V0 subunit a1a [Source:ZFIN;Acc:ZDB-GENE-030131-3027]	324307	234.1499	2.1841	1.1271	0.3276	3.4406	0.0006	0.0140	1.8534
ENSDARG00000074060	mitogen-activated protein kinase kinase kinase 14a [Source:ZFIN;Acc:ZDB-GENE-120215-80]	100004261	200.1351	2.1840	1.1269	0.2134	5.2813	0.0000	0.0000	4.6747
ENSDARG00000055314	minichromosome maintenance complex binding protein [Source:ZFIN;Acc:ZDB-GENE-030131-9676]	321119	74.4671	2.1836	1.1267	0.2400	4.6953	0.0000	0.0003	3.5893
ENSDARG00000019861	fibrinogen-like 2a [Source:ZFIN;Acc:ZDB-GENE-030131-9506]	565637	23.8458	2.1707	1.1182	0.3741	2.9892	0.0028	0.0404	1.3936
ENSDARG00000008363	MCL1 apoptosis regulator, BCL2 family member b [Source:ZFIN;Acc:ZDB-GENE-030825-1]	373102	417.1689	2.1691	1.1171	0.2908	3.8418	0.0001	0.0048	2.3187
ENSDARG00000034667	lipoprotein lipase-like [Source:NCBI gene;Acc:100331214]	100331214	123.7918	2.1658	1.1149	0.3622	3.0785	0.0021	0.0328	1.4847
ENSDARG00000022309	desmoplakin a [Source:ZFIN;Acc:ZDB-GENE-030131-2743]	324023	207.7286	2.1637	1.1135	0.3742	2.9759	0.0029	0.0414	1.3826
ENSDARG00000103038	phosphoinositide-3-kinase, regulatory subunit 3a (gamma) [Source:ZFIN;Acc:ZDB-GENE-040426-1978]	406311	241.0317	2.1621	1.1124	0.3366	3.3045	0.0010	0.0192	1.7160
ENSDARG00000075014	sequestosome 1 [Source:ZFIN;Acc:ZDB-GENE-040426-2204]	406452	852.1802	2.1613	1.1119	0.2865	3.8811	0.0001	0.0043	2.3709
ENSDARG00000024314	homocysteine-inducible, endoplasmic reticulum stress-inducible, ubiquitin-like domain member 1 [Source:ZFIN;Acc:ZDB-GENE-050913-47]	565499	379.2726	2.1591	1.1104	0.1955	5.6812	0.0000	0.0000	5.4298
ENSDARG00000100826	hypoxia inducible factor 1 subunit alpha, like [Source:ZFIN;Acc:ZDB-GENE-040426-1315]	393376	1874.0460	2.1574	1.1093	0.2425	4.5752	0.0000	0.0004	3.4004
ENSDARG00000030700	CTP synthase 1a [Source:ZFIN;Acc:ZDB-GENE-030131-808]	322089	108.0770	2.1538	1.1069	0.2145	5.1603	0.0000	0.0000	4.4466
ENSDARG00000041428	yrdC N(6)-threonylcarbamoyltransferase domain containing [Source:ZFIN;Acc:ZDB-GENE-070410-65]	797343	124.4562	2.1424	1.0992	0.2717	4.0461	0.0001	0.0025	2.5947
ENSDARG00000004017	sperm associated antigen 1a [Source:ZFIN;Acc:ZDB-GENE-030131-9443]	564953	114.7774	2.1410	1.0983	0.2108	5.2094	0.0000	0.0000	4.5512
ENSDARG00000103308	macrophage stimulating 1 [Source:ZFIN;Acc:ZDB-GENE-020806-3]	259260	72.5667	2.1372	1.0957	0.2731	4.0124	0.0001	0.0028	2.5493
ENSDARG00000098377	tumor necrosis factor receptor superfamily, member 11b [Source:ZFIN;Acc:ZDB-GENE-081104-76]	NA	35.6866	2.1337	1.0934	0.3370	3.2442	0.0012	0.0221	1.6555
ENSDARG00000014329	nucleophosmin 1a [Source:ZFIN;Acc:ZDB-GENE-021028-1]	266985	435.2869	2.1322	1.0923	0.2302	4.7454	0.0000	0.0002	3.6763

ensembl_gene_id	description	entrezgene_							-log10	
		id	baseMean	FC	log ₂ FC	lfcSE	stat	pvalue	padj	(FDRpval)
ENSDARG00000051853	galactosamine (N-acetyl)-6-sulfatase [Source:ZFIN;Acc:ZDB-GENE-070112-1152]	791159	70.4942	2.1238	1.0866	0.3180	3.4168	0.0006	0.0147	1.8314
ENSDARG00000075192	YME1-like 1a [Source:ZFIN;Acc:ZDB-GENE-091113-41]	793098	550.5073	2.1237	1.0866	0.2718	3.9976	0.0001	0.0030	2.5252
ENSDARG00000031336	hydroxysteroid (20-beta) dehydrogenase 2 [Source:ZFIN;Acc:ZDB-GENE-030804-21]	368367	564.9766	2.1214	1.0850	0.2027	5.3540	0.0000	0.0000	4.8194
ENSDARG00000098853	EH-domain containing 1a [Source:ZFIN;Acc:ZDB-GENE-040426-2518]	405810	127.5549	2.1134	1.0796	0.2719	3.9708	0.0001	0.0032	2.4902
ENSDARG00000011921	thioredoxin-like 1 [Source:ZFIN;Acc:ZDB-GENE-040426-701]	394113	246.6280	2.1133	1.0795	0.3190	3.3841	0.0007	0.0158	1.8001
ENSDARG00000013946	influenza virus NS1A binding protein b [Source:ZFIN;Acc:ZDB-GENE-030131-6266]	334334	898.0455	2.1098	1.0771	0.1827	5.8963	0.0000	0.0000	5.8672
ENSDARG00000097973	si:ch1073-190k2.1 [Source:ZFIN;Acc:ZDB-GENE-131127-449]	NA	65.0852	2.1093	1.0767	0.3686	2.9214	0.0035	0.0468	1.3295
ENSDARG00000038557	ankyrin repeat and sterile alpha motif domain containing 3 [Source:ZFIN;Acc:ZDB-GENE-080204-51]	100136846	157.7203	2.1055	1.0741	0.2301	4.6672	0.0000	0.0003	3.5403
ENSDARG00000013576	growth arrest and DNA-damage-inducible, beta b [Source:ZFIN;Acc:ZDB-GENE-050223-1]	497646	90.2710	2.0979	1.0689	0.3589	2.9781	0.0029	0.0413	1.3841
ENSDARG00000060322	zgc:153654 [Source:ZFIN;Acc:ZDB-GENE-060929-1102]	565601	38.8891	2.0912	1.0643	0.3461	3.0751	0.0021	0.0330	1.4811
ENSDARG00000099776	glutamate-ammonia ligase (glutamine synthase) a [Source:ZFIN;Acc:ZDB-GENE-030131-688]	100000775	9701.5890	2.0911	1.0642	0.2582	4.1218	0.0000	0.0020	2.6980
ENSDARG00000029751	WW domain binding protein 1-like b [Source:ZFIN;Acc:ZDB-GENE-050522-112]	553658	83.4866	2.0894	1.0631	0.2501	4.2512	0.0000	0.0013	2.8918
ENSDARG00000012044	polymerase (RNA) III (DNA directed) polypeptide G like a [Source:ZFIN;Acc:ZDB-GENE-040912-67]	447901	61.1600	2.0891	1.0629	0.3252	3.2681	0.0011	0.0210	1.6769
ENSDARG00000039931	solute carrier family 25 member 33 [Source:ZFIN;Acc:ZDB-GENE-040426-2183]	406436	237.6069	2.0886	1.0625	0.3620	2.9347	0.0033	0.0455	1.3418
ENSDARG00000041110	DnaJ (Hsp40) homolog, subfamily C, member 3a [Source:ZFIN;Acc:ZDB-GENE-030131-1264]	322544	67.1368	2.0806	1.0570	0.2747	3.8478	0.0001	0.0047	2.3276
ENSDARG00000055226	solute carrier family 7 member 7 [Source:ZFIN;Acc:ZDB-GENE-051127-5]	641560	42.1391	2.0798	1.0564	0.3626	2.9132	0.0036	0.0477	1.3219
ENSDARG00000045980	NA	NA	266.3305	2.0790	1.0559	0.3388	3.1168	0.0018	0.0300	1.5235
ENSDARG00000074221	zgc:172302 [Source:ZFIN;Acc:ZDB-GENE-081205-5]	561460	586.8474	2.0775	1.0549	0.3242	3.2532	0.0011	0.0216	1.6646
ENSDARG00000057648	deoxynucleotidyltransferase, terminal, interacting protein 2 [Source:ZFIN;Acc:ZDB-GENE-080513-5]	564961	250.1056	2.0768	1.0544	0.1793	5.8812	0.0000	0.0000	5.8432
ENSDARG00000061256	si:dkey-44g23.5 [Source:ZFIN;Acc:ZDB-GENE-041008-233]	567109	493.3077	2.0752	1.0532	0.2890	3.6448	0.0003	0.0083	2.0802

ensembl_gene_id	description	entrezgene_									-log10
		id	baseMean	FC	log ₂ FC	lfcSE	stat	pvalue	padj	(FDRpval)	
ENSDARG00000011515	ORAI calcium release-activated calcium modulator 1a [Source:ZFIN;Acc:ZDB-GENE-110721-1]	566671	31.6576	2.0734	1.0520	0.3386	3.1065	0.0019	0.0306	1.5137	
ENSDARG00000061375	sphingosine-1-phosphate lyase 1 [Source:ZFIN;Acc:ZDB-GENE-070410-24]	100037312	357.1437	2.0711	1.0504	0.2927	3.5884	0.0003	0.0095	2.0229	
ENSDARG0000006031	4-aminobutyrate aminotransferase [Source:ZFIN;Acc:ZDB-GENE-031006-4]	378968	3943.7982	2.0687	1.0487	0.1354	7.7430	0.0000	0.0000	10.8317	
ENSDARG0000005643	glycine C-acetyltransferase [Source:ZFIN;Acc:ZDB-GENE-060518-3]	402822	52.5743	2.0660	1.0469	0.3135	3.3398	0.0008	0.0176	1.7543	
ENSDARG00000022712	signal transducer and activator of transcription 3 (acute-phase response factor) [Source:ZFIN;Acc:ZDB-GENE-980526-68]	30767	764.5692	2.0654	1.0464	0.2406	4.3486	0.0000	0.0009	3.0351	
ENSDARG00000077785	activating transcription factor 5b [Source:ZFIN;Acc:ZDB-GENE-030131-2637]	567253	999.6203	2.0611	1.0434	0.1856	5.6222	0.0000	0.0000	5.3399	
ENSDARG00000058658	si:dkey-178e17.3 [Source:ZFIN;Acc:ZDB-GENE-081104-335]	100535682	40.8622	2.0604	1.0429	0.3176	3.2834	0.0010	0.0202	1.6939	
ENSDARG00000058323	transmembrane BAX inhibitor motif containing 1a [Source:ZFIN;Acc:ZDB-GENE-041010-69]	449819	80.3199	2.0559	1.0397	0.3010	3.4541	0.0006	0.0136	1.8650	
ENSDARG00000104708	DEAD (Asp-Glu-Ala-Asp) box helicase 24 [Source:ZFIN;Acc:ZDB-GENE-100716-4]	553462	163.2324	2.0555	1.0395	0.1773	5.8638	0.0000	0.0000	5.8051	
ENSDARG00000078615	inactive ubiquitin carboxyl-terminal hydrolase 53-like [Source:NCBI gene;Acc:101885715]	101885715	95.0435	2.0526	1.0374	0.2412	4.3006	0.0000	0.0011	2.9622	
ENSDARG00000036848	solute carrier family 43 member 2a [Source:ZFIN;Acc:ZDB-GENE-040426-964]	NA	1567.2886	2.0485	1.0346	0.2209	4.6832	0.0000	0.0003	3.5678	
ENSDARG00000088440	slingshot protein phosphatase 2a [Source:ZFIN;Acc:ZDB-GENE-030131-3810]	325085	144.4344	2.0455	1.0325	0.2356	4.3820	0.0000	0.0008	3.0801	
ENSDARG00000089245	dual specificity phosphatase 23b [Source:ZFIN;Acc:ZDB-GENE-040718-163]	436735	45.1123	2.0451	1.0322	0.2736	3.7728	0.0002	0.0059	2.2317	
ENSDARG00000042221	methylenetetrahydrofolate dehydrogenase (NADP+ dependent) 1 like [Source:ZFIN;Acc:ZDB-GENE-041001-133]	100034522	105.6054	2.0441	1.0314	0.3560	2.8975	0.0038	0.0491	1.3091	
ENSDARG00000045946	SEC24 homolog D, COPII coat complex component [Source:ZFIN;Acc:ZDB-GENE-070117-2501]	553407	222.7857	2.0423	1.0302	0.2767	3.7237	0.0002	0.0067	2.1746	
ENSDARG00000059815	ornithine decarboxylase antizyme 2b [Source:ZFIN;Acc:ZDB-GENE-070313-1]	790945	468.2966	2.0402	1.0287	0.2510	4.0986	0.0000	0.0022	2.6671	
ENSDARG0000002967	pdgfa associated protein 1b [Source:ZFIN;Acc:ZDB-GENE-040426-942]	393179	283.5424	2.0357	1.0255	0.1880	5.4538	0.0000	0.0000	5.0207	
ENSDARG00000075833	lymphatic vessel endothelial hyaluronic receptor 1a [Source:ZFIN;Acc:ZDB-GENE-031118-138]	560618	57.5508	2.0351	1.0251	0.3107	3.2987	0.0010	0.0195	1.7102	
ENSDARG00000102549	NA	NA	257.0867	2.0344	1.0246	0.1920	5.3363	0.0000	0.0000	4.7847	
ENSDARG00000100461	interleukin-1 receptor type 2 [Source:NCBI gene;Acc:101882195]	101882195	50.3447	2.0338	1.0242	0.3490	2.9347	0.0033	0.0455	1.3418	

ensembl_gene_id	description	entrezgene_							-log10	
		id	baseMean	FC	log ₂ FC	lfcSE	stat	pvalue	padj	(FDRpval)
ENSDARG00000055129	Pim-3 proto-oncogene, serine/threonine kinase [Source:ZFIN;Acc:ZDB-GENE-050809-111]	565041	1072.8021	2.0263	1.0188	0.3162	3.2220	0.0013	0.0233	1.6331
ENSDARG00000014232	si:dkey-121j17.5 [Source:ZFIN;Acc:ZDB-GENE-030131-4745]	326020	44.0902	2.0244	1.0175	0.3449	2.9503	0.0032	0.0441	1.3558
ENSDARG00000001873	phosphoglycerate dehydrogenase [Source:ZFIN;Acc:ZDB-GENE-030131-647]	321928	241.8541	2.0232	1.0166	0.1938	5.2462	0.0000	0.0000	4.6210
ENSDARG00000014956	diablo, IAP-binding mitochondrial protein b [Source:ZFIN;Acc:ZDB-GENE-070112-202]	570425	56.0820	2.0211	1.0151	0.2770	3.6645	0.0002	0.0078	2.1066
ENSDARG00000070961	leptin receptor [Source:ZFIN;Acc:ZDB-GENE-080104-1]	567241	458.3000	2.0178	1.0128	0.1808	5.6030	0.0000	0.0000	5.3003
ENSDARG00000070669	chemokine (C-X-C motif) receptor 3, tandem duplicate 3 [Source:ZFIN;Acc:ZDB-GENE-100922-34]	799527	178.8257	2.0157	1.0113	0.2583	3.9158	0.0001	0.0038	2.4167
ENSDARG00000043531	Jun proto-oncogene, AP-1 transcription factor subunit [Source:ZFIN;Acc:ZDB-GENE-030131-7859]	335916	489.0072	2.0146	1.0105	0.1569	6.4419	0.0000	0.0000	7.1645
ENSDARG00000098903	transcription factor binding to IGHM enhancer 3a [Source:ZFIN;Acc:ZDB-GENE-010919-2]	114834	369.5061	2.0133	1.0096	0.1957	5.1580	0.0000	0.0000	4.4444
ENSDARG00000013144	ATPase Na ⁺ /K ⁺ transporting subunit beta 1a [Source:ZFIN;Acc:ZDB-GENE-001127-3]	64267	1370.6973	2.0132	1.0095	0.2163	4.6682	0.0000	0.0003	3.5404
ENSDARG00000020031	claudin 11a [Source:ZFIN;Acc:ZDB-GENE-040718-369]	436897	95.1167	2.0124	1.0089	0.2650	3.8069	0.0001	0.0053	2.2772
ENSDARG00000055966	CASP8 and FADD-like apoptosis regulator a [Source:ZFIN;Acc:ZDB-GENE-030826-3]	373114	114.3377	2.0105	1.0076	0.2924	3.4455	0.0006	0.0139	1.8584
ENSDARG00000004177	family with sequence similarity 169 member Ab [Source:ZFIN;Acc:ZDB-GENE-091118-95]	553309	108.2832	2.0086	1.0062	0.3202	3.1427	0.0017	0.0279	1.5538
ENSDARG00000056057	gremlin 2, DAN family BMP antagonist a [Source:ZFIN;Acc:ZDB-GENE-131127-498]	100002201	44.8069	2.0077	1.0055	0.3455	2.9101	0.0036	0.0479	1.3193
ENSDARG00000100513	ribosomal protein S27 like [Source:ZFIN;Acc:ZDB-GENE-060331-65]	677743	87.0260	2.0045	1.0032	0.3369	2.9777	0.0029	0.0413	1.3839
ENSDARG00000070228	cyclin-dependent kinase 6 [Source:ZFIN;Acc:ZDB-GENE-060503-786]	100034507	151.8004	0.5000	-1.0001	0.2298	-4.3523	0.0000	0.0009	3.0379
ENSDARG00000042533	glutathione S-transferase mu, tandem duplicate 1 [Source:ZFIN;Acc:ZDB-GENE-030911-2]	324366	184.5341	0.4999	-1.0002	0.2685	-3.7250	0.0002	0.0067	2.1754
ENSDARG00000058050	SET and MYND domain containing 3 [Source:ZFIN;Acc:ZDB-GENE-051120-138]	569507	54.8722	0.4993	-1.0021	0.2381	-4.2085	0.0000	0.0015	2.8327
ENSDARG00000018423	sulfatase 2a [Source:ZFIN;Acc:ZDB-GENE-040426-759]	393910	327.5517	0.4986	-1.0040	0.2321	-4.3266	0.0000	0.0010	3.0032
ENSDARG00000057568	neurofilament, light polypeptide a [Source:ZFIN;Acc:ZDB-GENE-091117-1]	793912	176.2854	0.4979	-1.0060	0.3313	-3.0364	0.0024	0.0364	1.4388

ensembl_gene_id	description	entrezgene_					-log10				
		id	baseMean	FC	log ₂ FC	lfcSE	stat	pvalue	padj	(FDRpval)	
ENSDARG00000045308	polymerase (DNA directed), alpha 1 [Source:ZFIN;Acc:ZDB-GENE-030114-9]	317740	111.8891	0.4968	-1.0092	0.3115	-3.2400	0.0012	0.0223	1.6516	
ENSDARG00000011094	cyclin A2 [Source:ZFIN;Acc:ZDB-GENE-020418-1]	192295	76.5115	0.4941	-1.0170	0.3126	-3.2535	0.0011	0.0216	1.6646	
ENSDARG00000098237	fibrillin 2b [Source:ZFIN;Acc:ZDB-GENE-090112-3]	571786	34.5014	0.4940	-1.0174	0.3141	-3.2391	0.0012	0.0223	1.6510	
ENSDARG0000004049	myristoylated alanine-rich protein kinase C substrate a [Source:ZFIN;Acc:ZDB-GENE-050522-145]	554102	136.3426	0.4935	-1.0189	0.3225	-3.1599	0.0016	0.0269	1.5696	
ENSDARG00000051730	solute carrier family 7 member 10b [Source:ZFIN;Acc:ZDB-GENE-121105-2]	559395	110.3343	0.4908	-1.0268	0.2329	-4.4087	0.0000	0.0008	3.1224	
ENSDARG00000053262	ATPase Na ⁺ /K ⁺ transporting subunit beta 4 [Source:ZFIN;Acc:ZDB-GENE-070412-1]	100037383	884.3359	0.4905	-1.0277	0.2741	-3.7494	0.0002	0.0062	2.2045	
ENSDARG00000103732	proteolipid protein 1a [Source:ZFIN;Acc:ZDB-GENE-001202-1]	64264	117.6620	0.4899	-1.0295	0.1939	-5.3100	0.0000	0.0000	4.7294	
ENSDARG00000099621	si:ch211-69b22.5 [Source:ZFIN;Acc:ZDB-GENE-141216-348]	NA	49.6958	0.4890	-1.0322	0.2866	-3.6021	0.0003	0.0092	2.0344	
ENSDARG00000090615	CD59 molecule (CD59 blood group) [Source:ZFIN;Acc:ZDB-GENE-030131-7871]	567192	320.9261	0.4860	-1.0410	0.1903	-5.4706	0.0000	0.0000	5.0519	
ENSDARG00000019532	fatty acid desaturase 2 [Source:ZFIN;Acc:ZDB-GENE-011212-1]	140615	67.8130	0.4855	-1.0423	0.3367	-3.0958	0.0020	0.0314	1.5037	
ENSDARG00000102453	solute carrier family 1 member 2b [Source:ZFIN;Acc:ZDB-GENE-030131-7779]	335836	5810.2704	0.4849	-1.0443	0.2047	-5.1019	0.0000	0.0000	4.3426	
ENSDARG00000014233	septin 8b [Source:ZFIN;Acc:ZDB-GENE-070424-3]	571702	154.5063	0.4812	-1.0552	0.2878	-3.6661	0.0002	0.0078	2.1066	
ENSDARG00000016725	growth arrest and DNA-damage-inducible, gamma b, tandem duplicate 1 [Source:ZFIN;Acc:ZDB-GENE-040426-2321]	406507	74.5566	0.4812	-1.0552	0.2852	-3.7002	0.0002	0.0071	2.1468	
ENSDARG00000035697	spindlin b [Source:ZFIN;Acc:ZDB-GENE-050417-414]	550562	38.3279	0.4733	-1.0791	0.3038	-3.5523	0.0004	0.0105	1.9791	
ENSDARG00000001889	tubulin, alpha 1a [Source:ZFIN;Acc:ZDB-GENE-090507-4]	573216	761.2351	0.4729	-1.0804	0.2749	-3.9306	0.0001	0.0037	2.4329	
ENSDARG00000044047	solute carrier family 18 member B1 [Source:ZFIN;Acc:ZDB-GENE-050417-386]	550539	30.1390	0.4717	-1.0840	0.3227	-3.3596	0.0008	0.0168	1.7739	
ENSDARG00000068428	si:ch211-153j24.3 [Source:ZFIN;Acc:ZDB-GENE-041014-38]	564403	89.4712	0.4699	-1.0896	0.2580	-4.2238	0.0000	0.0014	2.8496	
ENSDARG00000022531	netrin 1b [Source:ZFIN;Acc:ZDB-GENE-990415-168]	30192	542.6343	0.4684	-1.0941	0.2056	-5.3220	0.0000	0.0000	4.7543	
ENSDARG00000091579	si:ch211-66e2.5 [Source:ZFIN;Acc:ZDB-GENE-131121-180]	100150500	130.4206	0.4683	-1.0945	0.1955	-5.5993	0.0000	0.0000	5.2964	
ENSDARG00000045367	tubulin, alpha 1b [Source:ZFIN;Acc:ZDB-GENE-030822-1]	373080	286.5420	0.4658	-1.1022	0.2371	-4.6486	0.0000	0.0003	3.5072	
ENSDARG00000009387	roundabout, axon guidance receptor, homolog 4 (Drosophila) [Source:ZFIN;Acc:ZDB-GENE-020809-1]	560765	263.6419	0.4619	-1.1144	0.1701	-6.5532	0.0000	0.0000	7.4166	
ENSDARG00000102340	pleiotrophin [Source:ZFIN;Acc:ZDB-GENE-030624-1]	368211	1125.9742	0.4564	-1.1317	0.1438	-7.8707	0.0000	0.0000	11.2369	
ENSDARG00000052470	insulin-like growth factor binding protein 2a [Source:ZFIN;Acc:ZDB-GENE-000125-12]	794176	36.8551	0.4549	-1.1364	0.3406	-3.3366	0.0008	0.0177	1.7509	

ensembl_gene_id	description	entrezgene_							-log10	
		id	baseMean	FC	log ₂ FC	lfcSE	stat	pvalue	padj	(FDRpval)
ENSDARG00000012881	solute carrier family 4 member 1a (Diego blood group) [Source:ZFIN;Acc:ZDB-GENE-010525-1]	84703	35.3343	0.4549	-1.1364	0.3114	-3.6491	0.0003	0.0082	2.0861
ENSDARG00000008803	myristoylated alanine-rich protein kinase C substrate b [Source:ZFIN;Acc:ZDB-GENE-030131-1921]	323201	1783.7971	0.4547	-1.1372	0.1957	-5.8116	0.0000	0.0000	5.7057
ENSDARG00000022437	CD81 molecule b [Source:ZFIN;Acc:ZDB-GENE-040808-52]	445280	62.8323	0.4540	-1.1393	0.2618	-4.3512	0.0000	0.0009	3.0373
ENSDARG00000079305	hemoglobin alpha embryonic-3 [Source:ZFIN;Acc:ZDB-GENE-990706-3]	30601	229.3064	0.4522	-1.1450	0.3603	-3.1774	0.0015	0.0259	1.5867
ENSDARG00000100074	NA	NA	36.7795	0.4515	-1.1471	0.3475	-3.3011	0.0010	0.0194	1.7129
ENSDARG00000056722	CD99 molecule-like 2 [Source:ZFIN;Acc:ZDB-GENE-030131-1986]	323266	935.9962	0.4482	-1.1577	0.2563	-4.5176	0.0000	0.0005	3.2973
ENSDARG00000104436	zgc:153426 [Source:ZFIN;Acc:ZDB-GENE-060929-220]	767746	752.8873	0.4432	-1.1740	0.2599	-4.5173	0.0000	0.0005	3.2973
ENSDARG00000089255	potassium inwardly-rectifying channel, subfamily J, member 11, like [Source:ZFIN;Acc:ZDB-GENE-050222-2]	100003678	29.5622	0.4420	-1.1780	0.3464	-3.4008	0.0007	0.0153	1.8156
ENSDARG00000088330	hemoglobin, alpha embryonic 1.1 [Source:ZFIN;Acc:ZDB-GENE-980526-80]	572729	195.3412	0.4378	-1.1917	0.3602	-3.3084	0.0009	0.0191	1.7185
ENSDARG00000103490	dihydropyrimidinase like 4 [Source:ZFIN;Acc:ZDB-GENE-050720-3]	553411	193.3580	0.4375	-1.1928	0.3474	-3.4337	0.0006	0.0142	1.8491
ENSDARG00000055216	tubulin, alpha 1c [Source:ZFIN;Acc:ZDB-GENE-061114-1]	573122	1896.7251	0.4349	-1.2012	0.3147	-3.8173	0.0001	0.0051	2.2892
ENSDARG00000039522	tubulin, beta 2A class IIa [Source:ZFIN;Acc:ZDB-GENE-050522-384]	554127	205.2141	0.4326	-1.2089	0.3040	-3.9767	0.0001	0.0032	2.4991
ENSDARG00000087197	c-ros oncogene 1 , receptor tyrosine kinase [Source:ZFIN;Acc:ZDB-GENE-020506-1]	245951	56.3467	0.4317	-1.2117	0.3778	-3.2070	0.0013	0.0242	1.6168
ENSDARG00000044541	protein phosphatase 1, regulatory (inhibitor) subunit 14Ba [Source:ZFIN;Acc:ZDB-GENE-060825-331]	564838	191.0421	0.4294	-1.2197	0.2596	-4.6984	0.0000	0.0003	3.5929
ENSDARG00000062152	chromatin assembly factor 1, subunit A (p150) [Source:ZFIN;Acc:ZDB-GENE-030131-5366]	563212	86.3599	0.4279	-1.2247	0.3390	-3.6122	0.0003	0.0090	2.0438
ENSDARG00000035873	four-jointed box kinase 1 [Source:ZFIN;Acc:ZDB-GENE-100422-10]	100001423	23.8932	0.4271	-1.2274	0.4127	-2.9740	0.0029	0.0415	1.3815
ENSDARG00000013072	matrix metalloproteinase 15b [Source:ZFIN;Acc:ZDB-GENE-070817-6]	100332426	58.5190	0.4266	-1.2290	0.2397	-5.1281	0.0000	0.0000	4.3939
ENSDARG00000032238	dynamamin 3a [Source:ZFIN;Acc:ZDB-GENE-040724-76]	557996	29.3164	0.4257	-1.2322	0.3403	-3.6205	0.0003	0.0089	2.0521
ENSDARG00000102793	solute carrier family 16 member 6a [Source:ZFIN;Acc:ZDB-GENE-110208-1]	564872	65.7380	0.4229	-1.2415	0.2973	-4.1753	0.0000	0.0017	2.7815
ENSDARG00000054400	si:ch211-198n5.11 [Source:ZFIN;Acc:ZDB-GENE-050411-52]	100004018	35.6997	0.4220	-1.2447	0.2952	-4.2161	0.0000	0.0014	2.8436
ENSDARG00000058292	selenophosphate synthetase 1 [Source:ZFIN;Acc:ZDB-GENE-030131-3670]	324947	64.1857	0.4171	-1.2614	0.3226	-3.9095	0.0001	0.0039	2.4090

ensembl_gene_id	description	entrezgene_					-log10			
		id	baseMean	FC	log ₂ FC	lfcSE	stat	pvalue	padj	(FDRpval)
ENSDARG00000073870	glycerophosphodiester phosphodiesterase domain containing 2 [Source:ZFIN;Acc:ZDB-GENE-081107-62]	563198	91.6095	0.4171	-1.2614	0.3404	-3.7062	0.0002	0.0070	2.1535
ENSDARG00000070453	GTP cyclohydrolase 1 [Source:ZFIN;Acc:ZDB-GENE-070720-5]	100192219	261.7950	0.4141	-1.2718	0.1595	-7.9761	0.0000	0.0000	11.5671
ENSDARG00000089233	chondroitin sulfate N-acetylgalactosaminyltransferase 1b [Source:ZFIN;Acc:ZDB-GENE-130530-957]	101886904	41.0687	0.4128	-1.2766	0.3393	-3.7621	0.0002	0.0060	2.2187
ENSDARG00000020676	dipeptidyl-peptidase 3 [Source:ZFIN;Acc:ZDB-GENE-030131-1247]	322527	89.3687	0.4123	-1.2781	0.3028	-4.2215	0.0000	0.0014	2.8496
ENSDARG00000054420	retinoid isomerohydrolase RPE65 c [Source:ZFIN;Acc:ZDB-GENE-081104-505]	100004076	31.4576	0.4122	-1.2786	0.3709	-3.4477	0.0006	0.0138	1.8589
ENSDARG00000056774	G protein-coupled receptor 37 like 1b [Source:ZFIN;Acc:ZDB-GENE-081104-324]	567796	221.4524	0.4081	-1.2930	0.2506	-5.1607	0.0000	0.0000	4.4466
ENSDARG00000041515	RAS protein activator like 1b (GAP1 like) [Source:ZFIN;Acc:ZDB-GENE-141212-314]	570938	43.2856	0.4065	-1.2988	0.3048	-4.2606	0.0000	0.0013	2.9020
ENSDARG00000052012	reticulon 4 receptor-like 2 a [Source:ZFIN;Acc:ZDB-GENE-040310-4]	403307	106.2661	0.4061	-1.3002	0.4308	-3.0182	0.0025	0.0379	1.4209
ENSDARG00000042845	oxytocin [Source:ZFIN;Acc:ZDB-GENE-030407-1]	352920	101.5910	0.4013	-1.3174	0.4017	-3.2799	0.0010	0.0203	1.6922
ENSDARG00000001676	glycoprotein M6Bb [Source:ZFIN;Acc:ZDB-GENE-030710-10]	503756	760.7708	0.3950	-1.3400	0.2349	-5.7037	0.0000	0.0000	5.4747
ENSDARG00000032836	parvalbumin 5 [Source:ZFIN;Acc:ZDB-GENE-050417-336]	335623	121.7103	0.3938	-1.3444	0.4123	-3.2604	0.0011	0.0214	1.6698
ENSDARG00000005454	transforming, acidic coiled-coil containing protein 3 [Source:ZFIN;Acc:ZDB-GENE-050522-327]	321283	40.4051	0.3915	-1.3527	0.3985	-3.3948	0.0007	0.0155	1.8101
ENSDARG00000039356	zgc:194209 [Source:ZFIN;Acc:ZDB-GENE-081022-75]	570908	24.6639	0.3881	-1.3654	0.3993	-3.4199	0.0006	0.0146	1.8349
ENSDARG00000022951	parathyroid hormone 2 [Source:ZFIN;Acc:ZDB-GENE-041102-1]	402812	69.3144	0.3825	-1.3865	0.3385	-4.0964	0.0000	0.0022	2.6663
ENSDARG00000078654	TPX2 microtubule nucleation factor [Source:ZFIN;Acc:ZDB-GENE-030131-9652]	107966129	39.7799	0.3786	-1.4013	0.4110	-3.4091	0.0007	0.0150	1.8243
ENSDARG00000037747	fascin actin-bundling protein 1b [Source:ZFIN;Acc:ZDB-GENE-120507-1]	570314	437.3911	0.3783	-1.4024	0.2794	-5.0200	0.0000	0.0001	4.1816
ENSDARG00000102858	sc:d189 [Source:ZFIN;Acc:ZDB-GENE-080303-11]	100002334	28.0748	0.3772	-1.4067	0.3761	-3.7404	0.0002	0.0064	2.1920
ENSDARG00000102478	ADAM metallopeptidase with thrombospondin type 1 motif 7 [Source:HGNC Symbol;Acc:HGNC:223]	560364	21.8064	0.3762	-1.4105	0.4078	-3.4592	0.0005	0.0135	1.8694
ENSDARG00000086300	family with sequence similarity 107 member A [Source:HGNC Symbol;Acc:HGNC:30827]	794256	450.2567	0.3758	-1.4120	0.1627	-8.6805	0.0000	0.0000	14.0126
ENSDARG00000103332	NA	NA	133.2161	0.3722	-1.4257	0.2792	-5.1057	0.0000	0.0000	4.3482
ENSDARG00000007697	fatty acid binding protein 7, brain, a [Source:ZFIN;Acc:ZDB-GENE-000627-1]	58128	777.8949	0.3586	-1.4794	0.2174	-6.8036	0.0000	0.0000	8.1112
ENSDARG00000012073	kinesin family member 15 [Source:ZFIN;Acc:ZDB-GENE-050622-16]	573988	29.2758	0.3507	-1.5116	0.5201	-2.9060	0.0037	0.0483	1.3163

ensembl_gene_id	description	entrezgene_							-log10	
		id	baseMean	FC	log ₂ FC	lfcSE	stat	pvalue	padj	(FDRpval)
ENSDARG00000020054	aldehyde oxidase 6 [Source:ZFIN;Acc:ZDB-GENE-050208-742]	570457	68.6292	0.3501	-1.5140	0.2596	-5.8325	0.0000	0.0000	5.7531
ENSDARG00000100573	cytoskeleton associated protein 2-like [Source:ZFIN;Acc:ZDB-GENE-030131-6690]	569937	31.2107	0.3462	-1.5304	0.4772	-3.2070	0.0013	0.0242	1.6168
ENSDARG00000102857	NA	NA	106.8560	0.3448	-1.5364	0.3068	-5.0076	0.0000	0.0001	4.1597
ENSDARG00000101670	kinetochore associated 1 [Source:ZFIN;Acc:ZDB-GENE-050208-92]	497376	35.6845	0.3443	-1.5384	0.4124	-3.7308	0.0002	0.0065	2.1840
ENSDARG00000004232	deltaB [Source:ZFIN;Acc:ZDB-GENE-980526-114]	30141	57.8040	0.3381	-1.5643	0.4393	-3.5608	0.0004	0.0103	1.9870
ENSDARG00000005058	non-SMC condensin I complex, subunit D2 [Source:ZFIN;Acc:ZDB-GENE-050506-59]	552978	54.1085	0.3354	-1.5760	0.4197	-3.7549	0.0002	0.0062	2.2108
ENSDARG00000071694	NDC80 kinetochore complex component [Source:ZFIN;Acc:ZDB-GENE-030131-904]	445386	29.1992	0.3336	-1.5837	0.5023	-3.1529	0.0016	0.0273	1.5642
ENSDARG00000094752	retinoid isomerohydrolase RPE65 b [Source:ZFIN;Acc:ZDB-GENE-050410-16]	100002865	62.2080	0.3307	-1.5964	0.3415	-4.6748	0.0000	0.0003	3.5522
ENSDARG00000070463	E2F transcription factor 3 [Source:ZFIN;Acc:ZDB-GENE-070112-882]	791146	23.4853	0.3150	-1.6667	0.4690	-3.5537	0.0004	0.0105	1.9803
ENSDARG00000098980	si:ch211-153f2.3 [Source:ZFIN;Acc:ZDB-GENE-081104-135]	100534664	21.3345	0.3135	-1.6733	0.4484	-3.7319	0.0002	0.0065	2.1850
ENSDARG00000078069	ribonucleotide reductase M2 polypeptide [Source:ZFIN;Acc:ZDB-GENE-990415-25]	30733	145.4702	0.3093	-1.6928	0.4002	-4.2297	0.0000	0.0014	2.8569
ENSDARG00000103849	malate dehydrogenase 1Ab, NAD (soluble) [Source:ZFIN;Acc:ZDB-GENE-030131-7655]	335715	82.0877	0.2909	-1.7813	0.2413	-7.3831	0.0000	0.0000	9.7461
ENSDARG00000037997	tubulin, beta 5 [Source:ZFIN;Acc:ZDB-GENE-031110-4]	386701	532.3828	0.2902	-1.7850	0.3724	-4.7935	0.0000	0.0002	3.7698
ENSDARG00000103996	spindle apparatus coiled-coil protein 1 [Source:ZFIN;Acc:ZDB-GENE-070928-7]	568360	17.9303	0.2878	-1.7967	0.4952	-3.6285	0.0003	0.0087	2.0609
ENSDARG00000038066	karyopherin alpha 2 (RAG cohort 1, importin alpha 1) [Source:ZFIN;Acc:ZDB-GENE-040718-22]	436607	30.0041	0.2854	-1.8090	0.5718	-3.1639	0.0016	0.0267	1.5727
ENSDARG00000043740	EF-hand calcium binding domain 11 [Source:ZFIN;Acc:ZDB-GENE-050417-348]	550510	13.7722	0.2854	-1.8092	0.5474	-3.3050	0.0009	0.0192	1.7164
ENSDARG00000105976	islet amyloid polypeptide [Source:NCBI gene;Acc:100334757]	100334757	22.0499	0.2820	-1.8263	0.6023	-3.0325	0.0024	0.0367	1.4353
ENSDARG00000010792	cell division cycle 25B [Source:ZFIN;Acc:ZDB-GENE-000330-5]	57925	53.3772	0.2706	-1.8860	0.4472	-4.2171	0.0000	0.0014	2.8441
ENSDARG00000096554	si:dkey-25o16.4 [Source:ZFIN;Acc:ZDB-GENE-030131-969]	567619	27.6208	0.2697	-1.8908	0.5279	-3.5816	0.0003	0.0097	2.0142
ENSDARG00000002403	nucleolar and spindle associated protein 1 [Source:ZFIN;Acc:ZDB-GENE-030827-5]	567446	27.3367	0.2409	-2.0535	0.6327	-3.2456	0.0012	0.0220	1.6567
ENSDARG00000074989	SPARC-like 1 [Source:ZFIN;Acc:ZDB-GENE-060130-6]	567331	51.9364	0.2375	-2.0741	0.3671	-5.6505	0.0000	0.0000	5.3874
ENSDARG00000076228	kinesin family member 2C [Source:ZFIN;Acc:ZDB-GENE-070912-298]	100136875	16.4955	0.2318	-2.1093	0.6025	-3.5010	0.0005	0.0121	1.9157
ENSDARG00000001558	kinesin family member C1 [Source:ZFIN;Acc:ZDB-GENE-000208-21]	30453	37.1189	0.2299	-2.1211	0.6029	-3.5179	0.0004	0.0116	1.9374
ENSDARG00000038882	structural maintenance of chromosomes 4 [Source:ZFIN;Acc:ZDB-GENE-020419-21]	192332	52.2183	0.2297	-2.1222	0.5119	-4.1455	0.0000	0.0018	2.7358

ensembl_gene_id	description	entrezgene_							-log10	
		id	baseMean	FC	log ₂ FC	lfcSE	stat	pvalue	padj	(FDRpval)
ENSDARG00000040224	kelch repeat-containing protein [Source:ZFIN;Acc:ZDB-GENE-030131-2126]	323406	14.6167	0.2276	-2.1356	0.6537	-3.2666	0.0011	0.0211	1.6765
ENSDARG00000100741	cell division cycle 20 homolog [Source:ZFIN;Acc:ZDB-GENE-040426-2044]	406353	18.3870	0.2233	-2.1629	0.6226	-3.4737	0.0005	0.0130	1.8877
ENSDARG00000017744	structural maintenance of chromosomes 2 [Source:ZFIN;Acc:ZDB-GENE-030131-105]	321452	35.4493	0.2227	-2.1666	0.5262	-4.1171	0.0000	0.0020	2.6914
ENSDARG00000103754	abnormal spindle microtubule assembly [Source:ZFIN;Acc:ZDB-GENE-050208-620]	554173	88.4246	0.2209	-2.1787	0.4690	-4.6450	0.0000	0.0003	3.5037
ENSDARG00000070239	kinetochore scaffold 1 [Source:ZFIN;Acc:ZDB-GENE-030131-5437]	327226	19.3276	0.2206	-2.1804	0.5938	-3.6718	0.0002	0.0077	2.1135
ENSDARG00000021172	cytochrome P450, family 2, subfamily AD, polypeptide 2 [Source:ZFIN;Acc:ZDB-GENE-020812-2]	259306	50.7188	0.2158	-2.2121	0.4443	-4.9789	0.0000	0.0001	4.1087
ENSDARG00000091150	marker of proliferation Ki-67 [Source:ZFIN;Acc:ZDB-GENE-030131-9771]	564521	189.9181	0.2066	-2.2749	0.6022	-3.7776	0.0002	0.0058	2.2369
ENSDARG00000098650	IQ motif containing GTPase activating protein 3 [Source:ZFIN;Acc:ZDB-GENE-160226-1]	100537977	20.5914	0.1984	-2.3332	0.6188	-3.7707	0.0002	0.0059	2.2296
ENSDARG00000016856	paraoxonase 2 [Source:ZFIN;Acc:ZDB-GENE-030131-7116]	335176	12.1348	0.1924	-2.3777	0.5911	-4.0224	0.0001	0.0027	2.5614
ENSDARG00000045167	discs, large (Drosophila) homolog-associated protein 5 [Source:ZFIN;Acc:ZDB-GENE-040912-160]	447853	21.3706	0.1637	-2.6113	0.7262	-3.5957	0.0003	0.0093	2.0295
ENSDARG00000054929	zgc:110540 [Source:ZFIN;Acc:ZDB-GENE-050327-77]	541538	16.0521	0.1633	-2.6145	0.7773	-3.3634	0.0008	0.0167	1.7780
ENSDARG00000087554	cyclin-dependent kinase 1 [Source:ZFIN;Acc:ZDB-GENE-010320-1]	80973	15.6050	0.1601	-2.6429	0.6745	-3.9182	0.0001	0.0038	2.4182
ENSDARG00000088711	lectin, galactoside-binding, soluble, 1 (galectin 1)-like 1 [Source:ZFIN;Acc:ZDB-GENE-030131-4905]	326706	12.2899	0.1402	-2.8344	0.8446	-3.3560	0.0008	0.0170	1.7708
ENSDARG00000055192	zgc:136930 [Source:ZFIN;Acc:ZDB-GENE-060312-16]	563946	118.5321	0.1387	-2.8496	0.5114	-5.5724	0.0000	0.0000	5.2542
ENSDARG00000030215	matrilin 1 [Source:ZFIN;Acc:ZDB-GENE-050307-3]	403023	57.9144	0.1182	-3.0805	0.9529	-3.2328	0.0012	0.0227	1.6438
ENSDARG00000077620	cell division cycle associated 7a [Source:ZFIN;Acc:ZDB-GENE-050417-29]	550236	13.6610	0.0868	-3.5268	1.0641	-3.3144	0.0009	0.0188	1.7249
ENSDARG00000102245	thymidine kinase 1, soluble [Source:ZFIN;Acc:ZDB-GENE-030131-5801]	327590	20.0258	0.0688	-3.8622	0.8198	-4.7110	0.0000	0.0002	3.6141
ENSDARG00000056248	si:dkey-183i3.5 [Source:ZFIN;Acc:ZDB-GENE-030131-8568]	566445	76.2276	0.0672	-3.8947	0.5973	-6.5202	0.0000	0.0000	7.3498
ENSDARG00000090268	keratin type 1 c19e [Source:ZFIN;Acc:ZDB-GENE-050506-95]	553371	102.5087	0.0497	-4.3308	0.8924	-4.8529	0.0000	0.0001	3.8678

